Functional Genomics of Chromatin Regulator Dependencies and Resistance Mechanisms in B-cell Lymphoma

Daniel Angelov

A thesis submitted to Trinity College Dublin for

the degree of Doctor of Philosophy

2026

Thesis supervisor: Professor Adrian P. Bracken

Smurfit Institute of Genetics

Trinity College Dublin, The University of Dublin

Declaration

I declare that this thesis has not been submitted as an exercise for a degree at this or any other university and it is entirely my own work. I confirm that the work has been completed in full compliance with relevant university policies, including the Academic Integrity policy, the Trinity Policy on Good Research Practice, and the guidance on AI and GenAI in Teaching, Learning, Assessment and Research.

I agree to deposit this thesis in the University's open access institutional repository or allow the Library to do so on my behalf, subject to Irish Copyright Legislation and Trinity College Library conditions of use and acknowledgement.

I consent to the examiner retaining a copy of the thesis beyond the examining period, should they so wish (EU GDPR May 2018).

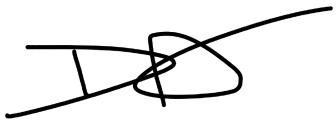

Daniel Angelov, January 2026

Summary

The polycomb repressive complexes 1 and 2 (PRC1 and 2) in mammals are multi-member protein complexes that catalyse chemical group additions to chromatin, functioning to maintain transcriptional repression and coordinate context-dependent gene programs. Germinal-centre lymphomas, the most common form of lymphoma, arise from B-cells that acquire recurrent mutations in chromatin regulatory genes during B-cell maturation. The catalytic subunit of Polycomb Repressive Complex 2 (PRC2), EZH2, is recurrently mutated in 25% of diffuse large B-cell lymphomas (DLBCL), causing increased H3K27me3 and decreased H3K27me2 levels, leading to hyper-repression of the gene programs required for normal B-cell terminal differentiation and exit from the germinal centre. EZH2 inhibitors provide clinical benefit, but resistance frequently develops, highlighting the need for alternative therapeutic targets. This project identifies multiple targetable chromatin regulatory genes as genetic sensitisers to EZH2 inhibition in B-cell lymphoma, including *BRD9*, *EP300*, *DOT1L*, *EHMT2* and *MEN1*. The PRC2 accessory protein AEBP2 was identified as a specific genetic dependency and EZH2 inhibitor sensitiser in B-cell lymphoma. While AEBP2 acts through PRC2, its essential role is surprisingly independent of canonical H3K27me3-mediated gene silencing. Instead, AEBP2 functions within a PRC2.2 complex lacking JARID2, using its zinc-finger domains to sample intergenic chromatin to sustain H3K27me2. The H3K36 methyltransferases, NSD1 and NSD2, which antagonise Polycomb function, were identified as genetic resistors to EZH2 inhibitors. While NSD2 does not physically interact with PRC2, its loss blunts gene de-repression in response to EZH2 inhibitors, potentially through effects at distal regulatory elements. Notably, loss of *AEBP2* or *NSD2* caused contrasting changes in intergenic H3K27me2 levels, driving sensitivity or resistance to PRC2 inhibitors, respectively. The work presented here identifies AEBP2-PRC2.2-maintained intergenic H3K27me2 as a therapeutic vulnerability in EZH2-mutant DLBCL and highlight dysregulated H3K27me2 as an underappreciated form of PRC2 dysfunction in cancer, with important therapeutic implications.

Publications & Manuscripts

Angelov D.[1], Nolan J.[1], Holland G., Nimmo D., Davies M., Monger C., Dillon E., Mucha M., Wang C., Lagan E., Malcolm A., Vandenberghe E., Flaus A., Chen C.W., Brien G.L., Conway E.[1,2], Bracken A.P[1,2]. (2025). AEBP2 Directed H3K27me2 by PRC2.2 Defines a Specific Chromatin Vulnerability in Diffuse Large B-Cell Lymphoma. *Manuscript in revision at Molecular Cell.*

Mucha M.[1], Lai Z.[1], McKenzie N.J.[1], Matrà F.[1], Boudes M., Flanigan S.F., Alejo-Vinogradova M.T., Monger C., Zhang Q., Nimmo D., Healy E., Silva A.J., **Angelov D.**, Reck D.M., Holland G., Atmaca Z.E., King H.E., Hamilton M., Glancy E., Nolan J., Weatheritt R.J., Bell O., Vermeulen M., Davidovich C.[1,2], Bracken A.P.[1,2] (2025) Auto-inhibition of PRC2 by the broadly expressed long isoform of AEBP2. EMBO J. In press.

[1]Authors contributed equally

[2]Co-senior authors

Acknowledgements

Firstly, I would like to extend a huge gratitude towards my supervisor, Professor Adrian Bracken. Starting in a basic science lab after seven years practising medicine was a shock to the system, but Adrian made this transition far easier than it should have been. His mentorship, teaching, and approachability is the primary reason I want to continue as a clinician-scientist for the rest of my career. Many thanks also to Dr James Nolan and Professor Elisabeth Vandenberghe, without whom I would never have had the opportunity to meet Professor Bracken and pursue this PhD project.

To all past and present members of the Bracken Lab, thank you for chatting science, sharing reagents, and creating a supportive environment. To the occupants of the “downstairs lab”, Dr Anto Doherty, Dr Eimear Lagan, Dr Gerry Brien and Ademar Silva; I was the buzzing bee in your ears for the first year of this project. From how to reverse pipette, to how to pool a library for sequencing, I’ll always be astounded and grateful for your patience with me. Drs Eimear Lagan and Dáire Gannon, you withstood hours of questions on CRISPR screens; without your kindness and time I couldn’t have performed such a fruitful CRISPR screen.

I would like to thank the Irish Cancer Society who funded this PhD research project, Dr Linsdey James for the NSD2 degrader, Grainne Holland for helping with structural analysis, generating AEBP2 mutants, and continuing the NSD2 story, Drs Darragh Nimmo and Craig Monger for bioinformatic support, and Dr James Nolan for starting the AEBP2 story.

Without the support of my wife Niamh McGlade, I never would’ve began or completed this PhD project. You have always been my number one supporter, and evenings with you and our beautiful son Roman are what I look forward to most in my day. To the Angelov and McGlade clans, thank you for your unconditional love and support over the years.

благодаря ви много на всички

In Memoriam

In the first 6 months of my PhD research project my mother developed B-cell lymphoma. She underwent a difficult treatment course and achieved a remission, however in the final 6 months of this research project her lymphoma relapsed and she never recovered. Her illness framed this PhD project in a sobering light, but provided me with the conviction to improve the understanding and treatments for blood cancers throughout my academic and clinical career.

In loving memory of my mother

Colette Angelov

November 11th 1957 – March 30th 2025

List of Figures and Tables

Chapter 1

Figure 1.1 Structure of Polycomb Repressive Complexes in Humans.

Figure 1.2 The Germinal Centre Reaction and Related B-cell Malignancies.

Figure 1.3 Mutations in Chromatin Regulatory Genes are Frequent in Germinal Centre Lymphoma and Lead to Aberrant Transcriptional Repression.

Figure 1.4 Targeting Chromatin Regulators in Cancer with Small Molecule Inhibitors.

Table 1 Clinical trials of EZH2 targeted therapies actively recruiting patients with haematological malignancies as on 30th January 2026.

Table 2 Clinical trials of EZH2 targeted therapies actively recruiting patients with solid organ malignancies as on 30th January 2026.

Chapter 3

Figure 3.1 Developing a genome-wide CRISPR screen system to identify sensitiser genes to EZH2 inhibition in B-cell lymphoma.

Figure 3.2 Genetic dependency profiles are similar across germinal centre B-cell lymphoma cell lines irrespective of *EZH2* mutation status.

Figure 3.3 *CARM1* is essential in B-cell lymphoma.

Figure 3.4 Pharmacological CARM1 inhibition is effective and specific in germinal centre B-cell lymphoma.

Figure 3.5 Mechanisms of action of EZH2 inhibition in sensitive lymphoma cells are likely divergent between EZH2-mutant and EZH2 wild-type lymphomas.

Figure 3.6 EZH2 inhibitor sensitiser genes are enriched for chromatin regulatory genes, many with already existing targeted therapeutics.

Figure 3.7 Dual targeting of BRD9 and PRC2 can enhance the anti-lymphoma efficacy in EZH2-mutant lymphoma cells.

Figure 3.8 *EP300* and *DOT1L* are essential in germinal centre lymphoma and appear to be PRC2 co-dependencies more broadly in cancer.

Figure 3.9 Dual targeting of PRC2 and the PI3K pathway may enhance efficacy in certain diffuse large B-cell lymphoma subtypes.

Figure 3.10 *EHMT2* loss sensitises lymphoma cells to EZH2 inhibition.

Figure 3.11 *MEN1* is a specific genetic dependency in germinal centre B-cell lymphoma.

Figure 3.12 *MEN1* is an EZH2 co-dependency but menin does not physically associated with PRC2.

Chapter 4

Figure 4.1 Divergent mechanisms of resistance to EZH2 inhibitors in EZH2-mutant versus EZH2 wild-type lymphomas.

Figure 4.2 EZH2 inhibitor ‘resister’ genes include known tumour suppressor genes along with several chromatin regulators.

Figure 4.3 *NSD2* or *NSD1* loss confer a survival advantage to B-cell lymphoma cells exposed to EZH2 inhibitors, in a dose-dependent fashion.

Figure 4.4 Bulk knock-out of *NSD2* using CRISPR, and PROTAC-mediated pharmacological degradation of NSD2 provide orthogonal evidence for mediating resistance to EZH2 inhibitors in EZH2-mutant lymphoma cells.

Figure 4.5 NSD2 does not possess any quantitatively significant protein interactors, and loss of NSD2 blunts the increases in H3K36me2 seen following EZH2 inhibitor treatment.

Figure 4.6 Isogenic *NSD1* and *NSD2* knockout EZH2-mutant lymphoma cell lines exhibit attenuated baseline proliferation rates and resistance to low dose EZH2 inhibition.

Figure 4.7 All three NSD isoforms are expressed in lymphoma cells, while NSD1 and NSD2 are chromatin bound, and their loss has variable effects on histone H3 post-translational modifications.

Figure 4.8 *NSD2* loss blunts gene activation following EZH2 inhibitor treatment of B-cell lymphomas.

Figure 4.9 *NSD2* loss globally redistributes H3K36me2 across the genome.

Figure 4.10 *NSD2* loss increases PRC2-dependent H3K27me3 and H3K27me2 enrichment genome-wide and at Polycomb target genes in EZH2-mutant lymphoma cells

Figure 4.11 Genome-wide overlap of H3K36me2 with H3K27ac identifies transcriptionally vulnerable loci.

Figure 4.12 *NSD2* loss modulates the chromatin response to EZH2 inhibition

Figure 4.13 *NSD2* loss remodels enhancer-associated chromatin states.

Figure 4.14 Developing NSD2 mutant constructs for further mechanistic exploration of NSD2-mediated resistance to EZH2 inhibitors in B-cell lymphoma.

Figure 4.15 The recurrent hypermorphic *NSD2* mutation, found in B-cell acute lymphoblastic leukaemia, may create genetic vulnerabilities to Polycomb and Menin.

Chapter 5

Figure 5.1 *AEBP2* and *PCGF1*/*PCGF5* are genetic dependencies in B-cell lymphoma.

Figure 5.2 *AEBP2* is a specific vulnerability in germinal centre B-cell lymphoma and is an EZH2 co-dependency in EZH2-mutant B-cell lymphoma.

Figure 5.3 AEBP2 is dispensable for global H3K27me3 and gene repression in B-cell lymphoma.

Figure 5.4 *AEBP2* loss, in contrast to *MTF2* loss, increases intergenic H3K27me3.

Figure 5.5 AEBP2 demonstrates a broader binding profile at Polycomb target genes and is bound more at intergenic regions compared with MTF2.

Figure 5.6 AEBP2 confers its essential function in germinal centre B-cell lymphoma in a PRC2 complex lacking JARID2.

Figure 5.7 EZH2-mutant B-cell lymphoma is specifically hypersensitive to loss of the zinc fingers of AEBP2.

Figure 5.8 AEBP2 chromatin binding via zinc fingers is critical for its role in lymphoma.

Figure 5.9 AEBP2 sustains residual H3K27me2 essential for continued proliferation of EZH2-mutant lymphoma.

Figure 5.10 AEBP2 contributes to genome-wide H3K27me2 and loss of AEBP2 leads to increased cPRC1, PRC2.1 and ultimately H3K27me3 at Polycomb target genes in embryonic stem cells.

Figure 5.11 AEBP2 is essential in EZH2 wild-type B-cell lymphoma, with different effects on PRC2 binding compared with EZH2-mutant lymphoma.

Figure 5.12 In addition to sensitising EZH2-mutant lymphoma cells to EZH2 inhibitors, targeting AEBP2 may overcome acquired EZH2 inhibitor resistance.

Abbreviations

ABC-DLBCL	Activated B-cell Diffuse Large B-cell Lymphoma
AC	Adenocarcinoma
AEBP2	AE Binding Protein 2
ALL	Acute Lymphoblastic Leukaemia
AML	Acute Myeloid Leukaemia
ARID1A	AT-rich interaction domain 1A
ATP	Adenosine Triphosphate
BCL	B-cell CLL/Lymphoma (gene)
BET	Bromodomain and extra-terminal
BL	Burkitt Lymphoma
BPLL	B-cell Prolymphocytic Leukaemia
BRD	Bromodomain
CARD	Caspase recruitment domain family member
CARM1	Coactivator-Associated Arginine Methyltransferase-1
Cas	CRISPR-associated (protein)
CBX	Chromobox
CDKN1A	Cyclin dependent kinase inhibitor 1A
CHOP	Cyclophosphamide, doxorubicin, vincristine, prednisone
CLL	Chronic Lymphocytic Leukaemia
CNA	Copy number abnormalities
CpG	Cytosine guanine dinucleotide (5'-C-phosphate-G-3')
CREBBP	cAMP-response element binding protein
CRISPR	Clustered regularly interspaced short palindromic repeats
CRPC	Castration Resistant Prostate Cancer
crRNA	CRISPR RNA
CTG	CellTiter-Glo® (reagent)
CVP	Cyclophosphamide, vincristine, prednisone
DLBCL	Diffuse Large B-cell Lymphoma
DLBCL-ABC	Diffuse Large B-cell Lymphoma – Activated B-Cell subtype
DLBCL-GCB	Diffuse Large B-cell Lymphoma – Germinal Centre B-cell subtype
DLBCL-NOS	Diffuse Large B-cell Lymphoma – Not Otherwise Specified subtype
DMEM	Dulbecco's modified eagle medium
DMG	Diffuse Midline Glioma
DMSO	Dimethylsulfoxide

DNA	Deoxyribonucleic acid
DNMT	DNA methyltransferase
DOT1L	Disruptor of Telomeric Silencing 1-like
DSB	Double strand DNA break
DTT	Dithiothreitol
EED	Embryonic ectoderm development
EHMT	Euchromatic Histone Lysine N-Methyltransferase
EMA	European medicines agency
EP300	E1A binding protein P300
EPOP	Elongin BC and Polycomb Repressive Complex 2 associated Protein
EZH	Enhancer of Zeste Homolog
FA	Formaldehyde
FACS	Fluorescence-activated cell sorting
FBS	Fetal bovin serum
FDA	Food and Drug Administration
FL	Follicular Lymphoma
GCB-DLBCL	Germinal Centre B-cell Diffuse Large B-cell Lymphoma
GFP	Green fluorescent protein
GO	Gene Ontology
HCC	Hepatocellular Carcinoma
HDAC	Histone deacetlyase
HDR	Homology-directed repair
HKMT	Histone lysine methyltransferase
HOX	Homeotic
ICGC	International Cancer Genome Consortium
IGV	Immunoglobulin variable region (gene)
IMDM	Iscove's MDM
IRF	Interferon Regulatory Factor
JARID2	Jumonji and AT-Rich Interaction Domain Containing 2
JMJD3	Jumonji Domain Containing 3, histone lysine demethylase
KDM	Lysine demethylase
KMT2	Lysine methyltransferase 2
LSD1	Lysine specific demethylase 1
MAPK	Mitogen associated protein kinase
MCL	Mantle Cell Lymphoma
MCRPC	Metastatic Castration Resistant Prostate Cancer
Me	Methyl

MEF2B	Myocyte enhancer factor 2B
MEN1	Multiple endocrine neoplasia 1
mESCs	Mouse embryonic stem cells
MM	Multiple Myeloma
MPN	Myeloproliferative Neoplasm
MPNST	Malignant Peripheral Nerve Sheath Tumour
MRT	Malignant Rhabdoid Tumour
MTF2	Metal Response Element Binding Transcription Factor 2
MYC	Myelocytomatosis
MYD	Myeloid differentiation primary response (gene)
NET	Neuroendocrine Tumour
NFkB	Nuclear factor kappa light chain enhancer of activated B cells
NGS	Next Generation Sequencing
NHEJ	Non-homologous End Joining
NHL	Non-Hodgkin Lymphoma
NSCLC	Non-small cell lung cancer
NSD	Nuclear receptor binding SET domain protein
PALI	PRC2 associated LCOR isoform
PBS	Phosphate buffered saline
PcG	Polycomb group
PCGF	Polycomb Group RING Finger
PCL	Polycomb-like
PEL	Primary Effusion Lymphoma
PHC	Polyhomeotic
PHF	PHD Finger Domain
PIK3CD	Phosphatidylinositol-4,5-bisphosphate 3-kinase catalytic subunit delta
PMSF	Phenylmethylsulfonyl fluoride
POU2F2	POU Class 2 Homeobox 2
PRC1	Polycomb Repressive Complex 1
PRC2	Polycomb Repressive Complex 2
PRDM	PR/SET Domain
PR-DUB	Polycomb repressive de-ubiquitinase
PRMT	Protein arginine methyltransferase
PTCL	Peripheral T-cell Lymphoma
PTM	Post Translational Modification
PVDF	Polyvinylidene difluoride
RB	Retinoblastoma

RING	Really Interesting New Gene
RNA	Ribonucleic acid
ROSA26	Reverse Orientation Splice Acceptor 26
RPMI	Roswell Park Memorial Institute
RYBP	RING1 and YY1 Binding Protein
SCC	Squamous cell carcinoma
SCLC	Small cell lung cancer
SCM	Sex combs midleg
SET	Su(var)3-9, Enhancer-of-zeste and Trithorax
sgRNA	Single guide RNA
SMARCA	SWI/SNF related, matrix associated, actin dependent regulator of chromatin subfamily A
SMZL	Splenic Marginal Zone Lymphoma
SUZ12	Suppressor of Zeste 12
SWI/SNF	Switch/Sucrose Non-Fermentable
TAD	Topological Associated Domain
Taz	Tazemetostat
TCGA	The Cancer Genome Atlas
TES	Transcription End Site
TNFRSF14	Tumour necrosis factor receptor superfamily member
TrxG	Trithorax group
TSS	Transcription Start Site
Ub	Ubiquitin
UTX	Ubiquitously Transcribed Tetratricopeptide Repeated Containing, X-linked
UTY	Ubiquitously Transcribed Tetratricopeptide Repeated Containing, Y-linked
VDJ	Variable-Diversity-Junctional (gene)
YAF	YY1 Associated Factor

Table of Contents

Declaration iii
Summary v
Publications & Manuscripts vii
Acknowledgments ix
In Memoriam xi
List of Figures xiii
Abbreviations xvii

CHAPTER 1 Introduction 1
1.1 Higher order structure of DNA and the role of chromatin in cellular identity 3
1.2 Chromatin modifications 4
1.3 Chromatin modifiers and their structures 5
1.4 Polycomb group proteins structure and function 7
1.5 B-cell physiology, the germinal centre and aetiology of germinal centre lymphoma 9
1.6 Mutations in chromatin modifying proteins and histones are common in cancer and germinal centre lymphoma 13
1.7 Epigenetic therapies and PRC2 inhibition for the treatment of GCB lymphoma 17
1.8 Resistance to EZH2 inhibitors has been demonstrated *in vitro* and *in vivo* 23
1.9 Research aims 24

CHAPTER 2 Methods 25
2.1 Cell culture methods 27
2.1.1 Cell culture and lentiviral production 27
2.1.2 Transduction of Cell Lines 28
2.1.3 Cell Proliferation Assays and Drug Treatments 29
2.1.4 Generating Cas9-Expressing Cell Lines 29
2.2 Protein Methods 30
2.2.1 Immunoblotting 30
2.2.2 Cellular Fractionation 31
2.2.3 Endogenous co-immunoprecipitation 31
2.2.4 Mass Spectrometry 32
2.3 Genetic/Genomic Methods 33
2.3.1 Genome-wide CRISPR-Cas9 Screen 33
2.3.2 Negative Selection Assays 34

2.3.3 Generating Isogenic Knockout Cell Lines Using CRISPR-Cas9 35
2.3.4 sgRNA Cloning 35
2.3.5 Generation of AEBP2 wild-type and mutant constructs 36
2.3.6 CUT&RUN-Rx 36
2.3.7 CUT&RUN-Rx Library Preparation 37
2.4 RNA Methods 37
2.4.1 RNA-seq 37
2.5 Computational Methods 38
2.5.1 Genome-wide CRISPR Screen Data Analysis 38
2.5.2 Mass Spectrometry Data Analysis 38
2.5.3 CUT&RUN-Rx Analysis 39
2.5.4 RNA-seq Analysis 40
2.5.5 Analysis of Flow Cytometric Assays 40

CHAPTER 3 Identifying Targetable Genes and Pathways Capable of Sensitising B-Cell Lymphoma Cells to EZH2 Inhibitors 41
3.1 Introduction 43
3.1.1 Functional Genomics Approaches to Precision Oncology 43
3.1.2 Applying CRISPR-Cas9 Systems in Functional Genomics 43
3.1.3 Recent Evidence for Chromatin Regulators as Genetic Dependencies in B-cell Lymphoma 46
3.2 Results 47
3.2.1 Developing a genome-wide CRISPR screen system to identify sensitiser genes to EZH2 inhibition in B-cell lymphoma 47
3.2.2 Genetic dependency profiles are similar across germinal centre B-cell lymphoma cell lines irrespective of *EZH2* mutation status 50
3.2.3 *CARM1* is essential in B-cell lymphoma 51
3.2.4 Pharmacological CARM1 inhibition is effective and specific in germinal centre B-cell lymphoma 56
3.2.5 Mechanisms of action of EZH2 inhibition in sensitive lymphoma cells are likely divergent between EZH2-mutant and EZH2 wild-type lymphomas 59
3.2.6 EZH2 inhibitor sensitiser genes are enriched for chromatin regulatory genes, many with already existing targeted therapeutics 59
3.2.7 Dual targeting of BRD9 and PRC2 can enhance the anti-lymphoma efficacy in EZH2-mutant lymphoma cells 64
3.2.8 *EP300* and *DOT1L* are essential in germinal centre lymphoma and appear to be PRC2 co-dependencies more broadly in cancer 65

3.2.9 Dual targeting of PRC2 and the PI3K pathway may enhance efficacy in certain diffuse large B-cell lymphoma subtypes 70
3.2.10 *EHMT2* loss sensitises lymphoma cells to EZH2 inhibition 71
3.2.11 *MEN1* is a specific genetic dependency in germinal centre B-cell lymphoma 76
3.2.12 *MEN1* is an EZH2 co-dependency but menin does not physically associate with PRC2 76
3.3 Discussion 82

CHAPTER 4 Loss of *NSD1* or *NSD2* Contributes to EZH2 Inhibitor Resistance Through Modulation of the H3K27-H3K36 Methylation Axis 85
4.1 Introduction 87
4.1.1 NSD protein structure and function 88
4.1.2 NSD proteins in cancer 89
4.2 Results 91
4.2.1 Divergent mechanisms of resistance to EZH2 inhibitors in EZH2-mutant versus EZH2 wild-type lymphomas 91
4.2.2 EZH2 inhibitor ‘resister’ genes include known tumour suppressor genes along with several chromatin regulators 91
4.2.3 *NSD2* or *NSD1* loss confers a survival advantage to B-cell lymphoma cells exposed to EZH2 inhibitors, in a dose-dependent fashion 96
4.2.4 Bulk knockout of *NSD2* using CRISPR, and PROTAC-mediated pharmacological degradation of NSD2 provide orthogonal evidence for mediating resistance to EZH2 inhibitors in EZH2-mutant lymphoma cells 97
4.2.5 NSD2 does not possess any quantitatively significant protein interactors, and loss of NSD2 blunts the increases in H3K36me2 seen following EZH2 inhibitor treatment 102
4.2.6 Isogenic *NSD1* and *NSD2* knockout EZH2-mutant lymphoma cell lines exhibit attenuated baseline proliferation rates and resistance to low dose EZH2 inhibition 103
4.2.7 All three NSD isoforms are expressed in lymphoma cells, while NSD1 and NSD2 are chromatin bound, and their loss has variable effects on histone H3 post-translational modifications 103
4.2.8 *NSD2* loss blunts gene activation following EZH2 inhibitor treatment of B-cell lymphomas 108
4.2.9 *NSD2* loss globally redistributes H3K36me2 across the genome 109

4.2.10 *NSD2* loss increases PRC2-dependent H3K27me3 and H3K27me2 enrichment genome-wide and at Polycomb target genes in EZH2-mutant lymphoma cells 114
4.2.11 Genome-wide overlap of H3K36me2 with H3K27ac identifies transcriptionally vulnerable loci 115
4.2.12 *NSD2* loss modulates the chromatin response to EZH2 inhibition 120
4.2.13 *NSD2* loss remodels enhancer-associated chromatin states 121
4.2.14 Developing NSD2 mutant constructs for further mechanistic exploration of NSD2-mediated resistance to EZH2 inhibitors in B-cell lymphoma 126
4.2.15 The recurrent hypermorphic *NSD2* mutation found in B-cell acute lymphoblastic leukaemia may create genetic vulnerabilities to Polycomb and Menin 127
4.3 Discussion 133
4.3.1 Targeting NSD in cancer 136

CHAPTER 5 AEBP2-Directed H3K27me2 Defines a Specific Vulnerability in EZH2-mutant Lymphoma 139
5.1 Introduction 141
5.2 Results 141
5.2.1 *AEBP2* and *PCGF1*/*PCGF5* are genetic dependencies in B-Cell lymphoma 141
5.2.2 *AEBP2* is a specific vulnerability in germinal centre B-cell lymphoma and is an *EZH2* co-dependency in EZH2-mutant B-cell lymphoma 143
5.2.3 AEBP2 is dispensable for global H3K27me3 and gene repression in B-cell Lymphoma 147
5.2.4 *AEBP2* loss, in contrast to *MTF2* loss, increases intergenic H3K27me3 150
5.2.5 AEBP2 demonstrates a broader binding profile at Polycomb target genes and is bound more at intergenic regions compared with MTF2 151
5.2.6 AEBP2 confers its essential function in germinal centre B-cell lymphoma in a PRC2 complex lacking JARID2 155
5.2.7 EZH2-mutant B-cell lymphoma is specifically hypersensitive to loss of the zinc fingers of AEBP2 160
5.2.8 AEBP2 chromatin binding via zinc fingers is critical for its role in lymphoma 161
5.2.9 AEBP2 sustains residual H3K27me2 essential for continued proliferation of EZH2-mutant lymphoma 166
5.2.10 AEBP2 contributes to genome-wide H3K27me2 and loss of AEBP2 leads to increased cPRC1, PRC2.1 and ultimately H3K27me3 at Polycomb target genes in embryonic stem cells 170

5.2.11 AEBP2 is essential in EZH2 wild-type B-cell lymphoma, with different effects on PRC2 binding compared with EZH2-mutant lymphoma 171
5.2.12 In addition to sensitising EZH2-mutant lymphoma cells to EZH2 inhibitors, targeting AEBP2 may overcome acquired EZH2 inhibitor resistance 176
5.3 Discussion 177

CHAPTER 6 General Discussion 181
6.1 General Summary 183
6.2 *AEBP2*^{L} joins *MEN1* and *DOT1L* as genes whose loss confer sensitivity to PRC2 Inhibitors, albeit via a distinct mechanism 183
6.3 AEBP2^{L} is in a JARID2-free form of PRC2.2 that mediates intergenic H3K27me2 deposition 184
6.4 The potential function of H3K27me2 in B-cell lymphoma 185
6.5 Altered H3K27me2 in cancers as an underappreciated modulator of resistance or sensitivity to EZH2 inhibitors 186
6.6 AEBP2^{L} as a potential therapeutic target 187
6.7 Conclusions 189

References 191

Appendices 242

CHAPTER 1

Introduction

1.1 Higher order structure of DNA and the role of chromatin in cellular identity

The total compliment of diploid DNA within a human cell, if stretched from one end to the other, would measure over 2 metres (Nurk et al., 2022; Piovesan et al., 2019). DNA is required to be condensed to the micrometre range in cells and to achieve this it is packaged into chromatin, the basic repeating unit of which is termed the nucleosome. The nucleosome consists of 147-bp of DNA wound around an octamer of four basically charged histone proteins (H2A, H2B, H3, H4) and one linker H1 protein in a repeating fashion (Bates, 2020; Kornberg, 1974; Kornberg & Lorch, 1999, 2020; Luger et al., 1997). In addition to the role of the nucleosome in DNA packaging, DNA wrapped around a nucleosome structure cannot interact with RNA polymerase II or transcription factors and thus nucleosomes have been suggested to directly regulate gene transcription (Kornberg & Lorch, 2020).

All cells in the human body originate from a single cell and possess the same DNA sequence inherited from two parents. In order for a single cell to divide and differentiate into the vast array of specialised cells within the human body genes must be strictly regulated in a context-dependent manner. Specific gene expression programs define cellular identity, and a number of regulatory mechanisms exist to coordinate such a complex process (Eisen et al., 1998; Liberzon et al., 2015; Wagner et al., 2016). The diverse array of chromatin modifications contribute to this regulatory process and are carried out by chromatin regulatory proteins, a biological process originally termed ‘epigenetics’ by Waddington in 1942 (Waddington, 1942a, 1942b). Alterations in chromatin structures such as DNA methylation at CpG islands, non-coding RNAs, and histone tail modifications can all regulate gene expression without changing the underlying DNA sequence (Allis & Jenuwein, 2016). In addition to transcriptional regulation, chromatin is also involved in many other cellular processes including replication, DNA repair and recombination, cell cycle control and X chromosome inactivation (Millan-Zambrano et al., 2022; Schuettengruber et al., 2017; Zentner & Henikoff, 2013).

1.2 Chromatin modifications

In order to regulate the required gene expression programs for specific cell types, chromatin must be highly dynamic to facilitate transcription factors and other regulatory elements binding to DNA, a process which is tightly regulated by histone post translational modifications (PTMs) and chromatin remodelling enzymes. Chromatin remodellers, such as members of the Switch/Sucrose non-fermentable (SWI/SNF) complex, are ATP-dependent enzymes that can disrupt the position of nucleosomes, uncovering specific DNA sequences to facilitate gene transcription (Bracken et al., 2019; Clapier et al., 2017; Mittal & Roberts, 2020; Roberts & Orkin, 2004). Histone PTMs are numerous and located primarily, but not exclusively, on the unstructured N-terminal histone protein tails (Bracken et al., 2019; Millan-Zambrano et al., 2022). The most well studied histone PTMs are the various modifications of lysine (K) residues in histone tails, which are discussed in more depth in Section 1.3, however modifications of other amino acids such as arginine, glutamine, serine and threonine, within histone proteins are also possible (Millan-Zambrano et al., 2022).

The addition of certain chemical modifications to histones can have diverse consequences on transcriptional regulation. For example, given the characteristic acidity of acetyl groups, their addition to positively charged lysine residues was originally shown to neutralise their charge, loosening the interaction of the histone protein with negatively charged DNA and facilitating transcription (Cosgrove et al., 2004; Shogren-Knaak et al., 2006). The addition of methyl groups however, can effect transcription in a dichotomous manner, depending on the specific site on the histone tail and the number of methyl groups added e.g. trimethylated lysine at position 27 of histone H3 (H3K27me3) is associated with transcriptional repression, whereas H3K36me2 is associated with transcriptional activation (Conway et al., 2015; Streubel et al., 2018). The plethora of covalent histone modifications that have been discovered have led to the ‘histone code hypothesis’, whereby the presence or absence of specific combinations of histone PTMs coordinate the transcriptional machinery to direct

cellular processes (Strahl & Allis, 2000; Turner, 1993). Consistent with this concept, recent work demonstrated that the transcriptional effects of individual histone PTMs depend strongly on their chromatin context, with alternative histone PTMs unable to fully substitute for canonical repressive marks such as H3K27me3 (Hedehus et al., 2025).

Finally, it has been shown to be overly reductive to consider chromatin modifications as simply ‘on’ and ‘off’ switches for transcriptional control. Bivalent chromatin is defined as nucleosomes possessing both transcriptionally active and repressive marks, H3K4me3 and H3K27me3 respectively (Bernstein et al., 2006). These bivalent domains can place a gene in a ‘poised’ state, whereby the temporary transcriptional silencing can be rapidly reversed to activate and facilitate dynamic changes in the transcriptional state required for certain cellular processes (Voigt et al., 2012). An example of the role of bivalent chromatin is presented in Section 1.5 on the germinal centre reaction in B-cells.

1.3 Chromatin modifiers and their structures

Enzymes that catalyse the addition of either methyl, ubiquitin, acetyl, sumo, or phosphoryl groups can be thought of as histone ‘writers’, while the enzymes catalysing the removal of these groups can be termed ‘erasers’, the function of which were original described as ‘on’ and ‘off’ switches relating to transcriptional regulation but which are now known to be much more complex (Allfrey et al., 1964). An additional category of ‘reader’ proteins function to recognise the specific histone PTMs and direct other proteins to interact with these domains such as bromodomain (BRD) and chromodomain containing proteins e.g. chromobox (CBX) proteins, BRD protein family (Fujisawa & Filippakopoulos, 2017; Hou et al., 2023).

Numerous histone lysine methyltransferases (HKMTs) exist, with the most well studied histone lysine methylation sites occurring at H3K27, H3K36, H3K9, H3K79, H3K4 and H4K20 (Husmann & Gozani, 2019). Many genes that encode HKMTs exist as paralogs, and can ‘write’ the same lysine mark on a specific histone e.g. NSD1, NSD2, NSD3 all write

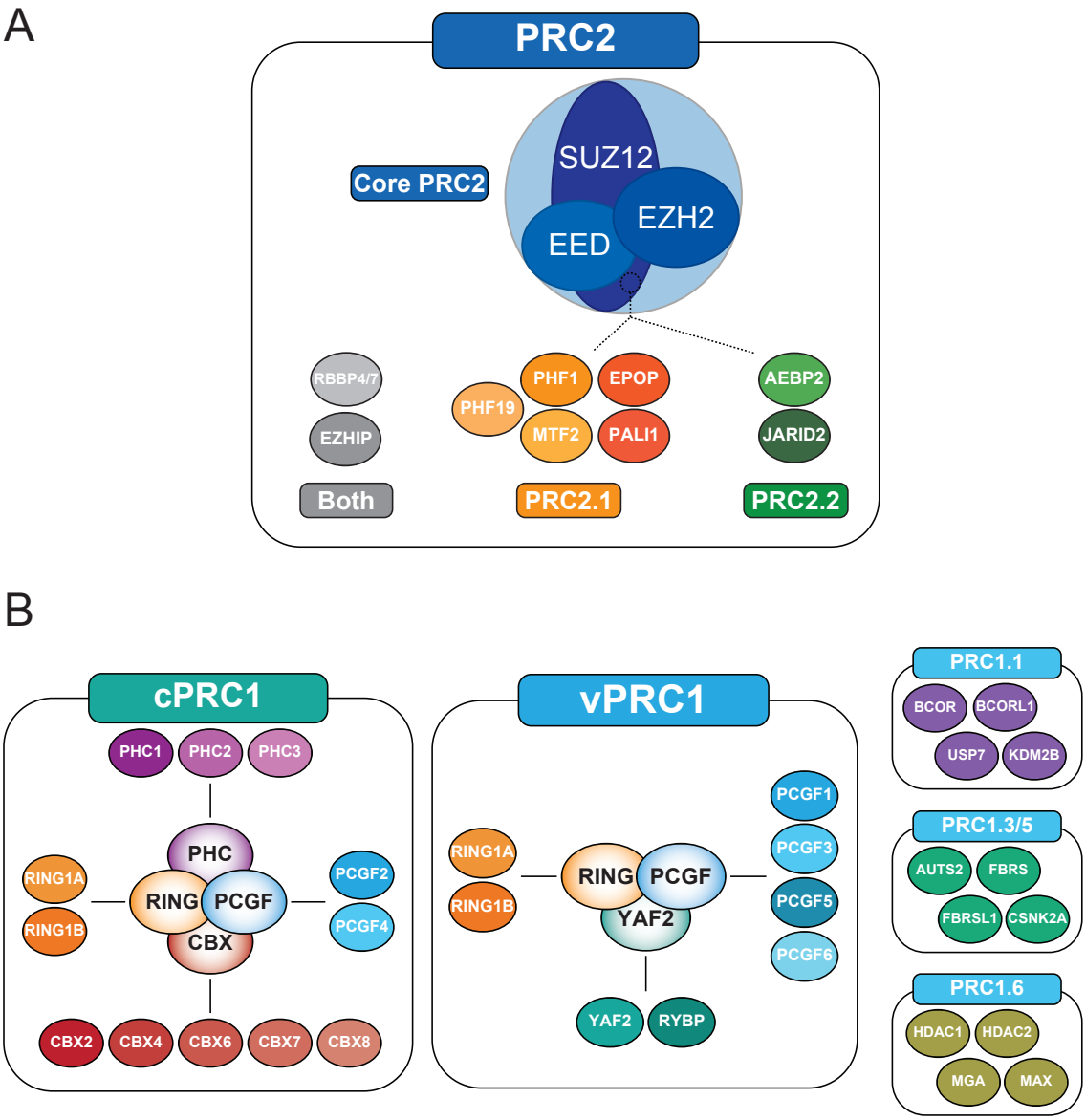

Figure 1.1: Structure of Polycomb repressive complexes in humans
A. Schematic representation of polycomb repressive complex 2 (PRC2) in humans. PRC2.1 shown (left) and PRC2.2 shown (right). Paralogs are indicated in dashed boxes. Alternative members indicated with dashed arrows. Adapted from (Deevy & Bracken, 2019).
B. Schematic representation of the two subtypes of Polycomb Repressive Complex 1 (PRC1) in humans.Canonical PRC1 shown (left) and variant PRC1 complex shown (right). Paralogs are indicated in dashed boxes. Adapted from (Bracken et al., 2019; Schuettengruber et al., 2017)

H3K36me1 and H3K36me2 (Y. Li et al., 2009; Rayasam et al., 2003; Shipman et al., 2024). Furthermore, while some HKMTs can only catalyse mono- or di-methylation, but not tri-methylation, such as the NSD proteins, other HKMTs like EZH2 is responsible for all-methylation of H3K27 (Cao et al., 2002; Kuzmichev et al., 2002).

1.4 Polycomb group proteins structure and function

Polycomb group (PcG) proteins were originally described in the Drosophila melanogaster model organism, after it was shown that mutations in the genes coding for PcG proteins affected the phenotypic distribution of the male sex comb organ (Lewis, 1978). It was subsequently observed that the antagonistic relationship between PcG and the Trithorax group (TrxG) proteins are critical in coordinating homeotic (Hox) gene expression patterns and maintaining proper spatial programming in Drosophila and higher organisms (Kennison & Tamkun, 1988; Schuettengruber et al., 2017). Polycomb group proteins are responsible for maintaining thousands of key developmental genes in a repressed state, preventing aberrant activation of these genes following cycles of cell division, and ensuring the maintenance of cellular identity throughout development (Bracken et al., 2006; Kim & Kingston, 2022; Margueron & Reinberg, 2011).

The Polycomb repressive complexes 1 and 2 (PRC1 and PRC2) are multi-protein complexes associated with states of transcriptional repression and are critical in maintaining gene repression (**Fig 1.1**). PRC2 is made up of the core component proteins embryonic ectoderm development (EED), suppressor of Zeste (SUZ12) and the SET domain containing enzymatic subunit enhancer of Zeste (EZH1 or EZH2)(Cao et al., 2002; Czermin et al., 2002; Deevy & Bracken, 2019; Kuzmichev et al., 2002; Muller et al., 2002). EED and SUZ12 stabilise the PRC2 complex and promote EZH2 catalytic activity, with EED binding H3K27me3 to allosterically stimulate PRC2 and facilitate the spreading of repressive chromatin domains (Cao & Zhang, 2004; Ciferri et al., 2012; Jiao & Liu, 2015; Pasini et al., 2004). EZH2 has been shown to generate the majority of global cellular H3K27me2/3 levels,

with EZH1 performing this function less prominently and found in less proliferative cellular contexts (Margueron et al., 2008; McCole et al., 2025). Notably, RBBP4, RBBP7 and EZHIP (a.k.a. CATACOMB) have all been shown to associate with core PRC2, with only EZHIP having an effect on PRC2 catalysis; inhibiting its activity (Cao et al., 2002; Hubner et al., 2019; Jain et al., 2020; Kuzmichev et al., 2002; Piunti et al., 2019).

PRC2 can be further subclassified depending on its accessory proteins; with PRC2.1 containing one of three Polycomb-like (PCL) proteins either MTF2, PHF1, or PHF19 along with EPOP or PALI1/2 while PRC2.2 contains AEBP2 and JARID2 (Conway et al., 2018; Hauri et al., 2016; Margueron & Reinberg, 2011; Smits et al., 2013). Depending on the subcomplex involved, PRC2 is recruited to unmethylated CpG islands in the promoters of Polycomb target genes through either its PCL protein interacting directly with DNA or through JARID2 binding to PRC1-mediated H2AK119Ub at these sites, although these are not the sole recruitment mechanisms (Bracken et al., 2019; Deevy & Bracken, 2019; Healy et al., 2019; Schuettengruber et al., 2017). The enzymatic component of PRC2, EZH1 or EZH2, is the sole histone methyltransferase responsible for mono-, di- and tri-methylating H3K27 (Cao et al., 2002; Czermin et al., 2002; Kuzmichev et al., 2002; Muller et al., 2002). The H3K27me3 mark is associated with the maintenance of transcriptional repression at the promoters of Polycomb target genes and recruits canonical PRC1 leading to chromatin compaction (Bracken et al., 2019; Højfeldt et al., 2019). In contrast, H3K27me1 is associated with gene bodies of actively transcribed regions, while H3K27me2 is less well characterised but is found distributed more non-specifically throughout the genome and may function to protect H3K27 from acetylation during DNA replication (Conway et al., 2015; Ferrari et al., 2014).

PRC1 complexes can be divided into ‘canonical’ (cPRC1) and ‘variant’ (vPRC1) depending on the presence of the specific Polycomb group RING finger (PCGF) paralog; with PCGF2 or PCGF4 defining cPRC1, and PCGF1/3/5/6 defining vPRC1 (Blackledge & Klose, 2021; Fursova et al., 2019b; Gao et al., 2012). While both cPRC1 and vPRC1 possess the

enzymatic RING1A or RING1B paralogs which mediate mono-ubiquitination of lysine residue 119 on histone H2A (H2AK119Ub), the majority of H2AK119Ub in the human body is proposed to be produced by the more catalytically active vPRC1, with cPRC1 functioning predominantly to compact chromatin and contribute to chromatin looping (Blackledge et al., 2014; Eagen et al., 2017; Eskeland et al., 2010; Fursova et al., 2019b; Grau et al., 2011; Ogiyama et al., 2018; Wang et al., 2004). The H2AK119Ub produced by vPRC1 is critical for maintaining repression of Polycomb target genes and recruiting PRC2 to chromatin (Blackledge et al., 2020; Tamburri et al., 2020). Canonical PRC1 incorporates one of the CBX paralogs, one of three Polyhomeotic (PHC) components, and one Sex Combs Midleg (SCM) subunit. These cPRC1 subunits contribute to recognising and binding H3K27me3, and compacting chromatin (Fischle et al., 2003; Frey et al., 2016; Isono et al., 2013; Min et al., 2003). In contrast, vPRC1 do not possess CBX or PHC proteins and rather contain one of RYBP or YAF2 paralogs, components which have been proposed to stimulate catalytic activity (Bracken et al., 2019; Ciapponi et al., 2024; Rose et al., 2016; Zhao et al., 2020).

Finally, antagonistic ‘eraser’ enzymes exist that can reverse the chromatin marks produced by both PRC1 and PRC2 chromatin ‘writer’ complexes. In the case of PRC1, this is the Polycomb repressive deubiquitinase (PR-DUB) complex, and in terms of PRC2 all three lysine demethylases 6A, 6B and 6C (KDM6A a.k.a. UTX, KDM6B a.k.a. JMJD3, KDM6C a.k.a. UTY) have H3K27me2/3 demethylase activity (Agger et al., 2007; Bonnet et al., 2022; Conway et al., 2021; Kooistra & Helin, 2012; Lan et al., 2007; Scheuermann et al., 2010; Swigut & Wysocka, 2007; Walport et al., 2014).

1.5 B-cell physiology, the germinal centre and aetiology of germinal centre lymphoma

The ‘germinal centre reaction’ is a critical physiological process by which memory B-cells and antibody-secreting plasma cells are produced in order for humans to achieve humoral immunity to external pathogens (De Silva & Klein, 2015; Klein & Dalla-Favera, 2008; Mesin

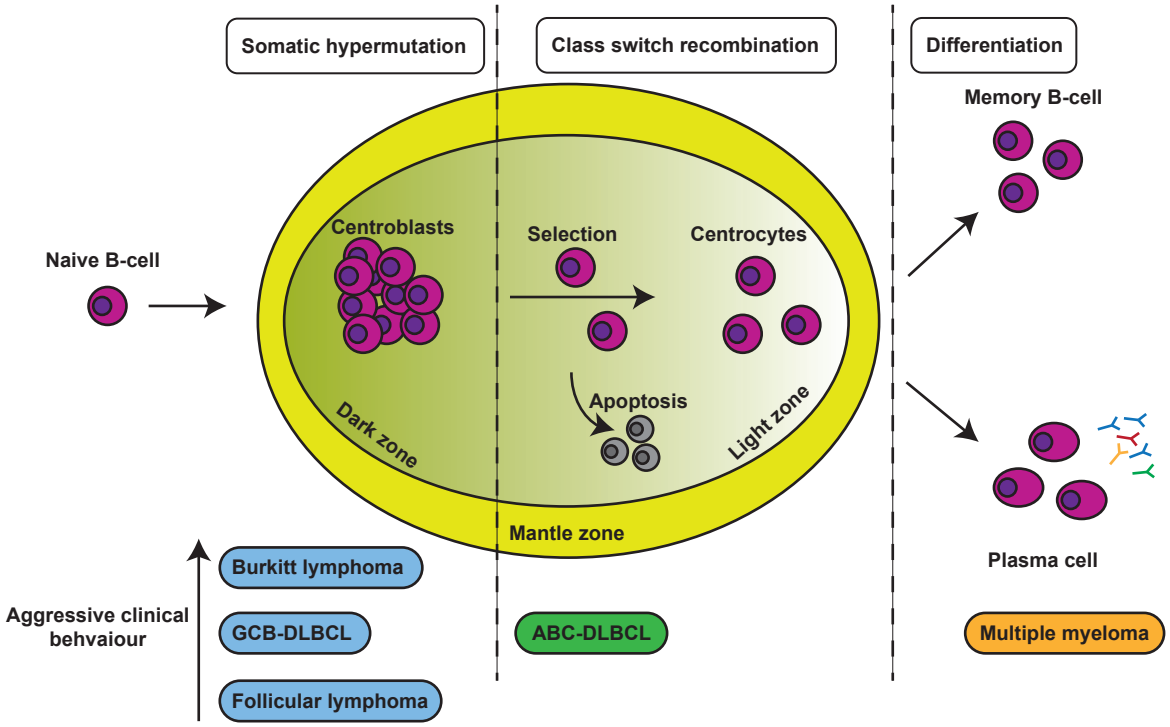

Figure 1.2: The Germinal Centre Reaction and Related B-cell malignancies.
Naïve B-cells enter the germinal centre within lymphoid organs, undergoing several molecular processes to permit immunoglobulin affinity maturation and differentiation to memory B-cells or plasma cells. Germinal centre lymphomas typically arise from centroblasts and centrocytes of the dark zone, compared to activated B-cell lymphomas arising from the light zone and beyond. Adapted from (Mlynarczyk et al., 2019)

et al., 2016). This physiological reaction is depicted in **Fig 1.2** and is described as follows. Naïve B-cells originate in the bone marrow from pre-B progenitor cells and are released into the blood stream through bone marrow capillaries. After a naïve B-cell encounters antigen, it will pass through a transient anatomical location within a lymphoid organ, such as a lymph node or the spleen, known as the germinal centre. Within the 'dark zone' of the germinal centre B-cells undergo massive hyperproliferation and somatic hypermutation of the their immunoglobulin variable region (*IGV*) genes and are termed centroblasts. Following immunoglobulin gene rearrangement, centroblasts are selected for based on the affinity of their B-cell receptors for the specific antigen encountered. Self-reactive B-cells and those with low affinity antibodies undergo apoptosis, whilst B-cells with high affinity antibodies undergo transit to the light zone of the germinal centre where they are termed centrocytes and undergo class switch recombination of their immunoglobulin genes to produce the various antibody isotypes. At this point, upon specific molecular signalling, B-cells can exit the germinal centre and terminally differentiate into either memory B-cells or antibody-secreting plasma cells. The germinal centre reaction is extensively reviewed in (Basso & Dalla-Favera, 2015; Mlynarczyk et al., 2019; Young & Brink, 2021).

The *BCL6* gene is known as the master regulator of the germinal centre reaction, and upregulation of BCL-6 protein is one of the prime initiators of this process, without which the germinal centre cannot form (Basso & Dalla-Favera, 2012; Kitano et al., 2011). The *MYC* gene is also a critical regulator of the germinal centre reaction where it is expressed in the initial expansion of naïve B-cells and involved in the recirculation of B-cells from the light zone to the dark zone of the germinal centre, with its absence leading to collapse of germinal centres *in vivo* (Calado et al., 2012; Dominguez-Sola et al., 2012). The enzymatic component of PRC2, EZH2, has been shown to be highly expressed in germinal centre B-cells and facilitates transcriptional repression of negative cell cycle regulatory genes, as well as genes involved in terminal differentiation of B-cells and exit from the germinal centre (Beguelin et al., 2013; Beguelin et al., 2017; Raaphorst et al., 2000; Velichutina et al., 2010). Somewhat uniquely for non-pluripotent stem cells, germinal centre B-cells possess bivalent

chromatin domains at specific loci i.e. genes marked with both the repressive H3K27me3 mark and the H3K4me3 mark associated with transcriptional activation. These bivalent domains are 'poised' to allow rapid transcriptional activation of the gene programs required to terminate the germinal centre reaction such *IRF4* and *PRDM1*, to facilitate terminal differentiation into plasma cells or memory B-cells (Beguelin et al., 2013; Caganova et al., 2013).

The term germinal-centre lymphoma can refer to any lymphoma arising from the germinal centre e.g. Burkitt lymphoma (BL), follicular lymphoma (FL) and germinal-centre diffuse large B-cell lymphoma (GCB-DLBCL) (Mlynarczyk et al., 2019). Although BL technically arises in the germinal centre, following an abnormal translocation in proliferating B-cells of the *MYC* proto-oncogene to the class switch region of the transcriptionally active B-cell immunoglobulin gene [t(8;14), t(2;8), t(8;22)], this lymphoma subtype is genetically distinct from FL and GCB-DLBCL given that the *MYC* translocation itself is sufficient to induce an extremely high grade neoplastic phenotype (Swerdlow et al., 2017). Therefore, for the rest of this PhD transfer report, the term 'germinal centre lymphoma' will refer to FL and GCB-DLBCL, both of which possess very similar mutational signatures and are arbitrarily distinguished histologically by the quantity of centrocytes and centroblasts as determined by morphological assessment.

FL is the most common form of low-grade NHL with roughly 195 cases per year in Ireland (NCRI, 2021). This form of NHL is characterised by the presence of the translocation between *BCL2* proto-oncogene and *IGH* enhancer region [t(14;18)] in ~90% of cases (Horsman et al., 1995; Rowley, 1988). This translocation occurs during VDJ recombination of immunoglobulin genes in the bone marrow, and in isolation, is insufficient for neoplastic transformation of B-cells (Kuppers et al., 1999; Roulland et al., 2014; Roulland et al., 2006). Additional mutations that occur in the mutation-prone germinal centre reaction contribute to malignant transformation of B-cells harbouring the t(14;18) translocation. These recurrent gene mutations are similar to those occurring in GCB-DLBCL and most frequently involve

chromatin regulators (discussed in Section 1.6). DLBCL is the most common form of high-grade NHL with ~420 cases per year in Ireland (NCRI, 2021). DLBCL is generally subdivided based on immunohistochemical patterns correlated with specific gene expression profile signatures into either GCB- or ABC-DLBCL, with GCB-DLBCL having a similar genetic profile to FL (Alizadeh et al., 2000; Mlynarczyk et al., 2019; Swerdlow et al., 2017). Importantly ABC-DLBCL, accounting for ~40% of DLBCL cases, arises from B-cells which are exiting or have exited the germinal centre (Scott et al., 2015). These lymphomas have a distinct gene expression profile with more frequent translocations of *BCL6*, mutations involving *MYD88*, *CD79B*, *CARD11* and aberrant NFkB signalling (Iqbal et al., 2007; Lenz et al., 2008; Morin et al., 2011; Ngo et al., 2011).

1.6 Mutations in chromatin modifying proteins and histones are common in cancer and GCB-lymphoma

Large scale collaborative research projects, such as The Cancer Genome Atlas (TCGA) and the International Cancer Genome Consortium (ICGC) have carried out sequencing studies that have uncovered genetic aberrations in almost all chromatin regulatory genes across a vast array of cancers, with subsequent mechanistic exploration of the mutations in chromatin regulators demonstrating their oncogenic nature (Cenik & Shilatifard, 2021; Cerami et al., 2012; Chang et al., 2016; Gao et al., 2013; Kadoch & Crabtree, 2015; Plass et al., 2013; Wilson & Roberts, 2011).

The most common recurrent genetic abnormalities in FL are copy number abnormalities (CNAs) and mutations in *TNFRSF14* (40-50%), along with mutations in the chromatin regulators *EZH2* (~12-20%), *KMT2D* (~76-90%) and *CREBBP* (~60-68%), *MEF2B* (~18%), *ARID1A* (~9%) and *SMARCA4* (5%) (Green et al., 2015; Launay et al., 2012; Okosun et al., 2014; Pasqualucci et al., 2011; Swerdlow et al., 2017). The various histone H1 proteins are also recurrently mutated in FL the most common being *HIST1H1E* (12%) and *HIST1H1C* (4%) (Green et al., 2015; Okosun et al., 2014). Similarly to FL, GCB-DLBCL is associated

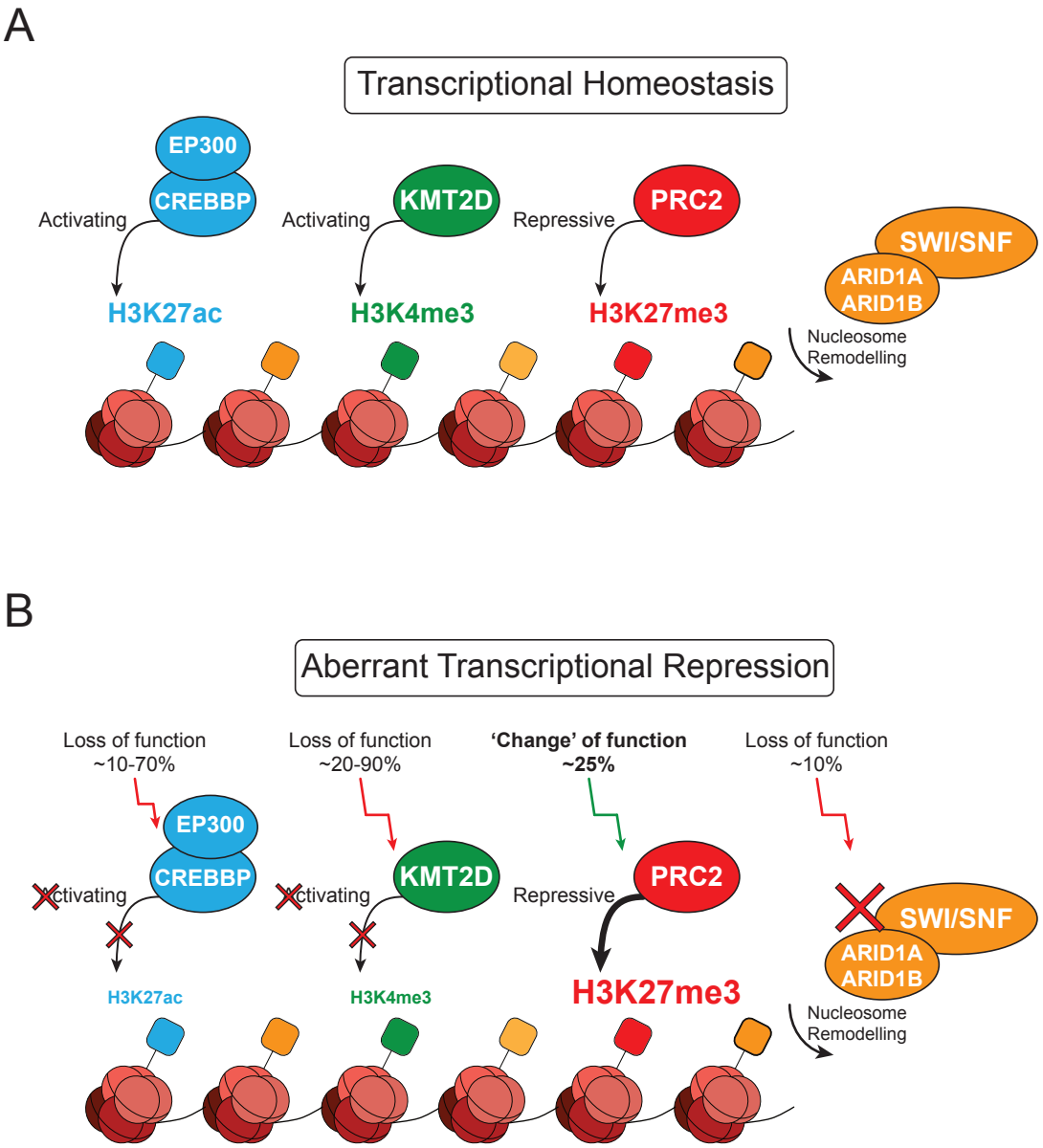

Figure 1.3: Mutations in chromatin regulatory genes are frequent in germinal centre lymphoma and lead to aberrant transcriptional repression.
A. In normal germinal centre B-cells there is transcriptional homeostais based on a balance of activating and repressive histone post-translational modifications, deposited by a variety of chromatin regulatory proteins. This process is tightly regulated such that B-cells undergoing maturation are agile enough to recirculate and proliferate in germinal centres following antigen exposure and differentiate and quiesce once the stimulus has abated.
B. The most frequent mutations found in germinal centre lymphoma include loss of function mutations in CREBBP/EP300, KMT2D and SWI/SNF members, and gain of function EZH2 mutations which all lead to aberrant repression of genes required for termination of the hyperproliferative germinal centre reaction. Adapted from (Kumar et al., 2021).

with recurrent genetic aberrations in the chromatin regulatory genes *EZH2* (20-25%), *KMT2D* (20-40%), *MEF2B* (15-20%), *CREBBP* (10-30%), as well as frequent *BCL2* translocations (~40%) and recurrent mutations in *TNFRS14* (30%) (Chapuy et al., 2018; Reddy et al., 2017; Schmitz et al., 2018; Swerdlow et al., 2017). Interestingly, recent studies have begun to shed light on the mechanisms of SWI/SNF mutations in germinal centre lymphoma, through modulation of chromatin accessibility and access to transcription factors that promote lymphomagenesis (Barisic et al., 2024; Deng et al., 2024).

Patients with germinal centre lymphomas usually have mutations in more than one chromatin regulatory gene (**Fig 1.3**), with one study demonstrating mutations of ≥1 chromatin modifying genes in 96% of FL samples, and mutations in ≥2 chromatin modifying genes in 76% of FL samples (Green et al., 2015; Lunning & Green, 2015; Morin et al., 2011). Another study examining sequencing and gene expression microarrays from CD20-sorted B-cells in FL patients, comparing diagnostic and relapse samples, demonstrated significant intratumoral heterogeneity. They proposed that some mutations which are more prevalent early in the disease (e.g. *CREBBP*) represent driver mutations, whilst mutations in *KMT2D* and *TNFRSF14* likely represent 'accelerator' mutations and result in disease progression (Green et al., 2013). The frequent monoallelic loss-of-function mutations in the histone acetyltransferases *CREBBP* and, less commonly *EP300*, in germinal centre lymphoma result in inadequate acetylation-mediated inactivation of BCL6 and acetylation-mediated activation of p53 promoting an oncogenic phenotype (Pasqualucci et al., 2011). Loss of *CREBBP* in murine models leads to germinal centre derived lymphoma and reduction in H3K27ac at enhancers resulting in aberrant transcriptionally repressed state (Jiang et al., 2017). Loss-of-function mutations in *KMT2D* result in reductions in H3K4me1/me2 at enhancers which have been shown to affect transcriptional programs to drive lymphomagenesis (Ortega-Molina et al., 2015; Zhang et al., 2015). However, germline mutations in *KMT2D* are insufficient to cause germinal centre lymphoma, highlighting the need for this mutation to cooperate with other genetic abnormalities in germinal centre lymphomas (Lindsley et al., 2016; Ng et al., 2010).

The recurrent *EZH2* mutation observed in germinal centre lymphomas was first described in 2010 by sequencing of germinal centre lymphoma patient samples (Bodor et al., 2011; Morin et al., 2010; Ryan et al., 2011). The hotspot mutation is usually clonal and almost always monoallelic, and results in a single amino acid change at tyrosine 646 in the SET domain responsible for coding the EZH2 protein's histone methyltransferase activity, with a number of less frequent mutations occurring at alternative codons in the SET domain including alanine 682 and alanine 692 (Bodor et al., 2013). This amino acid change results in augmented histone methyltransferase activity of EZH2 with a preference for di-methylated rather than monomethylated or unmethylated H3K27 substrate (Yap et al., 2011). The result of this *EZH2* 'change-of-function' mutation is globally increased H3K27me3 levels, an observation which is dependent on wild type EZH2 protein on the other allele mono- and di-methylating H3K27 (Conway et al., 2015). The *EZH2* mutation has been shown to give rise to germinal centre hyperplasia, enhances repression of negative regulators of the cell cycle such as CDKN1A, and traps B-cells in the germinal centre by preventing terminal differentiation, effects which in part are mediated by hyper-trimethylation of H3K27 at gene promoters resulting in aberrant gene repression (Beguelin et al., 2013). Mutant EZH2 cooperates with BCL6 to mediate hyper-repression of B-cell terminal differentiation genes, a process facilitated by CBX8 and non-canonical PRC1 (Béguelin et al., 2016). More recently, mutant EZH2 has been shown to initiate FL by disrupting the reliance of germinal centre B-cells on T follicular helper cells and instead facilitating an immunological dependency on follicular dendritic cells and an altered immune microenvironment (Beguelin et al., 2020). Finally, the *EZH2* mutation has also been recently shown to affect 3D chromatin architecture leading to transcriptional repression of entire topological associated domains (TADs) containing important tumour suppressor genes and genes involved in exit from the germinal centre (Donaldson-Collier et al., 2019).

Of interest in the field of chromatin biology and cancer is the fact that PRC2 can have diverse and seemingly dichotomous roles in the development of malignant phenotypes.

While the change-of-function *EZH2* mutations discussed in the previous paragraph are characteristic of germinal centre B-cell lymphoma and EZH2 overexpression has been demonstrated in a number of other cancers, paradoxically loss-of-function mutations in various PRC2 components have also been shown to be involved in a diverse array of malignancies including leukaemia, paediatric diffuse midline gliomas, and peripheral nerve sheath tumours (Bracken et al., 2003; Ernst et al., 2010; Kleer et al., 2003; Schwartzentruber et al., 2012; Varambally et al., 2002; Zhang et al., 2012). The context-dependent dichotomous tumour suppressor and oncogene roles that PRC2 can play have been proposed to relate to the role of PRC2 in maintaining repression of the specific oncogenic gene expression programs observed in the cancer type in question as well as the specific cell-of-origin (Comet et al., 2016). These diverse functional roles of PRC2 offer a rich background in which to study genetic modulators of response to PRC2 inhibition in lymphoma.

1.7 Epigenetic therapies and PRC2 inhibition for the treatment of GCB lymphoma

Given the altered epigenome associated with various malignant states, chromatin modifying enzymes are an attractive target in precision oncology (Helin & Dhanak, 2013). The first drug licensed by the FDA for the treatment of cancer that targeted a component of the epigenetic machinery was the DNA methyltransferase (DNMT) inhibitor azacitidine for acute myeloid leukaemia and myelodysplastic syndrome in 2004 (Feinberg & Tycko, 2004; Kaminskas et al., 2005; Sermer et al., 2019). Since then a number of additional therapies targeting various components of chromatin and DNA modification have been licensed by the FDA and EMA including histone deacetylase (HDAC) inhibitors, isocitrate dehydrogenase (IDH) inhibitors, and additional DNMT inhibitors, with these drugs predominantly indicated for the treatment of acute myeloid leukaemia, T-cell lymphoma, and multiple myeloma (Bates, 2020). Additional epigenetic therapies in clinical development include bromodomain and extra-terminal (BET) inhibitors, DOT1L histone

methyltransferase inhibitors, lysine-specific demethylase 1 (LSD1) inhibitors and specific HDAC6 inhibitors (Amengual et al., 2015; Dawson et al., 2011; Mertz et al., 2011; Nicosia et al., 2022; Schenk et al., 2012; Stein et al., 2018; Vogl et al., 2017).

The frontline therapy for DLBCL and FL has remained fairly similar for the last 20 years and consists of combined chemo-immunotherapy (Sehn & Salles, 2021). In DLBCL, the standard of care consists of six 3-week cycles of R-CHOP chemotherapy (Rituximab, Cyclophosphamide, Doxorubicin, Vincristine and Prednisolone). Due to clinical equipoise, the frontline treatment of symptomatic FL, in the absence of suspicion of high grade disease, is usually a physician's choice depending on a number of patient and disease factors including risk stratification, patient co-morbidities and preference, and therapeutic goals. The recommendations include either six 3-week cycles of rituximab or obinutuzumab combined with chemotherapy consisting of either CHOP, CVP, or bendamustine (Dreyling et al., 2021; McNamara et al., 2020).

To date, the only FDA and EMA licensed epigenetic therapy for B-cell lymphoma is the EZH2 inhibitor Tazemetostat, which was licensed initially by the FDA in June 2020 for relapsed/refractory follicular lymphoma with *EZH2* mutations (U.S. Food and Drug Administration, 2020). The phase II trial demonstrated an objective response rates of 69%, and somewhat surprisingly, given the widespread role of PRC2 in transcriptional regulation, EZH2 inhibition was associated with relatively minimal toxicity in patients (Morschhauser et al., 2022). Although EZH2 inhibition is active mouse models of DLBCL, it has less activity in humans in this context (Italiano et al., 2018; McCabe, Ott, et al., 2012). EZH2 inhibitor resistance is also an ongoing issue in a variety of cancer contexts (Drosos et al., 2022; Kazansky et al., 2024; Kim & Roberts, 2016; Yamagishi et al., 2024). Given the lack of substantial toxicity, and the requirement of most haematological malignancies to require therapeutic combinations, future development of EZH2 inhibitors in B-cell lymphoma appears to be combination therapy driven (NCT04224493, NCT02889523)(Morschhauser et al., 2022; Scholze et al., 2020). There are both past and current clinical trials investigating

the role of HDAC inhibitors, DNMT inhibitors, other EZH2 inhibitors, BET inhibitors and PRMT inhibitors in B-cell lymphoma, all of which are early phase I/II trials with mixed results (El-Khoueiry et al., 2023; Harb, 2018; Kirschbaum et al., 2011; Moreno et al., 2023; Ogura et al., 2014; Puvvada et al., 2016; Rosenthal et al., 2023; Schweizer, 2022; Younes et al., 2016).

Clinical trials of EZH2 inhibitors which are actively recruiting as of 30.01.2026 on https://clinicaltrials.gov are listed in **Table 1** (haematological malignancies) and **Table 2** (solid tumours). Interestingly, and somewhat paradoxically, EZH2 inhibitors have also shown promise in myeloid leukaemias with inactivating *EZH2* mutations (Alqazzaz et al., 2024), however previous work in SWI/SNF-mutant cancers has demonstrated non-catalytic roles of EZH2, which may explain the efficacy of EZH2 inhibitors in EZH2 loss-of-function tumours (K. H. Kim et al., 2015). Finally, EZH2 inhibitors are now being investigated to enhance chimeric antigen receptor (CAR) T-cell efficacy by reshaping the epigenetic state of the engineered T-cells, shifting the therapeutic focus away from the tumour and toward intrinsic modulation of CAR T-cell function in the treatment of B-cell lymphomas (Isshiki et al., 2025; Porazzi et al., 2025)(NCT05934838).

Novel therapeutic approaches targeting chromatin dysregulation in germinal centre lymphoma are being rationally devised based on pre-clinical studies exploring the mechanisms of lymphomagenesis in this context. For example, loss of H3K27 acetylation at enhancer loci of specific genes seen in CREBBP-mutant lymphoma cell lines correlate with the same loci that are repressed by the histone deacetylase HDAC3, and thus targeted inhibition of HDAC3 with a HDAC inhibitor could mitigate the CREBBP loss-of-function (Hatzi et al., 2013; Jiang et al., 2017). Similarly, the frequent *KMT2D* mutations that result in hypomethylation of H3K4 at enhancers, which is phenocopied by the physiological role of histone lysine demethylase KDM5, could be targeted using KDM5 inhibitors, to restore levels of H3K4 methylation (Heward et al., 2021). Equally, given the frequency of *ARID1A* mutations in germinal centre lymphoma, targeting ARID1B may be another effective

EZH2 Inhibitor	Inhibitor Class	Tumour Type	NCT Number	Disease / Indication	Phase
AXT-1003	EZH2 degrader	Haematological	NCT06484985	Non-Hodgkin Lymphoma	Phase I
HH285	EZH1/2 dual	Haematological	NCT06909877	Relapsed/Refractory PTCL	Phase Ib/II
SHR-2554	EZH2 selective	Haematological	NCT06519526	Relapsed/Refractory PTCL	Phase I/II
SHR-2554	EZH2 selective	Haematological	NCT05896046	Relapsed/Refractory Hodgkin Lymphoma	Phase I/II
SHR-2554	EZH2 selective	Haematological	NCT06173999	Peripheral T-cell Lymphoma	Phase Ib/II
SHR-2554	EZH2 selective	Haematological	NCT06122389	Relapsed/Refractory PTCL	Phase III
Tazemetostat	EZH2 selective	Haematological	NCT05983965	T-cell Lymphoma	Phase I
Tazemetostat	EZH2 selective	Haematological	NCT05627245	GC-derived B-cell lymphoma | T-cell lymphoma	Phase I
Tazemetostat	EZH2 selective	Haematological	NCT05934838	FL | MCL | DLBCL	Phase I
Tazemetostat	EZH2 selective	Haematological	NCT05618366	DLBCL | Follicular Lymphoma	Phase I
Tazemetostat	EZH2 selective	Haematological	NCT05627232	Relapsed/Refractory AML	Phase Ib
Tazemetostat	EZH2 selective	Haematological	NCT06824701	Indolent B-cell NHL	Phase Ib
Tazemetostat	EZH2 selective	Haematological	NCT05994235	Follicular Lymphoma	Phase II
Tazemetostat	EZH2 selective	Haematological	NCT05890352	Relapsed/Refractory Large B-cell Lymphoma	Phase II
Tazemetostat	EZH2 selective	Haematological	NCT06242834	High Grade B-cell NHL	Phase II
Tazemetostat	EZH2 selective	Haematological	NCT04224493	Relapsed/Refractory Follicular Lymphoma	Phase III
Tazemetostat	EZH2 selective	Haematological	NCT05372354	Relapsed/Refractory Multiple Myeloma	Phase Ib/II
Zeprumetostat	EZH2 selective	Haematological	NCT07372352	Peripheral T Cell Lymphoma	Phase II
Valmetostat	EZH1/2 dual	Haematological	NCT05683171	Relapsed/Refractory Follicular Lymphoma	Phase I/II

Table 1: Clinical trials of EZH2 targeted therapies actively recruiting patients with haematological malignancies as on 30th January 2026.

EZH2 Inhibitor	Inhibitor Class	Tumour Type	NCT Number	Disease / Indication	Phase
Mevrometostat	EZH2 selective	Solid	NCT03460977	mCRPC | SCLC	Phase I
Mevrometostat	EZH2 selective	Solid	NCT06551324	Metastatic Castrate Resistant Prostate Cancer	Phase III
Mevrometostat	EZH2 selective	Solid	NCT07028853	Metastatic Castration Sensitive Prostate Cancer	Phase III
Mevrometostat	EZH2 selective	Solid	NCT06629779	Metastatic Castration-Resistant Prostate Cancer	Phase III
SHR-2554	EZH2 selective	Solid	NCT07175220	Locally Advanced or Metastatic NSCLC	Phase II
SHR-2554	EZH2 selective	Solid	NCT07311408	Gastric Cancer	Phase II
SHR-2554	EZH2 selective	Solid	NCT07102901	Advanced/Metastatic Gastric Cancer	Phase II
Tulmimetostat	EZH1/2 dual	Solid	NCT05942300	Recurrent Ovarian Cancer	Phase I
Tulmimetostat	EZH1/2 dual	Solid	NCT05467748	Non-Small Cell Lung Cancer	Phase Ib/II
Tulmimetostat	EZH1/2 dual	Solid	NCT07190300	Metastatic Hormone-Sensitive Prostate Cancer	Phase I/II
Valemetostat	EZH1/2 dual	Solid	NCT06244485	Advanced Solid Tumour	Phase I
Valemetostat	EZH1/2 dual	Solid	NCT07244341	Metastatic CRPC	Phase I
Valemetostat	EZH1/2 dual	Solid	NCT06294548	Hepatocellular Carcinoma	Phase Ib/II
Valemetostat	EZH1/2 dual	Solid	NCT06644768	Metastatic/Advanced NSCLC	Phase Ib/II
Valemetostat	EZH1/2 dual	Solid	NCT06632977	Castrate Resistant Prostate Cancer	Phase II
XNW5004	EZH2 selective	Solid	NCT06022757	Advanced Solid Tumours	Phase Ib/II

Table 2: Clinical trials of EZH2 targeted therapies actively recruiting patients with solid organ malignancies as on 30th January 2026.

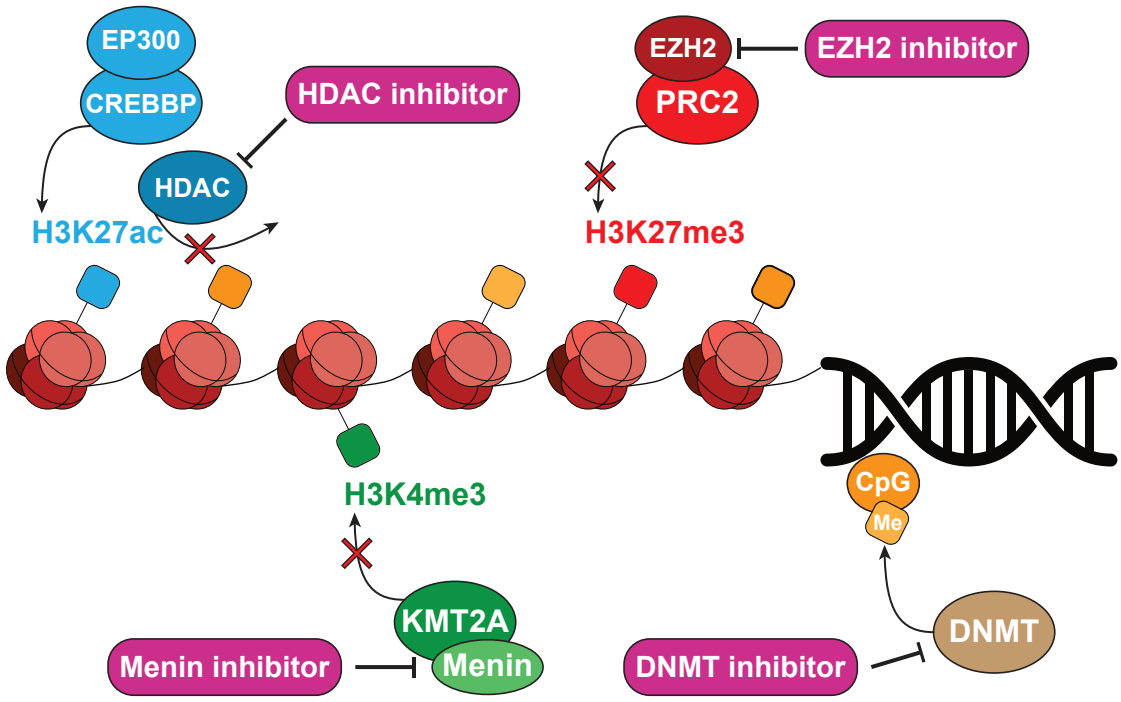

Figure 1.4: Targeting chromatin regulators in cancer with small molecule inhibitors
Illustration of the most advanced-stage epigenetic therapies currently in clinical use in precision haemato-oncology and their targets.

strategy (Helming et al., 2014; Lin et al., 2025). A schematic of the most impactful epigenetic therapies is provided in **Figure 1.4**.

1.8 Resistance to EZH2 inhibitors has been demonstrated *in vitro* and *in vivo*

Despite impressive objective response rates in the phase II trial of Tazemetostat in relapsed/refractory follicular lymphoma, patients derived median duration of responses of less than one year (Morschhauser et al., 2020). This highlights the challenge of acquired resistance to targeted therapies in cancer, which can relate to a multitude of adaptive mechanisms in the malignant cell population (Holohan et al., 2013; Milojkovic & Apperley, 2009). While specific resistance mechanisms to EZH2 inhibitors have not yet been described in B-cell lymphoma *in vivo*, a number of pre-clinical studies have shown various putative mechanisms of resistance including mutations in mutant EZH2 that alter drug binding, mutations in wild type EZH2 that facilitate the ongoing production of the H3K27me2 substrate necessary for lymphomagenesis, and upregulation of specific cell signalling pathways such as MAPK and PI3K pathways (Baker et al., 2015; Bisserier & Wajapeyee, 2018; Gibaja et al., 2016).

Studies investigating EZH2 inhibitors in other malignancies have shed further light on potential resistance mechanisms. Surprisingly, a translational study in T-cell lymphoma revealed that only 50% of resistance cases were attributed to PRC2 mutations that affected the binding of an EZH1/2 dual inhibitor (Yamagishi et al., 2024). Interestingly, changes in the epigenome including altered DNA methylation and mutations in chromatin regulators were implicated in other resistant cases in this study. Furthermore, other recent studies in paediatric malignant rhabdoid tumours and epithelioid sarcomas treated with EZH2 inhibitors have shown that resistance-associated somatic mutations may converge on dysregulation of the RB1/E2F axis or on regulators of H3K36 methylation (Drosos et al., 2022; Kazansky et al., 2023). Targeting other members of the PRC2 complex such as EED

may be effective in a subset of cases, however a greater understanding of the mechanisms underpinning resistance is required to advance therapeutic strategies in patients (He et al., 2017; Kim & Roberts, 2016; Qi et al., 2017; Tomassi et al., 2021).

1.9 Research Aims

Patients with germinal centre B-cell lymphomas treated with EZH2 inhibitors either do not respond, or develop resistance over time which may in part, be related to acquisition of mutations in chromatin regulatory genes. The hypothesis of this PhD research project is that this resistance to EZH2 inhibition may be overcome or prevented by elucidating and targeting these resistance pathways genetically or pharmacologically or by identifying sensitising genes to EZH2 inhibitor therapy with existing targeted therapies.

Aim 1:

Identify and validate genetic dependencies and EZH2 inhibitor sensitisers in B-cell lymphoma cells, focussing on pathways with existing pharmacological targets.

Aim 2:

Identify and validate genetic mediators of resistance to PRC2 inhibition in B-cell lymphoma cells and systematically evaluate the mechanisms of resistance.

Aim 3:

Develop a better understanding of the role of PRC2 in the development of B-cell lymphomas and uncover novel ways to target this complex.

CHAPTER 2

Methods

2.1 Cell culture methods

2.1.1 Cell Culture and Lentiviral Production

All cell lines were grown in a humidified incubator at 37°C, 5% CO2. Human B-cell lymphoma cell lines HT, OCI-LY18, Pfeiffer, WSU-DLCL2, DOHH2, Toledo, Raji, Daudi, RI-1 and U-2932 were all cultured in suspension in Roswell Park Memorial Institute medium - RPMI 1640 GlutaMAX (Gibco) supplemented with 10% (v/v) heat-inactivated fetal bovine serum (FBS) (Gibco) and 100U/ml penicillin/streptomycin (Gibco). Karpas-422 and SUDHL6 were cultured as above with 20% (v/v) heat-inactivated FBS. Human lymphoma cell lines OCI-LY1 and OCI-LY7 were cultured in suspension in Isocove Modified Dulbecco Media - IMDM (Gibco) supplemented with 20% (v/v) heat-inactivated FBS and 100U/ml penicillin/streptomycin. Human Burkitt Lymphoma cell lines Raji and Daudi and ABC-lymphoma cell lines RI-1 and U-2932 were a gift from Dr. Diego Pasini at the European Institute of Oncology, Milan. All other lymphoma cells were a gift from Professor Jude Fitzgibbon at St. Bart's Cancer Institute, London, UK.

The human malignant rhabdoid tumour cell line G401, Ewing sarcoma cell line A673, melanoma cell line IGR1, human embryonal carcinoma cell line NTERA-2, and HEK293T cells were cultured as adherent monolayers in Dulbecco's Modified Eagle Medium high glucose (DMEM) (Sigma) supplemented with 10% (v/v) heat-inactivated FBS (Gibco), and 100U/ml penicillin/streptomycin (Gibco).

Mouse embryonic stem cells (mESCs) were maintained on 0.1% gelatin-coated culture dishes and split every 2 days using 0.25% Trypsin-EDTA (Gibco). mESCs were cultured under 2i/LIF conditions in Glasgow Minimum Essential Medium (GMEM) (Sigma) supplemented with 20% heat-inactivated FBS, 100u/ml penicillin/streptomycin, 50μM β-mercaptoethanol (Sigma), 1:100 GlutaMAX (Gibco), 1:100 non-essential amino acids (Gibco), 1mM sodium pyruvate (Gibco), 1:500 homemade Leukaemia Inhibitory Factor (LIF), 3μM GSK inhibitor CHIRON9902 (Millipore) and 1μM MEK inhibitor PD0325901

(Millipore). On days that mESCs were being used as spike-in normalisation for CUT&RUN, cells were dissociated using 1-2ml of Accutase (Stem Cell Technologies) per 10cm tissue culture dish, to avoid interference with the assay's performance.

All cells except for mESCs were propagated by splitting 8:1 – 12:1 every 2-3 days. Adherent cells were dissociated with 0.25% Trypsin-EDTA (Gibco), prior to neutralisation with fresh media and re-seeding.

Lentiviral particles were produced using a second-generation lentiviral system in HEK293T cells. HEK293T cells were transfected with a lentiviral expression vector (sgRNA/shRNA/cDNA) or a pooled sgRNA library together with a viral envelope (VSVG) and packaging vector (PAX8) using polyethylenimine (PEI) (Polysciences) following a standard transfection protocol. For example, for one T75 flask, the recipe would consist of 4µg of individual sgRNA plasmids, 2µg of the viral packaging PAX8 plasmid and 3µg of the viral envelope VSV-G plasmid, combined with 27µl polyethylenimine in 500µl Opti-MEM (Gibco). These quantities were adjusted proportionally based on the surface area of the culture vessel. Viral supernatant was harvested 72hr post-transfection, sterile filtered through a 0.45µm polyethersulfone (PES) filter and stored at -80°C.

2.1.2 Transduction of Cell Lines

Cell lines were seeded at a density of 3.75 x10^5 cells/ml in a 96-well plate or 1 x10^6 cells/ml in a 6-well plate in complete medium containing polybrene (10µg/ml – homemade). Lentiviral supernatant supplemented with polybrene was added to appropriate wells, the plate was sealed with parafilm and centrifuged at 1700RPM at room temperature for 2 hours. Viral supernatant was then removed and fresh complete medium was added to the cells. Antibiotic selection or cell sorting was performed ≥24 hours post-transduction.

2.1.3 Cell Proliferation Assays and Drug Treatments

Suspension cells were seeded at a density of 4 x10^5 cells/ml in a 24-well plate. All drug treatment experiments used 0.01% DMSO (vehicle) as a negative control. For all compounds tested, a 1000x concentration was generated for each dilution such that an identical volume of drug could be added to each well no matter the concentration of drug, thereby limiting any potential effect from varying volumes of DMSO. Cells were split and reseeded every 3 days with fresh media and drug at a splitting ratio of 1:5. Viability was assessed at each 3-day timepoint, by taking a 50µl aliquot of cells from each well and plating into a 96-well white opaque plate followed by the addition of 50µl of CellTiter-Glo Luminescent Cell Viability Assay (Promega). The 96-well plate was agitated for 2 minutes to allow cell lysis. The plate was then protected from light for 10 minutes to allow luminescence signal stabilisation. Luminescence was then read on a microplate reader (Biotek Synergy 2) and each sample's viability was normalised to the percentage viability in the DMSO control. In some cell proliferation assays, cells were also counted at each 3-day timepoint using a haemocytometer as an orthogonal approach to validating cell viability.

2.1.4 Generating Cas9-Expressing Cell Lines

Doctors James Nolan, Eric Conway, and Marlena Mucha had previously generated stable Cas9 expression in all cell lines used in this research project except for Raji, Daudi, RI-1 and U2932. The following procedure was applied to those latter four cell lines, and furthermore to uninfected WSU-DLCL2 and HT to generate fresh Cas9 expression in order to account for any potential loss of Cas9 efficiency over time. Cell lines were seeded at a density 1 x106 cells/ml in a 6-well plate in complete medium containing polybrene (10µg/ml – homemade). Lentivirus supernatant containing lentiCas9-Blast (Sanjana et al., 2014), supplemented with polybrene, was added to appropriate wells. A negative control well was included that received complete medium instead of the lentivirus supernatant. The plate was sealed with parafilm and centrifuged at 1700RPM at room temperature for 2 hours. The lentiviral supernatant was discarded and cells were resuspended and re-plated into a new

6-well plate. This process was repeated twice to achieve a ‘triple infection’ of the parental cell line in order to increase the chances of generating highly efficient and stable Cas9 expression. Blasticidin 10µg/ml (Invitrogen) was added 72 hours after the first lentiviral transduction and cells were cultured in antibiotic for 10-14 days until the negative control cells had fully perished and the experimental cells were growing well. Cas9 expression was confirmed by immunoblot and Cas9 activity determined using the pXPR plasmid (Doench et al., 2014).

2.2 Protein Methods

2.2.1 Immunoblotting

Whole cell pellets were washed with ice cold PBS and lysed in either high salt buffer (50mM Tris-HCl pH 7.2, 1mM EDTA pH 7.4, 300mM NaCl) or RIPA buffer (25 mM Tris-HCl. pH 7.6, 150mM NaCl, 1% NP-40, 1% Sodium Deoxycholate, 0.1% SDS) supplemented with 1x protease inhibitor cocktail (ThermoFisher Scientific). Protein lysates were sonicated using a Sonifier SFX150 (Branson) or Bioruptor Pico (Diagenode), followed by rotation for 20 minute rotation at 4°C and clarification by centrifugation at 14000rpm for 20 minutes. Protein quantification was performed using the Bradford assay by comparing standard protein quantifications with samples read spectrophotometrically by a microplate reader at 595nm wavelength. Denatured protein lysates were separated using 4-12% gradient Bolt Bis-Tris Plus (Invitrogen) gel or 4-12% gradient NuPAGE Bis-Tris (Invitrogen) gel and transferred to nitrocellulose (0.2µm, Amersham) or PVDF (0.45µm, Immobilon-FL) membranes respectively. Membranes were blocked against non-specific binding in 5% fat milk for 30-60 minutes, then probed with primary and secondary antibodies. The PageRulerTM Plus pre-stained protein ladder (Thermo Scientific) was used to determine protein sizes on the membrane. Images were viewed using the Odyssey Fc Imager (LI-COR) and protein levels quantified using Image Studio software (LI-COR).

2.2.2 Cellular Fractionation

Whole cell pellets were washed with ice cold PBS and lysed on ice for 30 minutes in pre-extraction buffer (20mM HEPES pH 7.6, 50mM NaCl, 0.5% Triton X-100, 3mM MgCl2, 300mM Sucrose) supplemented with 1x protease inhibitor cocktail (ThermoFisher Scientific). Half of the protein lysate was take for the “Total” fraction. The remaining lysate was then centrifuged at 14000rpm for 10min at 4°C. The supernatant was collected for the “Soluble” fraction. The remaining protein pellet was washed and disturbed in pre-extraction buffer and centrifuged again at 14000rpm for 10min at 4°C and resuspended in pre-extraction buffer as the “Insoluble” or “Chromatin-Bound” fraction. An equal volume of 2x sample buffer (2x Bolt™ LDS Sample Buffer [ThermoFisher Scientific], 5% β-mercaptoethanol, 10mM dithiothreitol) was added to each fraction, samples were boiled at 99°C for 5 minutes and sonicated at 60% amplitude for a total of 30 seconds. Resulting lysates were then immunoblotted as described above.

2.2.3 Endogenous Co-Immunoprecipitation

Human lymphoma cells were harvested by centrifugation, washed twice with ice cold PBS, and resuspended in Buffer A (25mM HEPES pH 7.6, 5mM MgCl2, 25mM KCl, 0.05mM EDTA, 10% (v/v) glycerol, 0.1% NP-40, 1mM DTT, combined with protease inhibitors) and incubated with rotation at 4°C for 10 minutes. Cell nuclei were pelleted by centrifugation at 500rcf at 4°C for 10 minutes. Nuclei were lysed in Buffer C (10mM HEPES pH 7.6, 3mM $MgCl_2$, 100mM KCl, 0.5mM EDTA, 10% (v/v) glycerol, 1mM DTT, combined with protease inhibitors). Then, 300mM $(NH_4)_2SO_4$ dissolved in Buffer C was added to the samples which were rotated at 4°C for 10 minutes. Samples were ultracentrifuged at 350,000rcf for 15 minutes at 4°C using an SW 55 Ti swinging-bucket rotor in a Beckman Coulter Optima L-100XP. The supernatant was collected and nuclear extracts were precipitated by adding 300mg $(NH_4)_2SO_4$ for each 1ml of sample. The samples were incubated on ice for 20 minutes before repeating ultracentrifugation using the same parameters as above. Nuclear pellets were resuspended in IP buffer (300mM NaCl, 50mM Tris-HCl pH 7.5, 1mM EDTA,

1% (v/v) Triton-X100, 1mM DTT, combined with protease inhibitors) and protein quantification and sample normalisation was carried out using the Bradford assay. An input sample was retained at this time. For each co-IP, 1µl Benzonase Nuclease (Sigma-Aldrich) and 1µg of the respective antibody was added to 1mg of nuclear protein. Samples were rotated at 4°C overnight. The next day washed Protein G Dynabeads (Invitrogen) were added to each sample followed by rotation at 4°C for 2 hours. For immunoblotting, beads were washed five times with IP buffer with a 5 minute incubation step with samples rotating at 4°C between each wash. Samples were eluted from the beads by adding 50µl 1x Bolt LDS Sample Buffer (ThermoFisher Scientific) and heated to 95°C for 10 minutes. For mass spectrometry, beads were washed four times with IP buffer followed by two cold PBS washes with a 5 minute incubation step with samples rotating at 4°C between each wash. Dried beads were then stored at -80°C until further processing.

2.2.4 Mass Spectrometry

Molly Davies and Dr. Eugene Dillon, both of the Conway Institute in University College Dublin carried out this portion of the IP-MS experiment. Beads from the co-immunoprecipitation were washed with phosphate buffered saline and 8M urea was added to a volume of 200µl. Following this, 5mM DTT was added to the beads and incubated at 60°C for 30 minutes. Then, 9mM iodoacetemide solution was added to the beads and incubated in the dark at room temperature for 30 minutes. 2.2mM $CaCl_2$ was added to the beads followed by addition of 12.8mM ammonium bicarbonate pH 8. Following this, 1µg of sequencing grade trypsin (Sigma-Aldrich) was added to each reaction and incubated at 37°C overnight on a thermomixer at 350rpm. The next morning, 1% trifluoroacetic acid was added to stop the reaction. The tryptic digests were then desalted using ZipTips (Millipore) according to the manufacturer's protocol. Peptides (500-1000ng) were loaded onto Evotips as per manufacturer's instructions (EvoSep). Briefly, Evotips were activated by soaking them in isopropanol, primed with 20µL buffer B (Acetonitrile, 0.1% FA) by centrifugation for 1 min at 700rcf. Tips were soaked in isopropanol and equilibrated with 20µL buffer A (MS grade water, 0.1% FA) by centrifugation. Another 20µL buffer A was loaded onto the tips

and the samples were added on top of that. Tips were centrifuged and washed with 20µl buffer A followed by overlaying the C18 material in the tips with 100µL buffer A and a short 20 second spin.

The samples were analysed by the Mass Spectrometry Resource (MSR) in University College Dublin on a Bruker TimsTOF Pro mass spectrometer connected to a Evosep One chromatography system. Peptides were separated on an 8 cm analytical C18 column (Evosep, 3µm beads, 100µm ID) using the pre-set 30 samples per day gradient on the Evosep one. The Bruker TimsTOF Pro mass spectrometer was operated in positive ion polarity with TIMS (Trapped Ion Mobility Spectrometry) and PASEF (Parallel Accumulation Serial Fragmentation) modes enabled. The accumulation and ramp times for the TIMS were both set to 100ms., with an ion mobility (1/k0) range from 0.62 to 1.46 Vs/cm. Spectra were recorded in the mass range from 100 to 1,700 m/z. The precursor (MS) Intensity Threshold was set to 2,500 and the precursor Target Intensity set to 20,000. Each PASEF cycle consisted of one MS ramp for precursor detection followed by 10 PASEF MS/MS ramps, with a total cycle time of 1.16 seconds.

2.3 Genetic/Genomic Methods

2.3.1 Genome-Wide CRISPR-Cas9 Screen

Human lymphoma cell lines (WSU-DLCL2 and HT) with stable Cas9 expression were transduced with lentivirus containing the Brunello genome-wide library of sgRNAs with a coverage of 500x (500 cells per sgRNA) and a low multiplicity of infection (MOI) of 0.15 as previously described (Doench, 2018; Doench et al., 2016). During transduction, media was supplemented with 10µg/ml polybrene to improve transduction efficiency. Two control wells were included, one with no lentivirus to which no puromycin was added, and one with no lentivirus to which puromycin was added. Approximately 24 hours after transduction, cells were selected in 2µg/ml puromycin for 48 hours. At this timepoint (T0), for each cell line, two aliquots of cells were collected to take forward for serial passaging. To one aliquot, the

EZH2 inhibitor Tazemetostat IC20 was added at a concentration of ~IC20 dose (25nM) and to the other aliquot 0.01% (v/v) DMSO was added. Cells were counted and propagated forward maintaining a 500x coverage of each sgRNA every 3 days. The genome-wide CRISPR screen was carried out in both cell lines in two biological replicates. Cells were cultured in Tazemetostat or DMSO for 24 days in total, at which point (T24) cells in both conditions were harvested and genomic DNA extracted with the NucleoSpin Blood L (Macherey-Nagel) kit following the manufacturer's instructions. PCR inhibitors were removed with the OneStep PCR Inhibitor Removal (Zymo Research) kit prior to PCR amplification following the manufacturer's instructions. The barcoded sgRNA sequences were PCR amplified using the following recipe and PCR steps: DreamTaq Hot Start Green (50µl), P5 index primer 100µM (0.5µl), P7 index primer 100µM (0.5µl) at 95°C for 60 seconds, 28 cycles of 95°C for 30s, 53°C for 30s, 72°C for 30s; then 72°C for 10min. After PCR amplification, DNA fragments were purified using the GeneJET PCR Purification Kit (Thermo Scientific) as per the manufacturer's instructions. PCR products were then separated by a 2% agarose gel electrophoresis, gel purified using the QIAquick Gel Extraction Kit (Qiagen) and isopropanol precipitated. Size distributions of the PCR products were determined using the D1000 ScreenTape (Agilent) on the 4200 TapeStation System (Agilent). Pooled libraries were diluted and processed for 75-bp single-end sequencing using an Illumina NextSeq500.

2.3.2 Negative Selection Assays

sgRNAs targeting regions of proteins of interest highlighted by the two CRISPR screens were cloned into plasmids containing either a GFP (LRG2.1) (Tarumoto et al., 2018) or RFP (ipUSEPR) (Yang et al., 2021) reporter. Lentivirus was produced for these sgRNAs and transduced in Cas9-expressing human cell lines at a target MOI of 0.3-0.5. This resulted in a heterogenous population, where ~50% of cells possessed a GFP-tagged sgRNA targeting a validation gene and ~50% were untagged with no sgRNA. Following GFP positivity over time, it could be determined whether the particular sgRNA resulted in positive, negative, or neutral selection of the transduced cells i.e. specific sgRNAs could invoke a cell competition

advantage or disadvantage compared to uninfected cells. Following transduction of cells, the lentiviral-containing media was removed, fresh media applied and the cells were cultured for a period of 21-45 days (approx. 12 cell population doublings). The cells were split every 3 days at an appropriate ratio with GFP abundance quantified every 3 days using the Guava easyCyte HT system 12 (Luminex). Sequences of these sgRNAs can be found in Appendix II.

2.3.3 Generating Isogenic Knockout Cell Lines Using CRISPR-Cas9

NSD1 and NSD2 single knockout cells were generated in two EZH2-mutant lymphoma cell lines (WSU-DLCL2 and Karpas-422). Cells were transduced (as described in Section 2.1.2) with a single sgRNA from the Brunello library targeting NSD1 or NSD2 in a 6-well plate. Two different sgRNAs targeting each gene in separate wells were utilised to increase the chances of generating a successful knockout. One additional well for each cell line was transduced with an sgRNA targeting ROSA26 in order to generate isogenic negative control cell lines to account for any phenotypic changes that may have arisen during the cell sorting procedure. Following transduction, cells were grown in T25 cell culture flasks and at 48 hours the GFP^{high} population of cells was collected by FACS using the BD FACSAria Fusion High Performance Cell Sorter by Doctors Barry Moran and Orlaith Walsh in the Trinity Biomedical Sciences Institute Core Flow Facility. Individual GFP^{high} cells were seeded in each well of a 96-well plate and individual clones were expanded and knockout confirmed by immunoblot.

2.3.4 sgRNA Cloning

For green fluorescent protein (GFP) tagged sgRNA cloning LRG2.1 (Tarumoto et al., 2018) was used. For red fluorescent protein (RFP) tagged sgRNA with a puromycin resistance gene cloning iPUSEPR (Yang et al., 2021) was used. For sgRNA cloning. LRG2.1 and iPUSEPR plasmids were linearised with BsmBI (NEB) followed by incubation for 1 hour with calf intestinal phosphatase and purification of the digested plasmid by DNA gel

electrophoresis (0.7% agarose). For each validation gene, the sequences of the two most significant Brunello library sgRNAs from the genome-wide CRISPR-Cas9 screen were chosen for sgRNA cloning. Purified digested vector was ligated to annealed and phosphorylated oligonucleotides and transformed using competent DH5α E. coli cells. Sanger sequencing confirmed that cloned sgRNA sequences were correct. David Reck, PhD student in the Bracken Lab performed some of the sgRNA cloning.

2.3.5 Generation of AEBP2 wild-type and mutant constructs

The ectopic expression of the wild-type and mutant hAEBP2 constructs was performed using in-house lentiviral expression vectors derived from PLENTI EF1A FLAG/HA (Conway et al., 2018). Human AEBP2-L (NM_001114176.1) ORF was available in the gateway cloning-compatible entry vector PCR8 (pCR8/GW/TOPO cloning – Invitrogen). Zinc-finger mutant hAEBP2 ORFs were generated by Q5 Site-Directed Mutagenesis (NEB) as per the manufacturer's protocol and sequences were confirmed using Sanger sequencing. Expression clones were then generated using Gateway LR Clonase II (ThermoFisher). The AEBP2 ZF mutant constructs were generated by Gráinne Holland.

2.3.6 CUT&RUN-Rx

For each CUT&RUN-Rx, human lymphoma cells were combined with mESC (1:10 cell ratio), which served as a 10% exogenous genome "spike-in" for normalisation during downstream bioinformatic analysis. Cells were fixed with 0.1% formaldehyde for 1 minute, then quenched with 125mM glycine for 5 minutes and washed with PBS at room temperature. Nuclei were extracted by incubating samples in ice cold nuclear extraction buffer (20mM HEPES pH 7.5, 10mM KCl, 0.1% Triton X-100, 20% Glycerol, 1x protease inhibitor cocktail and 0.5mM spermidine) for 10 minutes. Extracted nuclei were centrifuged at 600rcf and 4°C and resuspended in cold nuclear extraction buffer (100µl per sample). The CUT&RUN was performed as per Epicypher CUT&RUN protocol v1.5.1. CUT&RUN

DNA was purified using the Monarch DNA Clean-up kit (New England Biolabs) using a 5:1 binding buffer: sample ratio and following the manufacturer's instructions.

2.3.7 CUT&RUN-Rx Library Preparation

The standard protocol of the NEBNext® Ultra™ II DNA Library prep kit (New England Biolabs) was used for library preparation of the CUT&RUN-Rx samples. Of note, PCR enrichment of adaptor-ligated DNA utilised a total of 14 cycles of denaturation at 98°C for 15 seconds and annealing/short extension at 60°C for 10 seconds. The purified PCR product was quantified using a Qubit fluorometer and fragment size distribution was analysed on an Agilent Tapestation 4200 (Agilent) using D1000 ScreenTape assay (Agilent). Pooled libraries were diluted and processed for 150-bp paired-end sequencing using an Illumina NovaSeqX plus platform.

2.4 RNA Methods

2.4.1 RNA-seq

For the NSD2-KO +/- EZH2 inhibitor experiment, total RNA was isolated from CTRL and NSD2-KO isogenic Karpas-422 (EZH2-mutant lymphoma) cells following 6 days of treatment with 100nM Tazemetostat or DMSO control, using the RNeasy Mini Kit (Qiagen) according to the manufacturer's instructions. For the PRC2 related experiment, total RNA was isolated from WSU-DLCL2 (EZH2-mutant lymphoma) cells 7 days after CRISPR-Cas9 sgRNA-mediated knockout of Luciferase (control), EED, AEBP2, MTF2, and NSD2 using the RNeasy Mini Kit (Qiagen) according to the manufacturer's instructions. RNA-seq libraries were prepared by Novogene as follows; mRNA was purified from total RNA using poly-T oligo-attached magnetic beads. Following fragmentation, first strand of cDNA was synthesised using random hexamers, followed by second strand synthesis using dTTP. cDNA was subject to end repair, A-tailing, adapter ligation before being size selected and amplified for final library generation. Libraries were quantified using a Qubit fluorometer and assessed using Bioanalyser and qRT-PCR for quality control. Libraries were sequenced

paired-end to an approximate read depth of 55 million paired-end reads on Illumina NovaSeqX plus platform.

2.5 Computational Methods

2.5.1 Genome-Wide CRISPR Screen Data Analysis

The MAGeCK algorithm was used to calculate CRISPR beta scores for the genome-wide CRISPR screen using the mle module, comparing sgRNA abundance of gDNA from the end of the screen in DMSO and Tazemetostat conditions, with the original plasmid pool (Li et al., 2014). Common essential genes were defined using the Achilles 19Q3 list of genes and were removed before generating plots using Prism 10 for MacOS (GraphPad). Dr. Craig Monger, a bioinformatician in the Bracken Lab, carried out the MAGeCK analysis.

2.5.2 Mass Spectrometry Data Analysis

Bruker mass spectrometric data from the Tims-Tof was processed using the MaxQuant (version 2.0.3.0) incorporating the Andromeda search engine. To identify peptides and proteins, MS/MS spectra were matched against a homo sapiens uniprot database containing 82,427 entries (release 2023_03). All searches were performed using the default setting of MaxQuant, using the unspecific enzyme setting and a false discovery rate of 1% on the peptide and protein level. The database searches were performed with acetylation (protein N terminus) and oxidation (M) as variable modifications. For the generation of label free quantitative (LFQ) ion intensities for protein profiles, signals of corresponding peptides in different nano-HPLC MS/MS runs were matched by MaxQuant in a maximum time window of 1 min. The ‘proteinGroups.txt’ output file was filtered for contaminants and reverse hits using Perseus version 2.0.10.0. Volcano plots were generated using Perseus version 2.0.10.0. For stoichiometric analysis, iBAQ values for IgG control were first subtracted from each experimental replicate. The subsequent iBAQ value of each identified protein was normalised to the respective bait protein in each IP. The stoichiometry values were averaged across replicates, reported as the mean. Plots were formatted using

GraphPad PRISM version 10.5.0. The generation of the proteinGroups.txt file was carried out by Dr. Eugene Dillon in the Conway Institute of University College Dublin.

2.5.3 CUT&RUN-Rx Analysis

Firstly, adapters from paired-end sequencing reads were trimmed using fastp (Chen, Zhou, et al., 2018). In order to perform alignments with exogenous spike-in mouse reference genome, a human-mouse hybrid genome was created by appending the mouse mm10 genome build to the hg38 human genome build prior to indexing. Reads were aligned to the hybrid genome using Bowtie2 (Langmead & Salzberg, 2012) in the -very sensitive mode. SAMtools (H. Li et al., 2009) was used to keep reads with a mapping quality >2, separate the mouse and human reads, remove duplicate reads, and convert SAM to BAM files. The normalisation factor generated by the spike-in for each antibody was calculated using the formula for normalised reference-adjusted reads per million (RRPM) (1 per million spike-in reads). The bamCoverage module from the deepTools2 (Ramirez et al., 2016) suite was used to generate RRPM normalised bigwig files for genome browser visualisation. Of note, NSD2 CUT&RUNs were cpm-normalised instead, due to the fact that the mouse ESC spike-in cells do not express NSD2. Average plots and tornado plots were generated using computeMatrix from the deepTools2 suite, while boxplots were generated using ggplot2 in R (Wickham, 2016), after producing matrices using the deepTools2 suite multiBigwigSummary. Regions that overlapped with a custom hg38 blacklist were excluded from analyses. Peak calling for H3K27ac peaks was performed using the MACS2 algorithm (Zhang et al., 2008) for narrow peaks, using matched IgG as a control. Peaks were filtered to retain high-confidence regions and converted to BED format. Candidate enhancers were defined from H3K27ac peaks by excluding promoter-proximal and exonic regions. Promoters were defined as TSS ±2Kb using gene annotations from hg38. The remaining regions represented intronic and intergenic regions. Gene Ontology (GO) enrichment analysis was performed using the EnrichR platform (Kuleshov et al., 2016). During the course of this research project Dr. Darragh Nimmo performed the first pass of much of the

bioinformatics, however the final versions of analyses and plots contained in this thesis were generated by myself, to preserve uniformity across analyses.

2.5.4 RNA-seq Analysis

For each pair of FASTQ files, BBDuk from BBTools (Bushnell, 2014) package was used to trim adaptors and low-quality reads. Filtered reads were aligned to the hg38 homo sapiens reference genome (GRCh38.98) using HISAT2 (Pertea et al., 2016)(version 2.2.1). The SAMtools program (H. Li et al., 2009) was used to convert SAM files to sorted BAM files. Next, featureCounts (Liao et al., 2014)(version 1.6.4) was used to count reads per gene, which had been assigned to gene identifier features annotated by the Ensembl 98 hg38 genome annotation. The resulting read counts table was imported into R, where the DESeq2 package (Love et al., 2014)(version 1.48.0) was used to identify differentially expressed genes with a fold-change of >1.5, a baseMean expression of >20, and adjusted p values <0.05. Adjusted p values were calculated in DESeq2 using the Benjamini–Hochberg (BH) procedure to control the false discovery rate (FDR). Differential expression results were visualised using volcano plots. Genes were highlighted in red (upregulated) or blue (downregulated) if they met all of the following criteria: adjusted p value <0.05, minimum 1.5-fold change, and base mean expression >20. Non-significant genes are shown in grey. Plots were generated using ggplot2 (Wickham, 2016).

2.5.5 Analysis of Flow Cytometric Assays

FCS files generated on the Guava easyCyte HT flow cytometer (Luminex) were imported to FlowJo v10 Software (BD Biosciences) where gating on singlets was carried out based on cells in an uninfected well and GFP positive populations determined. In all flow cytometric based assays, each timepoint was normalised to the initial day 3 timepoint to account for minor differences in cell seeding densities between wells.

CHAPTER 3

Identifying Targetable Genes and Pathways Capable of Sensitising B-Cell Lymphoma Cells to EZH2 Inhibitors

3.1 Introduction

3.1.1 Functional Genomics Approaches to Precision Oncology

The paradigm of precision oncology was exemplified with the use of tyrosine kinase inhibitors in the treatment of chronic myeloid leukaemia (Cortes et al., 2021; Druker et al., 2002; Lydon, 2009). Following the discovery of the t(9;22) Philadelphia chromosome and its resultant fusion oncoprotein BCR-ABL, rational drug development led to the discovery of the initial tyrosine kinase inhibitor imatinib (Bartram et al., 1983; Druker et al., 1996; Rowley, 1973). Chronic myeloid leukaemia went from a form of blood cancer requiring chemotherapy and often allogeneic stem cell transplantation, to a chronic illness that required a daily oral medication to maintain durable remissions (Druker, 2009). Functional genomics approaches have subsequently elucidated not only the genetic characteristics of many cancer types, but also enhanced the mechanistic understanding of these genetic alterations in cancer. This has enabled the oncology research community to develop targeted therapies that can take aim at the genetic lesion directly e.g. enzyme inhibitors, protein degraders; or indirectly such as harnessing the immune system to target malignant cells as is the case with immune checkpoint inhibitors.

3.1.2 Applying CRISPR-Cas9 Systems in Functional Genomics

Clustered, regularly interspaced, short palindromic repeats (CRISPR) are an ancient adaptive defence system, found in bacteria and archaea which, following transcription into CRISPR-derived RNAs (crRNAs), can recognise specific sequences of foreign DNA. Using effector DNA endonucleases, termed CRISPR-associated (Cas) proteins, these systems can then mediate double stranded DNA breaks (DSB) at the target sequences and destroy invading nucleic acids (Barrangou et al., 2007; Horvath & Barrangou, 2010; Jinek et al., 2012; Wiedenheft et al., 2012). Expression of *Streptococcus pyogenes* Cas9 in mammalian cells has led to the ability to use target sgRNAs against short sequences within genes of interest to facilitate genome editing both *in vitro* and *in vivo* (Cong et al., 2013; Mali et al., 2013; Wang et al., 2013; Yang et al., 2013). Mammalian cells will repair DSBs using either

homology-directed repair (HDR) or non-homologous end joining (NHEJ), the latter mechanism being error-prone and often the more common mechanism employed by the cell. NHEJ will frequently result in nucleotides being inserted or deleted (indels) into the DNA sequence, which can cause frameshift mutations and premature stop codons if occurring in protein coding regions (Hartenian & Doench, 2015). By facilitating genetic knock-out, knock-in, activation, or inhibition, CRISPR-Cas9 makes it possible to manipulate gene expression in order to study downstream functional and phenotypic consequences in diverse cellular contexts. An important point to consider when carrying out CRISPR genetic screens is that the Cas9 effector can have off-target effects, depending on the specific sgRNA sequence, the genomic loci targeted, the presence of copy number aberrations, and the number of base mismatches between the sgRNA and the target sequence (Aguirre et al., 2016; Fu et al., 2013; Hsu et al., 2013).

CRISPR-Cas9 screens have become an integral tool in the molecular biologist's arsenal for approaching functional genomics questions. These screens can be used to identify genetic dependencies in a variety of cancer types, which subsequently inform novel rational therapeutic targets in specific malignancies (Bock et al., 2022; Feng et al., 2022; Radko-Juettner et al., 2024; Tzelepis et al., 2016; T. Wang et al., 2014). Conventional chemotherapy typically employs non-specific anti-proliferative therapies that target rapidly dividing cells, while more recent advances in cancer therapeutics may target intrinsic vulnerabilities of the cancer's cell of origin e.g. proteosome inhibitors in multiple myeloma and anti-CD20 antibodies in lymphoma (Freeman & Sehn, 2018; Lim et al., 2010; Moreau et al., 2012). By utilising CRISPR screens, it is possible to ascertain genes that are preferentially essential in a specific and molecularly defined subset of a malignancy, an approach which has been recently applied to multiple myeloma by the Broad Institute (de Matos Simoes et al., 2023). Furthermore, large public CRISPR screen datasets such as the Cancer Dependency Map (DepMap)(Tsherniak et al., 2017), have made it possible to carry out co-dependency mapping whereby the phenotypes of two distinct gene knockouts can be correlated across a wide range of cancer contexts to assess for novel functional

interactions (Kim et al., 2019; Wainberg et al., 2021). Identifying genetic dependencies in cancer can also be integrated into large scale drug sensitivity screens, to match therapeutic targets with available drug compounds in a high-throughput manner (Garnett et al., 2012; Iorio et al., 2016).

A recent chromatin biology related example demonstrating the power of functional genomics approaches to effect meaningful translational outcomes in cancer research is the role of menin inhibitors in acute leukaemia. *KMT2A*-rearranged (*KMT2A*-r) acute leukaemias are associated with poor survival in both children and adults with conventional chemotherapeutic approaches unsatisfactory (Neff & Armstrong, 2013). Menin was originally shown to contribute to leukaemogenesis in *KMT2A*-r acute leukaemia in 2005 (Yokoyama et al., 2005). In 2015, the first menin inhibitors were published, demonstrating both *in vitro* and *in vivo* activity in *KMT2A*-r acute leukaemia by directly antagonising the leukaemic gene expression profile (Borkin et al., 2015). Using CRISPR-Cas9 based assays, coupled with gene expression and chromatin occupancy profiling in cells treated with/without menin inhibitor, the menin-KMT2A genetic dependency was broadened to *NUP98*-rearranged and NPM1-mutant acute leukaemia, greatly expanding the number of patients that could potentially benefit from menin inhibitors (Heikamp et al., 2022; Kuhn et al., 2016). By 2023, the results of the first phase I clinical trial using a menin inhibitor were published with a 30% complete remission rate in patients with relapsed/refractory acute leukaemia (Issa et al., 2023). In under 20 years, pursuing a functional genomics approach to a molecularly defined malignancy yielded the ability for clinicians to treat patients with a targeted therapy, the very definition of precision oncology.

Lastly, while small molecular inhibitors of oncoproteins represent a rational approach to targeting gain-of-function oncogene-driven cancers, loss of tumour suppressor genes occurs more frequently in cancer (Vogelstein et al., 2013) and cannot be targeted by the paradigm of ‘inhibitors’. For this reason, using CRISPR screens to identify cancer-specific targetable genetic vulnerabilities in loss-of-function tumour suppressor gene-mutated

cancers represents the next generation approach to developing precision oncology therapies and cures. This is particularly relevant in rare cancers with no current effective treatment options such as malignant rhabdoid tumours, where recent work using functional genomics approaches has identified *DCAF5* as a synthetic lethality in *SMARCB1*-mutated cancers (Radko-Juettner et al., 2024).

3.1.3 Recent Evidence for Chromatin Regulators as Genetic Dependencies in B-cell Lymphoma

A recent scientific report used genome-wide CRISPR-Cas9 screens in K-562 cells to investigate the role of chromatin regulators in modulating bivalent chromatin domains (Sparbier et al., 2023). Somewhat paradoxically, despite the menin-KMT2A complex mediating the H3K4me3 mark associated with active transcription, inhibition of menin either genetically or pharmacologically was shown to phenocopy PRC2 inhibition. This effect was shown to be related to aberrant KMT2A methyltransferase activity at bivalent genes after being released from active gene sites upon menin inhibition, which leads to a differentiation blockade of proliferating B-cells in the germinal centre resulting in a malignant phenotype. Another recent study used a bioinformatic approach to publicly available CRISPR-Cas9 screens to suggest that redistribution of the menin-KMT2A complex in EZH2-mutant lymphoma by elevated H3K27me3 levels drives a malignant gene expression profile by activating genes implicated in lymphomagenesis such as *mTORC1* (Chen et al., 2023).

The aim of this results chapter was to identify and validate novel genetic dependencies and sensitisers to PRC2 inhibition in germinal centre B-cell lymphoma, focusing on genes and pathways with existing drug targets.

3.2 Results

3.2.1 Developing a genome-wide CRISPR screen system to identify sensitiser genes to EZH2 inhibition in B-cell lymphoma

A number of optimisation steps were undertaken prior to performing the genome-wide CRISPR-Cas9 dropout screens. The optimal end timepoint was chosen as 24 days, to reflect a number of factors including (i) allowing at least 12 cell population doublings in order to observe a signal following a genetic perturbation; (ii) allowing enough time for the EZH2 inhibitor to produce phenotypic effects (can take at least 7 days based on prior Bracken Lab experience); and (iii) experience from prior experiments in the Bracken Lab that full depletion of an sgRNA targeting an essential gene (e.g. *RPA3*) took ~24 days in WSU-DLCL2 and HT. Due to the observation that B-cell lymphomas can respond to EZH2 inhibitors irrespective of *EZH2* mutation status (Morschhauser et al., 2020), an EZH2-mutant (WSU-DLCL2) and an EZH2 wild-type (HT) lymphoma cell line were chosen for this screen. These cell lines had been transduced with lentivirus containing a FLAG-tagged Cas9 vector and a blasticidin selectable marker (lentiCas9-Blast) by Dr James Nolan. The lentivirus containing the Brunello genome-wide library of 76,441 sgRNAs (Doench et al., 2016) was previously prepared by Dr Gerard Brien in the Bracken Lab.

A 24-day dose-response curve to Tazemetostat was performed in both cell lines and the dose chosen for each cell line was decided as the dose of drug that would inhibit cell proliferation by 20% (IC20) at 24 days, 22.83nM for WSU-DLCL2 and 25.5nM for HT (**Figure 3.1A**). The reason for choosing this dose was to avoid excess toxicity by day 24 in the experimental group compared to the control group to enable accurate sgRNA quantity comparisons. The multiplicity of infection (MOI) is defined as the ratio of lentiviral integrants to the infected cells. The desired multiplicity of infection (MOI) when undertaking genome-wide CRISPR-Cas9 dropout screens is 0.1-0.3, as recommended by the Broad Institute (Doench, 2018). This low MOI effectively ensures one lentiviral integrant is delivered to a single cell, limiting the risk of multiple sgRNAs targeting different genes being transduced

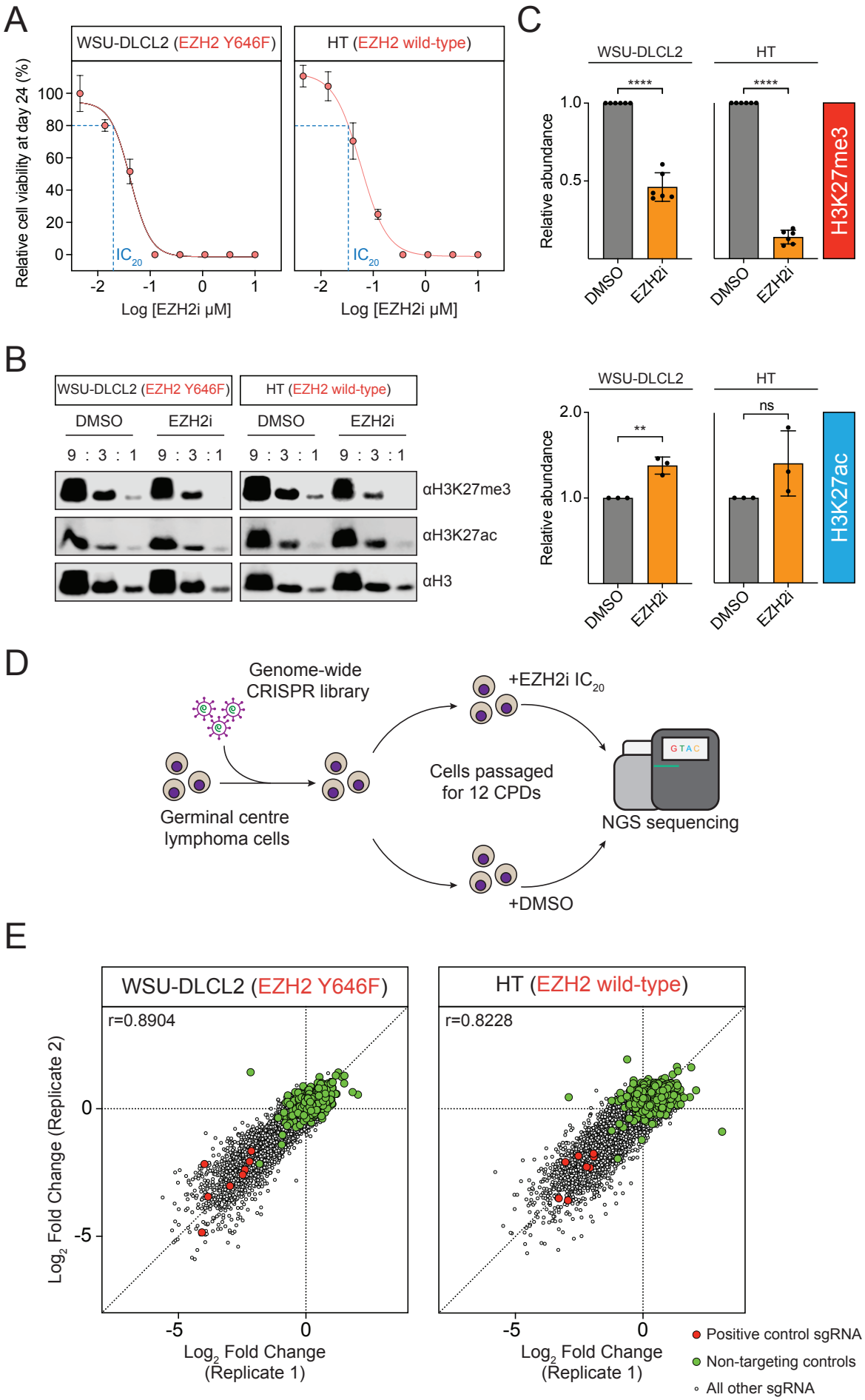
A
WSU-DLCL2 (EZH2 Y646F)
HT (EZH2 wild-type)
Relative cell viability at day 24 (%)
IC20
Log [EZH2i μM]
B
WSU-DLCL2 (EZH2 Y646F)
HT (EZH2 wild-type)
DMSO
EZH2i
9 : 3 : 1
αH3K27me3
αH3K27ac
αH3
C
WSU-DLCL2
HT
Relative abundance
H3K27me3
H3K27ac
ns
D
Genome-wide CRISPR library
Germinal centre lymphoma cells
+EZH2i IC20
Cells passaged for 12 CPDs
+DMSO
NGS sequencing
E
r=0.8904
r=0.8228
Log2 Fold Change (Replicate 2)
Log2 Fold Change (Replicate 1)
Positive control sgRNA
Non-targeting controls
All other sgRNA

Figure 3.1: Developing a genome-wide CRISPR screen system to identify sensitiser genes to EZH2 inhibition in B-cell lymphoma.
A. Relative cell viability (normalised to DMSO control) at day 24 in WSU-DLCL2 and HT lymphoma cells treated with varying concentrations of Tazemetostat over 24 days. The IC20 value is denoted by the dotted line. Cell viability was measured by CellTiter-Glo. Data are reported as the mean of three biological replicates ± SD.
B. Immunoblots from whole cell lysates of the indicated histone modifications in the indicated lymphoma cells, treated with either Tazemetostat or DMSO, harvested at the end of the genome-wide CRISPR screen. Lysate dilutions are indicated by 9:3:1.
C. Relative quantification of immunoblot analyses of H3K27 methylation and acetylation abundance in the indicated lymphoma cells. Signal intensity values were normalised to the histone H3 loading control and then expressed relative to the DMSO condition to identify the effects of EZH2 inhibition. Data values represent technical replicates from the two biological CRISPR screen replicates, and their mean values ± SD are plotted as bars.
D. Schematic of the genome-wide CRISPR-Cas9 screen performed in germinal center B-cell lymphoma cells. CPD, cell population doublings; EZH2i, EZH2 inhibitor (Tazemetostat).
E. Genome-wide CRISPR screen data illustrating the correlation between biological replicates. Gene scores are represented by the mean Log2 fold change in abundance of the 4 sgRNAs targeting each gene between the original plasmid library pool and day 24 (end of the screen). Positive controls (PCNA, RPL9, RPL23A, RPA3, POLR2C, POLR2D, GAPDH, CDK1) are highlighted in red while the 1000 non-targeting controls are shown in green. Grey datapoints represent all other sgRNAs in the Brunello library. Results shown for WSU-DLCL2 and HT cell lines.

into cells which could lead to non-specific toxicity. A lentiviral titration was undertaken in both cell lines and a volume of lentivirus that achieved an MOI 0.15 was chosen.

At the end timepoint of the CRISPR screen, additional cells were harvested in order to perform immunoblots for histone H3 modifications. In both WSU-DLCL2 and HT cell lines, treatment with IC20 Tazemetostat resulted in significant global reductions in H3K27me3 along with expected concomitant increases in H3K27ac (**Figure 3.1B and C**). The schematic for the CRISPR screen workflow is shown in **Figure 3.1D**. Following sequencing of the CRISPR screen, to ensure a high quality dataset, the relative abundances of positive and negative control sgRNAs were assessed using PinAPL-Py (Spahn et al., 2017). In both replicates of both cell lines, the non-targeting controls contained within the Brunello library broadly fell around 0 as expected, while genes chosen as positive controls (*RPA3*, *POLR2C*, *POLR2D*, *GAPDH*, *CDK1*, *PCNA*, *RPL9*, *RPL23A*), based on previous CRISPR screens performed in the Bracken Lab, showed strong depletion (**Figure 3.1E**).

3.2.2 Genetic dependency profiles are similar across germinal centre B-cell lymphoma cell lines irrespective of *EZH2* mutation status

Next, CRISPR Beta scores were calculated by Dr. Craig Monger, using the MAGeCK algorithm (Li et al., 2014). MAGeCK ranks genes in a CRISPR screen by integrating a number of attributes of the raw sequencing data including the read count, individual sgRNA effect, aggregated sgRNA effects for a specific gene, and individual sgRNA p values, to produce a Beta score. This value represents the strength of the effect of knocking out a gene on cell viability. I carried out all analysis after filtering out common essential genes (Achilles 19Q3)(Dempster, 2019; McFarland et al., 2018; Tsherniak et al., 2017). Beta scores for all genes in the two CRISPR screens were numerically ranked and shown as XY plots (**Figure 3.2A**). To determine the degree of shared genetic dependencies between EZH2-mutant and EZH2 wild-type lymphomas, all genes with a Beta score ≤-0.5 were compared and a significant overlap was observed (**Figure 3.2B**). A stricter overlap definition

was then applied, looking at the top 200 dependencies in each cell line, which again demonstrated a significant overlap (**Figure 3.2C**). Gene ontology (GO) of all genes with a Beta score ≤-0.5 was carried out using GOrilla (Eden et al., 2009) which again showed a significant overlap of GO Molecular Function terms between the two cell lines indicating a shared biology across two germinal centre lymphoma cell lines (**Figure 3.2D**). To validate these findings across a broader set of cell lines, the 462 overlapping dependencies (Beta score ≤-0.5) were compared with >1000 cancer cell lines in the Cancer Dependency Map (DepMap) which showed that 206 of these genes are selectively dependent in germinal centre B-cell lymphoma cell lines (n=13). The top 50 of these were plotted, highlighting key chromatin regulators, core PRC2 and known regulators of B-cell development (**Figure 3.2E-G**).

3.2.3 *CARM1* is essential in B-cell lymphoma

Having first confirmed a high quality CRISPR screen dataset, then demonstrating that genetic dependencies appear to be broadly shared amongst germinal centre B-cell lymphomas, I wanted to look specifically at genetic dependencies that had not been previously described, with a focus on chromatin regulatory genes. Previous genome-wide CRISPR screens in Diffuse Midline Glioma (DMG) cells possessing the oncohistone H3K27M, performed in the Bracken Lab, had identified *CARM1* as a genetic dependency in that context. Given that DMG cells are also dependent on core PRC2, I reasoned that *CARM1* may also be a dependency in EZH2-mutant lymphoma. Strikingly, *CARM1* scored as strongly as *EZH2* as a dependency in both WSU-DLCL2 and HT CRISPR screens (**Figure 3.3A**). Then, analysing data from the Cancer Dependency Map (https://depmap.org/portal), I observed that the only two cancer types with a CHRONOS dependency score of ≤ -0.5 for *CARM1* were Mature B-cell neoplasms (encompassing B-cell lymphoma) and B-cell acute lymphoblastic leukaemia (the most common childhood malignancy). What was fascinating was that *CARM1* seemed to be selectively dependent in B-cell derived malignancies (**Figure 3.3B**). To obtain further granularity on the specific B-cell malignancies contributing to the strong genetic dependency score of *CARM1*, I looked

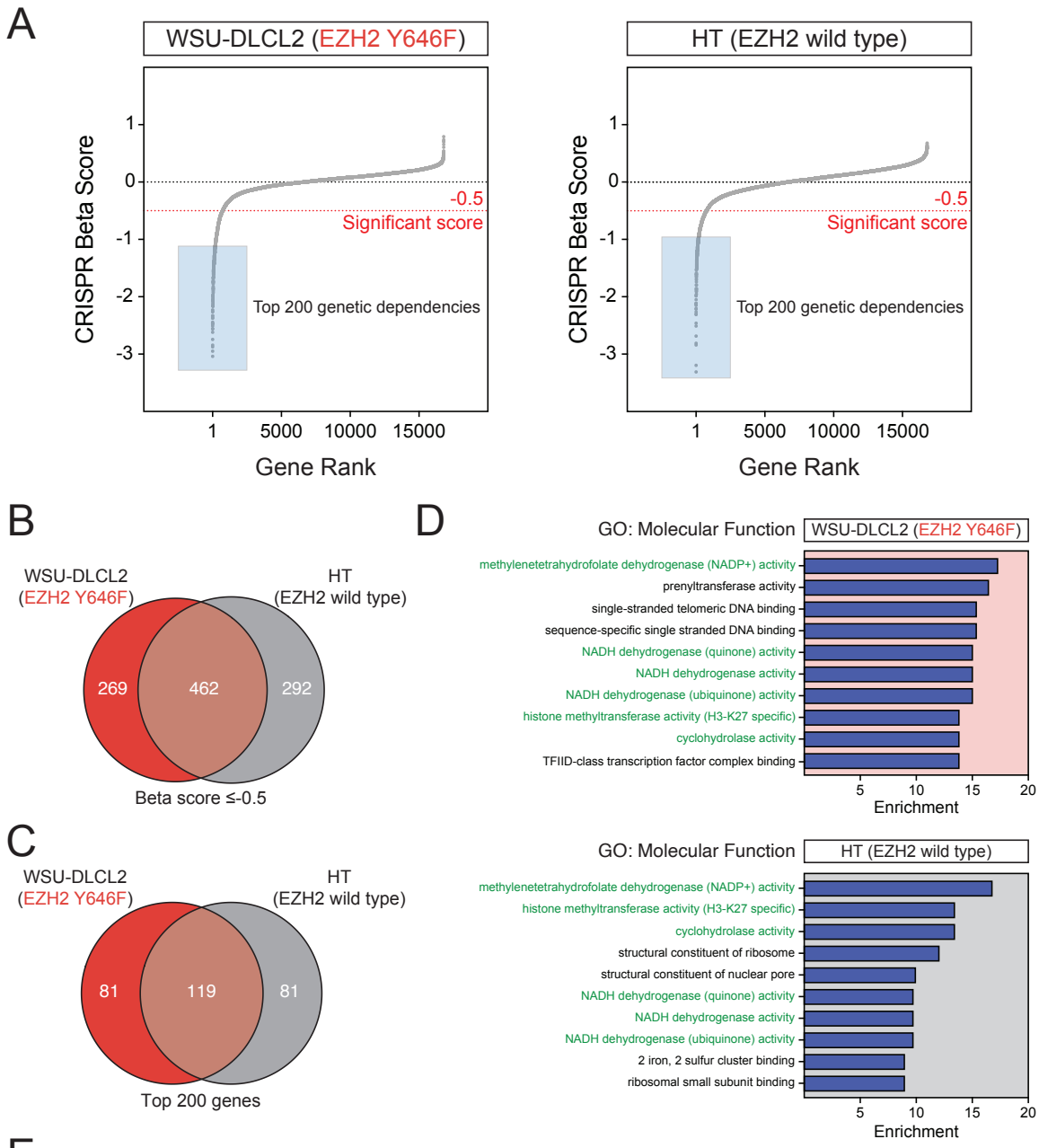
A
WSU-DLCL2 (EZH2 Y646F)
HT (EZH2 wild type)
CRISPR Beta Score
-0.5
Significant score
Top 200 genetic dependencies
Gene Rank
B
WSU-DLCL2 (EZH2 Y646F)
HT (EZH2 wild type)
269
462
292
Beta score ≤-0.5
C
81
119
81
Top 200 genes
D
GO: Molecular Function
methylenetetrahydrofolate dehydrogenase (NADP+) activity
prenyltransferase activity
single-stranded telomeric DNA binding
sequence-specific single stranded DNA binding
NADH dehydrogenase (quinone) activity
NADH dehydrogenase activity
NADH dehydrogenase (ubiquinone) activity
histone methyltransferase activity (H3-K27 specific)
cyclohydrolase activity
TFIID-class transcription factor complex binding
Enrichment
structural constituent of ribosome
structural constituent of nuclear pore
2 iron, 2 sulfur cluster binding
ribosomal small subunit binding
E
462 overlapping dependencies
342 of these present in Depmap
206 selectively dependent in GCB-DLBCL
Top 50 plotted
F
Top 50 selective dependencies (GCB-DLBCL vs all other cancers)
-Log10(q value)
Gene Rank
EZH2
BCL6
EED
POU2F2
CARM1
EP300
SUZ12
MEF2B
PIK3CD
PRC2
Known regulators of B-cell development
Selected chromatin regulators
G
Top 50 selective dependencies
1. EBF1
2. FNIP1
3. GCLC
4. SH3GL1
5. GLS
6. CCND3
7. EZH2
8. NMNAT1
9. EED
10. FLVCR1
11. BCL6
12. GSS
13. MBNL1
14. TTC7A
15. FPGS
16. MBD2
17. TADA1
18. CEPT1
19. MTF1
20. POU2F2
21. AK2
22. CARM1
23. POU2AF1
24. EP300
25. RHOA
26. SLC7A1
27. ATP1B3
28. TAF5L
29. ITSN2
30. ADIPOR2
31. CYB561A3
32. AKT2
33. SUZ12
34. FLCN
35. ATIC
36. ELOF1
37. PCYT2
38. CHCHD3
39. FECH
40. CYB5B
41. DLST
42. CDS2
43. MEF2B
44. RFK
45. ARF6
46. VPS39
47. RER1
48. TAF13
49. PIK3CD
50. DARS2

Figure 3.2: Genetic dependency profiles are similar across germinal centre B-cell lymphoma cell lines irrespective of *EZH2* mutation status.

A. Genome-wide CRISPR screen data gene ranked based on sgRNA enrichment or depletion at the end of screen (Day 24) in DMSO treated lymphoma cell lines indicated relative to the original plasmid pool as the control. Differential Beta-score between Day 24 and plasmid pool was calculated using the MAGeCK algorithm (Li et al., 2014). A negative Beta score indicates genetic dependency. Results shown for WSU-DLCL2 and HT cell lines. Common essential genes, as defined by depmap.org (Achilles, 19Q3), were removed. The top 200 genetic dependencies are highlighted.

B. Proportional Venn Diagram overlap of all genes with a Beta score ≤-0.5 in WSU-DLCL2 and HT cell lines.

C. Proportional Venn Diagram overlap of the top 200 genetic dependencies in WSU-DLCL2 and HT cell lines.

D. Gene ontology enrichment for Molecular Function of all genes with a Beta score ≤-0.5 in WSU-DLCL2 and HT cell lines using the GOrilla tool (Eden et al., 2009). Enrichment values were calculated using the equation Enrichment = (b/n) / (B/N), where N - is the total number of genes, B - is the total number of genes associated with a specific GO term, n - is the number of genes in the target set, and b - is the number of genes in the target set associated with a specific GO term. Overlapping GO terms between the two cell lines are highlighted in green.

E. Schematic of approach used to validate the results of the in-house genome-wide CRISPR screens performed in WSU-DLCL2 and HT cell lines with dependency data of all germinal centre B-cell lymphoma cell lines (n=13) contained in the Cancer Dependency Map (Depmap.org).

F. The Top 50 selective dependencies in germinal centre B-cell lymphoma cells compared to all other cancers in the Cancer Dependency Map. Core PRC2 components are highlighted in blue, known regulators of B-cell development in green, and selected other chromatin regulators in orange. p-values were calculated using a one-sided Mann–Whitney U test and were Benjamini–Hochberg adjusted for a false discovery rate q value.

G. The Top 50 selective dependencies in germinal centre B-cell lymphoma cells compared to all other cancers in the Cancer Dependency Map provided in a rank list.

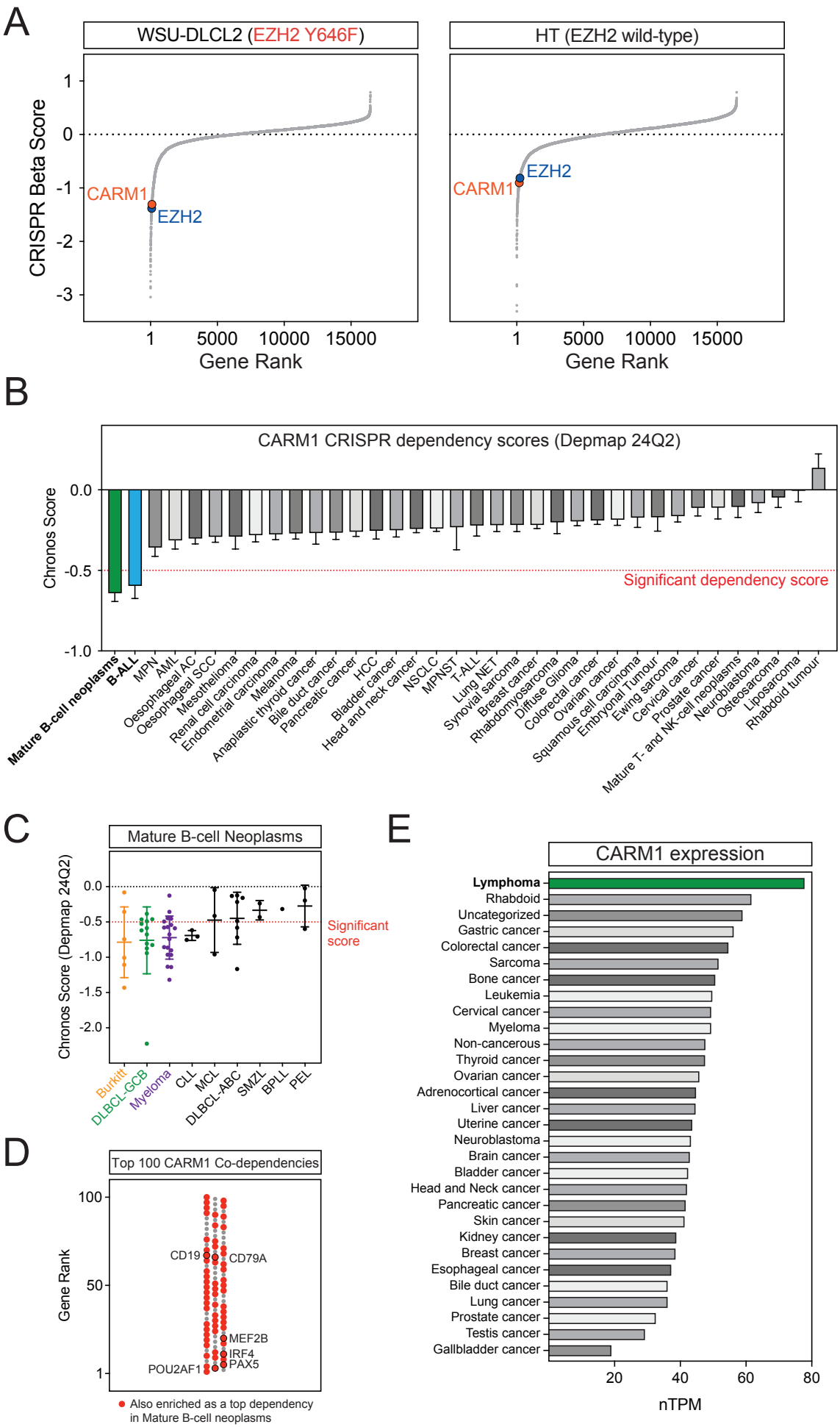
A
WSU-DLCL2 (EZH2 Y646F)
HT (EZH2 wild-type)
CRISPR Beta Score
CARM1
EZH2
Gene Rank
B
CARM1 CRISPR dependency scores (Depmap 24Q2)
Chronos Score
Significant dependency score
Mature B-cell neoplasms
B-ALL
MPN
AML
Oesophageal AC
Oesophageal SCC
Mesothelioma
Renal cell carcinoma
Endometrial carcinoma
Melanoma
Anaplastic thyroid cancer
Bile duct cancer
Pancreatic cancer
HCC
Bladder cancer
Head and neck cancer
NSCLC
MPNST
T-ALL
Lung NET
Synovial sarcoma
Breast cancer
Rhabdomyosarcoma
Diffuse Glioma
Colorectal cancer
Ovarian cancer
Squamous cell carcinoma
Embryonal Tumour
Ewing sarcoma
Cervical cancer
Prostate cancer
Mature T- and NK-cell neoplasms
Neuroblastoma
Osteosarcoma
Liposarcoma
Rhabdoid tumour
C
Mature B-cell Neoplasms
Chronos Score (Depmap 24Q2)
Significant score
Burkitt
DLBCL_GCB
Myeloma
CLL
MCL
DLBCL-ABC
SMZL
BPLL
PEL
D
Top 100 CARM1 Co-dependencies
Gene Rank
CD19
CD79A
MEF2B
IRF4
PAX5
POU2AF1
Also enriched as a top dependency in Mature B-cell neoplasms
E
CARM1 expression
Lymphoma
Rhabdoid
Uncategorized
Gastric cancer
Colorectal cancer
Sarcoma
Bone cancer
Leukemia
Cervical cancer
Myeloma
Non-cancerous
Thyroid cancer
Ovarian cancer
Adrenocortical cancer
Liver cancer
Uterine cancer
Neuroblastoma
Brain cancer
Bladder cancer
Head and Neck cancer
Pancreatic cancer
Skin cancer
Kidney cancer
Breast cancer
Esophageal cancer
Bile duct cancer
Lung cancer
Prostate cancer
Testis cancer
Gallbladder cancer
nTPM

Figure 3.3: *CARM1* is essential in B-cell lymphoma
A. Genome-wide CRISPR screen data in the indicated lymphoma cell lines gene ranked based on sgRNA enrichment at day 24 vs day 3. Differential CRISPR beta-score between D24 and D3 timepoints calculated using the MAGeCK algorithm. A negative beta score indicates genetic dependencies. Experiment performed in n=2 biological replicates.
B. CRISPR dependency scores for *CARM1* in the indicated cancer types based on DepMap CHRONOS score from the DepMap 24Q2 dataset (data represents mean ± SEM).
C. DepMap CHRONOS scores for *CARM1* in “Mature B-cell Neoplasms” subdivided into the indicated B-cell neoplasm subtypes. A signficant score of <-0.5 is denoted.
D. Gene rank plot of the top 100 *CARM1* co-dependencies based on DepMap 24Q2, with genes that are also enriched as top dependencies in Mature B-cell Neoplasms highlighted in red. Some examples of key B-cell dependencies are illustrated.
E. CARM1 expression by cancer type based on data from The Human Protein Atlas. Expression is denoted by normalised transcripts per million.

at all cell lines contained under the heading ‘Mature B-cell Neoplasms’ in DepMap. I noted that Burkitt lymphoma and germinal centre lymphoma cell lines appeared selectively dependent on *CARM1* (**Figure 3.3C**). This is notable as Burkitt lymphoma, although distinct from DLBCL, is also derived from germinal centre B-cells. Furthermore, investigation of the top 100 *CARM1* co-dependencies within DepMap demonstrated that the majority of these genes are also enriched as top dependencies in Mature B-cell neoplasms (**Figure 3.3D**). Finally, looking at publicly available expression data across multiple cancers, CARM1 expression appeared to be greatest in lymphomas (**Figure 3.3E**). Taken together, *CARM1* appears to be a selective dependency in B-cell malignancies arising from germinal centre B-cells.

3.2.4 Pharmacological CARM1 inhibition is effective and specific in germinal centre B-cell lymphoma

The initial focus of this PhD research project was to identify candidate novel targets as well as EZH2 inhibitor sensitisers in germinal centre B-cell lymphomas using functional genomics. Although *CARM1* has not been described as essential in B-cell lymphoma, a selective CARM1 arginine methyltransferase inhibitor, TP-064, has been developed initially based on promising results in multiple myeloma (Nakayama et al., 2018). Based on the results of Section 3.2.3 I performed cell viability assays across several different cancer cell lines exposed to TP-064. Consistent with the previous section, Burkitt lymphoma and germinal centre B-cell lymphoma cell lines were sensitive to CARM1 inhibition. In contrast, DLBCL-ABC subtype cell lines, which have a different genetic background to germinal centre lymphomas, and MRT, which are dependent on core PRC2, were not sensitive to CARM1 inhibition (**Figure 3.4A-C**). These results support testing CARM1 inhibitors across a broader panel of germinal centre B-cell lymphoma cell lines along with B-cell lymphoma xenografts (Veazey et al., 2020).

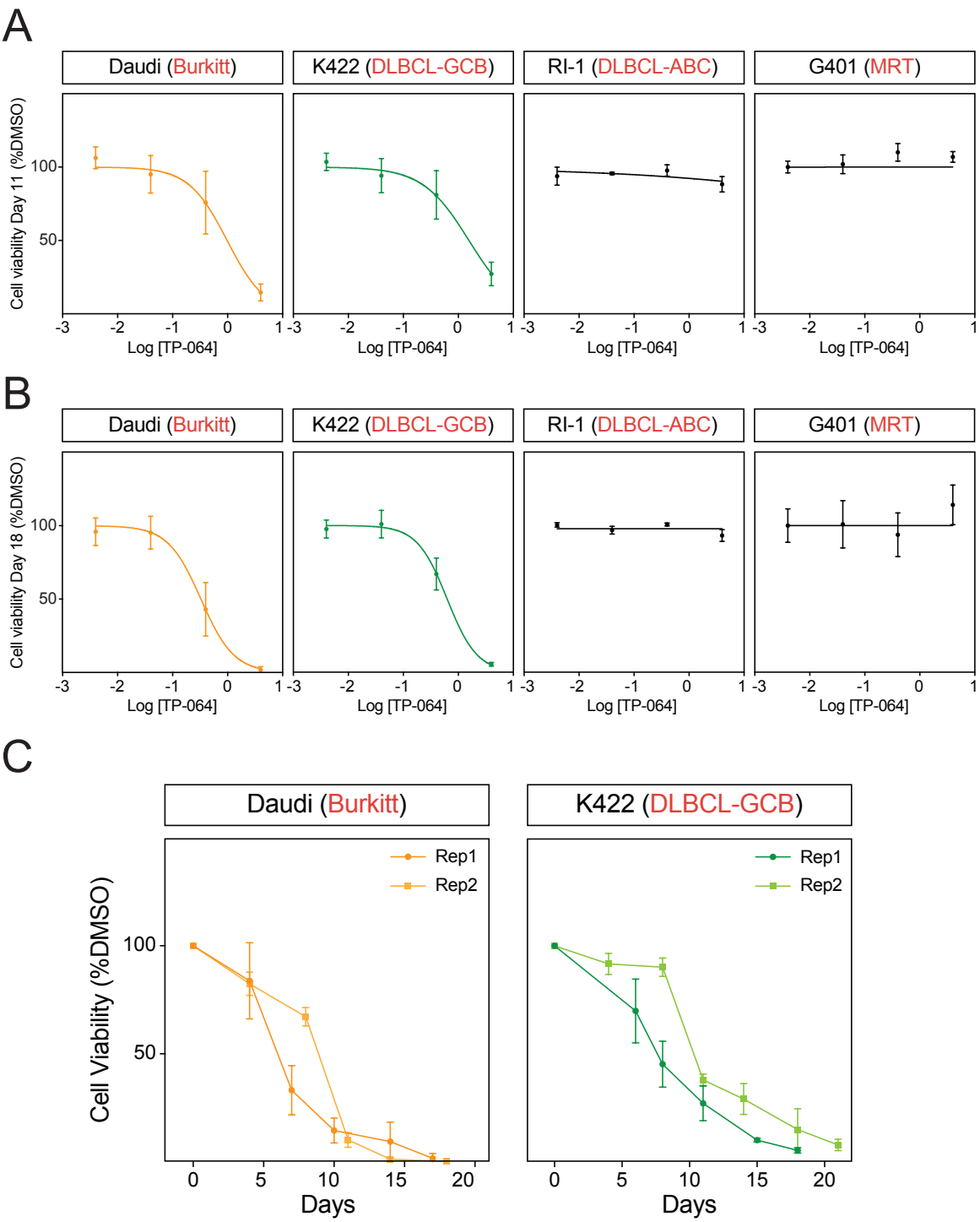

Figure 3.4: Pharmacological CARM1 inhibition is effective and specific in germinal centre B-cell lymphoma.

A. Cell viability results, normalised to DMSO control, at day 11 in the indicated cell lines treated with the CARM1 inhibitor TP-064 (data represents mean ± SD, n = 2 biological).

B. Cell viability results, normalised to DMSO control, at day 18 in the indicated cell lines treated with the CARM1 inhibitor TP-064 (data represents mean ± SD, n = 2 biological).

C. Cell viability results, normalised to DMSO control, in the indicated cell lines treated with 4μM of the CARM1 inhibitor TP-064, illustrating viability over time (data represents mean ± SD, n = 2 biological).

3.2.5 Mechanisms of action of EZH2 inhibition in sensitive lymphoma cells are likely divergent between EZH2-mutant and EZH2 wild-type lymphomas

Although earlier results in **Figure 3.2** provided evidence for a shared genetic dependency landscape across two germinal centre B-cell lymphomas irrespective of *EZH2* mutation status, I wanted to discern whether mechanisms of EZH2 inhibitors differed between EZH2-mutant and EZH2 wild-type cells. Given the altered chromatin landscape of EZH2-mutant lymphoma cells, with elevated H3K27me3 and severely reduced H3K27me2 levels, and the fact that fewer patients in the EZH2 wild-type cohort respond to EZH2 inhibitors, I hypothesised that the overlap of shared genetic sensitisers between WSU-DLCL2 and HT would be far smaller. Firstly, looking at the hockey stick plots, it was clear that the EZH2-mutant cell line had more genes with a EZH2i vs DMSO Beta score ≤ -0.5 (**Figure 3.5A**). When all genes with a Beta score ≤ -0.5 were overlapped there were very few shared sensitisers between WSU-DLCL2 and HT (**Figure 3.5B**). Next, I decided to focus solely on EZH2i sensitisers in EZH2-mutant lymphoma, and took the top 100 sensitisers to perform gene ontology (GO) analysis (**Figure 3.5C**). As expected, and providing further quality control validation of the CRISPR screen itself, enriched GO molecular function terms including predominantly methyltransferase activity and DNA/chromatin binding, while enriched GO cell process terms also included chromatin-specific terms (**Figure 3.5D-E**).

3.2.6 EZH2 inhibitor sensitiser genes are enriched for chromatin regulatory genes, many with already existing targeted therapeutics

Next, to identify specific genes whose loss sensitises EZH2-mutant lymphoma cells to the EZH2 inhibitor Tazemetostat, I compared CRISPR Beta scores between cells treated with DMSO (Control) and those exposed to a low dose (IC20) of Tazemetostat (**Figure 3.6A**). In the context of Beta scores generated between EZH2i and DMSO, a negative score indicates a gene whose loss sensitises cells to EZH2 inhibition, whereas a positive score indicates

A

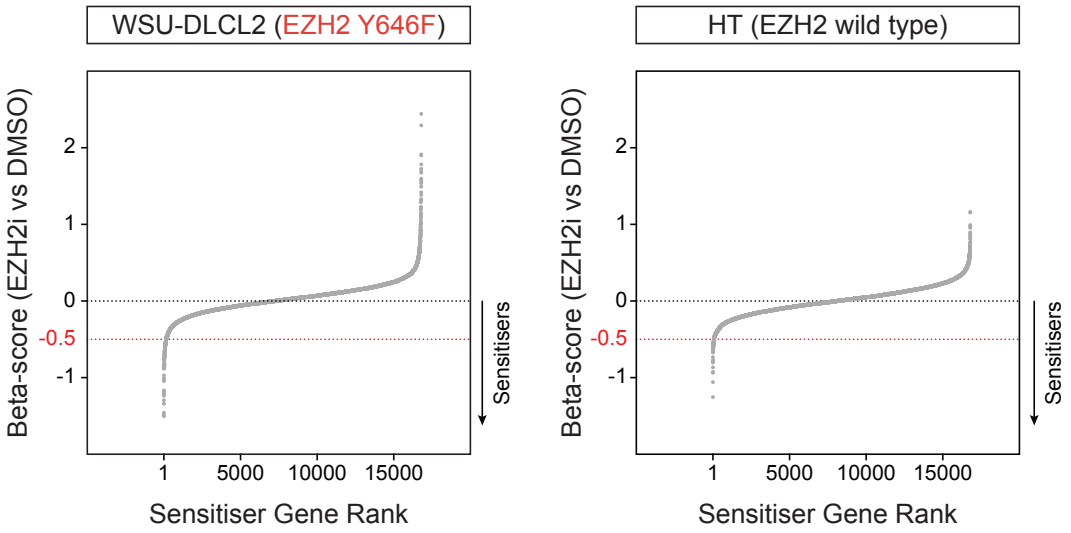
WSU-DLCL2 (EZH2 Y646F)
HT (EZH2 wild type)
Beta-score (EZH2i vs DMSO)
2
1
0
-0.5
-1
Sensitisers
1
5000
10000
15000
Sensitiser Gene Rank

B

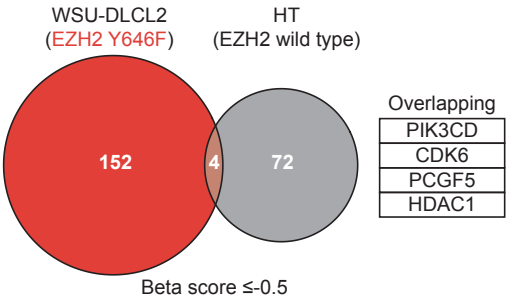
WSU-DLCL2
(EZH2 Y646F)
HT
(EZH2 wild type)
152
4
72
Overlapping
PIK3CD
CDK6
PCGF5
HDAC1
Beta score ≤-0.5

C

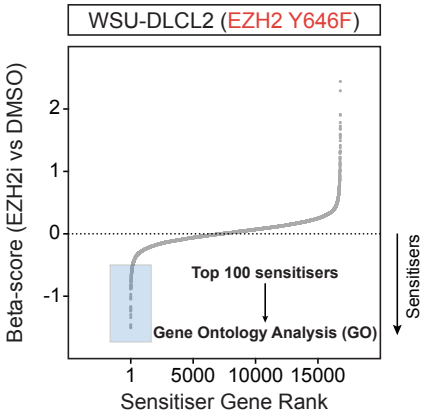
WSU-DLCL2 (EZH2 Y646F)
Beta-score (EZH2i vs DMSO)
2
1
0
-1
Top 100 sensitisers
Gene Ontology Analysis (GO)
Sensitisers
1
5000
10000
15000
Sensitiser Gene Rank

D

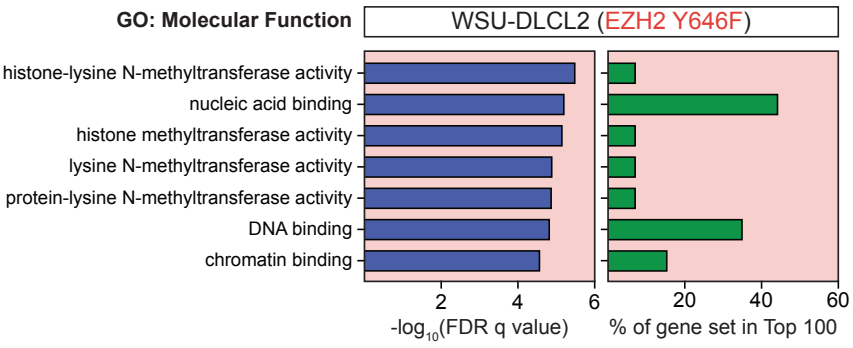
GO: Molecular Function
WSU-DLCL2 (EZH2 Y646F)
histone-lysine N-methyltransferase activity
nucleic acid binding
histone methyltransferase activity
lysine N-methyltransferase activity
protein-lysine N-methyltransferase activity
DNA binding
chromatin binding
2
4
6
-log10(FDR q value)
20
40
60
% of gene set in Top 100

E

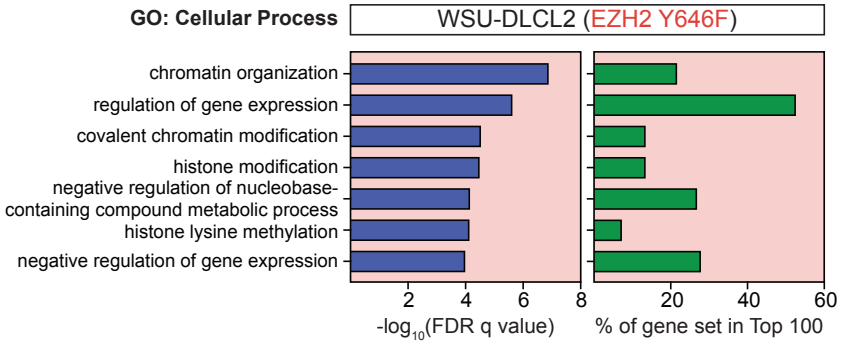
GO: Cellular Process
WSU-DLCL2 (EZH2 Y646F)
chromatin organization
regulation of gene expression
covalent chromatin modification
histone modification
negative regulation of nucleobase-containing compound metabolic process
histone lysine methylation
negative regulation of gene expression
2
4
6
8
-log10(FDR q value)
20
40
60
% of gene set in Top 100

Figure 3.5: Mechanisms of action of EZH2 inhibition in sensitive lymphoma cells are likely divergent between EZH2-mutant and EZH2 wild-type lymphomas.

A. Genome-wide CRISPR screen data in WSU-DLCL2 and HT lymphoma cells gene ranked based on sgRNA enrichment in low dose EZH2i treatment (Tazemetostat IC20) relative to DMSO control. Differential Beta-score between EZH2i and DMSO conditions calculated using the MAGeCK algorithm (Li et al., 2014). A negative Beta score indicates sensitiser genes, while a positive Beta score indicates resister genes. Common essential genes, as defined by depmap.org (Achilles, 19Q3), were removed.

B. Proportional Venn Diagram overlap of all genes with a Beta score ≤-0.5 in WSU-DLCL2 and HT cell lines.

C. Strategy showing that the top 100 candidate mediators of sensitisation to EZH2 inhibitors in EZH2-mutant lymphoma (WSU-DLCL2) were selected for gene ontology (GO) analysis.

D. Gene ontology enrichment for “Molecular Function” of the top 100 gene sensitisers in the WSU-DLCL2 cell line using the GOrilla tool (Eden et al., 2009). Enrichment p-values were calculated using a Fisher’s exact test and were Benjamini–Hochberg adjusted to obtain a False Discovery Rate (FDR) corrected q value (left). The percentage of genes within a given gene set that scored among the top 100 candidate mediators of sensitisation are shown (right).

E. Gene ontology enrichment for “Cellular Process” of the top 100 gene sensitisers in the WSU-DLCL2 cell line using the GOrilla tool (Eden et al., 2009). Enrichment p-values were calculated using a Fisher’s exact test and were Benjamini–Hochberg adjusted to obtain a False Discovery Rate (FDR) corrected q value (left). The percentage of genes within a given gene set that scored among the top 100 candidate mediators of sensitisation are shown (right).

A

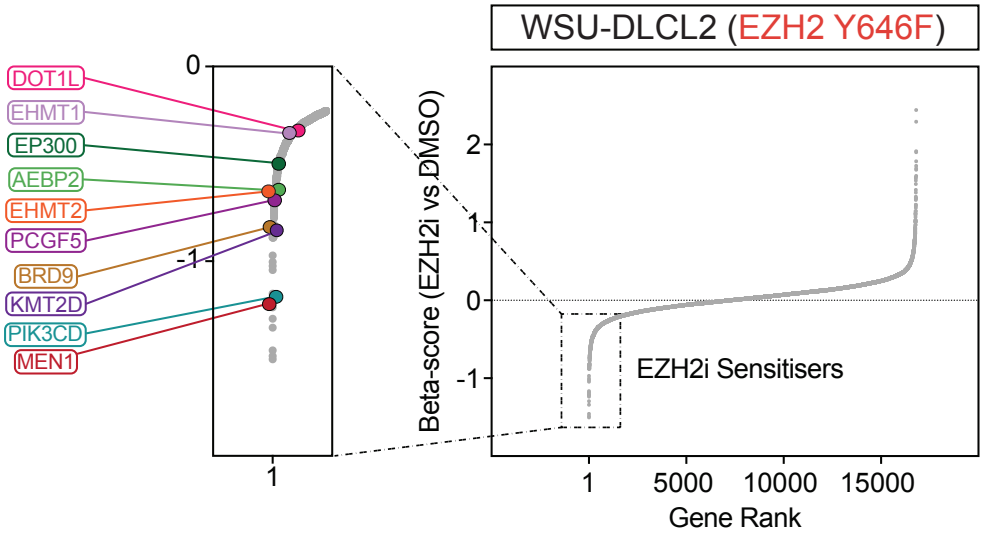
WSU-DLCL2 (EZH2 Y646F)
DOT1L
EHMT1
EP300
AEBP2
EHMT2
PCGF5
BRD9
KMT2D
PIK3CD
MEN1
0
-1
1
Beta-score (EZH2i vs DMSO)
2
1
0
-1
EZH2i Sensitisers
1
5000
10000
15000
Gene Rank

B

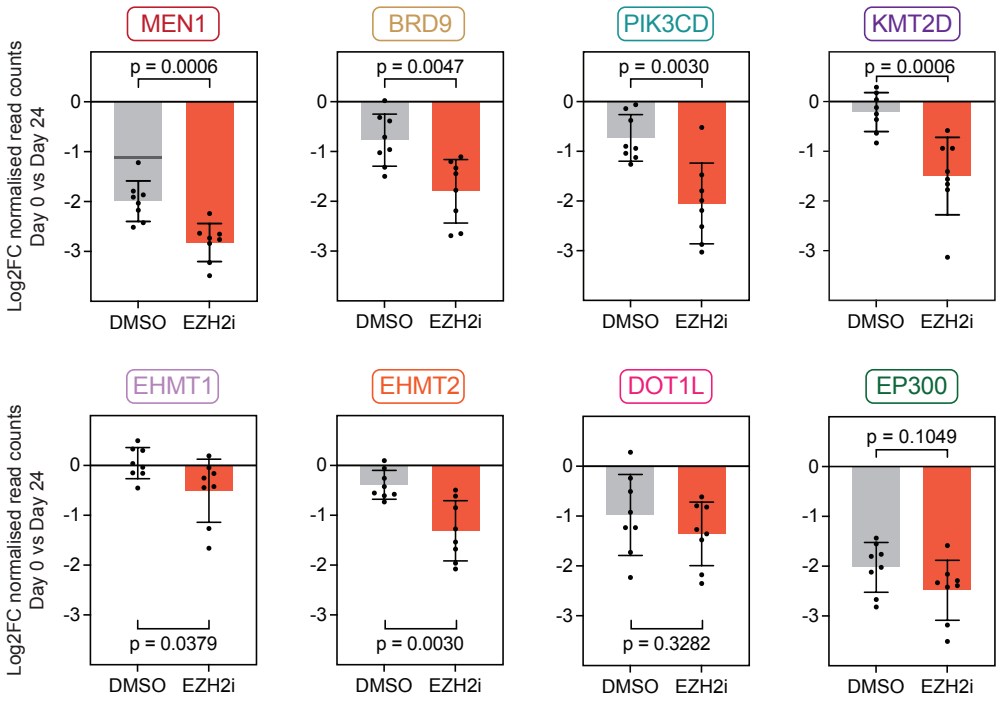
MEN1
BRD9
PIK3CD
KMT2D
EHMT1
EHMT2
DOT1L
EP300
Log2FC normalised read counts
Day 0 vs Day 24
p = 0.0006
p = 0.0047
p = 0.0030
p = 0.0006
p = 0.0379
p = 0.0030
p = 0.3282
p = 0.1049
DMSO
EZH2i

Figure 3.6: EZH2 inhibitor sensitiser genes are enriched for chromatin regulatory genes, many with already existing targeted therapeutics.

A. Genome-wide CRISPR screen data in WSU-DLCL2 lymphoma cells gene ranked based on sgRNA enrichment in low dose EZH2i treatment (Tazemetostat IC_{20}) relative to DMSO control. Differential Beta-score between EZH2i and DMSO conditions calculated using the MAGeCK algorithm (Li et al., 2014). Specific sensitiser genes with pre-existing drug targets are highlighted.

B. Bar charts illustrating log2-fold change of individual sgRNAs relative to T0 from either

Tazemetostat-treated or DMSO-treated cells (p value calculated by Mann-Whitney test).

genes whose loss confer resistance. *AEBP2*, a PRC2.2 accessory component, ranked 71 out of 16,808 genes, identifying it as a strong sensitiser to EZH2 inhibition, alongside two previously characterised sensitizer genes, *MEN1* (7/16,808)(Sparbier et al., 2023) and *DOT1L* (561/16,808)(Nguyen et al., 2025) (**Figure 3.6A**). The only other PRC2 accessory component to score in the screen was the PRC2.1-specific component *MTF2* which, in contrast to *AEBP2*, displayed a moderate resistance phenotype (16,448/16,808). The significance and mechanisms of *AEBP2* dependency in B-cell lymphoma, and its contrast with *MTF2* will be investigated further in Chapter 5. Additionally, I noted frequent chromatin regulatory genes as well as genes with existing drug targets scoring strongly as genetic sensitisers, which I then chose to prioritise in follow up experiments including *BRD9* (32/16,808), *KMT2D* (28/16,808), *EHMT1* (516/16,808), *EHMT2* (68/16,808), *EP300* (157/16,808), and *PIK3CD* (9/16,808)(**Figure 3.6B**).

3.2.7 Dual targeting of BRD9 and PRC2 can enhance the anti-lymphoma efficacy in EZH2-mutant lymphoma cells

I first decided to investigate BRD9, a member of the non-canonical BAF complex (SWI/SNF) of ATP-dependent chromatin remodellers (Bracken et al., 2019). Dr Gerry Brien, a Bracken Lab collaborator, among others have previously shown through similar functional genomics approaches, that degradation of BRD9 is an attractive therapeutic option in synovial sarcoma (Brien et al., 2018; Livingston et al., 2025; McBride et al., 2018). Initially, I performed CRISPR-Cas9 negative selection assays with sgRNAs targeting BRD9 across a number of cancer cell lines. These assays showed variable results with two EZH2-mutant and one EZH2 wild-type lymphoma cell lines being mildly vulnerable to *BRD9* loss, and an MRT cell line also demonstrating sensitivity to BRD9 loss (**Figure 3.7A**), consistent with previous published data (Wang et al., 2019).

Given these findings, a novel PROTAC degrader compound for BRD9, dBRD9-A (courtesy of Dr Brien) was tested in the EZH2-mutant lymphoma context. Immunoblots in WSU-

DLCL2 cells following multiple time course exposures to 100nM dBRD9-A showed significant and sustained protein degradation (**Figure 3.7B**) and protein quantification demonstrated full degradation of BRD9 by dBRD9-A at day 6 (**Figure 3.7C**). Next, cells were treated for 6 days with either 22.5nM Tazemetostat (IC20 dose), 100nM dBRD9-A or a combination of both and cell viability was measured. The BRD9 degrader drug alone had no appreciable effect on EZH2-mutant cell proliferation at 6 days, correlating with the modest effect that BRD9-targeting sgRNAs had on two EZH2-mutant lymphoma cell lines in **Figure 3.7A**. However, validating the EZH2i sensitiser phenotype that BRD9 demonstrated in the CRISPR screen, the combination of dBRD9-A and EZH2i resulted in additive inhibition of cell proliferation over EZH2 inhibitor alone (**Figure 3.7D**).

3.2.8 *EP300* and *DOT1L* are essential in germinal centre lymphoma and appear to be PRC2 co-dependencies more broadly in cancer

While *EP300* and *DOT1L* did not score as strongly as other sensitiser gene hits in the genome-wide CRISPR screens, they were chosen for validation due to the aim at the outset to identify genetic dependencies and sensitisers that possessed existing drug targets. EP300 is a transcriptional co-activator and lysine acetyltransferase that acetylates a broad array of proteins including histones, is recurrently mutated in B-cell lymphoma, and has been suggested to be synthetically lethal with *CREBBP* in *CREBBP*-mutated lymphoma (Meyer et al., 2019; Pasqualucci et al., 2011; Weinert et al., 2018). DOT1L is a histone methyltransferase that catalyses all-methylation of lysine 79 on histone H3 (H3K79me1/2/3), and is aberrantly recruited to KMT2A containing complexes in *KMT2A*-rearranged acute leukaemias (Bernt et al., 2011; Feng et al., 2002; Krivtsov et al., 2008; Ng et al., 2002; Okada et al., 2005). DOT1L inhibitors have been developed for use in *KMT2A*-rearranged leukaemias, but their efficacy has been modest (Daigle et al., 2013; Stein et al., 2018).

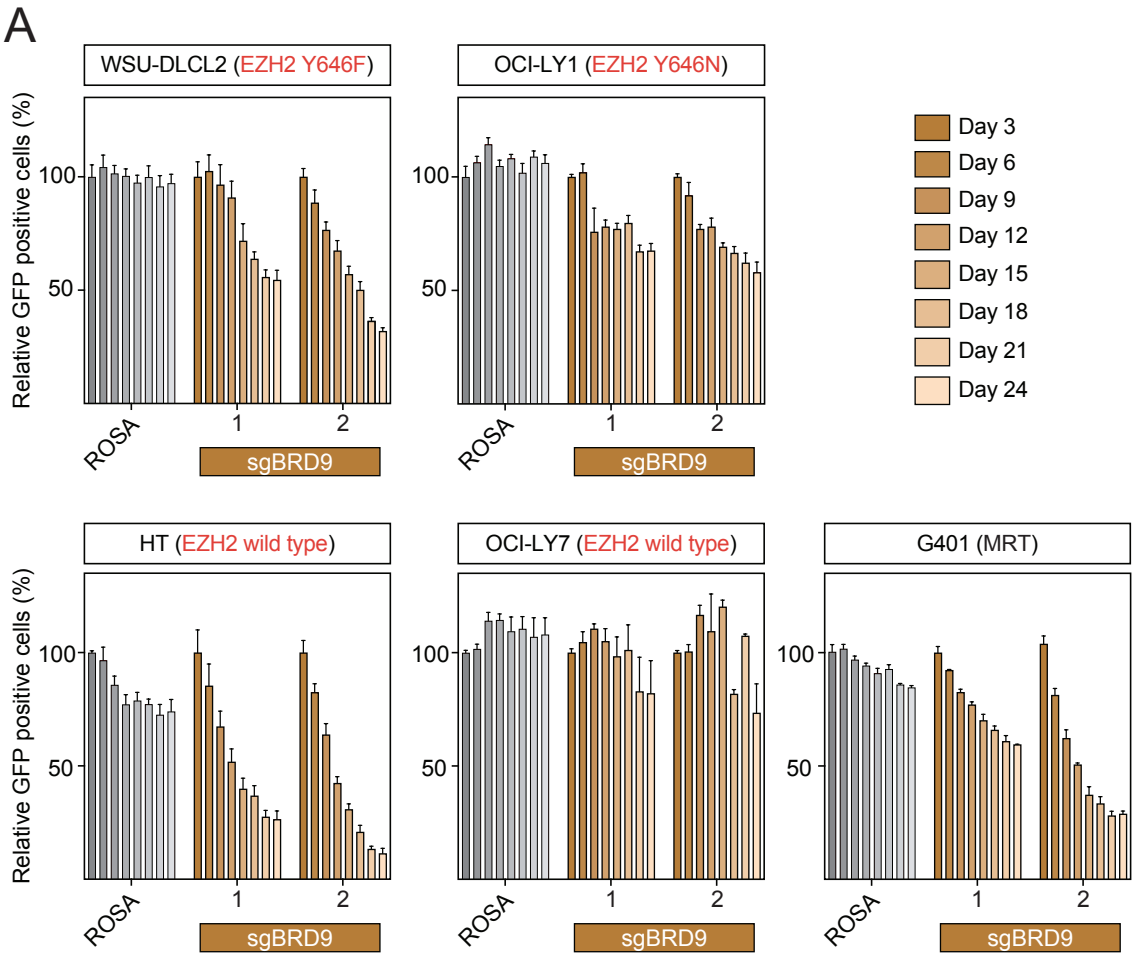
A
WSU-DLCL2 (EZH2 Y646F)
OCI-LY1 (EZH2 Y646N)
HT (EZH2 wild type)
OCI-LY7 (EZH2 wild type)
G401 (MRT)
Relative GFP positive cells (%)
100
50
ROSA
1
2
sgBRD9
Day 3
Day 6
Day 9
Day 12
Day 15
Day 18
Day 21
Day 24

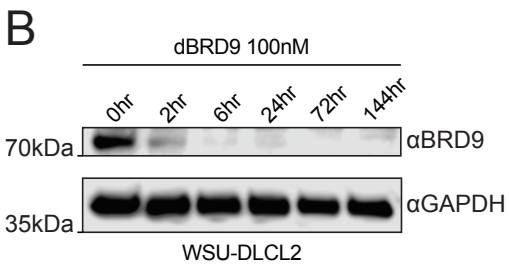
B
dBRD9 100nM
0hr
2hr
6hr
24hr
72hr
144hr
70kDa
αBRD9
35kDa
αGAPDH
WSU-DLCL2

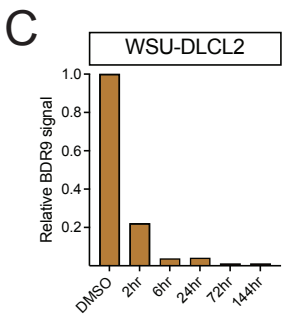
C
WSU-DLCL2
Relative BDR9 signal
1.0
0.8
0.6
0.4
0.2
DMSO
2hr
6hr
24hr
72hr
144hr

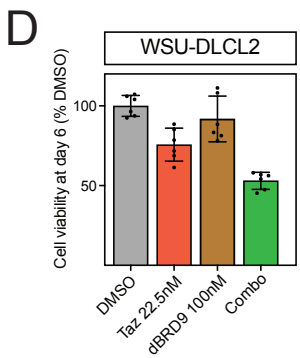
D
WSU-DLCL2
Cell viability at day 6 (% DMSO)
100
50
DMSO
Taz 22.5nM
dBRD9 100nM
Combo

Figure 3.7: Dual targeting of BRD9 and PRC2 can enhance the anti-lymphoma efficacy in EZH2-mutant lymphoma cells.

A.Growth competition assays in the indicated Cas9-expressing cell lines transduced with two independent BRD9-targeting sgRNAs. The relative GFP+ (sgRNA+) percentage is depicted at the indicated time points after transduction (n=4, data represented as mean ± SD).
B. Immunoblots of the indicated proteins in WSU-DLCL2 (EZH2-mutant lymphoma) cells treated with the 100nM of BRD9 degrader (dBRD9).
C. Relative quantification of immunoblot analyses of BRD9 abundance in WSU-DLCL2 (EZH2-mutant lymphoma) cells treated with the 100nM of BRD9 degrader (dBRD9) over the indicated timepoints. Signal intensity values were normalized to the GAPDH loading control.
D. Cell viability data in WSU-DLCL2 (EZH2-mutant lymphoma) cells treated with the indicat-ed compounds over 6 days (n=6, data represented as mean ± SD).

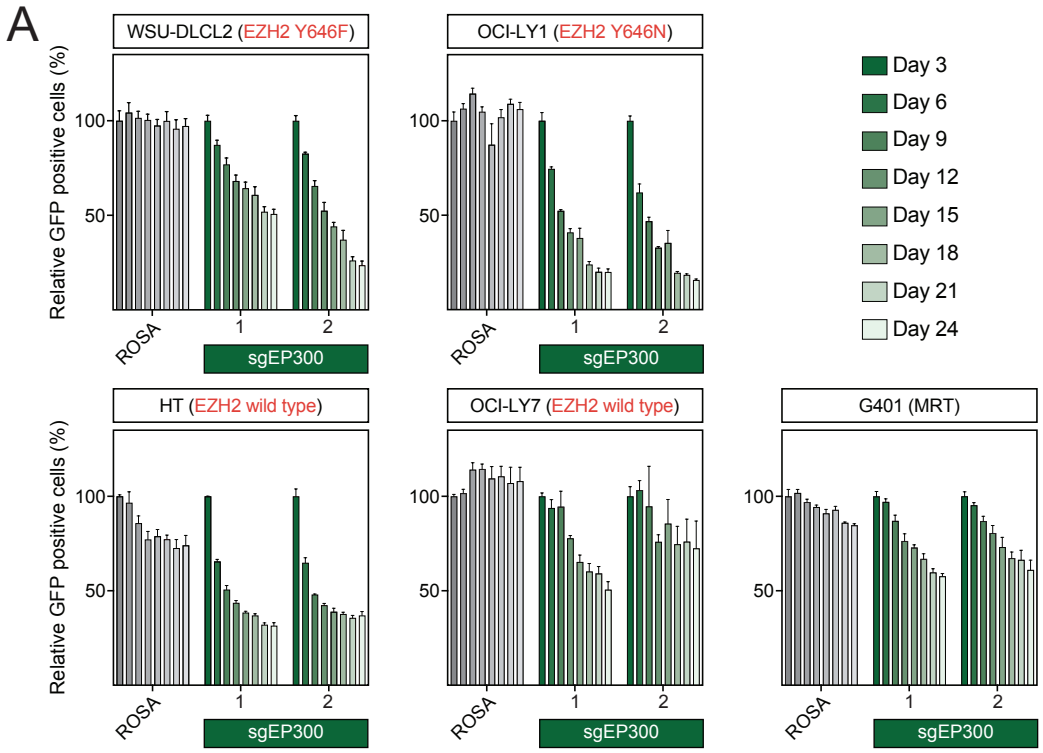
A
WSU-DLCL2 (EZH2 Y646F)
OCI-LY1 (EZH2 Y646N)
HT (EZH2 wild type)
OCI-LY7 (EZH2 wild type)
G401 (MRT)
Relative GFP positive cells (%)
100
50
ROSA
1
2
sgEP300
Day 3
Day 6
Day 9
Day 12
Day 15
Day 18
Day 21
Day 24

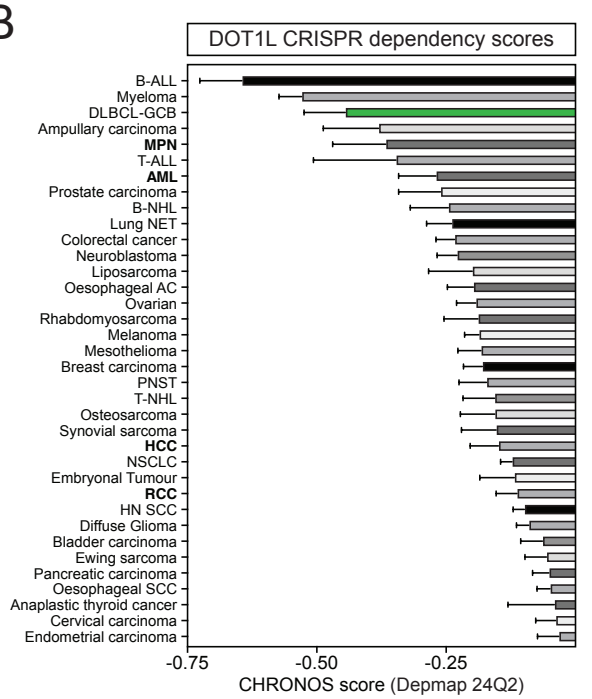
B
DOT1L CRISPR dependency scores
B-ALL
Myeloma
DLBCL-GCB
Ampullary carcinoma
MPN
T-ALL
AML
Prostate carcinoma
B-NHL
Lung NET
Colorectal cancer
Neuroblastoma
Liposarcoma
Oesophageal AC
Ovarian
Rhabdomyosarcoma
Melanoma
Mesothelioma
Breast carcinoma
PNST
T-NHL
Osteosarcoma
Synovial sarcoma
HCC
NSCLC
Embryonal Tumour
RCC
HN SCC
Diffuse Glioma
Bladder carcinoma
Ewing sarcoma
Pancreatic carcinoma
Oesophageal SCC
Anaplastic thyroid cancer
Cervical carcinoma
Endometrial carcinoma
-0.75
-0.50
-0.25
CHRONOS score (Depmap 24Q2)

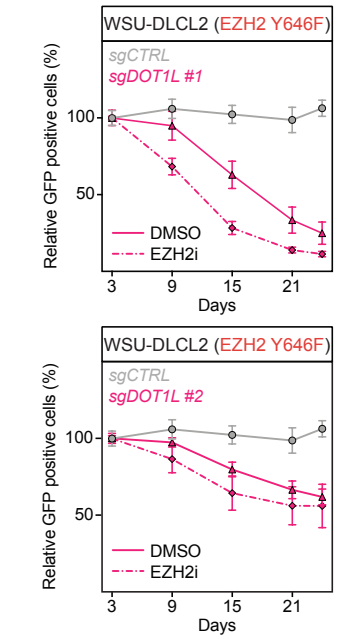
C
WSU-DLCL2 (EZH2 Y646F)
sgCTRL
sgDOT1L #1
Relative GFP positive cells (%)
100
50
DMSO
EZH2i
3
9
15
21
Days
WSU-DLCL2 (EZH2 Y646F)
sgCTRL
sgDOT1L #2
Relative GFP positive cells (%)
100
50
DMSO
EZH2i
3
9
15
21
Days

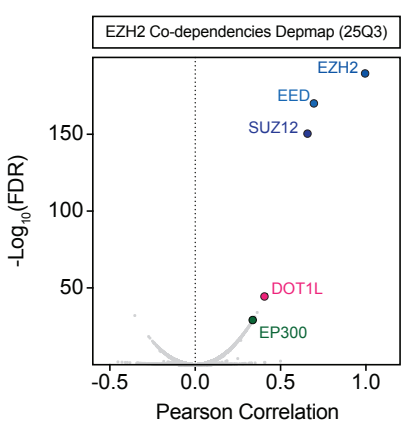
D
EZH2 Co-dependencies Depmap (25Q3)
EZH2
EED
SUZ12
DOT1L
EP300
-Log10(FDR)
150
100
50
-0.5
0.0
0.5
1.0
Pearson Correlation

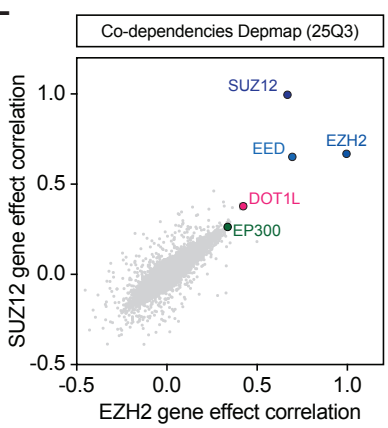
E
Co-dependencies Depmap (25Q3)
SUZ12
EED
EZH2
DOT1L
EP300
SUZ12 gene effect correlation
1.0
0.5
0.0
-0.5
-0.5
0.0
0.5
1.0
EZH2 gene effect correlation

Figure 3.8: *EP300* and *DOT1L* are essential in germinal centre lymphoma and appear to be PRC2 co-dependencies more broadly in cancer.

A. Growth competition assays in the indicated Cas9-expressing cells transduced with two independent *EP300*-targeting sgRNAs. The relative GFP+ (sgRNA+) percentage is depicted at the indicated time points after transduction (n=4, data represented as mean ± SD).

B. CRISPR dependency scores for *DOT1L* in the indicated cancer types based on DepMap CHRONOS score from the DepMap 24Q2 dataset, highlighting germinal centre DLBCL cell lines in green (data represents mean ± SEM).

C. Growth competition assays in Cas9-expressing WSU-DLCL2 (EZH2-mutant lymphoma) transduced with two independent sgRNAs targeting *DOT1L* followed by treatment with low dose EZH2i (Tazemetostat) (n=3, data represents mean ± SD).

D. *EZH2* co-dependencies derived from the gene effect scores of genome scale CRISPR screens in 1087 cancer cell lines in the Cancer Dependency Map (DepMap - https://depmap.org/portal/). The plot displays correlation between *EZH2* gene effect score and all other genes (calculated using Pearson's correlation coefficient). Core PRC2 are highlighted in blue, while *DOT1L* and *EP300* are highlighted in pink and green respectively.

E. *EZH2* and *SUZ12* co-dependencies derived from the gene effect scores of genome scale CRISPR screens in 1087 cancer cell lines in the Cancer Dependency Map (DepMap - https://depmap.org/portal/). The plot displays correlation between *EZH2* and *SUZ12* gene effect scores (calculated using Pearson's correlation coefficient). Core PRC2 are highlighted in blue, while *DOT1L* and *EP300* are highlighted in pink and green respectively.

Negative selection assays with sgRNAs targeting *EP300* demonstrated significant depletion in EZH2-mutant lymphoma cells (**Figure 3.8A**). Moving to *DOT1L*, germinal centre DLBCL cell lines were the third most dependent cancer type on this gene in DepMap, with the first and second most dependent cancer types being B-cell acute lymphoblastic leukaemia (B-ALL) and multiple myeloma, highlighting the B-cell malignancy tropism for *DOT1L* dependency (**Figure 3.8B**). Negative selection assays with sgRNAs targeting *DOT1L* in EZH2-mutant lymphoma cells treated with Tazemetostat further strengthened the finding of *DOT1L* as an EZH2i sensitiser in this context (**Figure 3.8C**). Turning back to the Cancer Dependency Map, *EZH2* genetic co-dependencies were calculated, with *EED* and *SUZ12* expectedly having the strongest correlation with *EZH2* gene scores given they are all contained in the same complex. Strikingly however, *EP300* and *DOT1L* were amongst the strongest *EZH2* co-dependencies across all genes and all cancer types (**Figure 3.8D**). As an orthogonal validation, *SUZ12* and *EZH2* co-dependencies were plotted on opposite axes, and again *DOT1L* and *EP300* were observed as equally co-dependent on both *SUZ12* and *EZH2* (**Figure 3.8E**).

3.2.9 Dual targeting of PRC2 and the PI3K pathway may enhance efficacy in certain diffuse large B-cell lymphoma subtypes

PIK3CD, a key component in the B-cell signalling pathway, and associated with B-cell lymphoma (Clayton et al., 2002; Okkenhaug et al., 2002; Srinivasan et al., 2009; Zhang et al., 2013), was noted to be a strong EZH2i sensitiser irrespective of *EZH2* mutation status. I attempted to validate these findings across a panel of cell lines exposed to *PIK3CD*-targeting sgRNAs in negative selection assays. Response to *PIK3CD* depletion was variable among lymphoma subtypes, but MRT cells appeared to be insensitive to its loss (**Figure 3.9A**). Next, to validate *PIK3CD* as an EZH2i sensitiser, negative selection assays +/- the EZH2 inhibitor Tazemetostat were performed and demonstrated that KO of *PIK3CD* sensitises WSU-DLCL2 and HT cells to EZH2 inhibitors (**Figure 3.9B**). Given that PI3K inhibitors are licensed for use in relapsed/refractory follicular lymphoma, it was logical to

then test a number of lymphoma cell lines with a combination of the PI3K inhibitor Idelalisib and Tazemetostat. A range of idelalisib doses were combined with 17nM Tazemetostat and cell viability was assessed after 5 days of treatment. While WSU-DLCL2, showed a clear additive effect in the PI3K and EZH2 inhibitor condition, this effect was not replicated in the other lymphoma cell lines. These findings may represent a cell line artefact in the WSU-DLCL2 cell line, but more likely reflect the significant differences in mechanisms of action between signalling pathway inhibitors such as PI3Kinase inhibitors and EZH2 inhibitors, the latter possessing a much longer onset of action in cells. A wider range of lower Idelalisib doses for a longer time course experiment e.g. 24 days would likely be necessary to identify a signal for EZH2i sensitisation by pharmacological assays.

3.2.10 *EHMT2* loss sensitises lymphoma cells to EZH2 inhibition

The genome-wide CRISPR screen interestingly highlighted the H3K9 methyltransferase EHMT2 (or G9A) as an EZH2 inhibitor sensitiser, but not as a genetic dependency in the germinal centre lymphoma context. EHMT2, and its paralog EHMT1, contribute to H3K9me1 and H3K9me2, histone post-translational modifications associated with constitutive heterochromatin at specific regions of the genome such as telomeres and centromeres (Mozzetta et al., 2014; Ogawa et al., 2002; Trojer & Reinberg, 2007; Wang et al., 2025). The idea of treating cancer cells with dual EZH2 and EHMT2 inhibition, to fully de-repress abnormally silenced gene expression programs has been evaluated (Curry et al., 2015; Liu et al., 2009; Vedadi et al., 2011). Using negative selection assays with sgRNAs targeting *EHMT2*, I saw minimal depletion in lymphoma cells (**Figure 3.10A**). This may be a real finding or could point to possible compensation from the paralog *EHMT1*. Following this I repeated negative selection assays in the presence of Tazemetostat and interestingly, in EZH2-mutant lymphoma cells, while DMSO treated cells remained relatively stable in the presence of sgRNA targeting *EHMT2*, cells exposed to EZH2 inhibition showed significant depletion (**Figure 3.10B**). Using an EHMT2 methyltransferase inhibitor (UNC0642) in isolation or in combination with an EZH2 inhibitor, I observed an additive effect on cell viability in 3 of 6 lymphoma cells (**Figure 3.10C**).

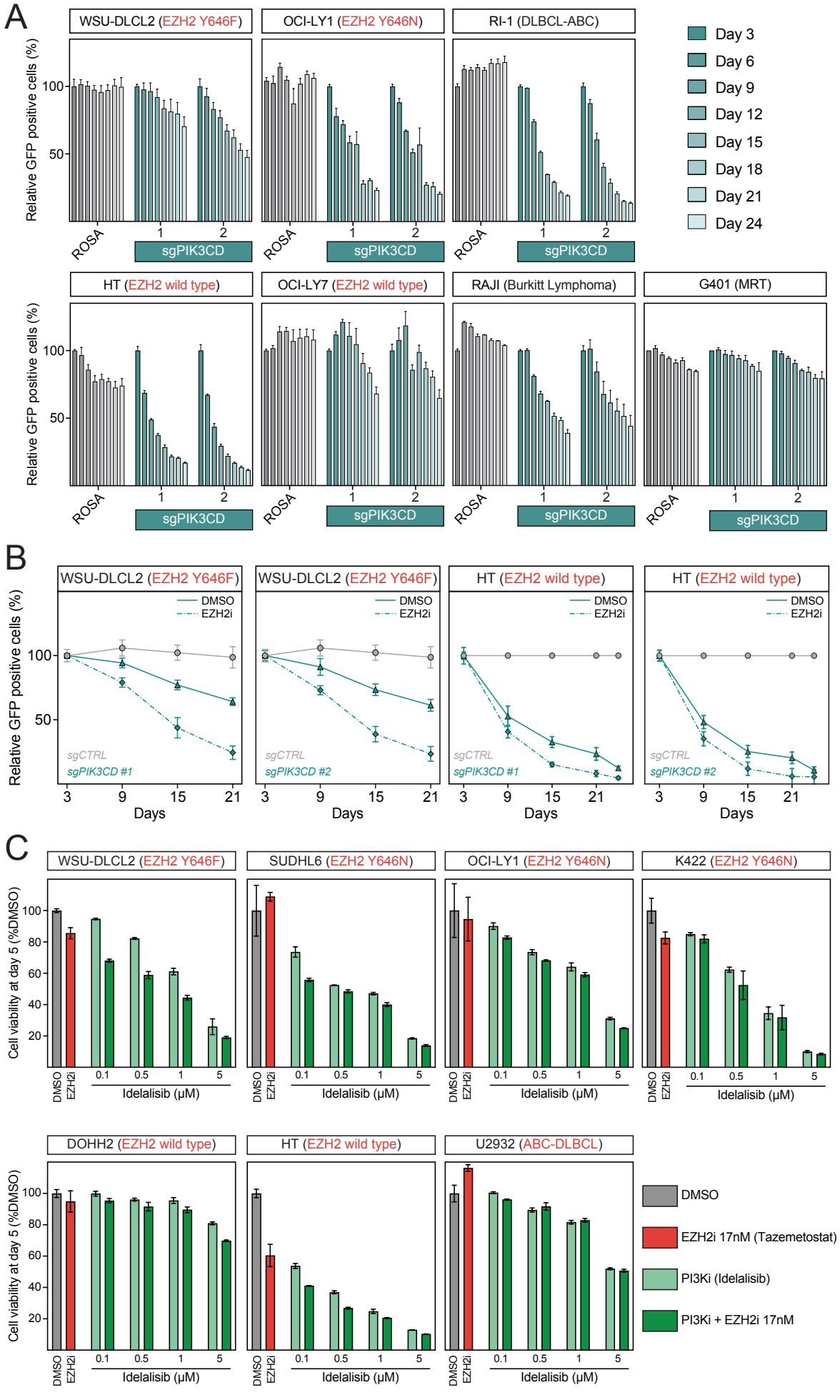
A
WSU-DLCL2 (EZH2 Y646F)
OCI-LY1 (EZH2 Y646N)
RI-1 (DLBCL-ABC)
HT (EZH2 wild type)
OCI-LY7 (EZH2 wild type)
RAJI (Burkitt Lymphoma)
G401 (MRT)
Relative GFP positive cells (%)
ROSA
sgPIK3CD
Day 3
Day 6
Day 9
Day 12
Day 15
Day 18
Day 21
Day 24
B
WSU-DLCL2 (EZH2 Y646F)
HT (EZH2 wild type)
DMSO
EZH2i
sgCTRL
sgPIK3CD #1
sgPIK3CD #2
Days
C
WSU-DLCL2 (EZH2 Y646F)
SUDHL6 (EZH2 Y646N)
OCI-LY1 (EZH2 Y646N)
K422 (EZH2 Y646N)
DOHH2 (EZH2 wild type)
HT (EZH2 wild type)
U2932 (ABC-DLBCL)
Cell viability at day 5 (%DMSO)
Idelalisib (μM)
DMSO
EZH2i 17nM (Tazemetostat)
PI3Ki (Idelalisib)
PI3Ki + EZH2i 17nM

Figure 3.9: Dual targeting of PRC2 and the PI3K pathway may enhance efficacy in certain diffuse large B-cell lymphoma subtypes.
A. Growth competition assays in the indicated Cas9-expressing cell lines transduced with two independent PIK3CD-targeting sgRNAs. The relative GFP+ (sgRNA+) percentage is depicted at the indicated time points after transduction (n=4, data represents mean ± SD).
B. Growth competition assays in the indicated Cas9-expressing lymphoma cells transduced with two independent sgRNAs targeting PIK3CD followed by treatment with low dose EZH2i (Tazemetostat) (n=3, data represents mean ± SD).
C. Cell viability data in the indicated lymphoma cells treated with the indicated compounds over 5 days (n=3, data represents mean ± SD).

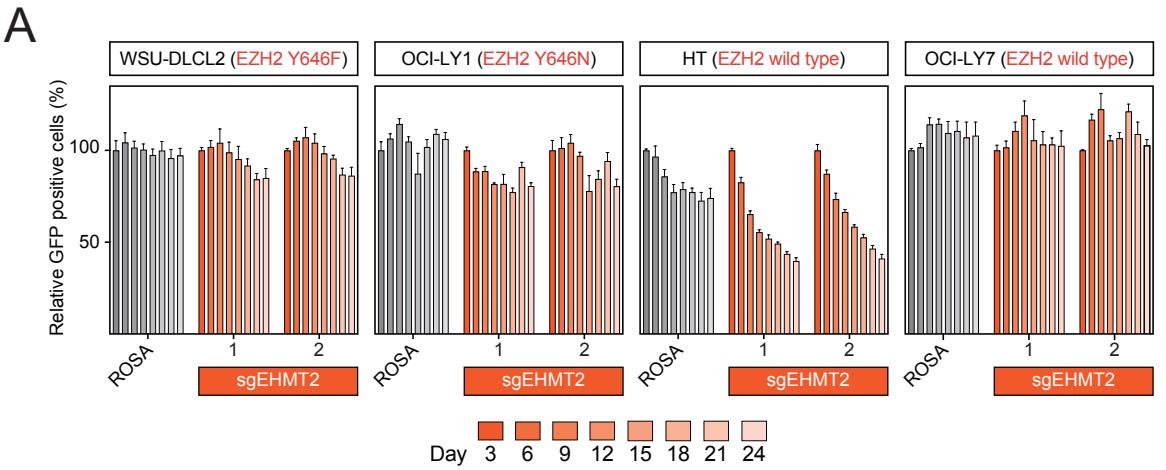
A
WSU-DLCL2 (EZH2 Y646F)
OCI-LY1 (EZH2 Y646N)
HT (EZH2 wild type)
OCI-LY7 (EZH2 wild type)
Relative GFP positive cells (%)
100
50
ROSA
1
2
sgEHMT2
Day 3 6 9 12 15 18 21 24

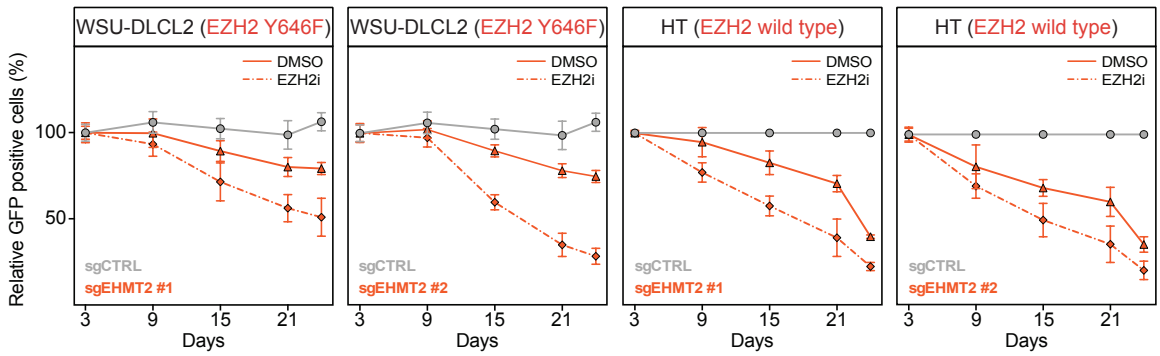
B
WSU-DLCL2 (EZH2 Y646F)
WSU-DLCL2 (EZH2 Y646F)
HT (EZH2 wild type)
HT (EZH2 wild type)
DMSO
EZH2i
Relative GFP positive cells (%)
100
50
sgCTRL
sgEHMT2 #1
sgEHMT2 #2
3 9 15 21
Days

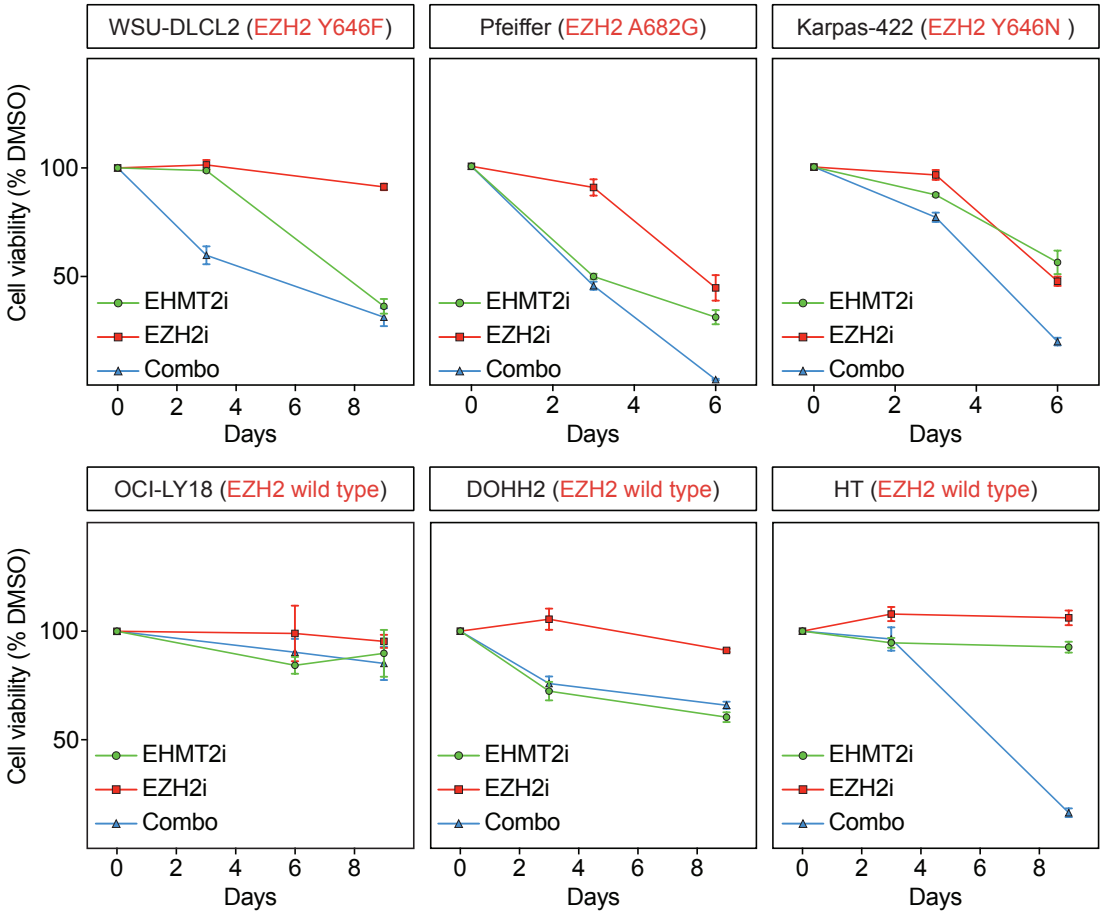
C
WSU-DLCL2 (EZH2 Y646F)
Pfeiffer (EZH2 A682G)
Karpas-422 (EZH2 Y646N)
OCI-LY18 (EZH2 wild type)
DOHH2 (EZH2 wild type)
HT (EZH2 wild type)
Cell viability (% DMSO)
100
50
EHMT2i
EZH2i
Combo
0 2 4 6 8
Days

Figure 3.10: *EHMT2* loss sensitises lymphoma cells to EZH2 inhibition.
A. Growth competition assays in the indicated Cas9-expressing cell lines transduced with two independent *EHMT2*-targeting sgRNAs. The relative GFP+ (sgRNA+) percentage is depicted at the indicated time points after transduction (n=4, data represents mean ± SD).
B. Growth competition assays in the indicated Cas9-expressing lymphoma cells transduced with two independent sgRNAs targeting *EHMT2* followed by treatment with low dose EZH2i (Tazemetostat) (n=3, data represents mean ± SD).
C. Cell viability data in the indicated lymphoma cells treated with the indicated compounds over 5 days (n=3, data represents mean ± SD).

3.2.11 *MEN1* is a specific genetic dependency in germinal centre B-cell lymphoma

During this PhD research project, two high profile research papers were published that described the synergism and interplay between the KMT2A scaffold protein Menin and PRC2 (Chen et al., 2023; Sparbier et al., 2023). Given the fact that Menin inhibitors have been developed over the past 10 years for *KMT2A*-rearranged acute leukaemias, this represents an optimal opportunity to repurpose an existing targeted therapy for a new indication, namely B-cell lymphoma. To validate the CRISPR screen results of *MEN1* being one of the strongest EZH2 inhibitor sensitiser genes, negative selection assays were performed for *MEN1* sgRNAs which demonstrated strong depletion in both EZH2-mutant, EZH2 wild-type and Burkitt lymphomas, but not in a melanoma cell or an activated B-cell subtype of DLBCL (**Figure 3.11A**). Next, I further validated this finding with data from DepMap showing that germinal centre B-cell lymphomas were the most dependent cancer type on *MEN1*, and that the absolute median CHRONOS scores for DLBCL-GCB cell lines was very strong, approximately that of pan essential genes (**Figure 3.11B**). Using publicly available expression data, *MEN1* expression was strongest in EZH2-mutant lymphoma, but also significantly higher in germinal centre B-cell lymphoma cell lines over other cancer types (**Figure 3.11C**). I then performed immunoblots to demonstrate that Menin and KMT2A are ubiquitously expressed at the protein level across a panel of B-cell lymphoma cell lines (**Figure 3.11D**).

3.2.12 *MEN1* is an EZH2 co-dependency but menin does not physically associate with PRC2

In the previous section I confirmed that *MEN1* is a dependency in germinal centre B-cell lymphoma, as well as other B-cell malignancies, that it is ubiquitously expressed in lymphoma cells and that its expression is correlated with *EZH2* mutation status. Next, I sought to validate *MEN1* as a specific EZH2 inhibitor sensitiser in B-cell lymphoma. Firstly,

I performed negative selection assays with sgRNAs targeting *MEN1* with or without Tazemetostat. These assays confirmed that *MEN1* loss acts as a sensitiser to PRC2 inhibitors in EZH2-mutant lymphoma (**Figure 3.12A**). To describe where Menin is located within the cell, I performed subcellular fractionations in *EZH2* and *MEN1* knockout cells and observed, expectedly, that Menin is primarily found in the insoluble chromatin-bound fraction, and that *MEN1* knockout did not alter EZH2 levels (**Figure 3.12B**). Given the observed synergy between Menin and EZH2, I questioned whether there was any physical contact between PRC2 and Menin. I performed endogenous co-immunoprecipitations of Menin and EED, and while Menin co-immunoprecipitated KMT2A as expected, it did not appear to interact with PRC2 (**Figure 3.12C**). Of note, this immunoblot possessed a number of presumed background bands, therefore, as an orthogonal validation, SUZ12 co-immunoprecipitations followed by mass spectrometry (IPMS) were performed later in this doctoral research project and will be discussed in Chapter 5.

I then performed an orthogonal pharmacological validation of this sensitiser effect, by combining the recently FDA approved Menin inhibitor Revumenib with Tazemetostat and demonstrated that dual therapy enhanced the anti-lymphoma efficacy in both EZH2-mutant and EZH2 wild-type lymphoma cells (**Figure 3.12D**). Further validation combining PRC2 inhibitor with genetic CRISPR-mediated *MEN1* or *EZH2* knockout confirmed the synergy between *MEN1* loss and EZH2 inhibition (**Figure 3.12E**). Finally, to look at the co-dependency between *MEN1* and PRC2 in an unbiased way, *MEN1* co-dependencies from DepMap were plotted. As expected, known COMPASS complex members *KMT2A*, *DOT1L* and *LEDGF* were the strongest co-dependencies, however strikingly, core PRC2 members were among the next strongest *MEN1* co-dependencies, highlighting the broader significance of this relationship in cancer (**Figure 3.12F**). The model for PRC2 and *MEN1* synergy is illustrated (**Figure 3.12G**).

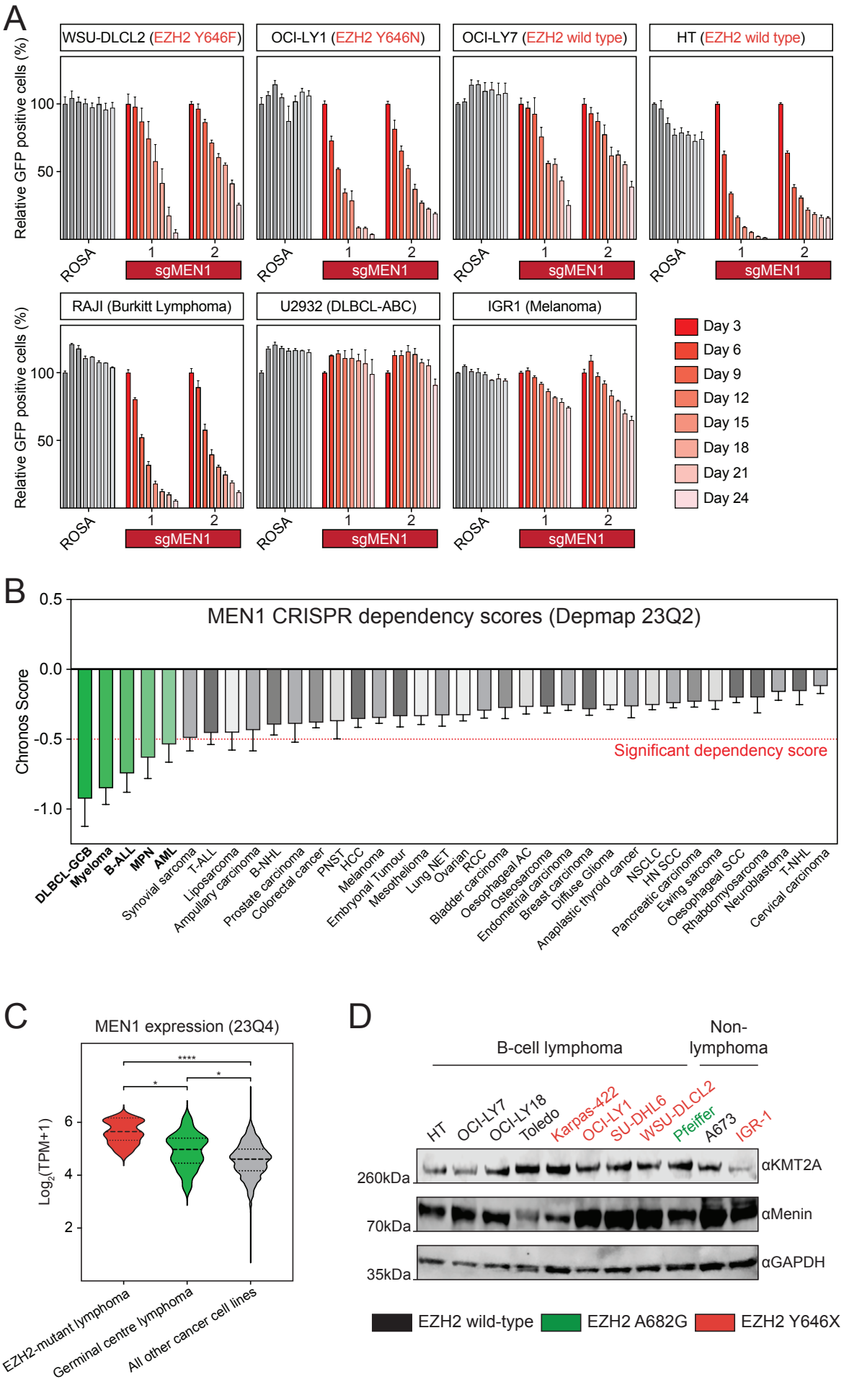
A
WSU-DLCL2 (EZH2 Y646F)
OCI-LY1 (EZH2 Y646N)
OCI-LY7 (EZH2 wild type)
HT (EZH2 wild type)
RAJI (Burkitt Lymphoma)
U2932 (DLBCL-ABC)
IGR1 (Melanoma)
Relative GFP positive cells (%)
100
50
ROSA
1
2
sgMEN1
Day 3
Day 6
Day 9
Day 12
Day 15
Day 18
Day 21
Day 24
B
MEN1 CRISPR dependency scores (Depmap 23Q2)
Chronos Score
0.5
0.0
-0.5
-1.0
Significant dependency score
DLBCL-GCB
Myeloma
B-ALL
MPN
AML
Synovial sarcoma
T-ALL
Liposarcoma
Ampullary carcinoma
B-NHL
Prostate carcinoma
Colorectal cancer
PNST
HCC
Melanoma
Embryonal Tumour
Mesothelioma
Lung NET
Ovarian
RCC
Bladder carcinoma
Oesophageal AC
Osteosarcoma
Endometrial carcinoma
Breast carcinoma
Diffuse Glioma
Anaplastic thyroid cancer
NSCLC
HN SCC
Pancreatic carcinoma
Ewing sarcoma
Oesophageal SCC
Rhabdomyosarcoma
Neuroblastoma
T-NHL
Cervical carcinoma
C
MEN1 expression (23Q4)
Log2(TPM+1)
6
4
2
****
*
*
EZH2-mutant lymphoma
Germinal centre lymphoma
All other cancer cell lines
D
B-cell lymphoma
Non-lymphoma
HT
OCI-LY7
OCI-LY18
Toledo
Karpas-422
OCI-LY1
SU-DHL6
WSU-DLCL2
Pfeiffer
A673
IGR-1
260kDa
70kDa
35kDa
αKMT2A
αMenin
αGAPDH
EZH2 wild-type
EZH2 A682G
EZH2 Y646X

Figure 3.11: *MEN1* is a specific genetic dependency in germinal centre B-cell lymphoma.

A. Growth competition assays in the indicated Cas9-expressing cell lines transduced with two independent *MEN1*-targeting sgRNAs. The relative GFP+ (sgRNA+) percentage is depicted at the indicated time points after transduction (n=4, data represents mean ± SD).

B. CRISPR dependency scores for *MEN1* in the indicated cancer types derived from the gene effect scores of genome scale CRISPR screens in 1087 cancer cell lines in the Cancer Dependency Map (DepMap - https://depmap.org/portal/)(24Q2 dataset). Cancer types in which the mean gene effect score is ≤ -0.5 are highlighted in green.

C. mRNA expression in the indicated cancer types derived from RNA-seq across 1087 cancer cell lines in the Cancer Dependency Map (DepMap - https://depmap.org/portal/)(23Q4 dataset) Values are log_2-transformed TPM + 1.

D. Immunoblots of the indicated proteins in the indicated cell lines. Cell lines are colour-coded based on EZH2 mutation status.

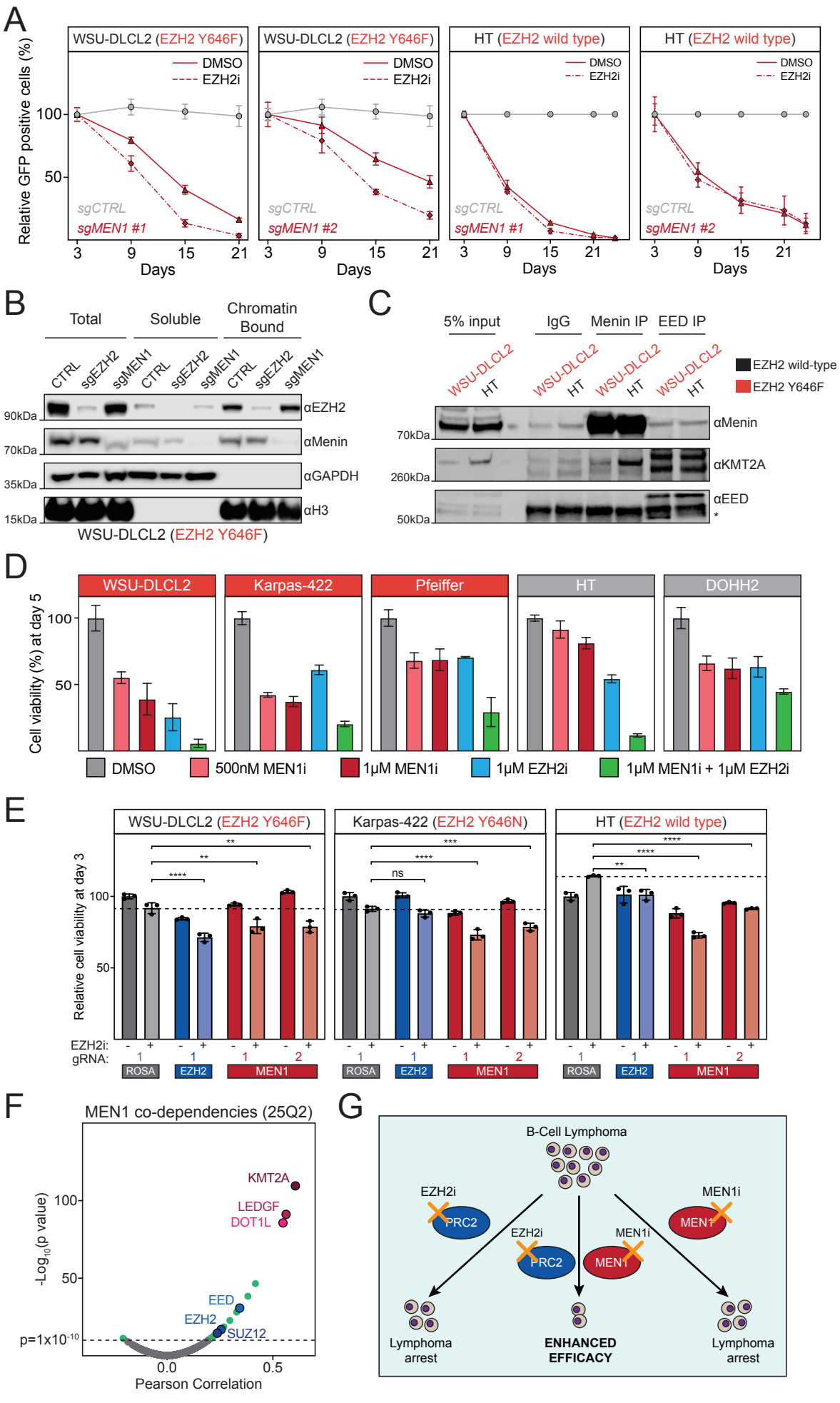
A
WSU-DLCL2 (EZH2 Y646F)
WSU-DLCL2 (EZH2 Y646F)
HT (EZH2 wild type)
HT (EZH2 wild type)
DMSO
EZH2i
Relative GFP positive cells (%)
100
50
sgCTRL
sgMEN1 #1
sgMEN1 #2
3
9
15
21
Days
B
Total
Soluble
Chromatin Bound
CTRL
sgEZH2
sgMEN1
90kDa
70kDa
35kDa
15kDa
αEZH2
αMenin
αGAPDH
αH3
WSU-DLCL2 (EZH2 Y646F)
C
5% input
IgG
Menin IP
EED IP
WSU-DLCL2
HT
EZH2 wild-type
EZH2 Y646F
70kDa
260kDa
50kDa
αMenin
αKMT2A
αEED
*
D
WSU-DLCL2
Karpas-422
Pfeiffer
HT
DOHH2
Cell viability (%) at day 5
100
50
DMSO
500nM MEN1i
1μM MEN1i
1μM EZH2i
1μM MEN1i + 1μM EZH2i
E
WSU-DLCL2 (EZH2 Y646F)
Karpas-422 (EZH2 Y646N)
HT (EZH2 wild type)
Relative cell viability at day 3
100
50
**
****
***
ns
EZH2i:
gRNA:
ROSA
EZH2
MEN1
F
MEN1 co-dependencies (25Q2)
-Log10(p value)
100
50
p=1x10-10
KMT2A
LEDGF
DOT1L
EED
EZH2
SUZ12
0.0
0.5
Pearson Correlation
G
B-Cell Lymphoma
EZH2i
MEN1i
PRC2
MEN1
Lymphoma arrest
ENHANCED EFFICACY
Lymphoma arrest

Figure 3.12: *MEN1* is an EZH2 co-dependency but menin does not physically associate with PRC2.

A. Growth competition assays in the indicated Cas9-expressing lymphoma cells transduced with two independent sgRNAs targeting MEN1 followed by treatment with low dose EZH2i (Tazemetostat) (n=3, data represents mean ± SD).

B. Immunoblots of the indicated proteins following subcellular fractionation in WSU-DLCL2 (EZH2-mutant lymphoma) cells transduced with sgRNAs targeting EZH2, MEN1 or control (ROSA26).

C. Immunoblots of the indicated proteins following endogenous co-immunoprecipitations of EED and Menin in the indicated lymphoma cell lines. Cell lines are colour-coded based on EZH2 mutation status. The * indicates the IgG background band.

D. Cell viability data in the indicated lymphoma cells treated with Menin inhibitor (Revumenib), EZH2i (Tazemetostat), or a combination of both over 5 days (n=3, data represents mean ± SD). EZH2-mutant lymphoma cell lines are indicated in red, with EZH2 wild-type cell lines indicated in grey.

E. Cell viability data in the indicated lymphoma cells treated with EZH2i 250nM (Tazemetostat) and the indicated sgRNAs over 3 days (n=3, data represents mean ± SD). Significance determined by ordinary three-way ANOVA with Tukey's multiple comparison test, *p value ≤ 0.05, **p value ≤ 0.01, ***p value ≤ 0.001, ****p value ≤ 0.0001.

F. MEN1 co-dependencies derived from the gene effect scores of genome scale CRISPR screens in 1087 cancer cell lines in the Cancer Dependency Map (Depmap - https://depmap.org/portal/). The plot displays correlation between the gene effect scores of MEN1 compared to all other genes (calculated using Pearson's correlation coefficient). Core PRC2 are highlighted in blue, while DOT1L, KMT2A and LEDGF are highlighted in purple. Co-dependent genes with a p value < $1x10^{-10}$ are also highlighted in green.

G. Model demonstrating how dual MEN1 and PRC2 loss results in enhanced efficacy in B-cell lymphoma.

3.3 Discussion

In this Chapter I have validated a number of recently discovered EZH2 inhibitor sensitisers including *DOT1L* (Göbel et al., 2025; Nguyen et al., 2025) and *MEN1* (Chen et al., 2023; Sparbier et al., 2023). I have described a novel germinal centre B-cell lymphoma dependency on *CARM1* which is targetable with an effective small molecule inhibitor. Finally, I've demonstrated a number of previously uncharacterised EZH2i sensitisers including *EP300*, *BRD9*, *EHMT2*/*G9A*, and *PIK3CD*, all of which possess available targeted agents and should be prioritised for further study.

The aim of this chapter was to identify novel targetable genes and pathways in germinal centre lymphoma cells. *EP300* is a histone acetyltransferase which, together with *CREBBP*, is recurrently mutated in B-cell lymphoma (Pasqualucci et al., 2011). *EP300* and *CREBBP* mutations in B-cell lymphoma are inactivating, which traditionally rendered them challenging to target therapeutically. However, a recent report has described a novel histone acetyltransferase activator as a way of targeting these mutations (Liu et al., 2025). This study demonstrated efficacy in *EZH2*-mutated B-cell lymphoma cell lines as well as in mouse models, and consideration should be given to studying the effects of this acetyltransferase activator in combination with PRC2 inhibition in B-cell lymphoma. Furthermore, EP300 is a substrate for CARM1, which it has also been suggested to interact with (An et al., 2004; Lee et al., 2005; Xu et al., 2001). Further study of the relationship between *CARM1* dependency and *EP300*-*EZH2* co-dependency in B-cell lymphoma could uncover novel insights into the specific chromatin vulnerabilities in these lymphomas. Interestingly, SMARCC1 is a known substrate of CARM1 (L. Wang et al., 2014; Wang & Roberts, 2014). Given the frequency of SWI/SNF mutations in germinal centre lymphomas and their contribution towards lymphomagenesis, further study of CARM1 in lymphoma should focus on the interplay between SWI/SNF components and CARM1 at specific genomic loci.

Turning to *MEN1* and repurposing Menin inhibitors for B-cell lymphoma. The *MEN1* co-dependency analysis confirmed *KMT2A*, *LEDGF* and *DOT1L*, as the top co-dependencies across all cancers. This most likely represents the strong signal from the known co-dependency on this COMPASS complex in *KMT2A*-rearranged acute leukaemia (Soto-Feliciano et al., 2023; Yokoyama et al., 2005). However, core PRC2 were among the top 20 *MEN1* co-dependencies in analyses in this PhD research project. Given the recently published compelling clinical data for Menin inhibitors in acute leukaemia (Arellano et al., 2025; Issa et al., 2023; Issa et al., 2025; Wang et al., 2024), and the fact that our research project represents the third independent group describing the strong co-dependency between *MEN1* and PRC2 (Chen et al., 2023; Sparbier et al., 2023), Menin inhibitors should now be tested in pre-clinical translational models of B-cell lymphoma xenografts in combination with PRC2 inhibitors.

Finally, *PIK3CD* as an EZH2i sensitiser gene hit is an interesting candidate for further development. *PIK3CD* encodes a kinase involved in the Akt signalling pathway (Manning & Toker, 2017). Small molecule PI3kinase inhibitors are reserved for patients with relapsed/refractory follicular lymphoma, and while effective at inducing remissions, are often associated with significant immune-mediated side effects including colitis, pneumonitis and life-threatening infections, limiting their use (Cheah & Fowler, 2016; Gopal et al., 2014; Gopal et al., 2017). EZH2 inhibitors may de-repress gene programs that make lymphoma cells more dependent on *PIK3CD*, and thus more susceptible to PI3K inhibition. Given *PIK3CD* scored within the top 10 Tazemetostat sensitisers, this relationship warrants further exploration and follow up.

In this chapter I have generated a genome-wide repository for genetic dependencies and EZH2 inhibitor sensitisers in B-cell lymphoma. These results have already helped multiple other members in the lab studying other PRC2-dependent cancers such as H3K27M-diffuse midline glioma. By comparing results of CRISPR screens in different cell lines, we can begin to form rational co-dependency maps that may be universal across cancer types, or unique

to specific cancer contexts. In the next chapter I will move on to focus on mechanisms of resistance to EZH2 inhibitors in germinal centre B-cell lymphoma in an effort to identify ways of mitigating resistance to these agents in patients.

CHAPTER 4

Loss of *NSD1* or *NSD2* Contributes to EZH2 Inhibitor Resistance Through Modulation of the H3K27-H3K36 Methylation Axis

4.1 Introduction

As well as identifying genetic sensitisers to the chosen therapy, CRISPR-Cas9 screens have also been used to identify genetic mediators of resistance (Doench et al., 2016; Drosos et al., 2022; Li et al., 2020; Patil et al., 2019). By treating Cas9-expressing lymphoma cells with EZH2 inhibitor, genes that become enriched throughout the CRISPR screen are likely those whose loss, or mutation, confer a survival advantage to the lymphoma cells over healthy cells. The rationale behind identifying genetic resisters is two-fold:

(i) To predict specific cellular pathways that may mediate resistance. In the example of this PhD research chapter, I wanted to predict patients unlikely to respond to PRC2 inhibition due to loss-of-function mutations in specific genes. EZH2 inhibitors could be avoided in these patients, representing an advance in precision oncology strategies in germinal centre B-cell lymphoma.

(ii) If a mutation is identified in a histone 'writer' protein that leads to EZH2 inhibitor resistance, a pharmacological inhibitor to the corresponding 'eraser' protein could restore functional levels of the specific histone PTM and may be able to prevent resistance in patients at the outset when treated with EZH2 inhibitors.

Clinical resistance to drugs targeting chromatin regulatory proteins have only recently been described. In a clinical trial evaluating menin inhibitors in patients with acute leukaemia, mutations in the *MEN1* gene that inhibit binding of the drug to the menin protein were enriched in ~39% of patients, leading to drug resistance by rescuing the aberrant pro-leukaemic gene expression profile seen in these patients (Perner et al., 2023). However, mutations in chromatin regulatory proteins other than the drug target, that bring about resistance *in vitro* or *in vivo*, have not yet been described.

4.1.1 NSD protein structure and function

The Nuclear receptor SET Domain (NSD) family of histone methyltransferases; NSD1, NSD2 and NSD3, function to mono- and di-methylate lysine 36 on histone H3 (H3K36) (Angrand et al., 2001; Huang et al., 1998; Kurotaki et al., 2001; Rayasam et al., 2003; Stec et al., 2001; Stec et al., 1998). Mono- and di-methylated H3K36, associated with transcriptional activation, is primarily enriched at gene promoters and enhancers (intergenic regions) while H3K36me3, which is only mediated by SETD2 methyltransferase, is found at gene bodies of actively transcribed genes (Kuo et al., 2011; Popovic et al., 2014; Shipman et al., 2024; Streubel et al., 2018; Sun et al., 2005; Weinberg et al., 2019; Yuan et al., 2009). NSD1 enhancer localisation is mediated by p300/CBP-catalysed H3K18ac, the genes of which (*EP300*/*CREBBP*) are recurrently mutated in germinal centre lymphoma (Pasqualucci et al., 2011; Sun et al., 2023). Importantly, the three NSD proteins are not the only methyltransferases capable of producing H3K36me1/2, with ASH1L, SETMAR and SMYD2 all possessing histone methyltransferase activity at H3K36 (Abu-Farha et al., 2008; Shipman et al., 2024; Wagner & Carpenter, 2012). SETD3 has previously been proposed to methylate H3K36 but this function has not been proven *in vivo* (Eom et al., 2011; Guo et al., 2019).

All three NSD proteins share several evolutionarily conserved domains including the catalytic SET domain, five plant homeodomains (PHD) domains, and two PWWP domains which read methylated H3K36 and facilitate NSD binding to histone H3 (Baker et al., 2008; Dhayalan et al., 2010; Rathert, 2021; Sankaran et al., 2016). The specificity of H3K36 dimethylation by NSD proteins has been proposed to result from an autoinhibitory mechanism (Qiao et al., 2011). A key point to note when interpreting *NSD1/2* knockout experiments in this PhD research project is the fact that all three NSD proteins can also methylate non-histone proteins which may alter the cellular phenotype (Lu et al., 2010; Saloura et al., 2017; Song et al., 2021; Topchu et al., 2022). Furthermore, despite the apparent redundancy in histone methyltransferase specificity between the NSD proteins, *Nsd1*-KO mice demonstrate embryonic lethality, while *Nsd2*-KO mice have severe

developmental and cardiac abnormalities and survive for only 10 days after birth (Nimura et al., 2009; Rayasam et al., 2003). These mouse models suggest that the NSD proteins are not necessarily functionally redundant, another point of consideration when assessing phenotypic experiments of NSD disruption in this PhD research chapter.

The H3K27me3 and H3K36me1/2 histone PTMs mark transcriptionally dichotomous gene loci, and are not found on the same H3 proteins (Young et al., 2009; Yuan et al., 2011). The NSD protein mediated H3K36me1/2 marks can inhibit PRC2 activity (Schmitges et al., 2011; Voigt et al., 2012) while the activity of all NSD proteins are inhibited by H2A ubiquitination, a mark mediated by PRC1 (Li et al., 2021; Yuan et al., 2013). Loss of *Nsd1* in mouse embryonic stem cells has been shown to result in globally increased H3K27me3 levels and reductions in H3K36me2 at promoter and intergenic regions (Streubel et al., 2018). The functional interplay between PRC1/2 and NSD proteins is important to consider when interpreting the results of this PhD research project chapter.

4.1.2 NSD proteins in cancer

NSD1 and *NSD3* have both been shown to be among translocation partner genes in *NUP98*-rearranged acute myeloid leukaemia, and both proteins have been shown to be overexpressed in a number of different malignancies (Angrand et al., 2001; Cancer Genome Atlas, 2015; French et al., 2014; Jaju et al., 2001; Khan, 2020; La Starza et al., 2004; Rathert, 2021; Rosati et al., 2002; Wang et al., 2007). Given the observation of recurrent loss-of-function mutations in certain cancers, *NSD1* has also been suggested as a tumour suppressor (Cancer Genome Atlas, 2015; Keck et al., 2015; Vougiouklakis et al., 2015). Recurrent point mutations E1099K and T1150A in the SET domain of *NSD2* cause hyperactivation of its histone lysine methyltransferase activity, causing global increases in H3K36me2 and concomitant reductions in H3K27me3; these mutations have been found in paediatric ALL (6-14%), mantle cell lymphoma (MCL) (10%), and rarely in chronic lymphocytic leukaemia (CLL) and MM (Bea et al., 2013; Ding et al., 2017; Fabbri et al., 2011; Jaffe et al., 2013; Oyer et al., 2014; Sato et al., 2021; Swaroop et al., 2019; J. Zhang

et al., 2014). Similar hyperactivating missense mutations have been identified in *NSD3* in CLL (Landau et al., 2013; Li et al., 2021). NSD2 has also been shown to be overexpressed, and contribute to carcinogenesis in several solid organ malignancies, via aberrant H3K36me2 regulation (C. He et al., 2019; Hudlebusch et al., 2011; Parolia et al., 2024; Sengupta et al., 2021; Zhao et al., 2021).

Multiple myeloma, a malignancy of terminally differentiated plasma cells, is characterised by significant clinical and molecular heterogeneity. Translocations involving the immunoglobulin heavy chain (*IGH*) locus are seen in 40-70% of patients with the t(4;14) translocation, bringing *NSD2* on chromosome 4 under the control of the *IGH* locus, occurring in 15-20% and conferring a worse overall survival on patients (Chesi et al., 1998; Keats et al., 2006; Moreau et al., 2002; Stewart, Bergsagel, et al., 2007; Stewart, Chang, et al., 2007). The t(4;14) translocation in MM has been extensively studied, and offers valuable insights into the altered epigenome associated with genetic *NSD2* aberrations. This translocation results in increased NSD2 expression and leads to genome-wide increases in H3K36me2 and reduced H3K27me3 conferring a gene expression program consistent with the development of multiple myeloma (Keats et al., 2005; Kuo et al., 2011; Martinez-Garcia et al., 2011; Popovic et al., 2014). The relationship between EZH2 and NSD2 is likely to be important not just in physiology but also in disease, given the observations of that H3K27me3 is reduced in specific genomic locations in multiple myeloma (Bennett et al., 2017).

The aim of this research chapter was to identify and validate genetic mediators of resistance to PRC2 inhibition in germinal centre B-cell lymphoma, and to systematically evaluate the mechanisms of resistance.

4.2 Results

4.2.1 Divergent mechanisms of resistance to EZH2 inhibitors in EZH2-mutant versus EZH2 wild-type lymphomas

In Chapter 3 I showed that while genetic dependencies were highly concordant in germinal centre lymphoma cells, EZH2 inhibitor sensitiser genes appeared to be EZH2 mutation-dependent. At the outset of this Chapter, I wanted to discern whether mechanisms of EZH2 inhibitor resistance differed between EZH2-mutant and EZH2 wild-type cells. Upon reviewing the Beta scores plotted in **Figure 4.1A**, it was evident that the number of genes with a score ≥ 0.5 were far higher in EZH2-mutant WSU-DLCL2 cells compared to HT EZH2 wild type cells following EZH2 inhibition. There was minimal overlap in the individual genes with a Beta score ≥0.5 between the two cell lines (**Figure 4.1B**). Notably, *NSD1* was one of the few overlapping genes, a finding that will be followed up in the next sections. Next, I applied the same strategy as in Chapter 3 and focussed solely on EZH2i sensitisers in EZH2-mutant lymphoma, taking the top 100 resister genes to perform gene ontology (GO) analysis (**Figure 4.1C**). Enriched GO terms included chromatin organisation, chromatin binding and H3K36 specific methyltransferase activity (**Figure 4.1D-E**).

4.2.2 EZH2 inhibitor 'resister' genes include known tumour suppressor genes along with several chromatin regulators

Turning my attention to specific EZH2 inhibitor resister genes, I found that the H3K36me2 methyltransferases NSD1 and NSD2 were among the top genes conferring resistance, respectively ranked 30th and 3rd out of 16,808 resister genes respectively (**Figure 4.2A**). Notably, the Bracken Lab and others have shown that loss of either *NSD1* or *NSD2* leads to global increases in H3K27me3 levels (Drosos et al., 2022; Martinez-Garcia et al., 2011; Popovic et al., 2014; Streubel et al., 2018). A previous study demonstrated that *NSD1* loss confers resistance to EZH2 inhibitors in MRT by reducing H3K36me2, a histone modification that was reported to be required for EZH2 inhibitor-induced gene activation

A

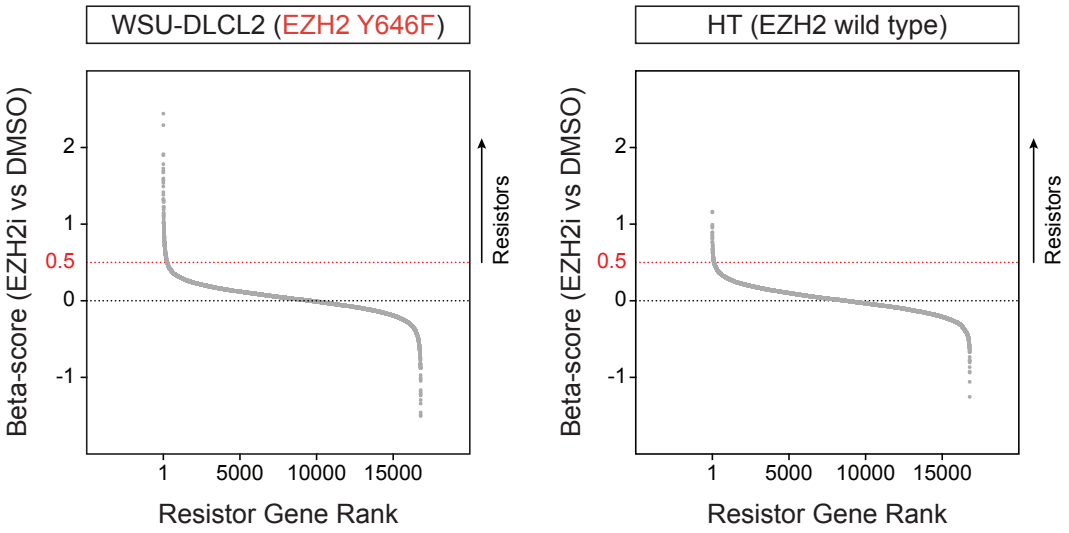

B

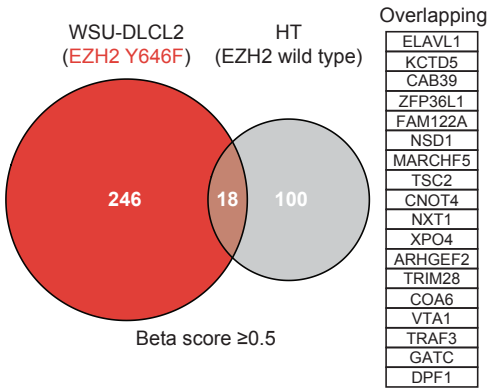

Overlapping
ELAVL1
KCTD5
CAB39
ZFP36L1
FAM122A
NSD1
MARCHF5
TSC2
CNOT4
NXT1
XPO4
ARHGEF2
TRIM28
COA6
VTA1
TRAF3
GATC
DPF1

C

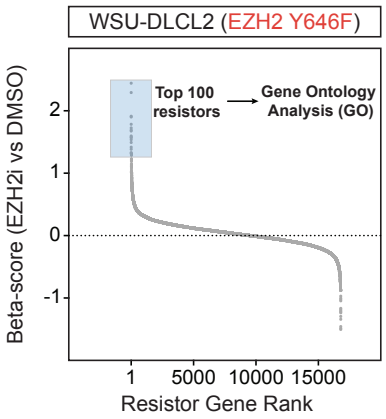

D

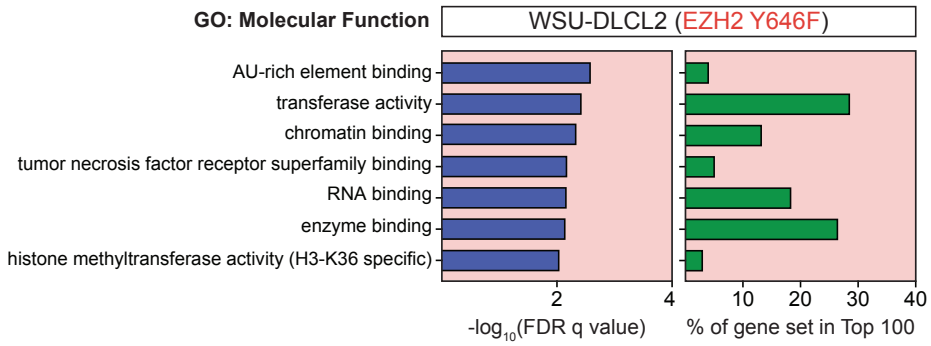

E

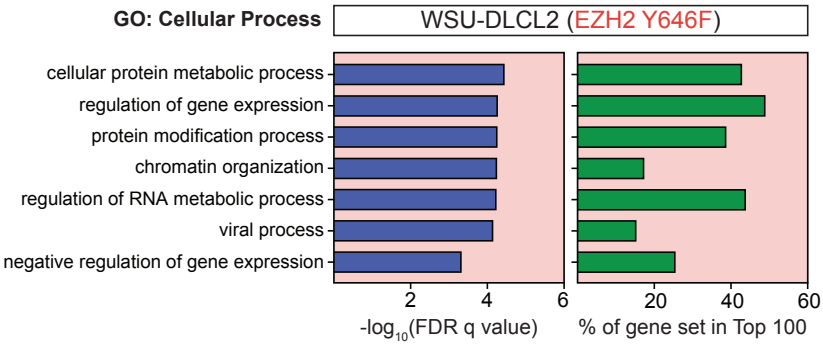

Figure 4.1: Divergent mechanisms of resistance to EZH2 inhibitors in EZH2-mutant versus EZH2 wild-type lymphomas.
A. Genome-wide CRISPR screen data in WSU-DLCL2 and HT lymphoma cells gene ranked based on sgRNA enrichment in low dose EZH2i treatment (Tazemetostat IC_{20}) relative to DMSO control. Differential Beta-score between EZH2i and DMSO conditions calculated using the MAGeCK algorithm (Li et al., 2014). A negative Beta score indicates sensitiser genes, while a positive Beta score indicates resistor genes. Common essential genes, as defined by depmap.org (Achilles, 19Q3), were removed.
B. Proportional Venn Diagram overlap of all genes with a Beta score ≥ 0.5 in WSU-DLCL2 and HT cell lines, with the 18 overlapping genes indicated.
C. Strategy showing that the top 100 candidate mediators of resistance to EZH2 inhibitors in EZH2-mutant lymphoma (WSU-DLCL2) were selected for gene ontology (GO) analysis.
D. Gene ontology enrichment for “Molecular Function” of the top 100 gene resistors in the WSU-DLCL2 cell line using the GOrilla tool (Eden et al., 2009). Enrichment p-values were calculated using a Fisher’s exact test and were Benjamini–Hochberg adjusted to obtain a False Discovery Rate (FDR) corrected q value (left). The percentage of genes within a given gene set that scored among the top 100 candidate mediators of resistance are shown (right).
E. Gene ontology enrichment for “Cellular Process” of the top 100 gene resistors in the WSU-DLCL2 cell line using the GOrilla tool (Eden et al., 2009). Enrichment p-values were calculated using a Fisher’s exact test and were Benjamini–Hochberg adjusted to obtain a False Discovery Rate (FDR) corrected q value (left). The percentage of genes within a given gene set that scored among the top 100 candidate mediators of resistance are shown (right).

A

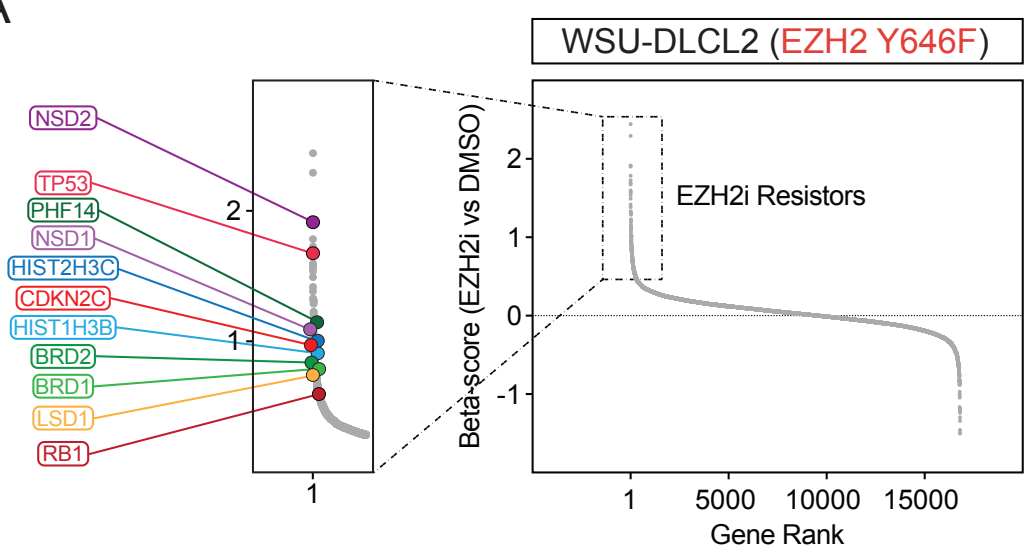
WSU-DLCL2 (EZH2 Y646F)
NSD2
TP53
PHF14
NSD1
HIST2H3C
CDKN2C
HIST1H3B
BRD2
BRD1
LSD1
RB1
2
1
1
Beta-score (EZH2i vs DMSO)
2
1
0
-1
EZH2i Resistors
1
5000
10000
15000
Gene Rank

B

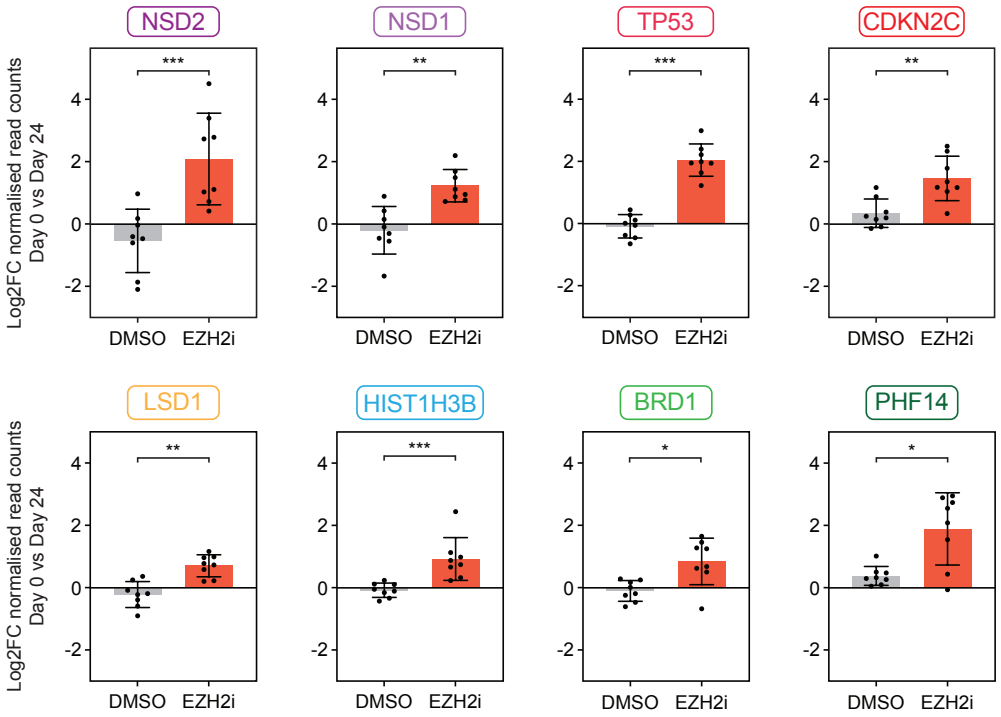
NSD2
NSD1
TP53
CDKN2C
LSD1
HIST1H3B
BRD1
PHF14
Log2FC normalised read counts
Day 0 vs Day 24
DMSO
EZH2i

Figure 4.2: EZH2 inhibitor 'resister' genes include known tumour suppressor genes along with several chromatin regulators.
A. Genome-wide CRISPR screen data in WSU-DLCL2 lymphoma cells gene ranked based on sgRNA enrichment in low dose EZH2i treatment (20nM Tazemetostat i.e. IC_{20}) relative to DMSO control. Differential Beta-score between EZH2i and DMSO conditions calculated using the MAGeCK algorithm (Li et al., 2014). Specific resistor genes are highlighted.
B. Bar charts illustrating log2-fold change of individual sgRNAs relative to T0 from either Tazemetostat-treated or DMSO-treated cells. p values were calculated by Mann-Whitney test. p*** <0.001, p** <0.01, p* <0.05.

and therapeutic efficacy, thus providing a potential mechanistic basis for the resistance phenotype (Drosos et al., 2022). Interestingly, the other known H3K36 methyltransferases, including NSD3, did not score as EZH2 inhibitor resisters. Similar to genetic sensitisers, the top mediators of resistance to EZH2 inhibitors clustered on chromatin regulatory genes and included tumour suppressor genes, as expected. Notable examples included *TP53* (8/16,808), *CDKN2C* (41/16,808), *LSD1* (86/16,808), *HIST1H3B* (49/16,808), *BRD1* (72/16,808), *PHF14* (25/16,808), *RB1* (160/16,808) (**Figure 4.2B**).

4.2.3 *NSD2* or *NSD1* loss confers a survival advantage to B-cell lymphoma cells exposed to EZH2 inhibitors, in a dose-dependent fashion

In order to validate *NSD2* and *NSD1* as genetic resisters to EZH2 inhibitors, I performed negative selection assays with sgRNAs targeting both genes in lymphoma cells treated with DMSO or Tazemetostat. In two EZH2-mutant lymphoma cell lines, while sgRNAs targeting *NSD2* alone did not affect the cellular phenotype, sgRNAs targeting *NSD1* in the DMSO condition appeared to deplete over time (**Figure 4.3A-B**). In EZH2-mutant lymphoma cells that were treated with Tazemetostat, sgRNAs targeting both *NSD1* and *NSD2* conferred a marked cellular fitness advantage. In EZH2 wild-type cells, targeting *NSD2* alone did not affect lymphoma cell phenotype while targeting *NSD1* alone conferred a modest survival disadvantage, however when treated with Tazemetostat, sgRNAs targeting either *NSD1* or *NSD2* conferred a survival advantage (**Figure 4.3C**). To assess specificity of *NSD1/NSD2* loss leading to EZH2 inhibitor resistance, I set out to demonstrate a dose-response in the resister phenotype. I performed CRISPR-Cas9 negative selection assays this time with increasing Tazemetostat doses, in an EZH2-mutant lymphoma cell line targeted with either *NSD1* or *NSD2* sgRNAs. As expected, I saw an increasing resister phenotype in *NSD1/NSD2* targeted cells with increasing doses of EZH2 inhibitor, providing further evidence for these genes being important mediators of resistance to PRC2 inhibition (**Figure 4.3D-E**).

4.2.4 Bulk knockout of *NSD2* using CRISPR, and PROTAC-mediated pharmacological degradation of NSD2 provide orthogonal evidence for mediating resistance to EZH2 inhibitors in EZH2-mutant lymphoma cells

Through initial CRISPR screen results and validatory cell competition assays in the previous sections, I have demonstrated that *NSD1* and *NSD2* are EZH2 inhibitor resister genes. To provide orthogonal validation to these findings, I employed an additional two approaches. First, I performed CRISPR 'bulk' knockout of *NSD1* and *NSD2*, by selecting for sgRNA-transduced lymphoma cells using puromycin selection. As this is not a clonal knockout, a heterogenous population of variable knockouts would be generated, however immunoblots demonstrated a reasonable knockout of *NSD1* and *NSD2* in at least one of the sgRNAs used for each gene (**Figure 4.4A**). Next, I monitored lymphoma cell growth in cells following bulk *NSD1* or *NSD2* knockout and saw that in EZH2-mutant lymphoma cells at day 21, *NSD2* loss protected cells from EZH2 inhibition in both sgRNAs used (**Figure 4.4B**). Using this approach however, it did not appear that 'bulk' *NSD1*-KO contributed to Tazemetostat resistance. The novel NSD2 PROTAC degrader compound UNC8153 (dNSD2; kind gift from Dr Lindsey James) has been shown to degrade NSD2 and reduce H3K36me2 levels in multiple myeloma, leukaemia and sarcoma cell lines *in vitro* (Hanley et al., 2023). Lymphoma cells were initially treated with a range of doses of this degrader compound and NSD2 protein levels were assessed by immunoblot, where it can be seen that NSD2 is significantly, although not fully, degraded with the 10μM dose (**Figure 4.4C**). Then, EZH2-mutant and wild-type lymphoma cells were treated with either low dose EZH2i inhibitor, 10μM dNSD2, or a combination of both. In the EZH2-mutant lymphoma cell line, the presence of the NSD2 degrader could cause resistance to Tazemetostat, a finding that was not replicated in the EZH2 wild-type lymphoma cell line (**Figure 4.4D**). This finding was seen at both 1μM and 10μM dNSD2 doses, suggesting that full NSD2 protein degradation was unnecessary to produce an EZH2 inhibitor resistance phenotype (**Figure 4.4E**). Given these findings, further NSD2-related mechanistic experiments were prioritised for EZH2-mutant lymphoma cells only.

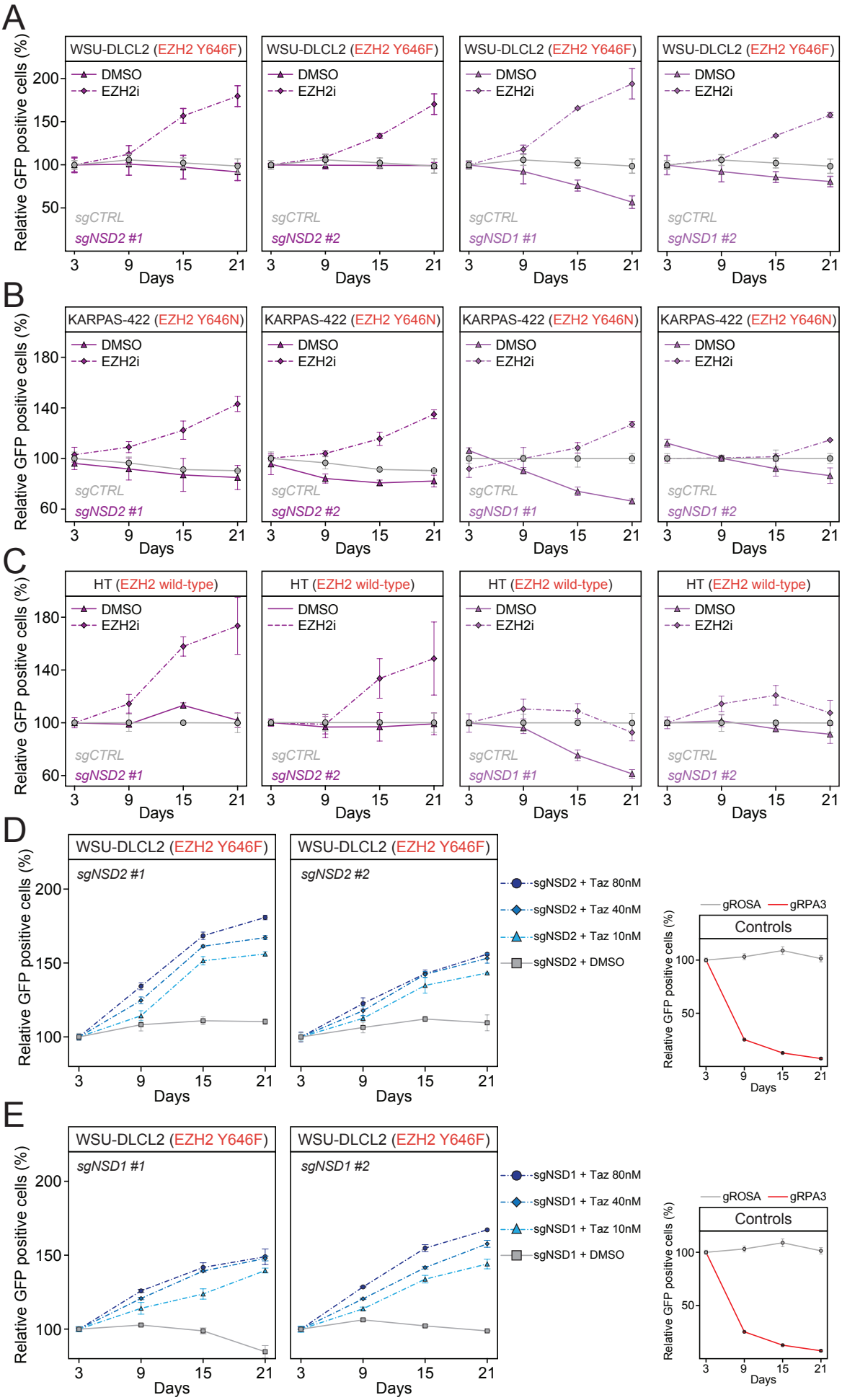
A
WSU-DLCL2 (EZH2 Y646F)
DMSO
EZH2i
Relative GFP positive cells (%)
sgCTRL
sgNSD2 #1
sgNSD2 #2
sgNSD1 #1
sgNSD1 #2
Days
B
KARPAS-422 (EZH2 Y646N)
C
HT (EZH2 wild-type)
D
sgNSD2 + Taz 80nM
sgNSD2 + Taz 40nM
sgNSD2 + Taz 10nM
sgNSD2 + DMSO
gROSA
gRPA3
Controls
E
sgNSD1 + Taz 80nM
sgNSD1 + Taz 40nM
sgNSD1 + Taz 10nM
sgNSD1 + DMSO

Figure 4.3: *NSD2* or *NSD1* loss confer a survival advantage to B-cell lymphoma cells exposed to EZH2 inhibitors, in a dose-dependent fashion.

A. Growth competition assays in Cas9-expressing WSU-DLCL2 (EZH2-mutant lymphoma) cells transduced with two independent NSD2 and NSD1-targeting sgRNAs followed by treatment with 20nM of the EZH2 inhibitor Tazemetostat. The relative GFP+ (sgRNA+) percentage is depicted at the indicated time points after transduction (n=4, data represents mean ± SD).

B. Growth competition assays in Cas9-expressing Karpas-422 (EZH2-mutant lymphoma) cells transduced with two two independent NSD2 and NSD1-targeting sgRNAs followed by treatment with 20nM of the EZH2 inhibitor Tazemetostat. The relative GFP+ (sgRNA+) percentage is depicted at the indicated time points after transduction (n=4, data represents mean ± SD).

C. Growth competition assays in Cas9-expressing HT (EZH2 wild-type lymphoma) cells transduced with two two independent NSD2 and NSD1-targeting sgRNAs followed by treatment with 20nM of the EZH2 inhibitor Tazemetostat. The relative GFP+ (sgRNA+) percentage is depicted at the indicated time points after transduction (n=4, data represents mean ± SD).

D. Growth competition assays in Cas9-expressing WSU-DLCL2 (EZH2-mutant lymphoma) cells transduced with two independent NSD2 and NSD1-targeting sgRNAs followed by treatment with the indicated EZH2i (Tazemetostat) doses. The relative GFP+ (sgRNA+) percentage is depicted at the indicated time points after transduction (n=3, data represents mean ± SD).

E. Growth competition assays in Cas9-expressing WSU-DLCL2 (EZH2-mutant lymphoma) cells transduced with two independent NSD2 and NSD1-targeting sgRNAs followed by treatment with the indicated EZH2i (Tazemetostat) doses. The relative GFP+ (sgRNA+) percentage is depicted at the indicated time points after transduction (n=3, data represents mean ± SD). The positive and negative controls are shown separately (right).

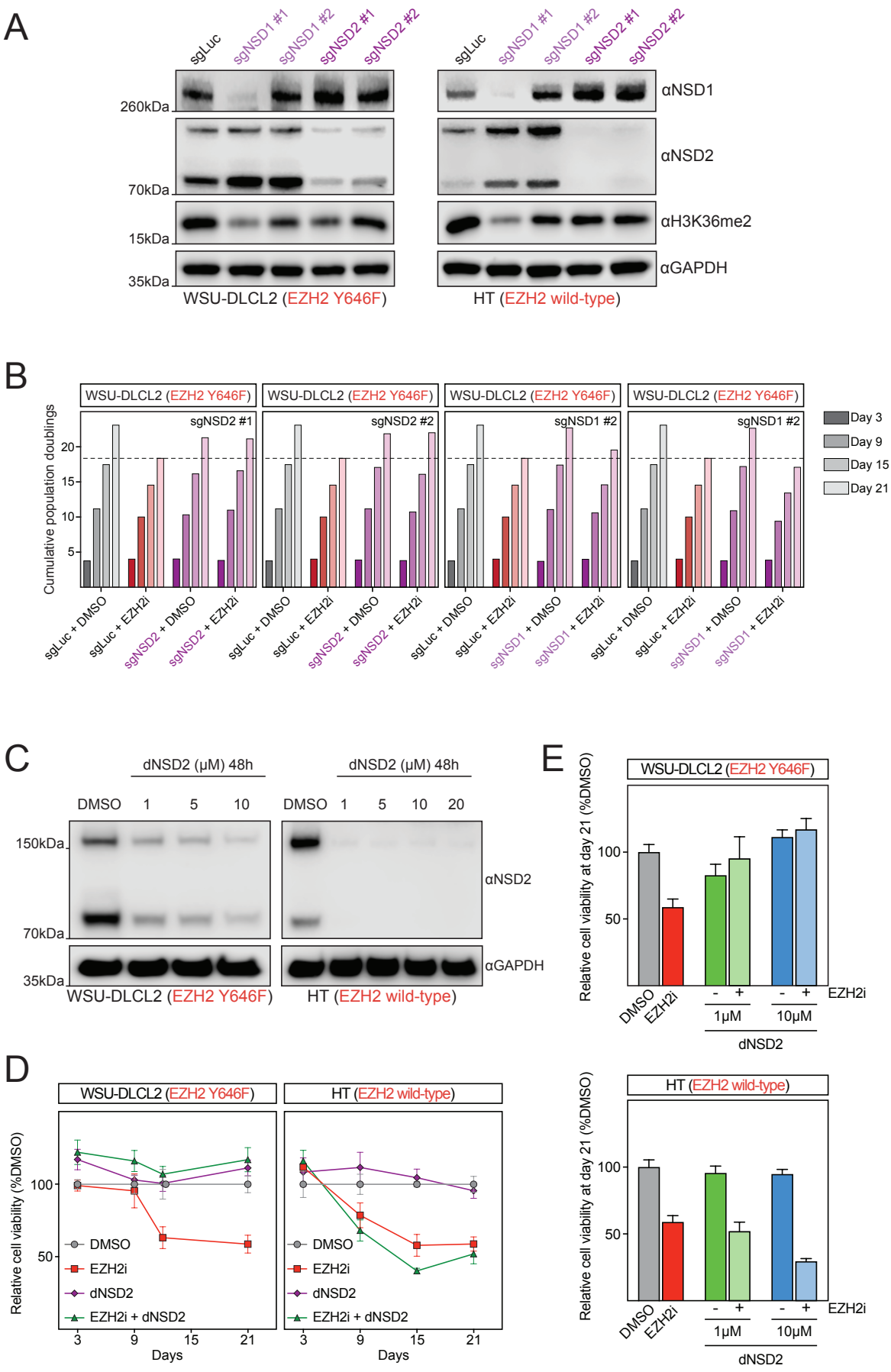
A
sgLuc
sgNSD1 #1
sgNSD1 #2
sgNSD2 #1
sgNSD2 #2
260kDa
70kDa
15kDa
35kDa
αNSD1
αNSD2
αH3K36me2
αGAPDH
WSU-DLCL2 (EZH2 Y646F)
HT (EZH2 wild-type)
B
WSU-DLCL2 (EZH2 Y646F)
sgNSD2 #1
sgNSD2 #2
sgNSD1 #2
sgNSD1 #2
Cumulative population doublings
Day 3
Day 9
Day 15
Day 21
sgLuc + DMSO
sgLuc + EZH2i
sgNSD2 + DMSO
sgNSD2 + EZH2i
sgNSD1 + DMSO
sgNSD1 + EZH2i
C
dNSD2 (μM) 48h
DMSO
1
5
10
20
150kDa
70kDa
35kDa
αNSD2
αGAPDH
WSU-DLCL2 (EZH2 Y646F)
HT (EZH2 wild-type)
D
WSU-DLCL2 (EZH2 Y646F)
HT (EZH2 wild-type)
Relative cell viability (%DMSO)
DMSO
EZH2i
dNSD2
EZH2i + dNSD2
Days
E
WSU-DLCL2 (EZH2 Y646F)
HT (EZH2 wild-type)
Relative cell viability at day 21 (%DMSO)
DMSO
EZH2i
1μM
10μM
dNSD2
EZH2i

Figure 4.4: Bulk knockout of *NSD2* using CRISPR, and PROTAC-mediated pharmacological degradation of NSD2 provide orthogonal evidence for mediating resistance to EZH2 inhibitors in EZH2-mutant lymphoma cells.

A. Immunoblots of the indicated proteins and histone modifications from whole cell lysates in the indicated lymphoma cells transduced with either a control sgRNA (Luciferase) or two individual sgRNAs targeting NSD2 or NSD1.

B. Cumulative population doublings in WSU-DLCL2 (EZH2-mutant lymphoma) cells transduced with either a control sgRNA (Luciferase) or two individual sgRNAs targeting NSD2 or NSD1 followed by treatment with DMSO control or 20nM of the EZH2 inhibitor Tazemetostat over 21 days.

C. Immunoblots of the indicated proteins from whole cell lysates in WSU-DLCL2 (EZH2-mutant lymphoma) and HT (EZH2 wild-type lymphoma) cells treated with either DMSO control or the NSD2 PROTAC degrader compound UNC8153 at the indicated concentrations.

D. Cell viability data in the indicated lymphoma cells treated with either DMSO control, 20nM of the EZH2 inhibitor Tazemetostat, 10μM of the NSD2 degrader UNC8153, or a combination of EZH2i and dNSD2 over 21 days (n=3, data represents mean ± SD).

E. Cell viability data at day 21 in the indicated lymphoma cells treated with either DMSO control, 20nM of the EZH2 inhibitor Tazemetostat, the NSD2 degrader UNC8153 at two concentrations, or a combination of EZH2i and dNSD2 at two concentrations (n=3, data represents mean ± SD).

4.2.5 NSD2 does not possess any quantitatively significant protein interactors, and loss of NSD2 blunts the increases in H3K36me2 seen following EZH2 inhibitor treatment

Given the findings so far in this chapter of NSD2 loss contributing to PRC2 inhibitor resistance, I reasoned that perhaps NSD2 may physically interact with PRC2 components or some other chromatin regulator. Seven isoforms of NSD2 are known to be produced by alternative splicing. **Figure 4.5A** illustrates the three most studied together with their protein domains and the epitope for the NSD2 antibody used throughout this PhD research project. Previous studies have shown a relatively bland NSD2 interactome, with PARP1, HSPA8 and RPL10 reported interactors (Huang et al., 2019; Wang et al., 2021). I performed endogenous co-immunoprecipitation of NSD2 followed by mass spectrometry, with the help of Molly Davies and Eugene Dillon (UCD). I observed that while the previously reported NSD2-interacting proteins were significant in the volcano plot, along with core PRC2 components, quantitative analysis using iBAQ values to calculate stoichiometry showed an absence of quantitatively significant interactors (**Figure 4.5B-D**). This provides evidence for NSD2 broadly acting in isolation in its functions.

Next, using the same bulk approach to NSD2 knockout, I cultured *NSD2*-KO WSU-DLCL2 cells +/- Tazemetostat for 9 days, noting again the resistance to PRC2 inhibition (**Figure 4.5E**). Then, after harvesting the cells for immunoblots, I observed the increases in H3K36me2 levels seen following EZH2 inhibition were blunted in *NSD2*-KO cells (**Figure 4.5F**), linking to previous work that showed that H3K36me2 levels are central to gene expression changes in PRC2 inhibited cells (Drosos et al., 2022).

4.2.6 Isogenic *NSD1* and *NSD2* knockout EZH2-mutant lymphoma cell lines exhibit attenuated baseline proliferation rates and resistance to low dose EZH2 inhibition

I sought to generate a genetically clean system with which I could explore the effects of *NSD2* loss on transcription and chromatin landscapes more robustly than with the NSD2 degrader or bulk CRISPR knockout approach, both of which produced incomplete knockout of *NSD1* or *NSD2*. To do this, I single cell sorted lymphoma cells transduced with sg*ROSA26*, sg*NSD1* or sg*NSD2* and grew out single cell clones (described in more detail in Section 2.3.3). Using this approach, I successfully generated clonal, isogenic, and complete *NSD2* and *NSD1* knockouts in two EZH2-mutant lymphoma cell lines, WSU-DLCL2 and Karpas-422 (**Figure 4.6A-B**). Given the previous findings that *NSD1*-KO in the absence of EZH2 inhibitor could cause negative consequences to the lymphoma cells, I performed the rest of the experiments in this chapter in the *NSD2*-KO cells. Initially, I noted in simple proliferation assays that the *NSD2*-KO cells grew slightly slower over time (**Figure 4.6C**). In cell viability assays I confirmed that this isogenic system was consistent with the CRISPR screen, and that these cells were resistant to low dose EZH2 inhibitors (**Figure 4.6D-F**). Then, I wanted to further explore this relationship with PRC2 inhibition by performing cell viability assays across a range of doses of Tazemetostat. Strikingly, over 18 days, it was clear that *NSD2*-KO conferred resistance to low dose, but not higher doses of EZH2 inhibition (**Figure 4.6G-H**).

4.2.7 All three NSD isoforms are expressed in lymphoma cells, while NSD1 and NSD2 are chromatin bound, and their loss has variable effects on histone H3 post-translational modifications

Following the previous sections that have contained a significant amount of functional data, I wanted to carry out a comprehensive characterisation of the *NSD2*-KO lymphoma cells. Firstly, I assessed expression of all three *NSD* paralogs and saw that they are all expressed,

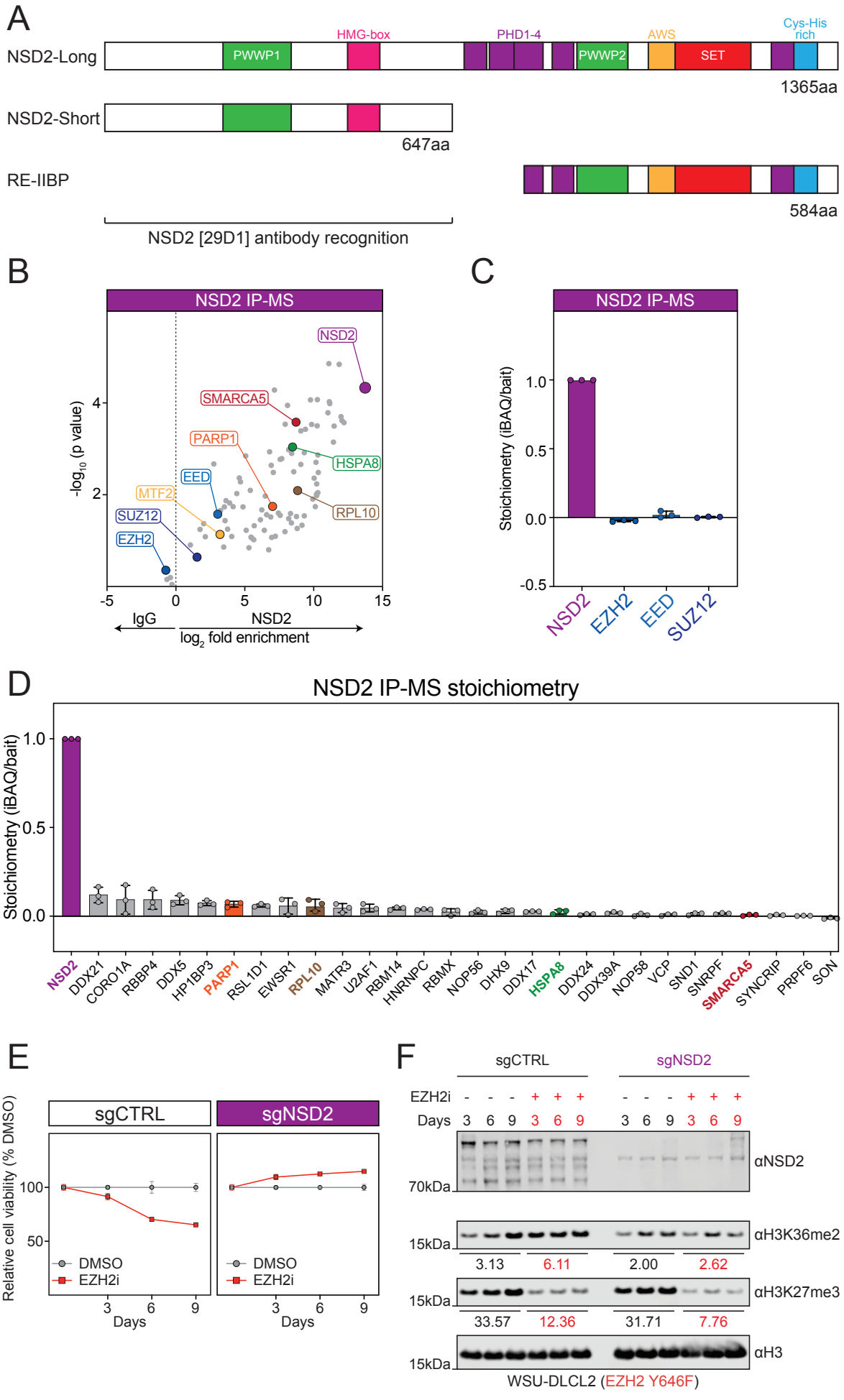
A
NSD2-Long
PWWP1
HMG-box
PHD1-4
PWWP2
AWS
SET
Cys-His rich
1365aa
NSD2-Short
647aa
RE-IIBP
584aa
NSD2 [29D1] antibody recognition
B
NSD2 IP-MS
NSD2
SMARCA5
PARP1
HSPA8
EED
MTF2
RPL10
SUZ12
EZH2
-log10 (p value)
IgG
NSD2
log2 fold enrichment
C
NSD2 IP-MS
Stoichiometry (iBAQ/bait)
NSD2
EZH2
EED
SUZ12
D
NSD2 IP-MS stoichiometry
Stoichiometry (iBAQ/bait)
NSD2
DDX21
CORO1A
RBBP4
DDX5
HP1BP3
PARP1
RSL1D1
EWSR1
RPL10
MATR3
U2AF1
RBM14
HNRNPC
RBMX
NOP56
DHX9
DDX17
HSPA8
DDX24
DDX39A
NOP58
VCP
SND1
SNRPF
SMARCA5
SYNCRIP
PRPF6
SON
E
sgCTRL
sgNSD2
Relative cell viability (% DMSO)
DMSO
EZH2i
Days
F
sgCTRL
sgNSD2
EZH2i
Days
70kDa
αNSD2
15kDa
αH3K36me2
3.13
6.11
2.00
2.62
αH3K27me3
33.57
12.36
31.71
7.76
αH3
WSU-DLCL2 (EZH2 Y646F)

Figure 4.5: NSD2 does not possess any quantitatively significant protein interactors, and loss of NSD2 blunts the increases in H3K36me2 seen following EZH2 inhibitor treatment.

A. Scaled diagrammatic representation of the three primary isoforms of NSD2 including the canonical NSD2-long isoform (MMSET type II), the NSD2-short isoform lacking the SET domain (MMSET type I), and the NSD2-short isoform containing the SET domain (RE-IIBP). The indicated protein domains were annotated using the Conserved Domains Database (CDD) hosted on the website of the National Center for Biotechnology Information. The epitope for the NSD2 antibody [clone 29D1] is shown.

B.Volcano plot illustrating protein enrichment in endogenous co-immunoprecipitations of NSD2 followed by mass spectrometry in WSU-DLCL2 (EZH2-mutant lymphoma) cells (n=3 biological replicates).

C. Bar plots depicting the stoichiometry of core PRC2 components from the IP-MS of NSD2 in WSU-DLCL2 (EZH2-mutant lymphoma) cells (n=3, data represents mean ± SD).

D. Bar plots demonstrating the stoichiometry of all proteins with log2 fold enirhchment ≥5 from the NSD2 IP-MS in WSU-DLCL2 (EZH2-mutant lymphoma) cells (n=3, data represents mean ± SD). The proteins PARP1 and SMARCA5 are highlighted.

E. Cell viability data in WSU-DLCL2 (EZH2-mutant lymphoma) cells transduced with either a control sgRNA (ROSA) or sgNSD2 and treated with DMSO or low dose EZH2 inhibitor (Tazemetostat) over 9 days (n=3, data represents mean ± SD).

F. Immunoblots of the indicated proteins and histone modifications from whole cell lysates in WSU-DLCL2 (EZH2-mutant lymphoma) cells transduced with either a control sgRNA (ROSA) or sgNSD2 and treated with DMSO or low dose EZH2 inhibitor (Tazemetostat). The numbers under the histone modification immunoblots indicate fluorescent signal normalised to the H3 loading control averaged in the DMSO-treated (black) or the EZH2i-treated (red) cells.

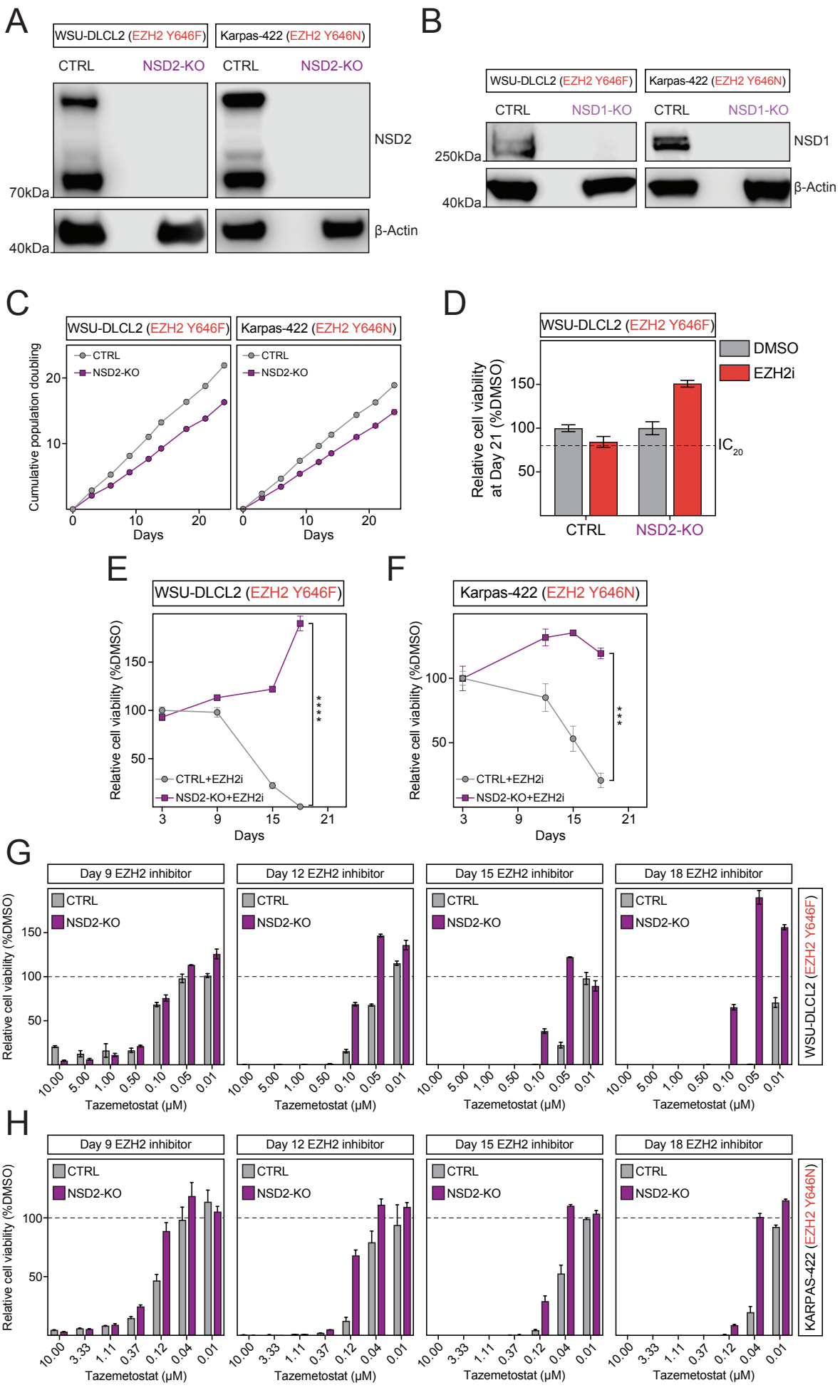
A
WSU-DLCL2 (EZH2 Y646F)
Karpas-422 (EZH2 Y646N)
CTRL
NSD2-KO
CTRL
NSD2-KO
NSD2
70kDa
40kDa
β-Actin
B
WSU-DLCL2 (EZH2 Y646F)
Karpas-422 (EZH2 Y646N)
CTRL
NSD1-KO
CTRL
NSD1-KO
NSD1
250kDa
40kDa
β-Actin
C
WSU-DLCL2 (EZH2 Y646F)
Karpas-422 (EZH2 Y646N)
CTRL
NSD2-KO
Cumulative population doubling
Days
D
WSU-DLCL2 (EZH2 Y646F)
DMSO
EZH2i
Relative cell viability at Day 21 (%DMSO)
IC20
CTRL
NSD2-KO
E
WSU-DLCL2 (EZH2 Y646F)
Relative cell viability (%DMSO)
CTRL+EZH2i
NSD2-KO+EZH2i
****
Days
F
Karpas-422 (EZH2 Y646N)
Relative cell viability (%DMSO)
CTRL+EZH2i
NSD2-KO+EZH2i
***
Days
G
Day 9 EZH2 inhibitor
Day 12 EZH2 inhibitor
Day 15 EZH2 inhibitor
Day 18 EZH2 inhibitor
CTRL
NSD2-KO
Relative cell viability (%DMSO)
Tazemetostat (μM)
WSU-DLCL2 (EZH2 Y646F)
H
Day 9 EZH2 inhibitor
Day 12 EZH2 inhibitor
Day 15 EZH2 inhibitor
Day 18 EZH2 inhibitor
CTRL
NSD2-KO
Relative cell viability (%DMSO)
Tazemetostat (μM)
KARPAS-422 (EZH2 Y646N)

Figure 4.6: Isogenic *NSD1* and *NSD2* knockout EZH2-mutant lymphoma cell lines exhibit attenuated baseline proliferation rates and resistance to low dose EZH2 inhibition.

A. Immunoblots of the indicated proteins from whole cell lysates in WSU-DLCL2 and Karpas-422 (EZH2-mutant lymphoma) cells which had been transduced with either a control sgRNA (ROSA) or sgNSD2, followed by single cell FACS sorting and grown out in culture.

B. Immunoblots of the indicated proteins from whole cell lysates in WSU-DLCL2 and Karpas-422 (EZH2-mutant lymphoma) cells which had been transduced with either a control sgRNA (ROSA) or sgNSD1, followed by single cell FACS sorting and grown out in culture.

C. Cell proliferation data in the indicated CTRL and *NSD2*-KO, EZH2-mutant lymphoma cells, as measured by counting cells every 3 days and calculating cumulative population doublings (n=3, data represents mean ± SD).

D. Cell viability data at day 21 in CTRL and *NSD2*-KO, WSU-DLCL2 cells, treated with either DMSO control or 20nM of the EZH2 inhibitor Tazemetostat (n=3, data represents mean ± SD). The IC_{20} line is indicated.

E. Cell viability data in CTRL and *NSD2*-KO, WSU-DLCL2 (EZH2-mutant lymphoma) cells treated with 50nM Tazemetostat over 18 days (n=3, data represents mean ± SD). Significance determined using unpaired t test, ****p value <0.0001.

F. Cell viability data in CTRL and *NSD2*-KO, Karpas-422 (EZH2-mutant lymphoma) cells treated with 41nM Tazemetostat over 18 days (n=3, data represents mean ± SD). Significance determined using unpaired t test, ***p value <0.001.

G. Cell viability data in CTRL and *NSD2*-KO, WSU-DLCL2 (EZH2-mutant lymphoma) cells treated with the indicated concentrations of the EZH2 inhibitor Tazemetostat over 18 days (n=3, data represents mean ± SD).

H. Cell viability data in CTRL and *NSD2*-KO, Karpas-422 (EZH2-mutant lymphoma) cells treated with the indicated concentrations of the EZH2 inhibitor Tazemetostat over 18 days (n=3, data represents mean ± SD).

but that *NSD2*-KO led to slight increases in NSD1 expression in WSU-DLCL2 (**Figure 4.7A**). Unsurprisingly, given the NSD2 IPMS showed no significant PRC2 interactors, *NSD2*-KO or *NSD1*-KO did not alter basal levels of PRC2 proteins (**Figure 4.7B**). Interestingly, neither *NSD2*- or *NSD1*-KO had dramatic effects on H3K36me2 on a global level, both knockouts reducing this histone PTM modestly (**Figure 4.7B-C**). Neither knockout had any significant effect on H3K36me3, as expected. Given the antagonism between NSD proteins and Polycomb, I expected to see increases in H3K27me3 in *NSD1*- and *NSD2*-KO but this was not the case. I hypothesise that because H3K27me3 basal levels are already so high in EZH2-mutant lymphoma, the immunoblot signal is saturated and it is difficult to appreciate any further gains. It was notable however, that H3K27me2 levels appeared to increase significantly on a global level in *NSD2*-KO cells (**Figure 4.7D-E**). Overall these immunoblots confirmed total KO of the respective NSD protein and suggested that KO of one *NSD* may result in compensation by the other (**Figure 4.7F**). Finally, subcellular fractionations were performed to determine the cellular locations for NSD1 and NSD2 proteins and, as expected for chromatin modifying proteins, these were found in the chromatin-bound insoluble fraction (**Figure 4.7G-H**).

4.2.8 *NSD2* loss blunts gene activation following EZH2 inhibitor treatment of B-cell lymphomas

Given the fact that NSD2 scored better than NSD1 in the CRISPR screen, and that in negative selection assays *NSD1* loss appeared detrimental to lymphoma cell fitness in the absence of EZH2 inhibition, I decided to focus on the *NSD2*-KO isogenic system. To begin to tease out the mechanism of how *NSD2*-loss causes resistance to PRC2 inhibition in lymphoma cells, I treated isogenic *NSD2*-KO lymphoma cells with or without a moderate dose of Tazemetostat (100nM) over 6 days and performed RNA-sequencing. Consistent with previous work, EZH2 inhibitor treatment resulted in ~1000 upregulated differentially expressed genes (DEGs) in control cells. This is because loss of PRC2 function causes de-repression of genes marked by H3K27me3. In contrast, *NSD2*-KO cells treated with the

same dose of Tazemetostat experienced a significantly attenuated response, with fewer upregulated DEGs, suggesting a blunting of the effect of EZH2 inhibitor treatment on global gene expression profiles (**Figure 4.8A**). Comparing EZH2 inhibitor-responsive genes, I observed a significant overlap between conditions, and fascinatingly these included a significant number of genes involved in B-cell differentiation and exit from the germinal centre e.g. *PRDM1*, *CD4*, *CXCR4*, *MYD88* and immunoglobulin genes (**Figure 4.8B**). The overall magnitude of significant upregulated genes was markedly reduced in NSD2 deficient cells (**Figure 4.8C**), and gene-by-gene comparison highlighted widespread blunting of PRC2 inhibitor-mediated gene de-repression in the absence of NSD2 (**Figure 4.8D**). Gene ontology terms of upregulated DEGs were enriched for immune signalling, cytokine production and STAT-dependent pathways, key pathways in B-cell differentiation (**Figure 4.8E**) which were blunted following EZH2 inhibitor treated *NSD2*-KO cells. Taken together, this data highlights the requirement of NSD2 for full transcriptional activation following PRC2 inhibition in EZH2-mutant lymphoma.

4.2.9 *NSD2* loss globally redistributes H3K36me2 across the genome

Next, I wanted to determine patterns of H3K36me2 distribution upon *NSD2* loss, and to assess chromatin occupancy for NSD2. I performed CUT&RUN for IgG, NSD2 and H3K36me2 in the NSD2 isogenic system and first looked at genome browser tracks. Unsurprisingly, H3K36me2 tracks showed peaks at the promoters and gene bodies of active genes and H3K36me2 peaks were lost in *NSD2*-KO cells at a subset of loci including that highlighted (**Figure 4.9A)**. I noted that NSD2 appeared to be bound at certain H3K36me2-marked loci, with a peak that was lost in *NSD2*-KO cells. This is despite the significant levels of background noise visible with this antibody. Quantitative peak calling for H3K36me2 revealed a global reduction in both broad and narrow peaks following *NSD2* loss (**Figure 4.9B**).

I then divided the genome into 10kb bins and plotted H3K36me2 signal against NSD2 signal which showed that, under normal conditions, NSD2 binding is strongly associated with

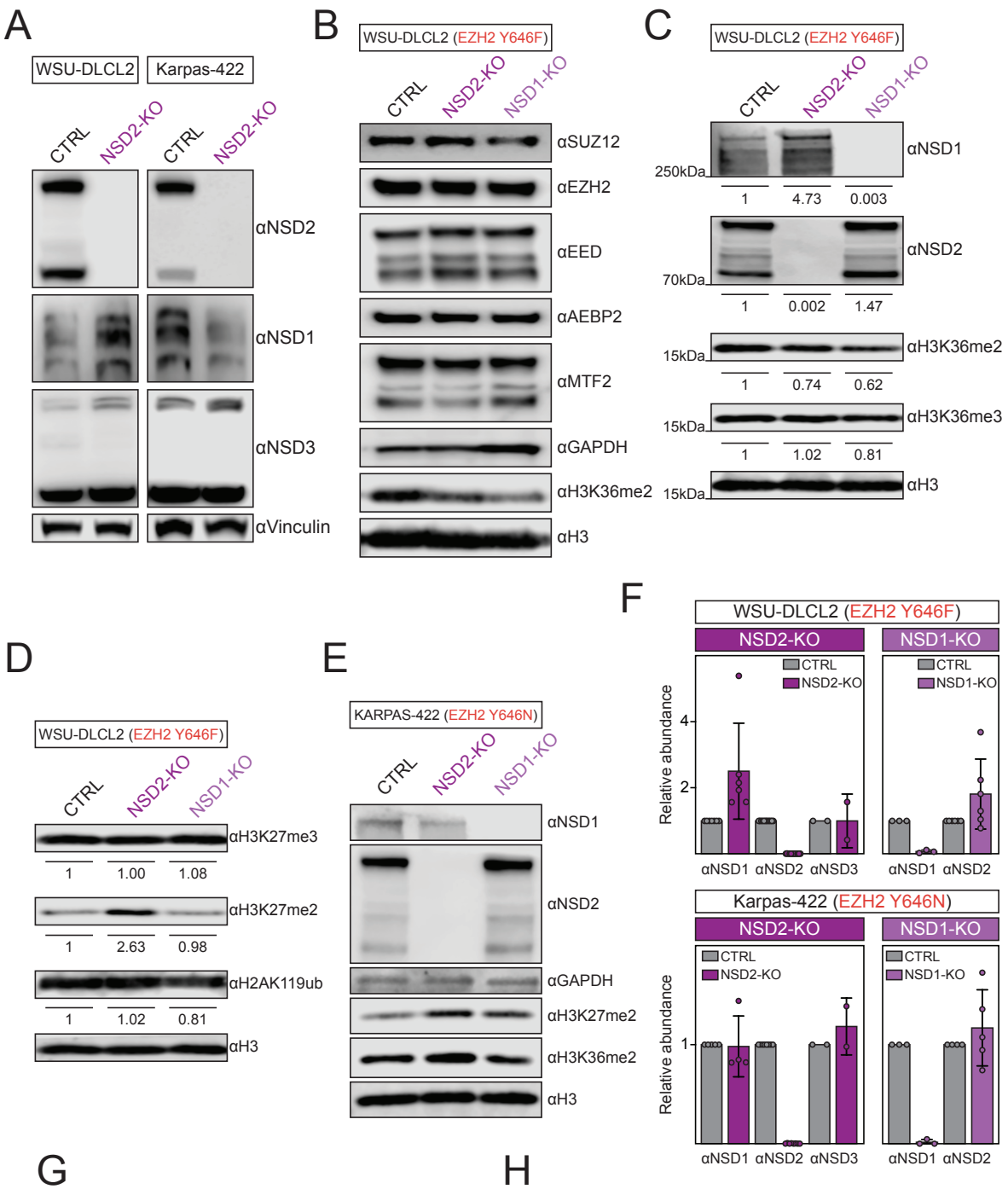
A
WSU-DLCL2
Karpas-422
CTRL
NSD2-KO
αNSD2
αNSD1
αNSD3
αVinculin
B
WSU-DLCL2 (EZH2 Y646F)
CTRL
NSD2-KO
NSD1-KO
αSUZ12
αEZH2
αEED
αAEBP2
αMTF2
αGAPDH
αH3K36me2
αH3
C
WSU-DLCL2 (EZH2 Y646F)
CTRL
NSD2-KO
NSD1-KO
250kDa
αNSD1
1
4.73
0.003
70kDa
αNSD2
1
0.002
1.47
15kDa
αH3K36me2
1
0.74
0.62
15kDa
αH3K36me3
1
1.02
0.81
15kDa
αH3
D
WSU-DLCL2 (EZH2 Y646F)
CTRL
NSD2-KO
NSD1-KO
αH3K27me3
1
1.00
1.08
αH3K27me2
1
2.63
0.98
αH2AK119ub
1
1.02
0.81
αH3
E
KARPAS-422 (EZH2 Y646N)
CTRL
NSD2-KO
NSD1-KO
αNSD1
αNSD2
αGAPDH
αH3K27me2
αH3K36me2
αH3
F
WSU-DLCL2 (EZH2 Y646F)
NSD2-KO
NSD1-KO
CTRL
NSD2-KO
CTRL
NSD1-KO
Relative abundance
4
2
αNSD1
αNSD2
αNSD3
αNSD1
αNSD2
Karpas-422 (EZH2 Y646N)
NSD2-KO
NSD1-KO
CTRL
NSD2-KO
CTRL
NSD1-KO
Relative abundance
1
αNSD1
αNSD2
αNSD3
αNSD1
αNSD2
G
WSU-DLCL2 (EZH2 Y646F)
Total
Soluble
Chromatin Bound
CTRL
NSD2-KO
NSD1-KO
70kDa
αNSD2
150kDa
αNSD1
100kDa
αEZH2
55kDa
αEED
35kDa
αGAPDH
15kDa
αH3
H
Karpas-422 (EZH2 Y646N)
Total
Soluble
Chromatin Bound
CTRL
NSD2-KO
NSD1-KO
70kDa
αNSD2
300kDa
αNSD1
35kDa
αGAPDH
15kDa
αH3

Figure 4.7: All three NSD isoforms are expressed in lymphoma cells, while NSD1 and NSD2 are chromatin bound, and their loss has variable effects on histone H3 post-translational modifications.

A. Immunoblots of the indicated proteins from whole cell lysates in CTRL, *NSD2*-KO, WSU-DLCL2 and Karpas-422 (EZH2-mutant lymphoma) cells.

B. Immunoblots of the indicated proteins and histone modifications from whole cell lysates in CTRL, *NSD2*-KO and *NSD1*-KO, WSU-DLCL2 (EZH2-mutant lymphoma) cells.

C. Immunoblots of the indicated proteins and histone modifications from whole cell lysates in CTRL, *NSD2*-KO and *NSD1*-KO, WSU-DLCL2 (EZH2-mutant lymphoma) cells. The signal of each immunoblot relative to the GAPDH (for proteins) and H3 (for histone modifications) loading controls is indicated under each immunoblot.

D. Immunoblots of the indicated histone modifications from whole cell lysates in CTRL, *NSD2*-KO and *NSD1*-KO, WSU-DLCL2 (EZH2-mutant lymphoma) cells. The signal of each immunoblot relative to the H3 loading control is indicated under each immunoblot.

E. Immunoblots of the indicated proteins and histone modifications from whole cell lysates in CTRL, *NSD2*-KO and *NSD1*-KO, Karpas-422 (EZH2-mutant lymphoma) cells.

F. Relative quantification of immunoblot analyses of NSD1, NSD2, NSD3 abundance in WSU-DLCL2 and Karpas-422 (EZH2-mutant lymphoma) cells. Signal intensity values were normalised to a loading control and then expressed relative to the control cells. Data values represent mean values ± SD of the indicated replicates.

G. Immunoblots of the indicated proteins from chromatin subcellular fractionations in CTRL, *NSD2*-KO and *NSD1*-KO, WSU-DLCL2 (EZH2-mutant lymphoma) cells.

H. Immunoblots of the indicated proteins from chromatin subcellular fractionations in CTRL, *NSD2*-KO and *NSD1*-KO, Karpas-422 (EZH2-mutant lymphoma) cells.

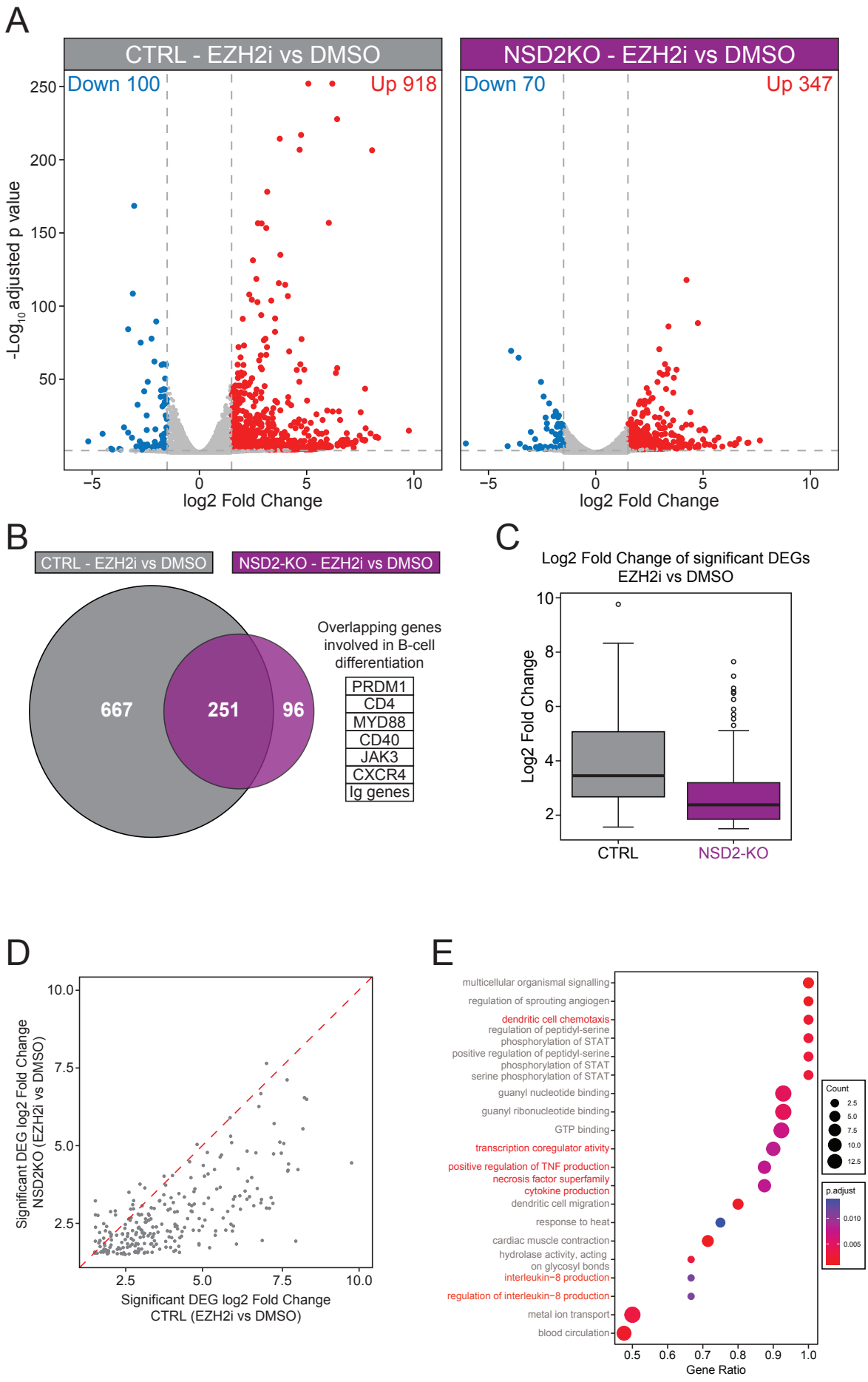
A
CTRL - EZH2i vs DMSO
Down 100
Up 918
NSD2KO - EZH2i vs DMSO
Down 70
Up 347
-Log10 adjusted p value
log2 Fold Change
B
CTRL - EZH2i vs DMSO
NSD2-KO - EZH2i vs DMSO
667
251
96
Overlapping genes involved in B-cell differentiation
PRDM1
CD4
MYD88
CD40
JAK3
CXCR4
Ig genes
C
Log2 Fold Change of significant DEGs EZH2i vs DMSO
Log2 Fold Change
CTRL
NSD2-KO
D
Significant DEG log2 Fold Change NSD2KO (EZH2i vs DMSO)
Significant DEG log2 Fold Change CTRL (EZH2i vs DMSO)
E
multicellular organismal signalling
regulation of sprouting angiogen
dendritic cell chemotaxis
regulation of peptidyl-serine phosphorylation of STAT
positive regulation of peptidyl-serine phosphorylation of STAT
serine phosphorylation of STAT
guanyl nucleotide binding
guanyl ribonucleotide binding
GTP binding
transcription coregulator ativity
positive regulation of TNF production
necrosis factor superfamily cytokine production
dendritic cell migration
response to heat
cardiac muscle contraction
hydrolase activity, acting on glycosyl bonds
interleukin−8 production
regulation of interleukin−8 production
metal ion transport
blood circulation
Gene Ratio
Count
p.adjust

Figure 4.8: *NSD2* loss blunts gene activation following EZH2 inhibitor treatment of B-cell lymphomas.

A. Volcano plots of RNA-seq depicting differentially expressed genes in CTRL and *NSD2*-KO, Karpas-422 (EZH2-mutant lymphoma) cells treated with DMSO control or 100nM of the EZH2 inhibitor Tazemetostat for 6 days. The number of genes differentially expressed both up (red) and down (blue) are indicated on the plots (n=3 biological replicates; significance cutoff: $p < 0.05$; minimum 1.5-fold change).

B. Venn diagram demonstrating overlap of differentially expressed genes upregulated (DEGs up) in CTRL and *NSD2*-KO, Karpas-422 lymphoma cells treated with DMSO control or 100nM of the EZH2 inhibitor Tazemetostat for 6 days.

C. Boxplots comparing differentially expressed genes upregulated (DEGs up) in CTRL and *NSD2*-KO, Karpas-422 lymphoma cells treated with DMSO control or 100nM of the EZH2 inhibitor Tazemetostat for 6 days. Boxes represent the interquartile range (25th–75th percentiles), the median is indicated within the boxes with a thick line, and whiskers extend to the most extreme values within 1.5x of the IQR. Values are represented by the Log2 Fold Change in EZH2i versus DMSO treated cells.

D. XY plot comparing log2 fold-change of differentially expressed genes upregulated (DEGs up) in CTRL cells (+/-EZH2i) on the x-axis with *NSD2*-KO cells (+/- EZH2i) on the y-axis.

E. Gene ontology analysis of the 918 genes upregulated in CTRL lymphoma cells treated with the EZH2 inhibitor Tazemetostat showing significantly enriched GO biological process and molecular function terms. The x-axis represents the gene ratio (the proportion of genes within the DEG list associated with each GO term), while dot size indicates the number of genes contributing to each term. Dot color corresponds to the adjusted p-value (FDR).

A-E. CTRL cells shown in grey, while NSD2-KO cells are denoted in purple.

H3K36me2 enrichment (**Figure 4.9C**). Notably, NSD2 binding and H3K36me2 signal were not perfectly correlated, indicating that NSD2 probably does not control all H3K36me2, a finding that corroborates immunoblots in Section 4.2.7. Furthermore, these results should be interpreted with caution, given the significant background noise in the NSD2 CUT&RUN, the proportion of 10kb bins above the diagonal are likely skewed, especially in low signal regions. Genomic annotation of H3K36me2 peaks validated the CUT&RUN assay; consistent with previously published work, the majority of peaks were at promoters, with enrichment at intergenic regions and gene bodies (**Figure 4.9D**). Next, fold-change analysis comparing *NSD2*-KO to CTRL cells further supported the relationship between NSD2 occupancy and H3K36me2, where a significant proportion of genomic bins lose H3K36me2 upon *NSD2* loss (**Figure 4.9E**). Crucially, not all regions behave in this way, suggesting an uncoupling of NSD2 and H3K36me2 at certain genomic loci. These regions where NSD2 is lost but H3K36me2 is unchanged or increased (Q2) were compared with Q3 regions in annotation analysis which only showed subtle changes between these quadrants (**Figure 4.9F**). Finally, in contrast to genome-wide, average plots at genes downregulated in *NSD2*-KO showed coordinated reductions in H3K36me2 and NSD2 signal alongside reduced H3K27ac, linking NSD2-dependent H3K36me2 redistribution to transcriptional repression (**Figure 4.9G-H**). Collectively, these data support a model in which *NSD2* loss results in redistribution of H3K36me2 at specific genomic regions with downstream consequences for gene expression.

4.2.10 *NSD2* loss increases PRC2-dependent H3K27me3 and H3K27me2 enrichment genome-wide and at Polycomb target genes in EZH2-mutant lymphoma cells

To investigate whether *NSD2* loss can influence Polycomb-mediated repression, I examined transcriptional and chromatin changes in EZH2-mutant lymphoma cells following *NSD2* knockout. Looking again at earlier RNA-seq analysis, this time focusing on *NSD2*-KO vs control in EZH2-mutant lymphoma cells, I noted widespread transcriptional

alterations, with substantial numbers of genes both upregulated and downregulated relative to control (**Figure 4.10A**). Genes downregulated upon *NSD2* loss were enriched for pathways related to immune signalling, lipid metabolism, and small GTPase regulation, consistent with increased transcriptional repression at specific genomic loci (**Figure 4.10B**). Given the established antagonism between H3K36 methylation and PRC2 activity, I next assessed PRC2 occupancy and H3K27 methylation states. At Polycomb group (PcG) target gene promoters, *NSD2* loss was associated with increased binding of PRC2 components SUZ12 and MTF2, accompanied by relatively minimal H3K27me3 changes, suggesting enhanced PRC2 engagement at these loci (**Figure 4.10C**). Genome-wide analyses illustrated modest H3K27me3 enrichment across broad chromosomal domains in Karpas-422 NSD2-KO cells, with a slightly more pronounced signal in WSU-DLCL2 *NSD2*-KO cells (**Figure 4.10D-E**). More strikingly, H3K27me2 levels were more significantly elevated across the entire genome (**Figure 4.10F-G**), suggesting NSD2 loss results in a coordinated expansion of repressive H3K27 methylation states rather than isolated, locus-specific effects. Collectively, this data is suggestive of a model in which NSD2-dependent H3K36me2 normally limits PRC2 activity or spreading, and that loss of NSD2 shifts the chromatin landscape toward increased PRC2 occupancy and H3K27 methylation, reinforcing Polycomb-associated repression in EZH2-mutant lymphoma cells.

4.2.11 Genome-wide overlap of H3K36me2 with H3K27ac identifies transcriptionally vulnerable loci

Building on the previous observation that *NSD2* loss enhances PRC2 occupancy and global H3K27 methylation in EZH2-mutant lymphoma cells, I next examined how NSD2-dependent H3K36me2 intersects with different chromatin states and how this balance is affected upon NSD2 loss. Genome browser views of CUT&RUN-Rx for H3K27me3, H3K36me2 and H3K27ac highlighted H3K36me2 and H3K27ac peaks coinciding at certain genomic loci, whereas H3K27me3 occupied largely distinct domains (**Figure 4.11A**), consistent with opposing chromatin contexts (Streubel et al., 2018; Xu et al., 2008; Yuan et

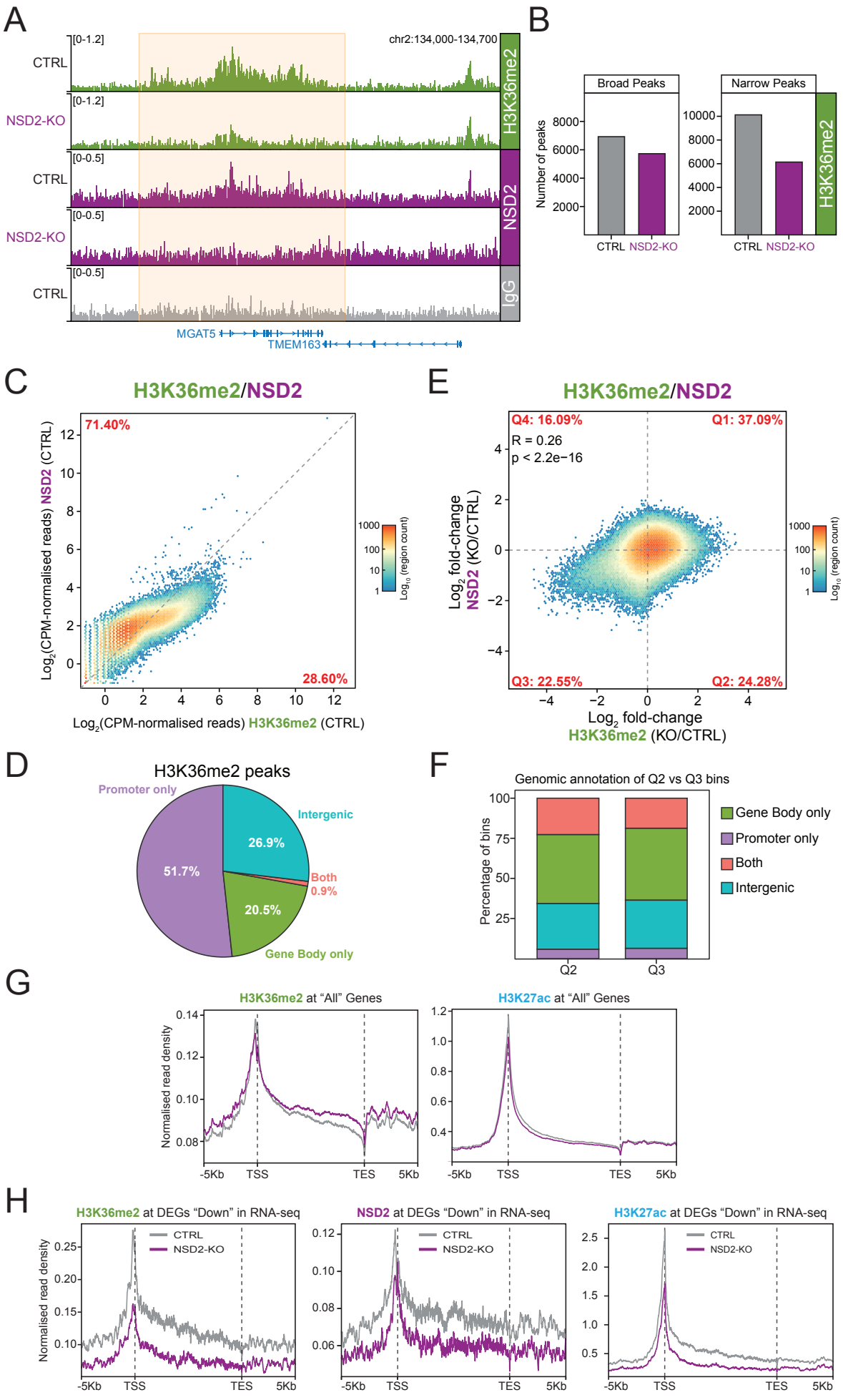
A
[0-1.2]
chr2:134,000-134,700
CTRL
NSD2-KO
H3K36me2
[0-0.5]
NSD2
IgG
MGAT5
TMEM163
B
Broad Peaks
Narrow Peaks
Number of peaks
CTRL NSD2-KO
C
H3K36me2/NSD2
71.40%
28.60%
Log2(CPM-normalised reads) NSD2 (CTRL)
Log2(CPM-normalised reads) H3K36me2 (CTRL)
Log10 (region count)
D
H3K36me2 peaks
Promoter only
Intergenic
Both
Gene Body only
51.7%
26.9%
0.9%
20.5%
E
H3K36me2/NSD2
Q4: 16.09%
Q1: 37.09%
R = 0.26
p < 2.2e−16
Q3: 22.55%
Q2: 24.28%
Log2 fold-change NSD2 (KO/CTRL)
Log2 fold-change H3K36me2 (KO/CTRL)
F
Genomic annotation of Q2 vs Q3 bins
Percentage of bins
Gene Body only
Promoter only
Both
Intergenic
Q2
Q3
G
H3K36me2 at "All" Genes
H3K27ac at "All" Genes
Normalised read density
-5Kb TSS TES 5Kb
H
H3K36me2 at DEGs "Down" in RNA-seq
NSD2 at DEGs "Down" in RNA-seq
H3K27ac at DEGs "Down" in RNA-seq
CTRL
NSD2-KO

Figure 4.9: *NSD2* loss globally redistributes H3K36me2 across the genome

A. Representative genome browser tracks showing H3K36me2 (green), NSD2 (purple), and IgG control (grey) signal in CTRL and *NSD2*-KO Karpas-422 (EZH2-mutant) lymphoma cells across the MGAT5/T-MEM163 locus. The highlighted region illustrates reduced H3K36me2 signal coinciding with reduced NSD2 occupancy in *NSD2*-KO cells.

B. Bar plots showing the total number of H3K36me2 peaks identified in CTRL and *NSD2*-KO Karpas-422 (EZH2-mutant) lymphoma cells using the MACS2 algorithm (Zhang et al., 2008) for broad peak calling (left) and narrow peak calling (right).

C. Density scatter plot comparing $\log_2$ CPM-normalised H3K36me2 signal (x-axis) and NSD2 signal (y-axis) in CTRL cells across 10kb genomic bins. The dashed diagonal indicates equal signal between marks. Percentages indicate the fraction of bins above or below the diagonal.

D. Genomic annotation of H3K36me2 peaks in CTRL Karpas-422 (EZH2-mutant) lymphoma cells. Peaks were classified as promoter-only, gene body-only, both promoter and gene body, or intergenic based on genomic overlap. Genomic annotation of H3K36me2 peaks was performed using HOMER with hg38 gene annotations (Heinz et al., 2010).

E. Density scatter plot showing the relationship between H3K36me2 $\log_2$ fold-change (*NSD2*-KO vs CTRL) on the x-axis, and NSD2 $\log_2$ fold-change (*NSD2*-KO vs CTRL) on the y-axis across 10kb genomic bins. Dashed lines indicate zero fold-change. Quadrants (Q1–Q4) denote bins with concordant or discordant changes between NSD2 and H3K36me2, with percentages shown for each quadrant. Pearson correlation coefficient (R) and corresponding two-sided p-value are indicated.

F. Stacked bar plots showing the genomic annotation of bins in Q2 (H3K36me2 gain with *NSD2* loss) and Q3 (concordant loss of *NSD2* and H3K36me2). Differences in annotation distributions between Q2 and Q3 were assessed using a chi-squared test of independence.

G. Metaplots of normalised CUT&RUN signal for H3K36me2 (Rx) (left), and H3K27ac (Rx) (right) across all genes in RNA-seq. Profiles are centered on transcription start sites (TSS) and scaled to transcription end sites (TES), with ±5 kb flanking regions shown.

H. Metaplots of normalised CUT&RUN signal for H3K36me2 (Rx) (left), NSD2 (CPM) (middle), and H3K27ac (Rx) (right) across genes downregulated in RNA-seq upon *NSD2* loss. Profiles are centered on transcription start sites (TSS) and scaled to transcription end sites (TES), with ±5 kb flanking regions shown.

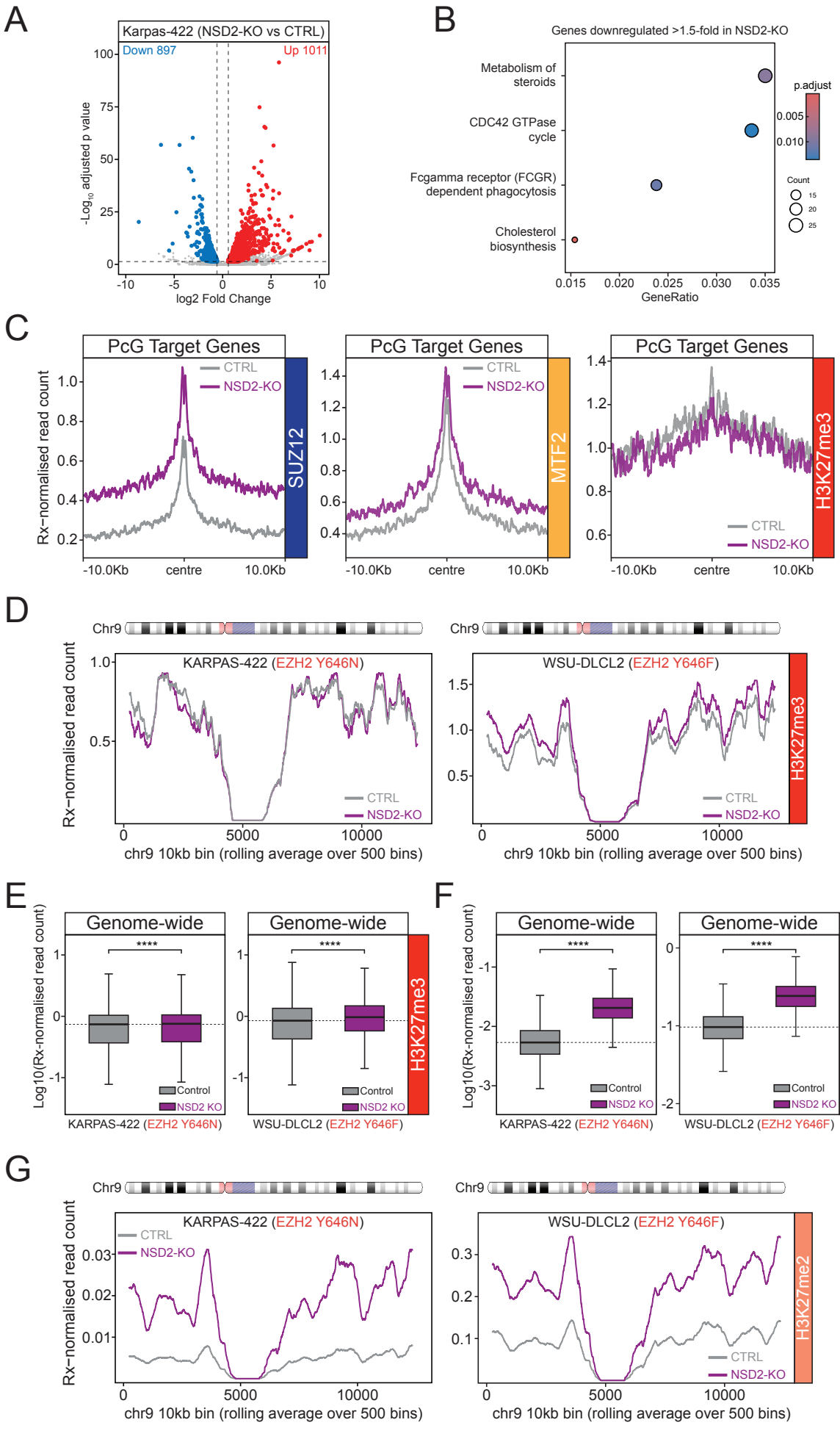
A
Karpas-422 (NSD2-KO vs CTRL)
Down 897
Up 1011
-Log10 adjusted p value
log2 Fold Change
B
Genes downregulated >1.5-fold in NSD2-KO
Metabolism of steroids
CDC42 GTPase cycle
Fcgamma receptor (FCGR) dependent phagocytosis
Cholesterol biosynthesis
p.adjust
Count
GeneRatio
C
PcG Target Genes
CTRL
NSD2-KO
Rx-normalised read count
SUZ12
MTF2
H3K27me3
-10.0Kb
centre
10.0Kb
D
Chr9
KARPAS-422 (EZH2 Y646N)
WSU-DLCL2 (EZH2 Y646F)
chr9 10kb bin (rolling average over 500 bins)
E
Genome-wide
Log10(Rx-normalised read count)
Control
NSD2 KO
H3K27me3
F
H3K27me2
G

Figure 4.10: *NSD2* loss increases PRC2-dependent H3K27me3 and H3K27me2 enrichment genome-wide and at Polycomb target genes in EZH2-mutant lymphoma cells.

A. Volcano plots of RNA-seq depicting differentially expressed genes in CTRL and *NSD2*-KO, Karpas-422 (EZH2-mutant lymphoma) cells. The number of genes differentially expressed both up (red) and down (blue) are indicated on the plots (n=3 biological replicates; significance cutoff: $p < 0.05$; minimum 1.5-fold change).

B. Reactome/Gene Ontology analysis of genes downregulated >1.5 fold in *NSD2*-KO cells compared with control cells.

C. Average plots showing spike-in normalized H3K27me3 CUT&RUN-Rx enrichment for the indicated antibodies at PRC2 target genes in CTRL and *NSD2*-KO Karpas-422 (EZH2-mutant) lymphoma cells.

D. Rolling average plots presenting H3K27me3 CUT&RUN-Rx signal across the whole of chromosome 9 in CTRL and *NSD2*-KO Karpas-422 and WSU-DLCL2 (EZH2-mutant) lymphoma cells. Visualised using 10kb genomic windows.

E. Boxplots of H3K27me3 CUT&RUN-Rx signal at genome-wide 10kb bins in CTRL and *NSD2*-KO Karpas-422 and WSU-DLCL2 (EZH2-mutant) lymphoma cells. Significance determined using pairwise Wilcoxon rank-sum tests, ****p value ≤ 0.0001.

F. Boxplots of H3K27me2 CUT&RUN-Rx signal at genome-wide 10kb bins in CTRL and *NSD2*-KO Karpas-422 and WSU-DLCL2 (EZH2-mutant) lymphoma cells. Significance determined using pairwise Wilcoxon rank-sum tests, ****p value ≤ 0.0001.

G. Rolling average plots presenting H3K27me2 CUT&RUN-Rx signal across the whole of chromosome 9 in CTRL and *NSD2*-KO Karpas-422 and WSU-DLCL2 (EZH2-mutant) lymphoma cells. Visualised using 10kb genomic windows.

al., 2011). Quantitative analyses across increasing genomic footprints showed minimal overlap between H3K36me2 and H3K27me3, and between H3K27ac and H3K27me3, even at large scales, while H3K36me2 and H3K27ac shared a modest degree of genomic space which increased proportionally with footprint size (**Figure 4.11B-D**), supporting a partial association of H3K36me2 with transcriptionally active regions.

Following *NSD2* loss, regions previously marked by both H3K36me2 and H3K27ac showed redistribution in genomic annotation, with reduced promoter and gene body association and increased localisation to intergenic regions (**Figure 4.11E**), suggesting a loss of focused enrichment at transcriptionally relevant loci. Integrating previous RNA-seq with chromatin occupancy experiments, I noted that genes associated with shared H3K36me2/H3K27ac domains exhibit significantly greater transcriptional downregulation compared with other genes in *NSD2*-KO cells (**Figure 4.11F**), and are enriched among downregulated transcripts genome-wide (**Figure 4.11G**). Together, these data support a model in which NSD2-dependent H3K36me2 contributes to the maintenance of active chromatin states that are antagonistic to PRC2-mediated repression, and that loss of *NSD2* shifts this balance toward Polycomb-dominated chromatin, leading to redistribution of active marks and preferential transcriptional vulnerability at H3K36me2/H3K27ac–associated loci. The current analysis does not account for indirect consequences of broader transcriptional reprogramming.

4.2.12 *NSD2* loss modulates the chromatin response to EZH2 inhibition

Next, I attempted to integrate the effect of PRC2 inhibition on histone post-translational modifications with NSD2 modulation in EZH2-mutant lymphoma cells. Using the same approach as in Section 4.2.9, I divided the genome into 10kb bins and plotted log2 fold-change of H3K27me3, H3K27me2, H3K27ac and H3K36me2 signal between Tazemetostat-treated cells versus DMSO control. I then plotted *NSD2*-KO cells on the y-axis and control cells on the x-axis. I observed that EZH2 inhibition was associated with widespread loss of H3K27me3 and H3K27me2, and gains in H3K27ac and H3K36me2 at

most genomic loci (**Figure 4.12A**). The effects of EZH2 inhibitor treatment on H3K36me2 levels have not been widely reported, and so this finding, along with **Figure 4.5F** add to our understanding of chromatin context modulation following PRC2 inhibition, and are in keeping with similar findings in childhood malignant rhabdoid tumours treated with EZH2 inhibitors (Drosos et al., 2022). An interesting feature in these analyses was that NSD2 knockout did not significantly alter the magnitude or direction of H3K27me3 or H3K27ac changes in response to EZH2 inhibition, however H3K27me2 was reduced more significantly with Tazemetostat in *NSD2*-KO cells, and H3K36me2 was not increased as much in response to Tazemetostat in *NSD2*-KO cells.

Then, I divided the genome into quartiles of H3K27me3 signal and mapped the log2 fold-change in RNA-seq expression, H3K36me2 and H3K27ac chromatin occupancy. I observed that the quartiles possessing the most abundant baseline H3K27me3 signal demonstrated the greatest degree of gene de-repression in response to EZH2 inhibition, and that this was blunted across the higher quartiles only in *NSD2*-KO cells (**Figure 4.12B**). I saw that H3K36me2 gained the most signal in the highest H3K27me3 quartiles and that across all quartiles, but particularly Q1 and Q2, this effect was blunted in *NSD2*-KO cells. Finally, although H3K27ac increased expectedly across H3K27me3 quartiles in EZH2 inhibitor-treated cells, there was no clear difference in the degree of increase between *NSD2*-KO and control cells.

4.2.13 *NSD2* loss remodels enhancer-associated chromatin states

Finally, given the significant changes in transcriptional responses to EZH2 inhibition in *NSD2* knockout lymphoma cells, and the identification of shared H3K27ac/H3K36me2 regions, I sought to characterise genomic elements that could represent sites of NSD2-dependent regulatory activity. Firstly, I quantitatively assessed H3K27ac narrow peaks and observed a moderate degree of overlap between *NSD2*-KO and control lymphoma cells, as well as substantial sets of condition-specific peaks (**Figure 4.13A**). Genomic annotation of all H3K27ac peaks in control cells, as well as unique peaks in control or *NSD2*-KO cells,

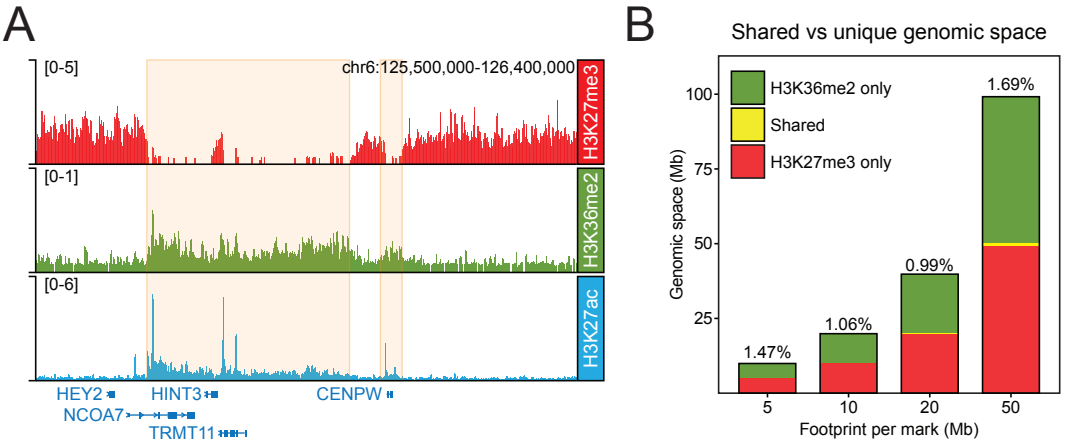
A
[0-5]
chr6:125,500,000-126,400,000
H3K27me3
[0-1]
H3K36me2
[0-6]
H3K27ac
HEY2
NCOA7
HINT3
TRMT11
CENPW

B
Shared vs unique genomic space
H3K36me2 only
Shared
H3K27me3 only
Genomic space (Mb)
100
75
50
25
1.47%
1.06%
0.99%
1.69%
5
10
20
50
Footprint per mark (Mb)

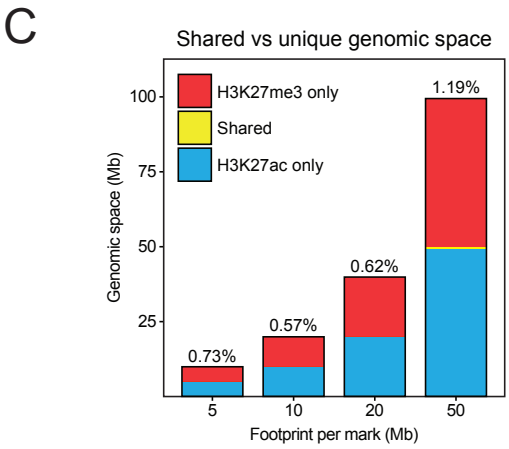
C
Shared vs unique genomic space
H3K27me3 only
Shared
H3K27ac only
Genomic space (Mb)
100
75
50
25
0.73%
0.57%
0.62%
1.19%
5
10
20
50
Footprint per mark (Mb)

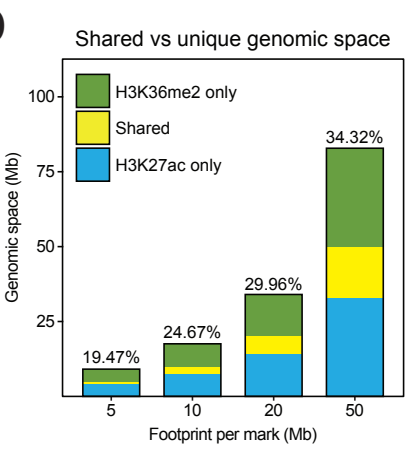
D
Shared vs unique genomic space
H3K36me2 only
Shared
H3K27ac only
Genomic space (Mb)
100
75
50
25
19.47%
24.67%
29.96%
34.32%
5
10
20
50
Footprint per mark (Mb)

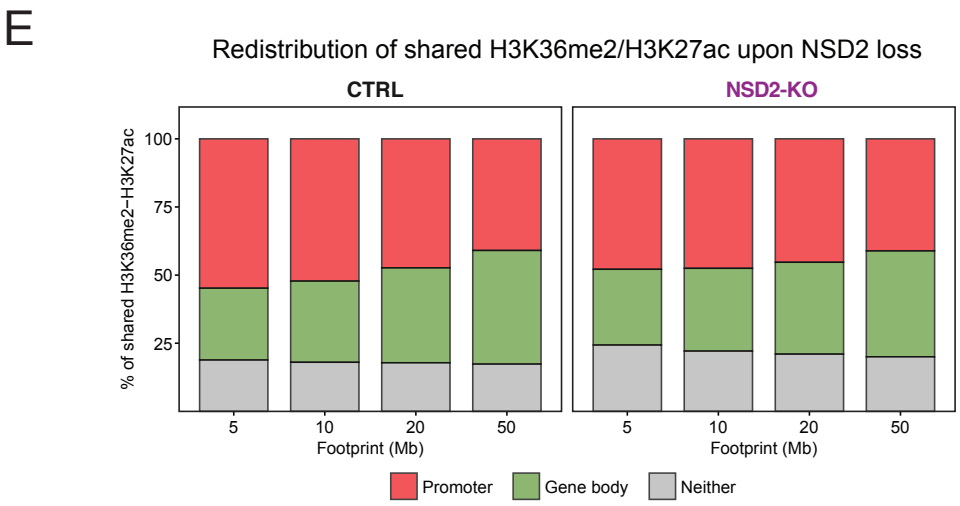
E
Redistribution of shared H3K36me2/H3K27ac upon NSD2 loss
CTRL
NSD2-KO
% of shared H3K36me2−H3K27ac
100
75
50
25
5
10
20
50
Footprint (Mb)
Promoter
Gene body
Neither

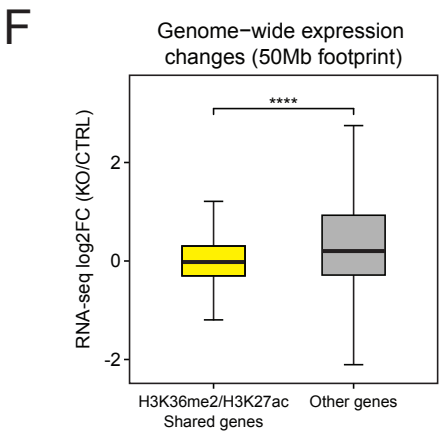
F
Genome−wide expression changes (50Mb footprint)
RNA-seq log2FC (KO/CTRL)
****
2
0
-2
H3K36me2/H3K27ac Shared genes
Other genes

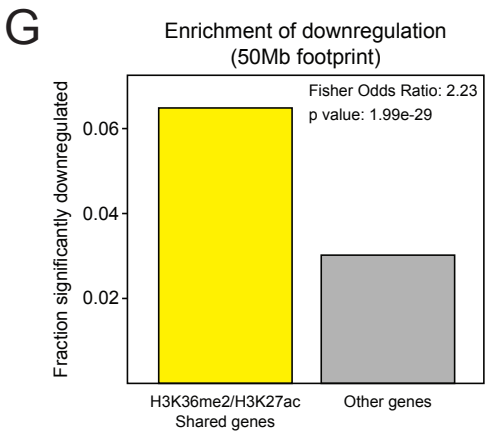
G
Enrichment of downregulation (50Mb footprint)
Fisher Odds Ratio: 2.23
p value: 1.99e-29
Fraction significantly downregulated
0.06
0.04
0.02
H3K36me2/H3K27ac Shared genes
Other genes

Figure 4.11: Genome-wide overlap of H3K36me2 with H3K27ac identifies transcriptionally vulnerable loci

A. Representative genome browser view illustrating the spatial relationship between H3K36me2 (green), H3K27me3 (red), and H3K27ac (blue) across a locus on chromosome 6 in CTRL Karpas-422 (EZH2-mutant) lymphoma cells. Highlighted regions indicate the dichotomous relationship between the repressive H3K27me3 post-translational modification and H3K27ac and H3K36me2.

B. Genome-wide overlap between H3K36me2 and H3K27me3 quantified using increasing genomic footprints (5, 10, 20, and 50 Mb per mark). Stacked bars indicate H3K36me2-only (green), H3K27me3-only (red), and shared (yellow) genomic space. Percentages above bars denote the fraction of shared overlap relative to total genomic space covered.

C. Genome-wide overlap between H3K27ac and H3K27me3 across increasing genomic footprints. Stacked bars show H3K27ac-only (blue), H3K27me3-only (red), and shared (yellow) regions, with percentages indicating shared overlap.

D. Genome-wide overlap between H3K36me2 and H3K27ac across increasing genomic footprints. Stacked bars show H3K36me2-only (green), H3K27ac-only (blue), and shared (yellow) genomic space. Percentages indicate the fraction of shared overlap, revealing substantial co-localization at larger footprints.

E. Genomic annotation of shared H3K36me2/H3K27ac regions in CTRL and *NSD2*-KO Karpas-422 lymphoma cells. Shared regions were classified as promoter, gene body, or intergenic, and proportions are shown for each footprint size, highlighting redistribution toward intergenic regions upon NSD2 loss.

F. RNA-seq log2 fold-change (*NSD2*-KO vs CTRL) for genes associated with shared H3K36me2/H3K27ac regions compared with all other genes (50 Mb footprint). Boxplots show median and interquartile range; whiskers represent 1.5x IQR. Statistical significance was assessed using a two-sided Wilcoxon rank-sum test (****, $p < 0.0001$).

G. Enrichment of transcriptional downregulation among genes associated with shared H3K36me2/H3K27ac regions compared with other genes (50 Mb footprint). Bars represent the fraction of significantly downregulated genes (adjusted $p < 0.05$). Enrichment was assessed using Fisher's exact test; odds ratio and p-value are indicated.

A

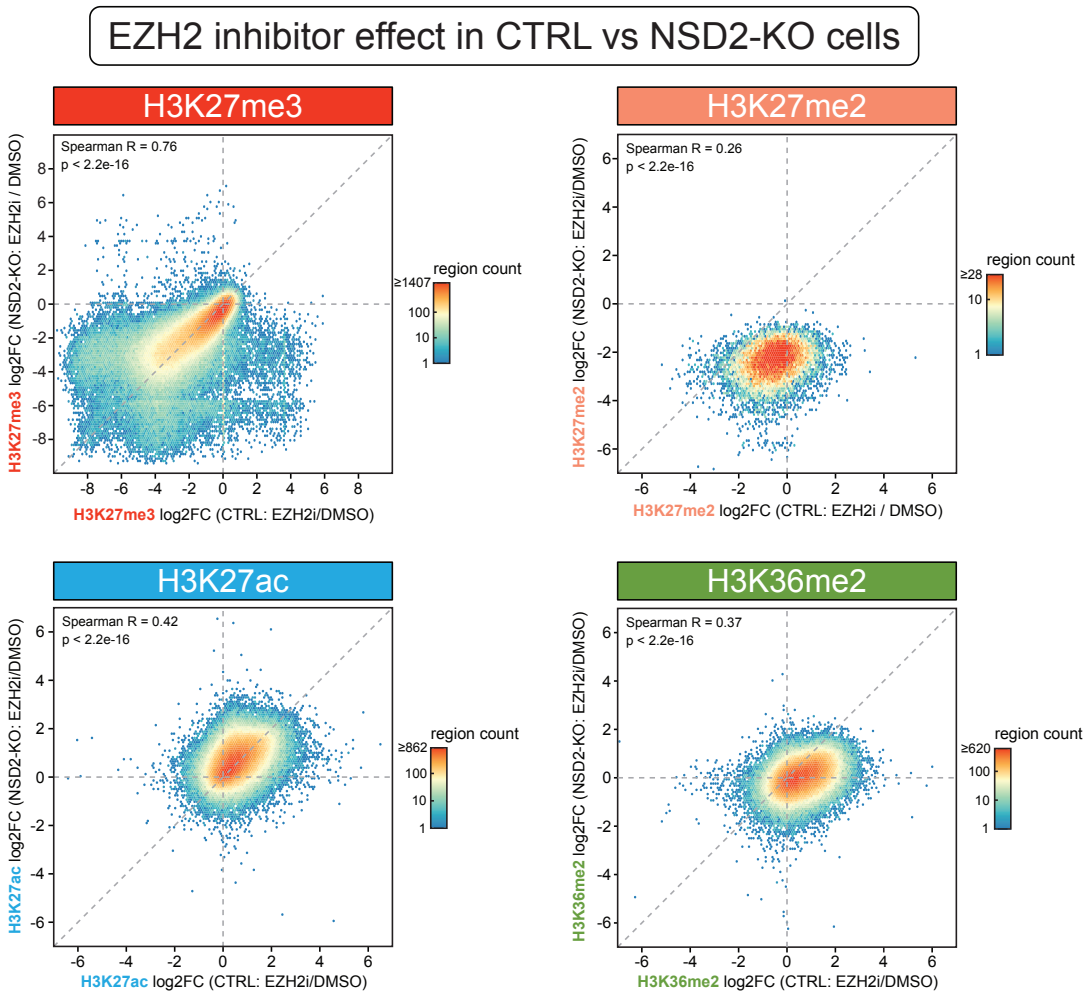
EZH2 inhibitor effect in CTRL vs NSD2-KO cells
H3K27me3
Spearman R = 0.76
p < 2.2e-16
H3K27me3 log2FC (NSD2-KO: EZH2i / DMSO)
H3K27me3 log2FC (CTRL: EZH2i/DMSO)
region count
≥1407
100
10
1
H3K27me2
Spearman R = 0.26
p < 2.2e-16
H3K27me2 log2FC (NSD2-KO: EZH2i/DMSO)
H3K27me2 log2FC (CTRL: EZH2i / DMSO)
region count
≥28
10
1
H3K27ac
Spearman R = 0.42
p < 2.2e-16
H3K27ac log2FC (NSD2-KO: EZH2i/DMSO)
H3K27ac log2FC (CTRL: EZH2i/DMSO)
region count
≥862
100
10
1
H3K36me2
Spearman R = 0.37
p < 2.2e-16
H3K36me2 log2FC (NSD2-KO: EZH2i/DMSO)
H3K36me2 log2FC (CTRL: EZH2i/DMSO)
region count
≥620
100
10
1

B

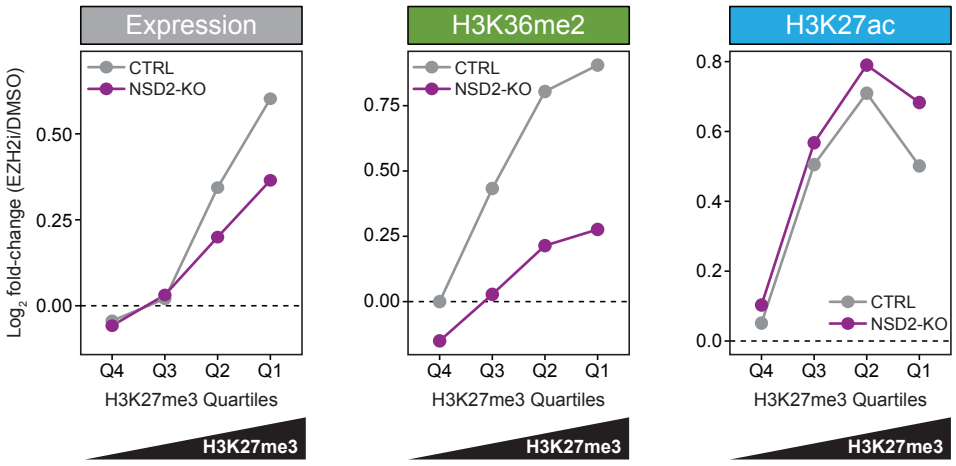
Expression
H3K36me2
H3K27ac
CTRL
NSD2-KO
Log2 fold-change (EZH2i/DMSO)
Q4
Q3
Q2
Q1
H3K27me3 Quartiles
H3K27me3

Figure 4.12: *NSD2* loss modulates the chromatin response to EZH2 inhibition

A. Hexbin scatter plots comparing $\log_2$ fold-change of CUT&RUN signal of H3K27ac, H3K27me2, H3K27me3 and H3K36me2 induced by EZH2 inhibition (EZH2i vs DMSO) in CTRL (x-axis) versus *NSD2*-KO (y-axis) cells across the entire genome. Each point represents a 10kb genomic bin, coloured by regional density. Spearman correlation coefficients are shown, with p-values calculated using two-sided Spearman rank correlation tests.

B. Line plots illustrating the average EZH2i-induced $\log_2$ fold-change in gene expression, H3K36me2, and H3K27ac across genomic quartiles (Q1–Q4), stratified by chromatin context. Genes are separated into quartiles based on H3K27me3 levels in CTRL Karpas-422 cells. Responses in CTRL and *NSD2*-KO lymphoma cells are shown. Dashed horizontal lines indicate no change.

demonstrated that *NSD2*-KO unique peaks seemed to be less promoter based and more enriched at intergenic and intronic regions, which could represent candidate enhancer regions (**Figure 4.13B**).

I defined candidate enhancer regions based on H3K27ac peaks by excluding promoter-proximal regions (TSS ±2 kb) and annotated exons using hg38 gene annotations, resulting in a set of intronic and distal intergenic enhancer-like elements. I then profiled chromatin occupancy for NSD2, Polycomb components and associated histone post-translational modifications. Expectedly, NSD2 binding was lost at these candidate enhancers in *NSD2*-KO cells, accompanied by significant reductions in both H3K36me2 and H3K27ac at these regions. Furthermore, I observed increased SUZ12 binding at these elements alongside a strong increase in H3K27me2 and H3K27me3 signal at these regions, indicating acquisition of Polycomb-associated features at loci that are active in control cells (**Figure 4.13C**).

Collectively, these findings suggest that *NSD2* loss is associated with alteration of chromatin landscapes at candidate enhancer regions, characterised by loss of active histone marks and increased Polycomb-associated repressive histone post-translational modifications. While this data is consistent with a role for NSD2 in regulating active distal regulatory elements, and is consistent with a recent report on NSD1 roles in a model system,. Further experiments including chromatin capture techniques such as Hi-C would be required to link these candidate enhancers to target gene promoters and associated transcriptional changes.

4.2.14 Developing NSD2 mutant constructs for further mechanistic exploration of NSD2-mediated resistance to EZH2 inhibitors in B-cell lymphoma

So far I have explored in detail the functional consequences of NSD2 loss on lymphoma cell fitness upon EZH2 inhibition, the consequences of NSD2 loss on H3K36me2 and

H3K27ac redistribution across the genome, focussing on distal regulatory elements, and the effects of NSD2 loss on blunting the transcriptional response to EZH2 inhibitors. To further explore mechanisms of NSD2 function in EZH2-mutant lymphoma I decided to clone the hypermorphic NSD2 E1099K mutant which results in excessive H3K36me2 deposition and is found in a number of blood cancers (Oyer et al., 2014; Pierro et al., 2020; Swaroop et al., 2019), as well as a catalytically dead NSD2 mutant (**Figure 4.14A**). These ORFs were kindly provided by Dr Gerry Brien who had generated them previously.

I planned for these mutants to be used in functional assays, to firstly be able to perform FLAG CUT&RUN assays to circumvent the issue of high background in the endogenous NSD2 CUT&RUNs. Secondly, I wanted to determine the contribution of the SET domain to the EZH2 inhibitor resistance phenotype seen in the lymphoma cells. By producing excessive H3K36me2 at the expense of H3K27me3, the hypermorphic NSD2 mutant in theory should not only rescue the resistance phenotype, but should be toxic to the EZH2-mutant lymphoma cells. To check whether these constructs could be expressed in human cells, I performed transient transfections in HEK293T cells (**Figure 4.14B**). I was successfully able to transiently express the NSD2 wild-type, E1099K and catalytically dead constructs (**Figure 4.14C**). To my surprise, even in these HEK293T models, I was able to observe the expected differential changes on H3K36me2 levels with each NSD2 construct (**Figure 4.14D**). These constructs will be invaluable moving forward in EZH2-mutant lymphoma cells.

4.2.15 The recurrent hypermorphic *NSD2* mutation found in B-cell acute lymphoblastic leukaemia may create genetic vulnerabilities to Polycomb and Menin

In the last section in this chapter on NSD2 I decided to focus on NSD2 dysfunction in other types of blood cancers. Using data from the Cancer Dependency Map I first mapped cancer cell mutations across the protein domains of NSD2. Mutations of the enzymatic SET domain

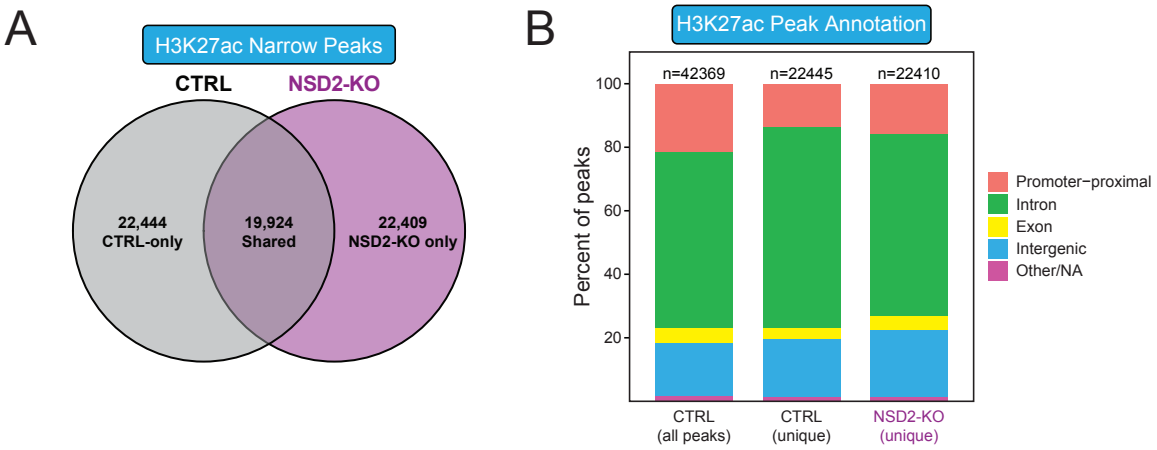

C

Candidate Enhancers

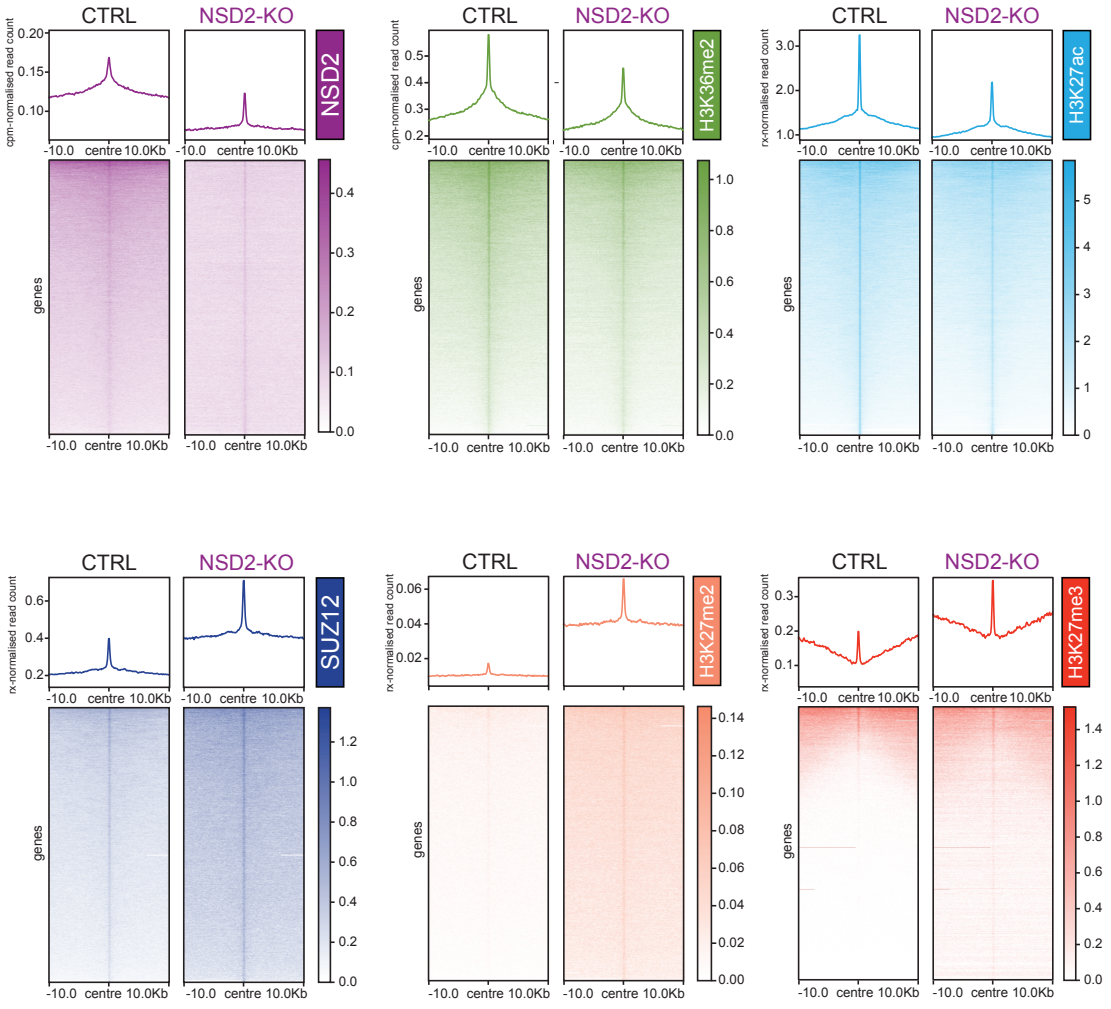

Figure 4.13: *NSD2* loss remodels enhancer-associated chromatin states

A. Venn diagram illustrating the overlap of H3K27ac narrow peaks using the MACS2 algorithm (Zhang et al., 2008) in CTRL and *NSD2*-KO Karpas-422 (EZH2-mutant) lymphoma cells. Peaks were considered shared only if they exhibited ≥50% reciprocal overlap, defining a stringent set of robustly conserved regions. Condition-specific peaks represent loci gained or lost upon *NSD2* deletion.

B. Stacked bar plot demonstrating the genomic distribution of H3K27ac peaks for all CTRL cell peaks, CTRL-specific peaks, and *NSD2*-KO-specific peaks (reciprocal overlap ≥50%). Peaks were annotated relative to hg38 gene features using HOMER (Heinz et al., 2010) and classified as promoter-proximal, intronic, exonic, intergenic, or other/unassigned. Values are shown as the percentage of peaks within each category; total peak numbers are indicated above each bar.

C. Average plots (top) and tornado plots (bottom) of CUT&RUN profiles for NSD2, H3K36me2, H3K27ac, SUZ12, H3K27me2, and H3K27me3 centred on candidate enhancer regions (±10 kb from enhancer centres) in CTRL and *NSD2*-KO Karpas-422 (EZH2-mutant) lymphoma cells. Candidate enhancers were defined as H3K27ac peaks with promoter-proximal (TSS ±2 kb) and exonic regions removed. Regions were sorted by mean H3K27ac signal in CTRL cells. Average plots illustrate the average signal across all regions, while tornado plots depict signal intensity per region, while line plots represent the average signal across all regions.

B

Transient Transfection:

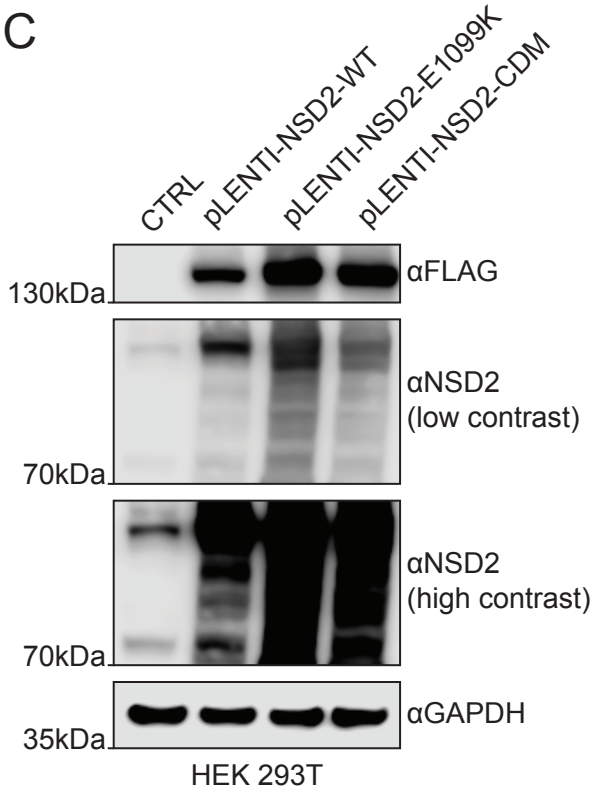

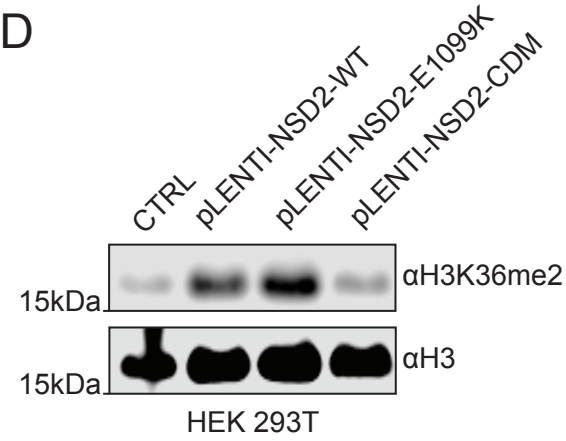

Figure 4.14: Developing NSD2 mutant constructs for further mechanistic exploration of NSD2-mediated resistance to EZH2 inhibitors in B-cell lymphoma.

A. Diagrammatic representation of the HA/FLAG-tagged NSD2 wild-type long, NSD2 hyperactive mutant (E1099K), and NSD2 catalytically dead mutant constructs. The PWWP and SET domains are indicated. CDM indicates the catalytically dead mutant.

B. Schematic of transient transfection in HEK 293T cells of NSD2 constructs.

C. Immunoblots from whole cell lysates of the indicated proteins in HEK 293T cells expressing the indicated NSD2 protein constructs following transient transfection.

D. Immunoblots from whole cell lysates of the indicated histone proteins in HEK 293T cells expressing the indicated NSD2 protein constructs following transient transfection.

of *NSD2* were an outlier in terms of frequency, the most common being the recurrent E1099K mutation (**Figure 4.15A**). I was able to determine that the E1099K *NSD2* mutation was enriched in lymphoid cancer cell lines, most of these being cell lines from patients with B-cell acute lymphoblastic leukaemia (B-ALL), the most common malignancy in childhood (**Figure 4.15B**). I decided to plot the CHRONOS CRISPR dependency scores from RCH-ACV, a B-ALL cell line possessing the E1099K *NSD2* mutation. Strikingly, this cell line was dependent not only on core PRC2, but also seemingly on canonical PRC1 (**Figure 4.15C**). This stands to reason, and may represent the corollary of what I have discovered in this chapter. I have shown that in a PRC2-dependent cancer, EZH2-mutant lymphoma, loss of *NSD2* results in EZH2i resistance. Here, in NSD2-mutant B-ALL, hypermorphic NSD2 function appears to be associated with a genetic dependency on PRC2/cPRC1.

Given that in Chapter 3 I showed *MEN1* to be essential in PRC2-dependent lymphomas, I hypothesised that PRC2-dependent B-ALL may also be dependent on *MEN1*. Indeed, looking at CHRONOS dependency scores in all B-ALL cell lines in DepMap, there was a modest trend towards increased *MEN1* dependency in *NSD2*-mutated B-ALL cell lines (**Figure 4.15D**). Notably both NSD2-mutated and NSD2 wild-type B-ALL cell lines appeared significantly dependent on *MEN1* i.e. CHRONOS score ≤ -0.5. I then looked at cPRC1 component dependencies in B-ALL which showed a weak correlation between cPRC1 dependency and NSD2 mutation status. It must be stressed that these *in silico* data are preliminary and do not prove a link between cPRC1/PRC2 and NSD2-mutant B-ALL. However based on the signal seen here, and the fact that we have previously described a *CBX4*-dependency in a cancer context with a similar chromatin landscape to B-ALL (Lagan et al., 2025), I co-applied for a research grant with my supervisor Professor Bracken which led us to beginning a new stream of research in the lab investigating the interplay between Polycomb and NSD2 in B-ALL, which Gráinne Holland is now pursuing as her PhD research project.

4.3 Discussion

In this chapter I have shown that mechanisms of resistance to EZH2i inhibitors are likely dependent on *EZH2* mutation status. I demonstrated that, along with tumour suppressor genes, top genetic resister genes to EZH2 inhibitors are frequently chromatin regulatory genes including H3K36 methyltransferases. I have confirmed that both *NSD1* and *NSD2* loss, either via pharmacological or genetic means, cause dose-dependent resistance to EZH2 inhibitors in B-cell lymphoma. I showed that *NSD2* does not possess any significant protein interactors, and that loss of NSD2 blunts both gene de-repression and H3K36me2 increases characterised by EZH2 inhibitor therapy. I successfully performed endogenous NSD2 CUT&RUN and showed that NSD2 binds at some but not all H3K36me2 peaks, pointing to it acting at specific genomic loci.

NSD2 knockout leads to H3K36me2 and H3K27ac loss specifically at the promoters of genes controlled by NSD2. *NSD2* loss resulted in mild gains in genome-wide H3K27me3 and moderate gains in genome-wide H3K27me2, in contrast to in embryonic stem cells where increases in H3K27me3 were more stark, albeit with Nsd1 knock-down (Streubel et al., 2018). Interestingly, *NSD2* knockout-induced H3K27me3 gains in the lymphoma context were associated with enhanced lymphoma cell fitness, in contrast to a previous report (Kwok et al., 2023). However the most striking finding was at distal regulatory elements, termed candidate enhancers based on H3K27ac signal, where NSD2 knockout resulted in loss of H3K27ac/H3K36me2 and gains in Polycomb-associated H3K27me2/H3K27me3. This points to a role of NSD2 at enhancer elements where it antagonises Polycomb, and that gains in repressive histone marks at these regions when *NSD2* is lost may modulate sensitivity to EZH2 inhibitors. Notably, in *NUP98*::*NSD1* acute myeloid leukaemia, it has already been proposed that maintenance of H3K36 methylation and histone acetylation at distal regulatory regions antagonises Polycomb-mediated repression of key loci such as Hox-A, pointing to an important dichotomous relationship between NSD proteins and PRC2 at these DNA elements (Wang et al., 2007). Lastly, given that the *H3.3K36M* oncohistone

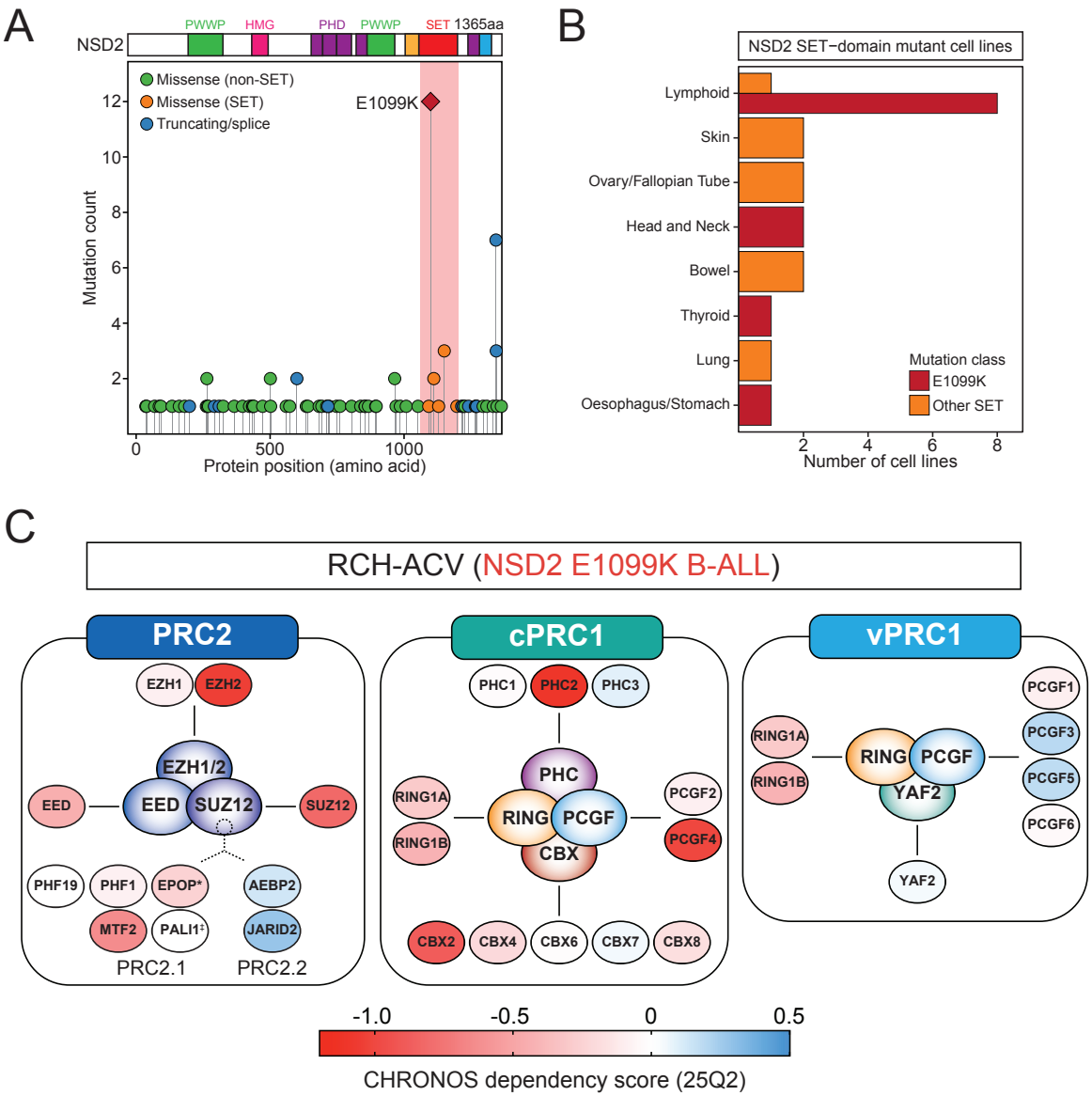
A
NSD2
PWWP
HMG
PHD
PWWP
SET
1365aa
Missense (non-SET)
Missense (SET)
Truncating/splice
E1099K
Mutation count
Protein position (amino acid)
B
NSD2 SET−domain mutant cell lines
Lymphoid
Skin
Ovary/Fallopian Tube
Head and Neck
Bowel
Thyroid
Lung
Oesophagus/Stomach
Mutation class
E1099K
Other SET
Number of cell lines
C
RCH-ACV (NSD2 E1099K B-ALL)
PRC2
EZH1
EZH2
EZH1/2
EED
SUZ12
PHF19
PHF1
EPOP*
AEBP2
MTF2
PALI1‡
JARID2
PRC2.1
PRC2.2
cPRC1
PHC1
PHC2
PHC3
PHC
RING1A
RING1B
RING
PCGF
CBX
PCGF2
PCGF4
CBX2
CBX4
CBX6
CBX7
CBX8
vPRC1
PCGF1
PCGF3
PCGF5
PCGF6
YAF2
-1.0
-0.5
0
0.5
CHRONOS dependency score (25Q2)
D
MEN1
CHRONOS score (25Q2)
NSD2 E1099K
NSD2 WT
E
NSD2 E1099K B-ALL
NSD2 WT B-ALL
CHRONOS score (25Q2)
CBX2
CBX4
PHC2
PHC1
RING1A

Figure 4.15: The recurrent hypermorphic *NSD2* mutation, found in B-cell acute lymphoblastic leukaemia, may create genetic vulnerabilities to Polycomb and Menin.

A. Lollipop plot demonstrating the distribution of NSD2 coding mutations mapped to amino acid position in cell lines from the Cancer Dependency Map (DepMap). Bars indicate the number of unique mutations at each amino acid residue. The SET domain (aa 1062–1203) is shaded and was defined using the Conserved Domain Database from the National Center for Biotechnology Information (NCBI). The lollipop markers are colored by the dominant "VariantInfo" derived consequence class observed at each residue. Synonymous, or silent, mutations were excluded during plot generation.

B. Bar plot showing the distribution and frequency of NSD2 SET domain mutations by cancer cell line lineage using the "OncotreeLineage" column in the Depmap-derived "Model.csv".

C. Heatmap representation of CRISPR dependency scores (CHRONOS scores) for all PRC2, canonical PRC1 (cPRC1), and variant PRC1 (vPRC1) members derived from CRISPR screens performed in the *NSD2* E1099K-mutated B-ALL cell line RCH-ACV, downloaded from the DepMap 25Q2 data release. * indicates a common essential gene as defined by Achilles 19Q3. ‡ indicates a gene that does not have CRISPR dependency data in DepMap and thus is represented with an arbitrary score of 0 on the plots.

D. CRISPR dependency scores (CHRONOS scores) for *MEN1* derived from genome-wide CRISPR screens downloaded from the DepMap 25Q2 data release. The data shows only B-cell acute lymphoblastic leukaemia cell lines for which CRISPR screen data exists (n=12) and these are divided into NSD2 E1099K-mutant B-ALL cell lines (n=4) and NSD2 wild-type B-ALL cell lines (n=8).

E. CRISPR dependency scores (CHRONOS scores) for canonical PRC1 members derived from genome-wide CRISPR screens downloaded from the DepMap 25Q2 data release. The data shows only B-cell acute lymphoblastic leukaemia cell lines for which CRISPR screen data exists (n=12) and these are divided into NSD2 E1099K-mutant B-ALL cell lines (n=4)(left) and NSD2 wild-type B-ALL cell lines (n=8)(right).

mutation, seen in chondroblastomas and some sarcomas, results in global reductions in H3K36 methylations, it would be fascinating to see whether cloning this mutant into lymphoma cells recapitulates resistance to EZH2 inhibitors (Behjati et al., 2013; Lu et al., 2016; Rajagopalan et al., 2021).

An interesting detail in this Chapter is the fact that *NSD2*-KO resulted in lymphoma cell resistance to low dose, but not higher doses, of EZH2 inhibitor. This makes sense from a translational cancer context; patients are treated with specific doses of EZH2 inhibitors, however not all lymphoma cells will be exposed *in vivo* to the maximal plasma concentration of the EZH2 inhibitor. This can be due to a multitude of factors including differences in blood supply, immunological niches, the complex lymphoma microenvironment and the presence of disease in sanctuary sites such as the central nervous system (CNS). Thus, some lymphoma cells will be exposed to lower EZH2 inhibitor concentrations, and may develop resistance over time due to loss of *NSD2*.

4.3.1 Targeting NSD in cancer

Despite the well documented evidence for genetic aberrations in the NSD genes in cancer and the resultant excess H3K36me2 driving oncogenic gene expression programs, efforts at developing inhibitors of the methyltransferase activity of NSD proteins were largely unsuccessful until recently. This may be in part due to the difficulty in assessing inhibition of NSD histone methyltransferase activity in vitro (Y. Li et al., 2009), as well as multiple pharmacological factors including a lack of histone methyltransferase specificity, lack of potency in vitro, and off-target effects (Coussens et al., 2018; Drake et al., 2014; Li et al., 2026; Morrison et al., 2018; Shen et al., 2019; Tisi et al., 2016). Progress on NSD2 inhibitors is being made, with two recently published scientific papers demonstrating effective and specific NSD2 inhibition in a number of cancer cell lines and xenograft models (Jeong et al., 2026; Li et al., 2026).

Given the difficulty in deriving an inhibitor of the NSD catalytic SET domain, a recent advance has been the development of inhibitors of the NSD protein N-terminal PWWP domain, which inhibits binding to H3K36me2, a requirement for locating NSD proteins onto chromatin (Bottcher et al., 2019; Dilworth et al., 2022; Ferreira de Freitas et al., 2021). Although these compounds lack bioactivity in cancer cell lines, the effective targeting of the PWWP domain has recently led to the development of a novel 'proteolysis-targeting chimera' (PROTAC) degrader compound targeting NSD2 called UNC8153 (Hanley et al., 2023). PROTAC molecules comprise a heterobifunctional molecule, one end with a ligand towards the protein of interest, in this case the PWWP domain of NSD2, and on the other end a ligand for an E3 ubiquitin ligase. The two ligands are joined by a linker domain and once the protein of interest is engaged, the E3 ubiquitin ligase ubiquitinates the protein targeting it for degradation by the proteosome (Bekes et al., 2022). UNC8153 demonstrated selectivity for NSD2 degradation, reduction in H3K36me2 and inhibition of proliferation in a multiple myeloma cell line (Hanley et al., 2023). A number of PROTAC compounds have recently entered clinical trials (NCT03888612, NCT04072952, NCT04336982, NCT04965753), thus offering a promising new form of drug target, particularly for challenging drug targets like the NSD proteins.

In this chapter I developed a list of EZH2 inhibitor resistance genes in B-cell lymphoma. I have progressed the understanding of NSD2-related mechanisms of resistance, however there were numerous other chromatin regulatory genes that scored in the genome-wide CRISPR screen that would be worthy of further exploration. It is notable that genes such as *BRD1* and *BRD2* have been implicated as readers of acetylated histones within histone acetyltransferase complexes (Kanno et al., 2004; LeRoy et al., 2008; Mishima et al., 2014). It stands to reason that while the repressive machinery of PRC2 is a dependency and EZH2 inhibitor sensitiser in germinal centre lymphomas, chromatin regulatory proteins involved in active chromatin domains, like NSD proteins but also readers such as BRD1/BRD2 would function as resistors to EZH2 inhibition. In developing isogenic *NSD1*- and *NSD2*-KO lymphoma cell lines, these will provide future lab members with a genetically clean system

with which to study the interplay between H3K27 and H3K36 methylations. Finally, my preliminary work looking at *NSD2*-mutated B-ALL dependencies on DepMap have led to a new project in this cancer context within the Bracken Lab. As a Paediatric Haematologist, this offers me an ability to stay involved and engaged in basic science research, and to try to integrate it with translational experiments in the clinic to develop mechanistically informed targeted therapies.

CHAPTER 5

AEBP2-Directed H3K27me2 Defines a Specific Vulnerability in EZH2-mutant Lymphoma

5.1 Introduction

In Chapter 1 I introduced the oncogenic recurrent *EZH2* SET domain mutation in germinal B-cell lymphomas, and its biochemical consequence of producing an aberrantly repressed chromatin landscape with hyper-trimethylation of H3K27, and concomitant reductions in H3K27me2. The main aim of this results chapter was to develop a better understanding of the role of PRC2 in the development of B-cell lymphomas and uncover novel ways to target this complex. An alternative avenue of PRC2 targeting in B-cell lymphoma is through PROTAC degrader compounds targeting EED (Hsu et al., 2020; Potjewyd et al., 2020). Dr. James Nolan, during his PhD research project in the Bracken Lab, demonstrated that these EED degraders can circumvent acquired mutations in *EZH2* that alter EZH2 inhibitor binding and result in toxicity to otherwise EZH2 inhibitor resistant B-cell lymphoma cells (Angelov et al., 2025; Bisserier & Wajapeyee, 2018). Dr Nolan along with other previous Bracken Lab members Drs Rachel McCole and Marlena Mucha performed extensive PRC2-tiled CRISPR screens, a saturated CRISPR screen targeting all PAM sequences of each PRC2 member, across a range of cancer contexts (Lagan et al., 2025). Through this work, the PRC2 accessory component AEBP2, originally identified by He et al., 1999, was initially characterised as a specific genetic dependency in B-cell lymphoma cells. **This results chapter will expand and broaden the understanding of *AEBP2* dependency, as well as *AEBP2* as an EZH2 inhibitor sensitiser in germinal centre B-cell lymphoma.**

5.2 Results

5.2.1 *AEBP2* and *PCGF1*/*PCGF5* are genetic dependencies in B-Cell lymphoma

In Chapter 3 I demonstrated the shared genetic dependency landscape among germinal centre lymphomas, I described *CARM1* as a novel genetic dependency, and characterised a number of previously undescribed genetic sensitisers to PRC2 inhibition. At the outset of the genome-wide CRISPR screen, I anticipated that accessory components of PRC2 would

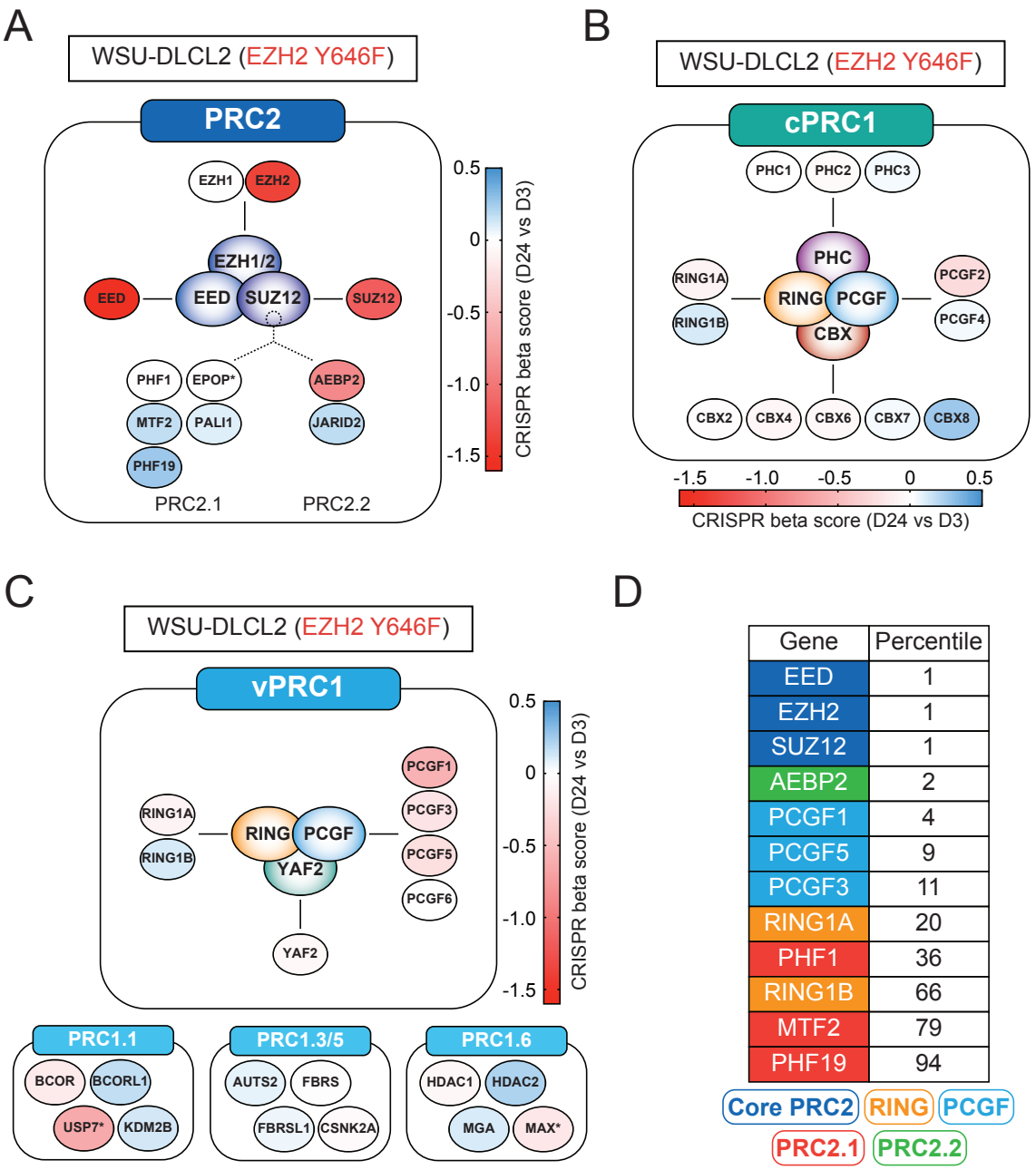

Figure 5.1: *AEBP2* and *PCGF1*/*PCGF5* are genetic dependencies in B-cell lymphoma.

A Heatmap representation of CRISPR dependency scores for all PRC2 members from the genome-wide CRISPR screen in WSU-DLCL2 (EZH2-mutant lymphoma). Screens were performed in 2 biological replicates.

B Heatmap representation of CRISPR dependency scores for all canonical PRC1 members from the genome-wide CRISPR screen in WSU-DLCL2 (EZH2-mutant lymphoma). Screens were performed in 2 biological replicates.

C Heatmap representation of CRISPR dependency scores for all variant PRC1 members from the genome-wide CRISPR screen in WSU-DLCL2 (EZH2-mutant lymphoma). Screens were performed in 2 biological replicates.

D Table representing the percentile rank for the indicated genes from the genome-wide CRISPR screen in WSU-DLCL2 (EZH2-mutant) lymphoma cells, based on CRISPR dependency score.

score as dependencies and/or sensitiser 'hits', but perhaps not as strongly as core PRC2 genes. I was interested to see if there was a difference between PRC2.1 and PRC2.2 accessory components, given their described independent roles (Deevy & Bracken, 2019; Glancy et al., 2023; Healy et al., 2019; Mucha et al., 2025). Drs James Nolan and Eric Conway, in the Bracken Lab, had recently described a dependency on the PRC2 accessory protein, AEBP2, in germinal centre lymphoma cells using a PRC2-tiled CRISPR screen (Angelov et al., 2025). Focusing on PRC2, and consistent with previous work (Knutson et al., 2012; McCabe, Ott, et al., 2012; Potjewyd et al., 2020; Qi et al., 2012; Qi et al., 2017), cells containing single guide RNAs (sgRNAs) targeting core PRC2 components (*EZH2*, *SUZ12* and *EED*) showed significant dropout in the EZH2-mutant lymphoma cell population over time (**Figure 5.1A**). Consistent with Dr Nolan's work, amongst the sgRNAs targeting PRC2 accessory components, only those targeting *AEBP2* were depleted. Interestingly, sgRNAs targeting the other PRC2.2 accessory component *JARID2* did not deplete. Turning my attention to canonical and variant PRC1 components, it was notable that only sgRNAs targeting *PCGF1* and *PCGF5* seemed to deplete among the other PRC1 genes (**Figure 5.1B-C**). In fact, other than the core PRC2 components, the only other Polycomb-related genes that scored in the top 10th percentile of genetic dependencies amongst all genes in the genome-wide CRISPR screen were *AEBP2*, *PCGF1* and *PCGF5* (**Figure 5.1D**).

5.2.2 *AEBP2* is a specific vulnerability in germinal centre B-cell lymphoma and is an *EZH2* co-dependency in EZH2-mutant B-cell lymphoma

In order to validate the CRISPR screen findings, and to examine whether *AEBP2* is universally essential in PRC2-dependent cancers, I performed validation assays in WSU-DLCL2 along with a SMARCB1-mutant extracranial malignant rhabdoid tumour (MRT) cell line G401, a cancer that is also dependent on core PRC2 (Malone & Roberts, 2024). To do this, I measured the depletion of GFP-tagged sgRNAs in CRISPR-Cas9 negative selection assays, targeting core PRC2 components (*EZH2*, *EED* and *SUZ12*) and PRC2.2 subunits

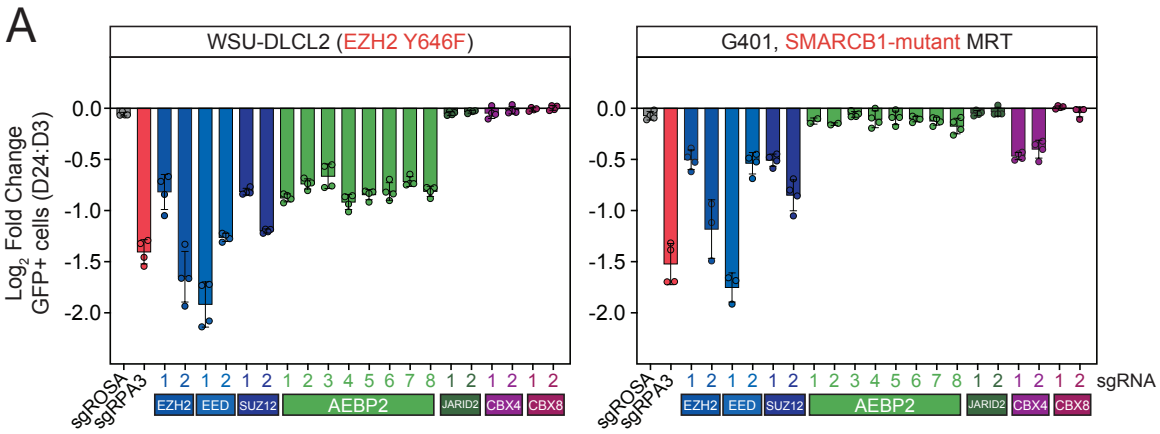
A
WSU-DLCL2 (EZH2 Y646F)
G401, SMARCB1-mutant MRT
Log2 Fold Change GFP+ cells (D24:D3)
0.0
-0.5
-1.0
-1.5
-2.0
sgROSA
sgRPA3
1 2 1 2 1 2 1 2 3 4 5 6 7 8 1 2 1 2 1 2
sgRNA
EZH2
EED
SUZ12
AEBP2
JARID2
CBX4
CBX8

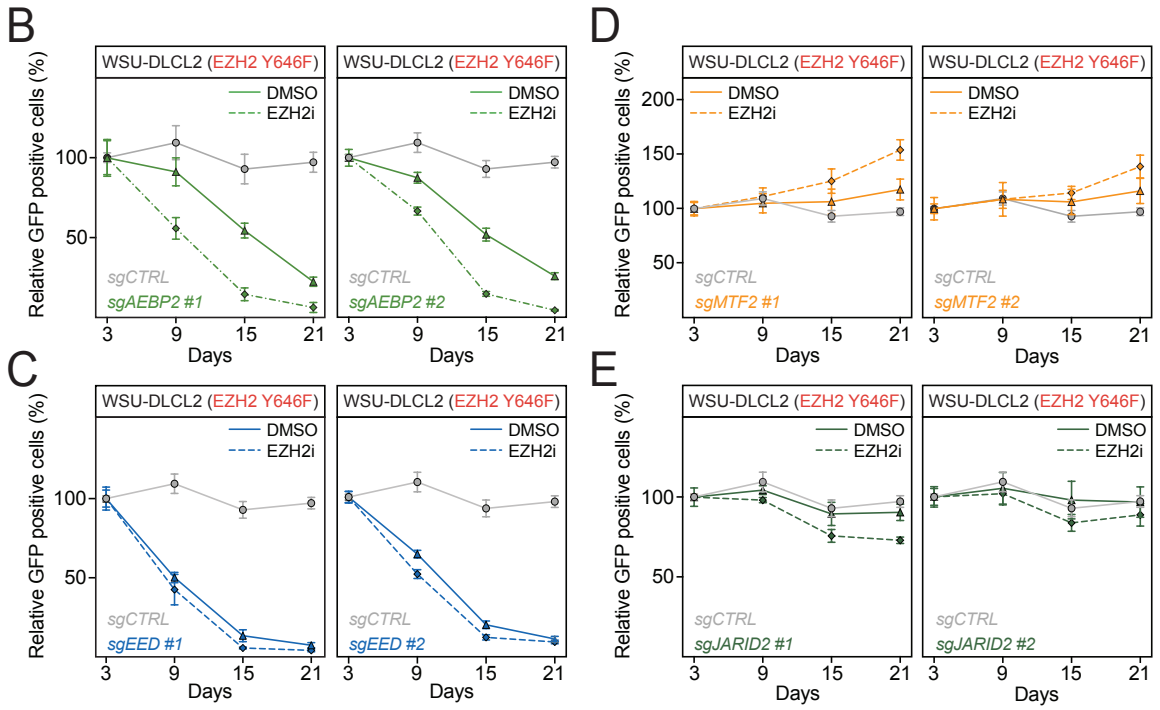
B
D
C
E
WSU-DLCL2 (EZH2 Y646F)
DMSO
EZH2i
Relative GFP positive cells (%)
100
50
200
150
sgCTRL
sgAEBP2 #1
sgAEBP2 #2
sgMTF2 #1
sgMTF2 #2
sgEED #1
sgEED #2
sgJARID2 #1
sgJARID2 #2
3 9 15 21
Days

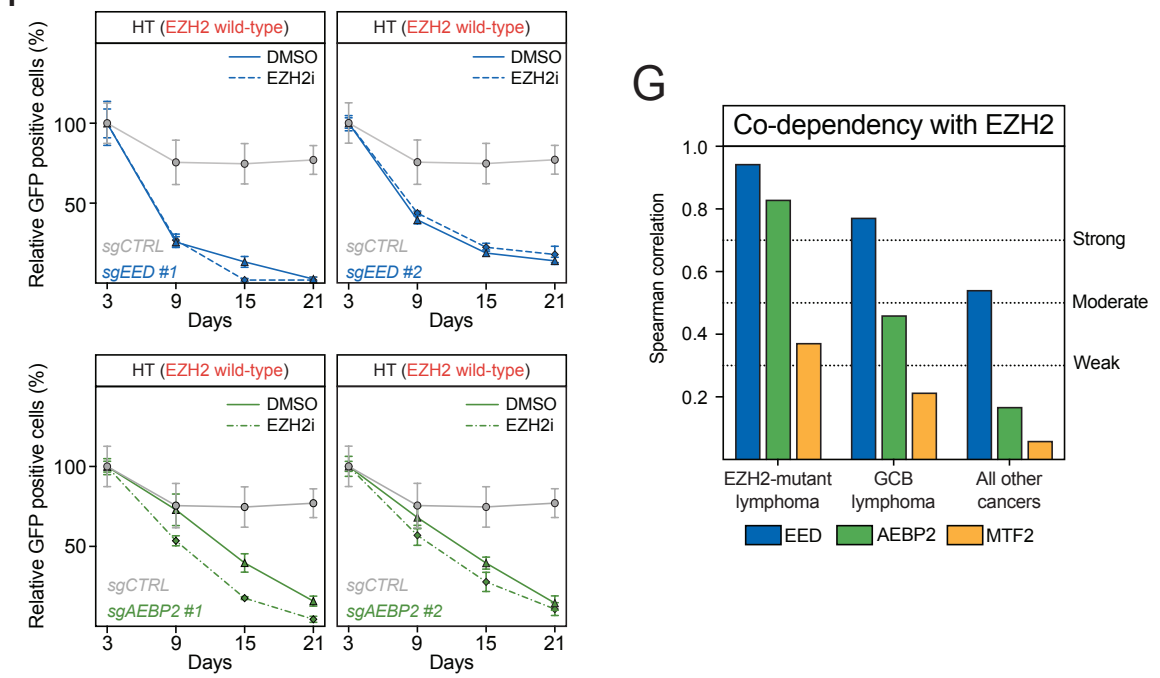
F
HT (EZH2 wild-type)
DMSO
EZH2i
Relative GFP positive cells (%)
100
50
sgCTRL
sgEED #1
sgEED #2
sgAEBP2 #1
sgAEBP2 #2
3 9 15 21
Days

G
Co-dependency with EZH2
Spearman correlation
1.0
0.8
0.6
0.4
0.2
Strong
Moderate
Weak
EZH2-mutant lymphoma
GCB lymphoma
All other cancers
EED
AEBP2
MTF2

Figure 5.2: *AEBP2* is a specific vulnerability in germinal centre B-cell lymphoma and is an EZH2 co-dependency in EZH2-mutant B-cell lymphoma.

A. Growth competition assays in Cas9-expressing WSU-DLCL2 (EZH2-mutant lymphoma) and G401 (SMARCB1-mutant malignant rhabdoid tumour) cell lines transduced with sgRNAs targeting the indicated genes (n=4, data represents mean ± SD).

B. Growth competition assays in Cas9-expressing WSU-DLCL2 (EZH2-mutant lymphoma) transduced with sgRNAs targeting *AEBP2* followed by treatment with low dose EZH2i (Tazemetostat) or DMSO control (n=3, data represents mean ± SD).

C. Growth competition assays in Cas9-expressing WSU-DLCL2 (EZH2-mutant lymphoma) transduced with sgRNAs targeting *EED* followed by treatment with low dose EZH2i (Tazemetostat) or DMSO control (n=3, data represents mean ± SD).

D. Growth competition assays in Cas9-expressing WSU-DLCL2 (EZH2-mutant lymphoma) transduced with sgRNAs targeting *MTF2* followed by treatment with low dose EZH2i (Tazemetostat) or DMSO control (n=3, data represents mean ± SD).

E. Growth competition assays in Cas9-expressing WSU-DLCL2 (EZH2-mutant lymphoma) transduced with sgRNAs targeting *JARID2* followed by treatment with low dose EZH2i (Tazemetostat) or DMSO control (n=3, data represents mean ± SD).

F. Growth competition assays in Cas9-expressing HT (EZH2 wild-type lymphoma) transduced with sgRNAs targeting the indicated genes followed by treatment with low dose EZH2i (Tazemetostat) or DMSO control (n=3, data represents mean ± SD).

G. Correlation scores for *EZH2* co-dependencies with either *EED* or *AEBP2*, produced using CHRONOS gene-effect scores in the Cancer Dependency Map (https://depmap.org/portal/). Co-dependencies are divided into EZH2-mutant lymphoma (n=6), germinal centre lymphoma (n=14) and all other cancer cell lines (n=1087).

(*AEBP2* and *JARID2*) while using canonical PRC1 components *CBX4* and *CBX8* as additional negative controls with sg*ROSA26*. Strikingly, sgRNAs directed against core PRC2 components caused robust depletion in both cancer types, whereas sgRNAs targeting *AEBP2* selectively depleted in lymphoma cells (**Figure 5.2A**). Unexpectedly, sgRNAs targeting *JARID2* did not score, suggesting that AEBP2 within PRC2.2, but not JARID2, is required for EZH2-mutant lymphoma cell survival. Interestingly, I discovered that the MRT cell line G401 appeared to be sensitive to *CBX4* depletion, a finding that I did not have the scope to follow up on in this research project, but which could have important scientific and clinical implications in a paediatric cancer subtype with a dismal prognosis.

Next, I further validated the CRISPR screen findings using CRISPR-Cas9 negative selection assays in the presence or absence of the EZH2 inhibitor Tazemetostat. Two independent sgRNAs targeting *AEBP2* sensitised WSU-DLCL2 EZH2-mutant lymphoma cells to Tazemetostat treatment, confirming AEBP2 as a genetic sensitiser (**Figure 5.2B**). As expected, sgRNAs targeting *EED* produced strong depletion given its essential nature in these lymphomas. The EZH2i-sensitising effects of targeting *EED* were difficult to observe due to such robust depletion in both DMSO and EZH2i conditions (**Figure 5.2C**). To contrast the effects of PRC2.2 loss, sgRNAs targeting the PRC2.1 component *MTF2* were employed. Here, the loss of *MTF2* conferred moderate resistance to Tazemetostat, while loss of *JARID2* had no phenotypic effects in either condition, consistent with findings from the genome-wide screen (**Figure 5.2D-E**). I then confirmed *AEBP2* as a genetic dependency and EZH2i-sensitiser in the EZH2 wild-type lymphoma cell line HT, expanding the significance of AEBP2 in germinal centre B-cell lymphoma (**Figure 5.2F**). To evaluate the broader relevance of *AEBP2* as an *EZH2* co-dependency, I analysed data from the Cancer Dependency Map (https://depmap.org/portal) to compare the strength of *EZH2*-*AEBP2* co-dependency in EZH2-mutant lymphomas versus other cancer types (**Figure 5.2G**). Notably, the co-dependency between *EZH2* and *AEBP2* was comparable to that between *EZH2* and *EED* in EZH2-mutant lymphoma, but much weaker in other cancer

types; EED being a core PRC2 component and a proposed therapeutic target in lymphoma (McCole et al., 2025; Potjewyd et al., 2020; Qi et al., 2017).

5.2.3 AEBP2 is dispensable for global H3K27me3 and gene repression in B-cell lymphoma

Given the dependency on *AEBP2* in germinal centre lymphoma, Dr James Nolan was previously unable to generate stable clonal (single cell) *AEBP2* knockout (KO) lymphoma cells. Therefore, to generate a system by which I could knock-out all isoforms of *AEBP2* and study its effects on gene expression and chromatin contexts, I attempted to instead bulk knock-out *AEBP2* using CRISPR-Cas9. As it was likely that, after generating a heterogenous population of variable *AEBP2* knockouts, the lymphoma cells would select out the *AEBP2*-KO cells over time, all experiments using this 'bulk' KO system were carried out over short time courses (<7 days). Furthermore, for every experimental replicate using the 'bulk' KO approach, additional cells were harvested and immunoblots were carried out to confirm an acceptable level of *AEBP2*-KO prior to proceeding with genomic experiments as seen in **Figure 5.3A**.

To better understand why *AEBP2* is an *EZH2* co-dependency in lymphoma, I first assessed global H3K27me3 levels by immunoblot after CRISPR-mediated depletion of AEBP2, using EED depletion as a control. Cells were harvested 5 days after CRISPR KO of the indicated genes. As expected, loss of *EED* reduced global H3K27me3 levels, whereas *AEBP2* depletion caused H3K27me3 levels to remain largely unchanged (**Figure 5.3A**)(Mucha et al., 2025). Similar findings were noted in the EZH2 wild-type cell line HT (**Figure 5.3B**). Thus, while loss of *EZH2* or *EED* reduces H3K27me3, the fact that *AEBP2* depletion does not, indicates that the *AEBP2*-*EZH2* co-dependency is unlikely to be related to global H3K27me3 levels. I included sgRNAs targeting *MTF2* and *NSD2* in this experiment to

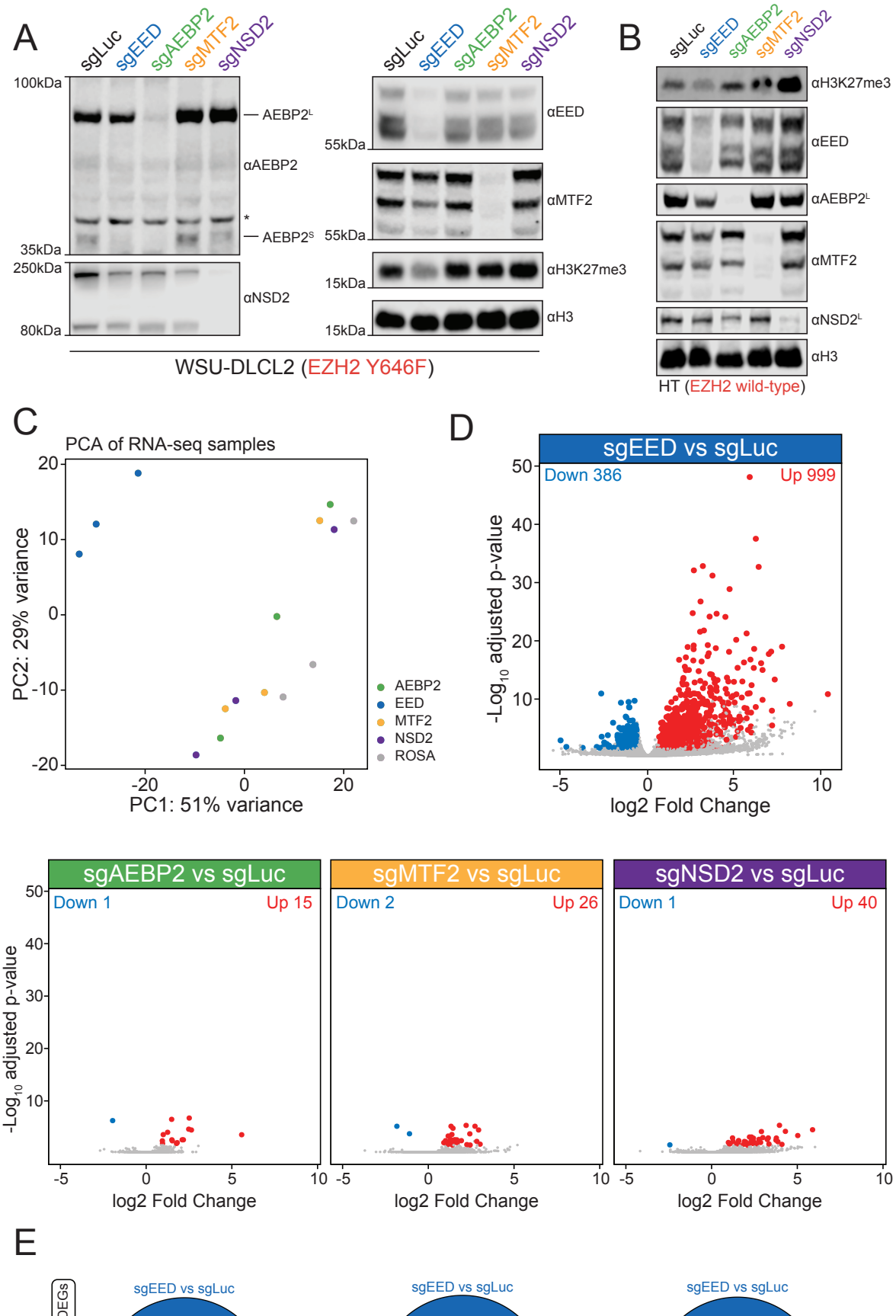
A
sgLuc
sgEED
sgAEBP2
sgMTF2
sgNSD2
100kDa
35kDa
250kDa
80kDa
AEBP2L
αAEBP2
AEBP2S
αNSD2
55kDa
15kDa
αEED
αMTF2
αH3K27me3
αH3
WSU-DLCL2 (EZH2 Y646F)
B
αH3K27me3
αEED
αAEBP2L
αMTF2
αNSD2L
αH3
HT (EZH2 wild-type)
C
PCA of RNA-seq samples
PC2: 29% variance
PC1: 51% variance
AEBP2
EED
MTF2
NSD2
ROSA
D
sgEED vs sgLuc
Down 386
Up 999
-Log10 adjusted p-value
log2 Fold Change
sgAEBP2 vs sgLuc
Down 1
Up 15
sgMTF2 vs sgLuc
Down 2
Up 26
sgNSD2 vs sgLuc
Down 1
Up 40
E
Overlap of upregulated DEGs
986
13
2
974
25
1
963
36
4

Figure 5.3: AEBP2 is dispensable for global H3K27me3 and gene repression in B-cell lymphoma.

A. Immunoblots of the indicated PRC2 proteins and histone modifications from whole cell lysates in WSU-DLCL2 (EZH2-mutant lymphoma) cells transduced with the indicated sgRNAs. The * denotes a background band. Experiment carried out in 3 biological replicates, with a representative example shown.

B. Immunoblots of the indicated PRC2 proteins and histone modifications from whole cell lysates in HT (EZH2 wild-type lymphoma) cells transduced with the indicated sgRNAs. Experiment carried out in 3 biological replicates, with a representative example shown.

C. PCA plot corresponding to RNA-seq performed in Cas9-expressing WSU-DLCL2 (EZH2-mutant lymphoma) cells transduced with sgRNAs targeting the indicated genes (n=3 biological replicates).

D. Volcano plots of RNA-seq depicting differentially expressed genes in Cas9-expressing WSU-DLCL2 (EZH2-mutant lymphoma) cells transduced with sgRNAs targeting the indicated genes. The number of genes differentially expressed both up (red) and down (blue) are indicated on the plots (n=3 biological replicates; significance cutoff: $p < 0.05$; minimum 1.5-fold change).

E. Venn diagram demonstrating overlap of differentially expressed genes upregulated (DEGs up) in WSU-DLCL2 lymphoma cells with CRISPR Cas9-mediated KO the indicated genes compared to control (sgLuciferase).

A-E. Core PRC2 complex is shown in blue, PRC2.1 accessory proteins are shown in orange, and PRC2.2 accessory proteins are shown in green. NSD2 is denoted in purple.

continue to contrast PRC2.1 and PRC2.2, and because in Chapter 4 I showed that *NSD2* loss also modulates H3K27me3 levels.

Next, I compared the transcriptional effects of core PRC2 depletion with those of *AEBP2* loss, using the same 'bulk' KO approach. Firstly, the PCA plot was striking for the *EED*-depleted cells lying significantly distinct from the other conditions (**Figure 5.3C**). Disruption of the core PRC2 component EED led to widespread transcriptional de-repression, consistent with reduced H3K27me3 levels. In contrast, *AEBP2* depletion caused minimal gene expression changes, similar to *MTF2* or *NSD2* loss (**Figure 5.3D**). Looking at overlapping differentially expressed genes, most of the few upregulated DEGs in *AEBP2*-KO did in fact overlap with DEGs in *EED*-KO (**Figure 5.3E**). This latter finding shows that, in addition to AEBP2 being dispensable for Polycomb target gene repression, *AEBP2* does not control its own distinct gene expression program in this cancer context.

Thus far in this Chapter, the results show that *AEBP2* is both a genetic dependency and a sensitiser to EZH2 inhibition in EZH2-mutant B-cell lymphoma, yet its loss does not lead to global H3K27me3 reduction or phenocopy activation of genes typically repressed by PRC2.

5.2.4 *AEBP2* loss, in contrast to *MTF2* loss, increases intergenic H3K27me3

Given the starkly opposing phenotypic consequences of *AEBP2* loss compared to *NSD2* loss (Chapter 4) on EZH2 inhibitor response, I hypothesised that the genome-wide profiles of H3K27me3 might differ between the two contexts. Although quantitative western blots showed little changes in the global levels of H3K27me3 in both AEBP2- and NSD2-deficient cells (**Figure 5.3A-B**), I reasoned that such bulk measurements might mask qualitative alterations in the distribution of H3K27me3, as was first reported for embryonic stem cells (ESCs) lacking accessory proteins (Healy et al., 2019; Højfeldt et al., 2019).

I previously examined the genome-wide distribution of H3K27me3 in *NSD2*-KO, EZH2-mutant lymphoma cells in Chapter 4, and showed that loss of this H3K36 methyltransferase led to increases in H3K27me3 at Polycomb target genes and as well as genome-wide. Given the known dichotomy between H3K36me2 and H3K27me3 this finding was not a surprise (Streubel et al., 2018). Here, I first performed 'bulk' KO of *AEBP2* and used *MTF2* KO as a positive control, given the fact that *MTF2* had an opposing phenotype in the genome-wide CRISPR screen and since it is known to reduce H3K27me3 at Polycomb target genes (Healy et al., 2019; Højfeldt et al., 2019; Sparbier et al., 2023) (**Figure 5.4A-B**).

To test the effects of *AEBP2* loss on H3K27me3 distribution, I performed spike-in normalised CUT&RUN (CUT&RUN-Rx) profiling for H3K27me3 and found that loss of *AEBP2* caused a genome-wide increase in H3K27me3, most notably at intergenic regions (**Figure 5.4C-F**). To my surprise, this was very similar to the effects of *NSD2* loss on H3K27me3. In contrast, *MTF2* loss caused a decrease in global H3K27me3 with more pronounced reductions at Polycomb target genes, as has been shown previously (Sparbier et al., 2023). Earlier in this Chapter I showed that *MTF2* loss promotes resistance to EZH2 inhibition. Taken together, these findings indicate that changes in H3K27me3 alone do not appear to account for the differential sensitivity of EZH2-mutant B-cell lymphoma cells to loss of *NSD2*, *MTF2*, *AEBP2* and core PRC2. Instead, they suggest AEBP2 has an additional, distinct function beyond modulation of H3K27me3 levels.

5.2.5 AEBP2 demonstrates a broader binding profile at Polycomb target genes and is bound more at intergenic regions compared with MTF2

To further investigate the role of AEBP2 in EZH2-mutant B-cell lymphoma, I profiled its genome-wide binding using CUT&RUN-Rx, comparing it to MTF2. Work from the Bracken Lab had previously shown that in chromatin immunoprecipitation assays of AEBP2, a more diffuse or high background signal along with a broader peak over Polycomb target genes

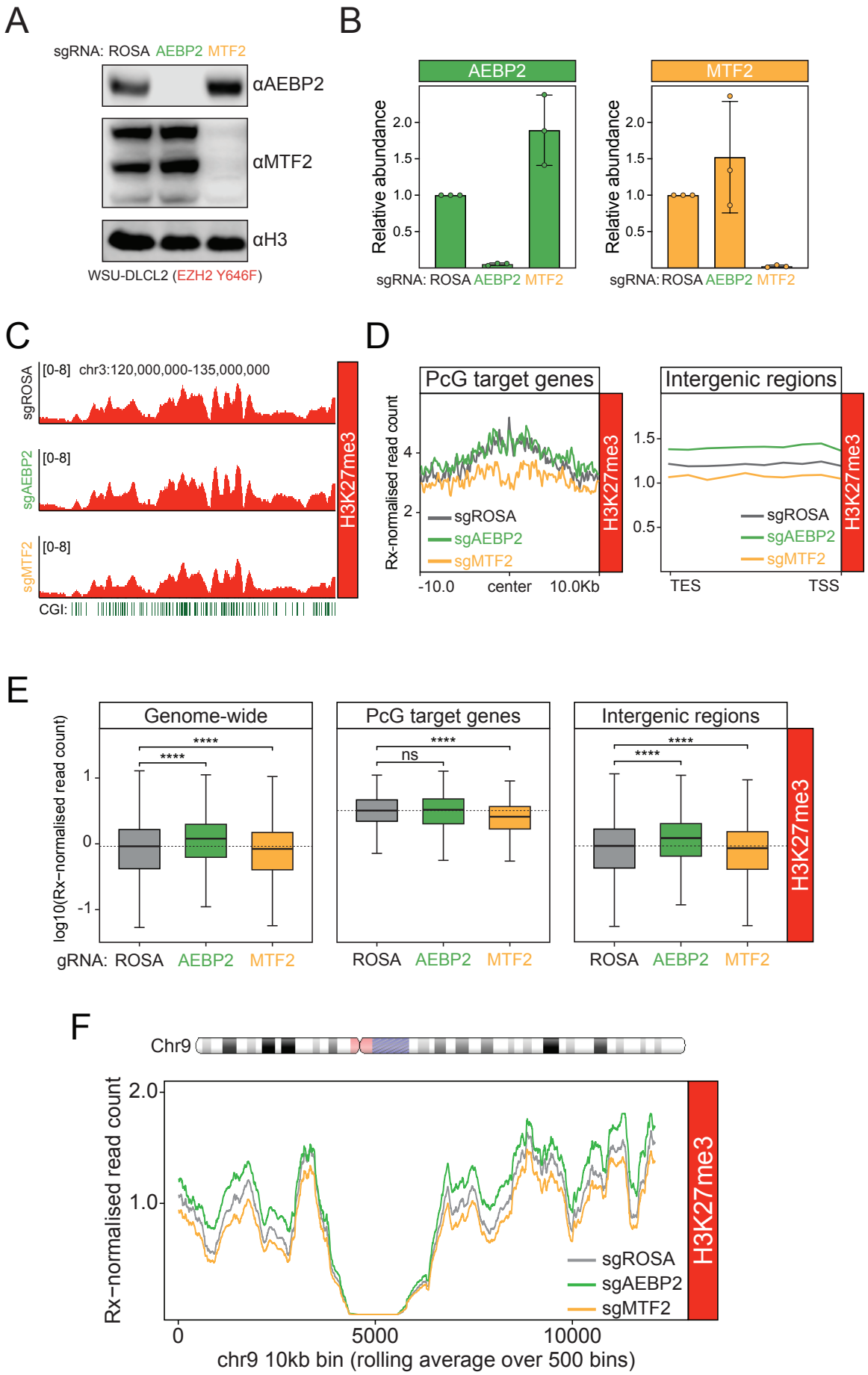
A
sgRNA: ROSA AEBP2 MTF2
αAEBP2
αMTF2
αH3
WSU-DLCL2 (EZH2 Y646F)
B
AEBP2
MTF2
Relative abundance
sgRNA: ROSA AEBP2 MTF2
C
sgROSA
sgAEBP2
sgMTF2
[0-8]
chr3:120,000,000-135,000,000
CGI:
H3K27me3
D
PcG target genes
Intergenic regions
Rx-normalised read count
sgROSA
sgAEBP2
sgMTF2
-10.0
center
10.0Kb
TES
TSS
H3K27me3
E
Genome-wide
PcG target genes
Intergenic regions
log10(Rx−normalised read count)
****
ns
gRNA: ROSA AEBP2 MTF2
ROSA AEBP2 MTF2
H3K27me3
F
Chr9
Rx−normalised read count
sgROSA
sgAEBP2
sgMTF2
H3K27me3
chr9 10kb bin (rolling average over 500 bins)

Figure 5.4: *AEBP2* loss, in contrast to *MTF2* loss, increases intergenic H3K27me3.

A. Immunoblots of the indicated proteins from whole cell lysates in Cas9-expressing WSU-DLCL2 cells transduced with sgRNAs targeting the indicated PRC2 genes (representative blot of n=3 biological replicates).

B. Relative quantification of immunoblot analyses of AEBP2 and MTF2 abundance in WSU-DLCL2 (EZH2-mutant lymphoma) cells. Signal intensity values were normalised to a loading control and then expressed relative to the sgROSA control cells. Data values represent 3 biological replicates, and their mean values ± SD are plotted as bars.

C. Genome browser representations showing H3K27me3 CUT&RUN-Rx sginal in WSU-DLCL2 (EZH2-mutant lymphoma) cells treated with sgRNAs targeting the indicated genes, at a representative PRC2 target site. CGI: CpG islands.

D. Average plots showing H3K27me3 CUT&RUN-Rx enrichment at PRC2 target genes and all intergenic sites in WSU-DLCL2 (EZH2-mutant lymphoma) cells transduced with sgRNAs targeting the indicated PRC2 genes. TES and TSS indicate Transcription End Site and Transcription Start Site, respectively.

E. Boxplots of H3K27me3 CUT&RUN-Rx signal at genome-wide 10kb bins, PRC2 target genes, and intergenic regions in Cas9-expressing WSU-DLCL2 (EZH2-mutant lymphoma) cells transduced with sgRNAs targeting the indicated PRC2 genes. Significance determined using pairwise Wilcoxon rank-sum tests, ****p value ≤ 0.0001.

F. Rolling average plots presenting H3K27me3 CUT&RUN-Rx signal across the whole of chromosome 9 in Cas9-expressing WSU-DLCL2 (EZH2-mutant lymphoma) cells transduced with sgRNAs targeting the indicated PRC2 genes. Visualised using 10kb genomic windows.

was seen compared with other Polycomb components (Healy et al., 2019). Looking at genome browser views of the CUT&RUN-Rx and comparing AEBP2 binding to MTF2 binding, I observed the same findings (**Figure 5.5A**). This may represent a biological phenomenon of more diffuse binding or high antibody background. It is notable that AEBP2 has been shown to bind to cPRC1-mediated H2AK119ub1, which is distributed broadly throughout the genome (Conway et al., 2021; Kasinath et al., 2021), suggesting that the observation of a high baseline CUT&RUN-Rx signal could be biological. Turning my attention to how AEBP2 and MTF2 are distributed throughout the genome, I found that while both proteins bound Polycomb target gene promoters, they appeared to display distinct preferences. While MTF2 appeared more strongly enriched at promoter-associated PRC2-binding sites, AEBP2, while also binding at Polycomb target promoters, appeared to show relatively greater occupancy at intergenic regions compared with MTF2 (**Figure 5.5B-E**).

I tested this hypothesis using CUT&RUN-Rx triplicate assays to look at the proportion of AEBP2 and MTF2 bound at intergenic regions compared to Polycomb target gene promoters, and showed that while both AEBP2 and MTF2 are mostly bound at Polycomb target genes, AEBP2 appeared significantly more bound at intergenic regions than MTF2 (**Figure 5.5F-G**). This pattern suggested to me that AEBP2 could also function outside of canonical Polycomb target gene promoters, potentially playing a distinct regulatory role at intergenic genomic regions. Furthermore, using CUT&RUN-Rx of the core PRC2 component SUZ12, *AEBP2*-KO cells showed an increase in SUZ12 binding at intergenic regions (**Figure 5.5H-I**), in keeping with the effects of *AEBP2*-KO on H3K27me3 levels shown in **Figure 5.4**. It was also notable that *MTF2*-KO led to greater reductions in SUZ12 binding at Polycomb target gene promoters compared with at intergenic regions, consistent with the effects on H3K27me3 seen in the previous Figure.

5.2.6 AEBP2 confers its essential function in germinal centre B-cell lymphoma in a PRC2 complex lacking JARID2

Although JARID2 is a well-established component of PRC2.2 alongside AEBP2, I was surprised to observe that sgRNAs targeting JARID2 were not depleted in the genome-wide CRISPR screen of EZH2-mutant lymphoma cells or in the validatory negative selection assays (**Figures 5.1 and 5.2**). To investigate the composition of PRC2 in EZH2-mutant B-cell lymphoma cells, I performed endogenous co-immunoprecipitation followed by mass spectrometry (IP-MS), using antibodies against AEBP2 or SUZ12 (**Figure 5.6A**)(Mass spectrometry portion carried out by Molly Davies and Eugene Dillon – UCD). This enabled me to capture all PRC2 formations as well as those specifically containing AEBP2. As expected, both AEBP2 and SUZ12 co-immunoprecipitated core PRC2 components; however, JARID2 peptides were not enriched in either IP-MS from EZH2-mutant B-cell lymphoma cells (**Figure 5.6B**).

Quantitative analysis of SUZ12 IP-MS revealed that MTF2 and AEBP2 were the predominant PRC2.1 and PRC2.2 accessory proteins, respectively, in these cells (**Figure 5.6C**). Notably, AEBP2 was detected only in complexes with core PRC2, with no evidence of quantitatively significant alternative interacting proteins, further supporting the idea that it exerts its functions exclusively through PRC2. These findings were replicated in the EZH2 wild-type cell line HT, again providing evidence of a shared mechanism of *AEBP2* dependency across germinal centre lymphomas (**Figure 5.6D-F**). The *AEBP2* gene locus encodes two main isoforms, AEBP2^{L} (long) and AEBP2^{S} (short), produced via alternative promoters (Kim et al., 2015; Kim et al., 2009; Mucha et al., 2025). Dr James Nolan previously showed, by immunoblot, that AEBP2^{L} is the predominant isoform across a panel of B-cell lymphoma cell lines. I performed a subcellular fractionation of a panel of B-cell lymphoma cell lines to confirm that JARID2 is not expressed, and that PRC2 core and accessory components are primarily chromatin bound (**Figure 5.6G**). I then used a publicly available dataset to confirm lack of JARID2 expression across a panel of B-cell lymphoma

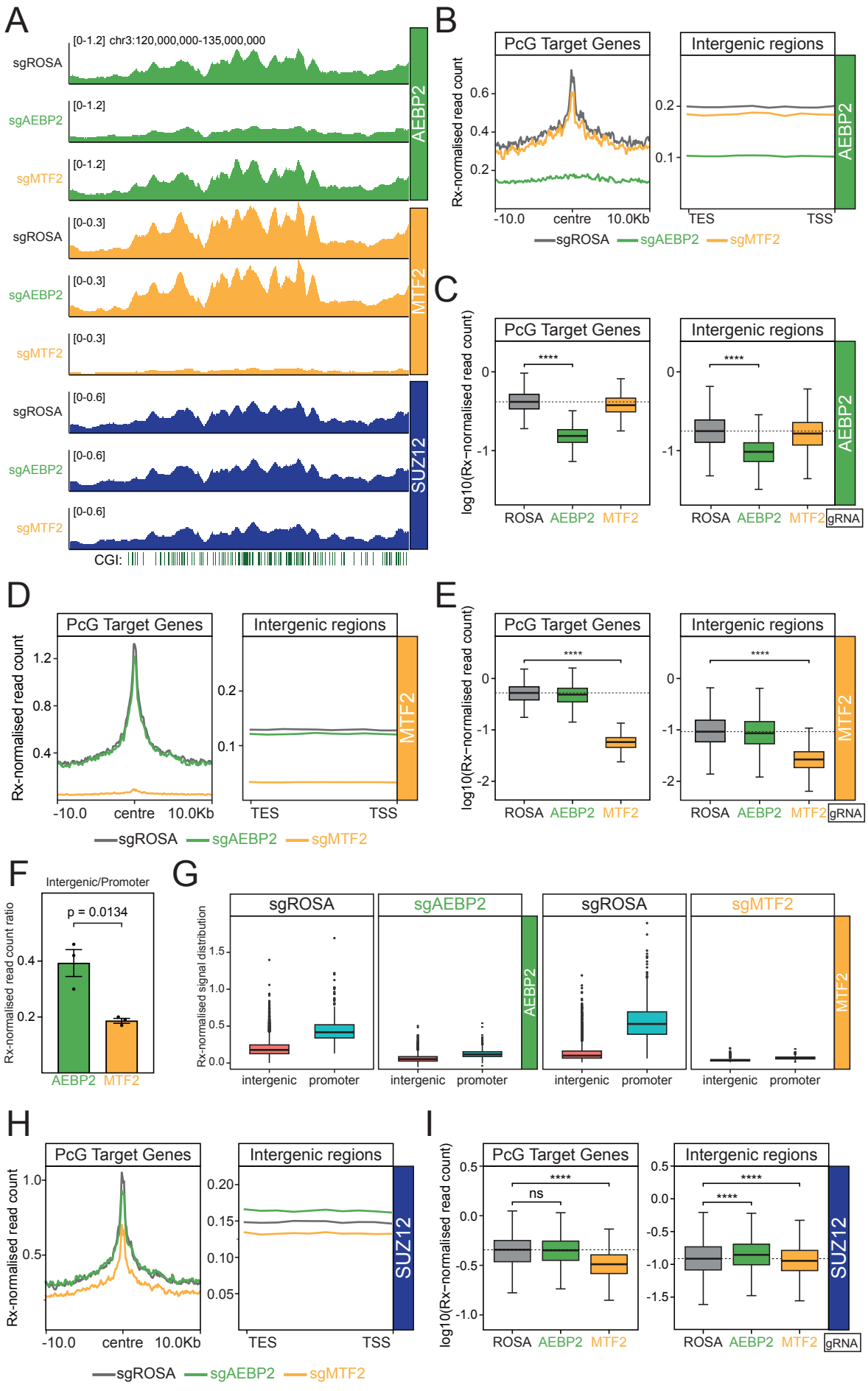
A
[0-1.2] chr3:120,000,000-135,000,000
sgROSA
sgAEBP2
sgMTF2
AEBP2
[0-0.3]
MTF2
[0-0.6]
SUZ12
CGI:
B
PcG Target Genes
Intergenic regions
Rx-normalised read count
-10.0
centre
10.0Kb
TES
TSS
sgROSA
sgAEBP2
sgMTF2
C
log10(Rx−normalised read count)
****
ROSA
AEBP2
MTF2
gRNA
D
E
F
Intergenic/Promoter
p = 0.0134
Rx-normalised read count ratio
G
sgROSA
sgAEBP2
sgMTF2
Rx-normalised signal distribution
intergenic
promoter
H
I
ns

Figure 5.5: AEBP2 demonstrates a broader binding profile at Polycomb target genes and is bound more at intergenic regions compared with MTF2.

A. Genome browser representations showing AEBP2, MTF2 and SUZ12 CUT&RUN-Rx reads in WSU-DLCL2 (EZH2-mutant lymphoma) cells treated with sgRNAs targeting the indicated genes, at a representative PRC2 target site. CGI: CpG islands.

B. Average plots showing AEBP2 CUT&RUN-Rx enrichment at PRC2 target genes and all intergenic sites in WSU-DLCL2 (EZH2-mutant lymphoma) cells transduced with sgRNAs targeting the indicated PRC2 genes. TES and TSS indicate Transcription End Site and Transcription Start Site, respectively.

C. Boxplots of AEBP2 CUT&RUN-Rx signal at PRC2 target genes and intergenic regions in WSU-DLCL2 (EZH2-mutant lymphoma) cells transduced with sgRNAs targeting the indicated PRC2 genes. Significance determined using pairwise Wilcoxon rank-sum tests, ****p value ≤ 0.0001.

D. Average plots showing MTF2 CUT&RUN-Rx enrichment at PRC2 target genes and all intergenic sites in WSU-DLCL2 (EZH2-mutant lymphoma) cells transduced with sgRNAs targeting the indicated PRC2 genes. TES and TSS indicate Transcription End Site and Transcription Start Site, respectively.

E. Boxplots of MTF2 CUT&RUN-Rx signal at PRC2 target genes and intergenic regions in WSU-DLCL2 (EZH2-mutant lymphoma) cells transduced with sgRNAs targeting the indicated PRC2 genes. Significance determined using pairwise Wilcoxon rank-sum tests, ****p value ≤ 0.0001.

F. Ratio of CUT&RUN-Rx signal at intergenic regions compared to PRC2-bound promoter regions for both AEBP2 and MTF2 (n=3, data represents mean ± SEM). Significance determined using unpaired t-test.

G. Boxplots of AEBP2 and MTF2 CUT&RUN-Rx signal at intergenic compared to promoter regions, in control (sgROSA) compared with the respective knock-out in a representative biological replicate corresponding to panel.

H. Average plots showing SUZ12 CUT&RUN-Rx enrichment at PRC2 target genes and all intergenic sites in WSU-DLCL2 (EZH2-mutant lymphoma) cells transduced with sgRNAs targeting the indicated PRC2 genes. TES and TSS indicate Transcription End Site and Transcription Start Site, respectively.

I. Boxplots of SUZ12 CUT&RUN-Rx signal at PRC2 target genes and intergenic regions in WSU-DLCL2 (EZH2-mutant lymphoma) cells transduced with sgRNAs targeting the indicated PRC2 genes. Significance determined using pairwise Wilcoxon rank-sum tests, ****p value ≤ 0.0001.

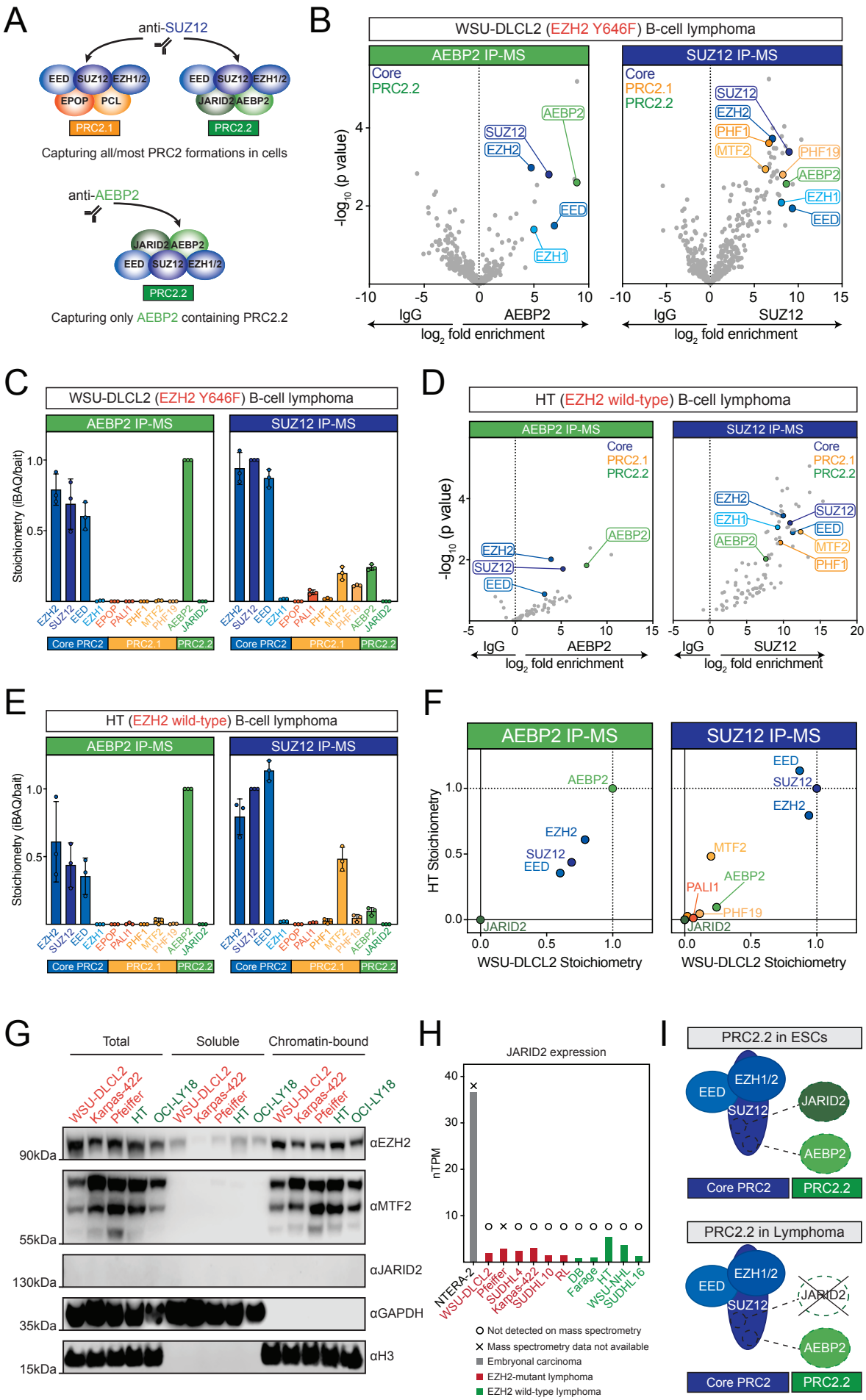
A
anti-SUZ12
EED
SUZ12
EZH1/2
EPOP
PCL
JARID2
AEBP2
PRC2.1
PRC2.2
Capturing all/most PRC2 formations in cells
anti-AEBP2
Capturing only AEBP2 containing PRC2.2
B
WSU-DLCL2 (EZH2 Y646F) B-cell lymphoma
AEBP2 IP-MS
SUZ12 IP-MS
Core
PRC2.1
PRC2.2
-log10 (p value)
lgG
AEBP2
SUZ12
log2 fold enrichment
C
Stoichiometry (iBAQ/bait)
Core PRC2
D
HT (EZH2 wild-type) B-cell lymphoma
E
F
HT Stoichiometry
WSU-DLCL2 Stoichiometry
G
Total
Soluble
Chromatin-bound
WSU-DLCL2
Karpas-422
Pfeiffer
HT
OCI-LY18
90kDa
55kDa
130kDa
35kDa
15kDa
αEZH2
αMTF2
αJARID2
αGAPDH
αH3
H
JARID2 expression
nTPM
Not detected on mass spectrometry
Mass spectrometry data not available
Embryonal carcinoma
EZH2-mutant lymphoma
EZH2 wild-type lymphoma
I
PRC2.2 in ESCs
PRC2.2 in Lymphoma

Figure 5.6: AEBP2 confers its essential function in germinal centre B-cell lymphoma in a PRC2 complex lacking JARID2.
A. Schematic of the SUZ12 co-IP-MS strategy to capture all PRC2 complexes, compared with the AEBP2 co-IP-MS strategy to capture only PRC2.2 complexes.
B. Volcano plots illustrating protein enrichment in endogenous co-immunoprecipitations followed by mass spectrometry of AEBP2 (left) and SUZ12 (right) in WSU-DLCL2 (EZH2-mutant lymphoma) cells (n=3 biological replicates).
C. Bar plots depicting stoichiometry from the IP-MS of AEBP2 (left) and SUZ12 (right) in WSU-DLCL2 (EZH2-mutant lymphoma) cells (n=3, data represents mean ± SD).
D. Volcano plots illustrating protein enrichment in endogenous co-immunoprecipitations followed by mass spectrometry of AEBP2 (left) and SUZ12 (right) in HT (EZH2 wild-type lymphoma) cells (n=3 biological replicates).
E. Bar plots depicting stoichiometry from the IP-MS of AEBP2 (left) and SUZ12 (right) in HT (EZH2 wild-type lymphoma) cells (n=3, data represents mean ± SD).
F. Comparison of the stoichiometry values for AEBP2 (left) and SUZ12 (right) IP-mass spectrometry experiments in two germinal centre B-cell lymphoma cell lines WSU-DLCL2 (EZH2-mutant) and HT (EZH2 wild-type) (n=3 biological replicates).
G. Immunoblots showing cellular fractionations in the indicated lymphoma cell lines demonstrating the lack of JARID2.
H. Bar plots depicting JARID2 expression data from the Human Protein Atlas derived from RNA-seq and mass spectrometry experiments. EZH2-mutant cells are coloured red, EZH2 wild-type cells are coloured green. NTERA-2, in grey, represents a human embryonal carcinoma cell line that is known to express JARID2, thus used as a control.
I. Schematic depictions of core PRC2 complex interacting with PRC2.2 accessory proteins in embryonic stem cells compared to B-cell lymphoma cells.
A-H. Core PRC2 complex is shown in blue, PRC2.1 accessory proteins are shown in orange, and PRC2.2 accessory proteins are shown in green.

cell lines (**Figure 5.6H**) (Jin et al., 2023). Collectively, these findings reveal a novel PRC2.2 configuration in EZH2-mutant B-cell lymphoma: a complex containing AEBP2^{L} but lacking JARID2, termed AEBP2^{L}-PRC2.2 (**Figure 5.6I**), distinct from the canonical JARID2-AEBP2-containing PRC2.2 characterised in mouse embryonic stem cells (ESCs).

5.2.7 EZH2-mutant B-cell lymphoma is specifically hypersensitive to loss of the zinc fingers of AEBP2

One possible explanation for the impaired proliferation following AEBP2 loss could be increased formation of MTF2-PRC2.1 complexes, due to reduced competition for SUZ12 binding (Chen, Jiao, et al., 2018; Glancy et al., 2021; Grijzenhout et al., 2016), leading to aberrant accumulation of H3K27me3. If this were the case, only the SUZ12-binding helix (SBH) of AEBP2 would be required for its function, while its zinc finger (ZF) domains would be dispensable. To investigate this, I re-analysed results from previous PRC2-tiled CRISPR screens in WSU-DLCL2 (EZH2-mutant lymphoma) and G401 (MRT), performed by Drs James Nolan, Eric Conway, and Marlena Mucha (Bracken Lab). With the help of Drs Eimear Lagan and Andrew Malcolm (Brien Lab) I looked at sgRNA depletion across *AEBP2*, *EZH2* (positive control), and *JARID2* (negative control), mapping sgRNA dropout to specific protein regions and identifying CRISPR-knockout hyper-sensitive (CKHS) sites using the ProTiler (He et al., 2019) algorithm (**Figure 5.7A-B**). Importantly, for a region to score as a CKHS, the algorithm requires runs of consecutive low-scoring sgRNAs and excludes those with poor-specificity.

As expected, the EZH2 SET domain scored as a CKHS region in both EZH2-mutant lymphoma and MRT. While two sgRNAs targeting the *AEBP2* PRC2-interacting region also showed strong dropout, intriguingly I observed strong depletion in the three ZF domains of AEBP2 in EZH2-mutant lymphoma but not MRT, indicating their functional importance is specific to this cancer context. In contrast, no hypersensitive regions were detected in JARID2, consistent with its non-essentiality in either cancer. For comparison, I separately

confirmed that *AEBP2*, *EZH2* and *JARID2* contain missense-intolerant regions in the general population (**Figure 5.7C**) (Sun et al., 2024), and though this does not imply cancer-specific dependency, it indicates that the ZFs of AEBP2 are specifically dependent in EZH2-mutant B-cell lymphoma.

To provide higher resolution within the zinc finger CKHS region block of AEBP2, a collaborator in the US, Dr. David Chen (Mayo Clinic) used a previously validated "smoothen" model (Mattson et al., 2024), to identify methionine 319 within ZF2, the central zinc-finger, as a candidate residue that may be critical for zinc-finger function, allowing us to validate the functional importance of the ZF domains of AEBP2 (**Figure 5.7D**).

5.2.8 AEBP2 chromatin binding via zinc fingers is critical for its role in lymphoma

Combining the results of the smoothen model with an NMR-determined structure of the AEBP2 ZFs (Sun et al., 2018)(**Figure 5.8A**), and with help from Professor Andrew Flaus (University of Galway), I hypothesised that substituting methionine 319 with aspartate (M319D), a residue in the ZF2 α-helix that forms to a hydrophobic core with ZF1, would preserve the overall structure of AEBP2 while specifically impairing zinc-finger-mediated chromatin binding, without affecting protein stability or PRC2 association (**Figure 5.8B**). Ectopic expression of wild-type AEBP2^{L}, AEBP2^{S} and the M319D AEBP2^{L} mutant (wild-type constructs generated by Dr Eric Conway, mutant generated by Gráinne Holland) in EZH2-mutant lymphoma cells confirmed stable expression (**Figure 5.8C**), while FLAG co-immunoprecipitations showed that the M319D mutant retained PRC2 binding capability (**Figure 5.8D**). However, subcellular fractionation analysis showed a reduced chromatin association for the M319D mutant compared to wild-type AEBP2^{L} (**Figure 5.8E**).

Next, I performed functional rescue assays and found that the M319D mutant was unable to restore proliferation in *AEBP2* knockout lymphoma cells (**Figure 5.8F**). Based on the fact

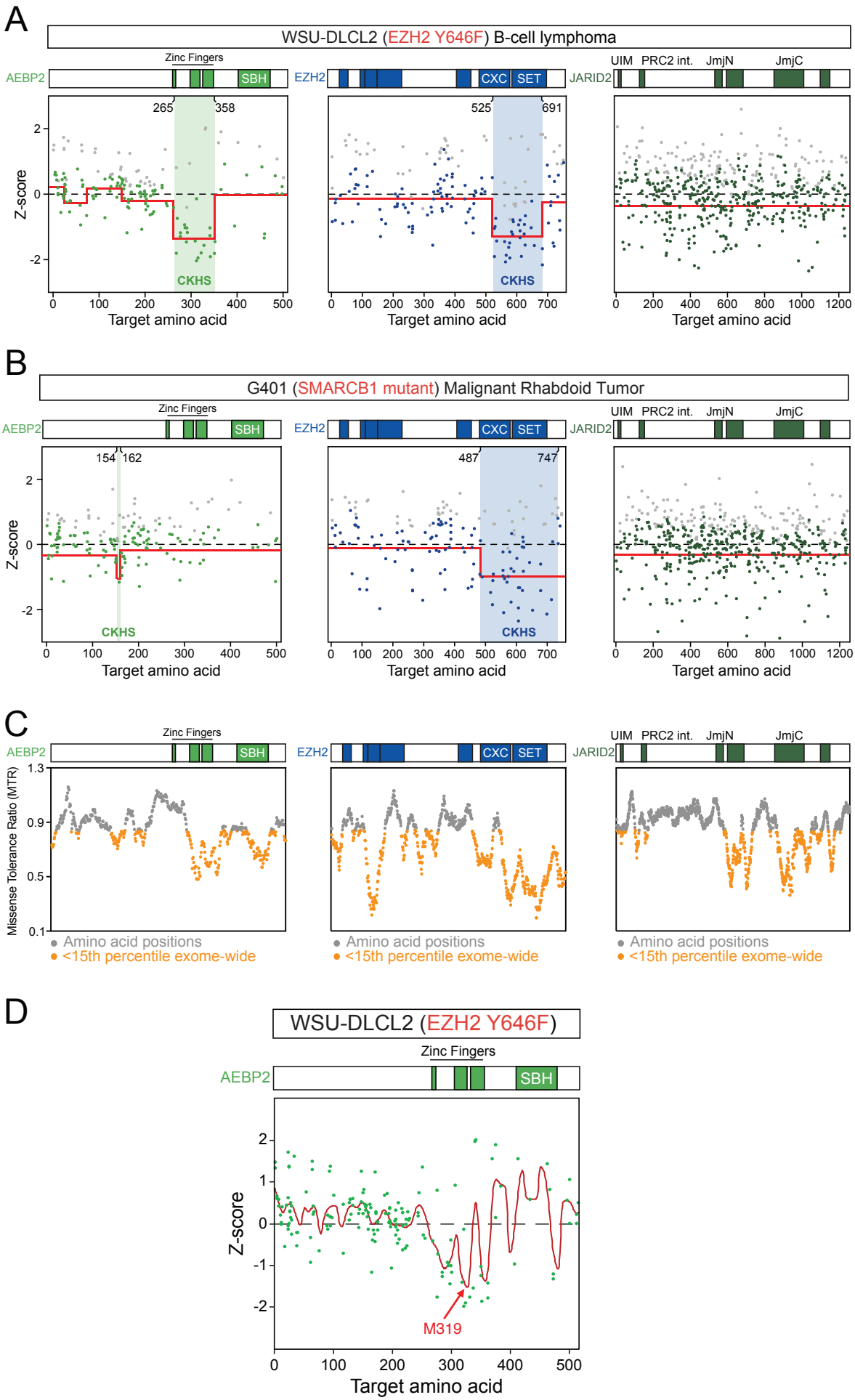
A
WSU-DLCL2 (EZH2 Y646F) B-cell lymphoma
Zinc Fingers
AEBP2
SBH
EZH2
CXC
SET
JARID2
UIM
PRC2 int.
JmjN
JmjC
265
358
525
691
Z-score
CKHS
Target amino acid
B
G401 (SMARCB1 mutant) Malignant Rhabdoid Tumor
154
162
487
747
C
Missense Tolerance Ratio (MTR)
Amino acid positions
<15th percentile exome-wide
D
WSU-DLCL2 (EZH2 Y646F)
M319

Figure 5.7: EZH2-mutant B-cell lymphoma is specifically hypersensitive to loss of the zinc fingers of AEBP2.
A CRISPR tiling screen results of AEBP2, EZH2 and JARID2 in WSU-DLCL2 (EZH2-mutant lymphoma) cells (n=2 biological replicates). sgRNAs are indicated by dots mapped to the target amino acid. CRISPR-knockout hyper-sensitivity (CKHS) regions are indicated in the shaded regions. The average depletion of sgRNAs targeting a protein segment is indicated by the red line (Z-score). The relevant domains of each protein are indicated. SBH indicates the SUZ12-binding helix domain.
B CRISPR PRC2-tiling screen results of AEBP2, EZH2 and JARID2 in G401 (SMARCB1-mutant MRT) cells (n=2 biological replicates). sgRNAs are indicated by dots mapped to the target amino acid. CRISPR-knockout hyper-sensitivity (CKHS) regions are indicated in the shaded regions. The average depletion of sgRNAs targeting a protein segment is indicated by the red line (Z-score). The relevant domains of each protein are indicated. SBH indicates the SUZ12-binding helix domain.
C Missense Tolerance Ratio plots representing regional intolerance to missense mutations using the RGC-ME database of missense mutations in healthy individuals (https://rgc-research.regeneron.com/me/home). We used a sliding window of 31 amino acids across AEBP2, EZH2 and JARID2. Amino acids in the top 15% of those intolerant to missense mutations genome wide are colored orange. The relevant domains of each protein are indicated. SBH indicates the SUZ12-binding helix domain.
D CRISPR-tiling screen results of AEBP2 in WSU-DLCL2 (EZH2-mutant lymphoma) cells (n=2 biological replicates) with sgRNAs indicated by dots mapped to the target amino acid and analysis carried out using the “smoothen” model(ref). The average depletion of sgRNAs targeting a protein segment is indicated by the red line (Z-score). The relevant domains of each protein are indicated. SBH indicates the SUZ12-binding helix domain. The zinc finger 2 M319 residue is highlighted.

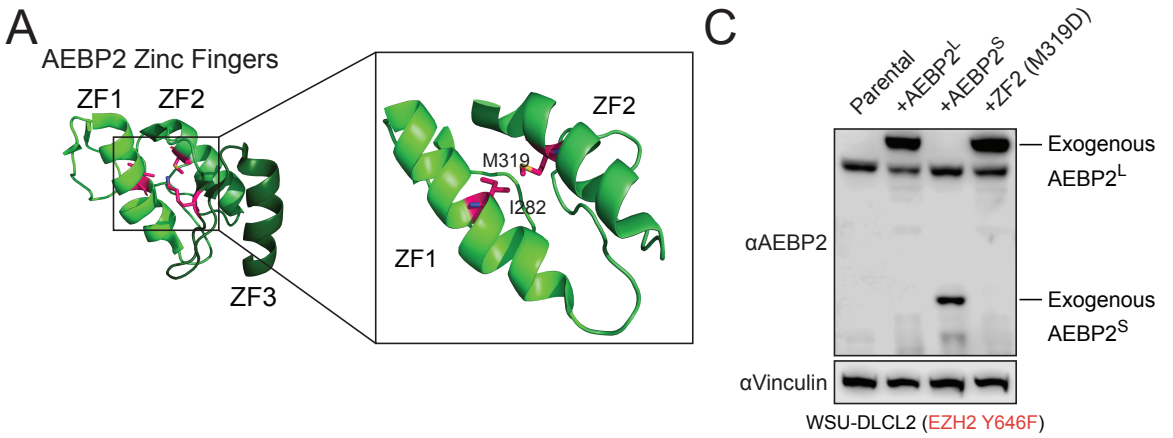
A
AEBP2 Zinc Fingers
ZF1
ZF2
ZF3
M319
I282
C
Parental
+AEBP2L
+AEBP2S
+ZF2 (M319D)
Exogenous AEBP2L
Exogenous AEBP2S
αAEBP2
αVinculin
WSU-DLCL2 (EZH2 Y646F)

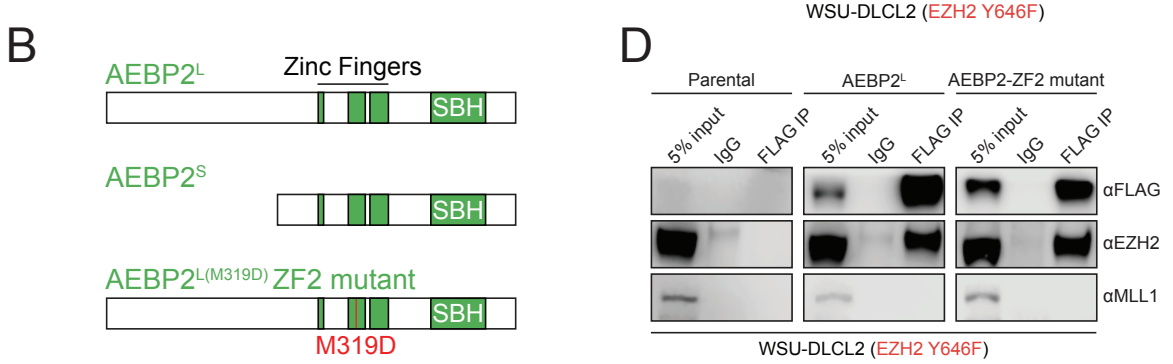
B
AEBP2L
Zinc Fingers
SBH
AEBP2S
AEBP2L(M319D) ZF2 mutant
M319D
D
Parental
AEBP2L
AEBP2-ZF2 mutant
5% input
IgG
FLAG IP
αFLAG
αEZH2
αMLL1
WSU-DLCL2 (EZH2 Y646F)

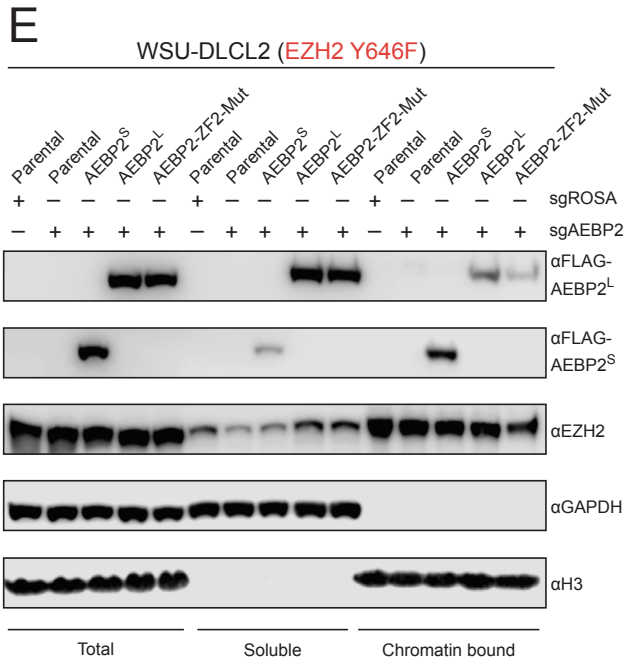
E
WSU-DLCL2 (EZH2 Y646F)
Parental
AEBP2S
AEBP2L
AEBP2-ZF2-Mut
sgROSA
sgAEBP2
αFLAG-AEBP2L
αFLAG-AEBP2S
αEZH2
αGAPDH
αH3
Total
Soluble
Chromatin bound

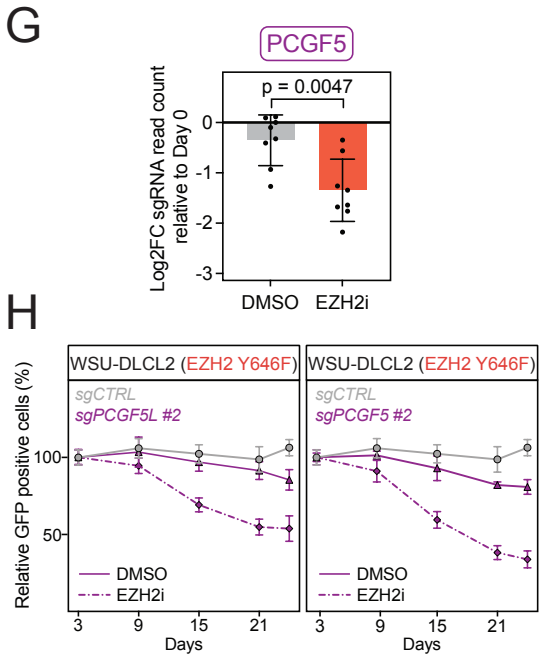
G
PCGF5
p = 0.0047
Log2FC sgRNA read count relative to Day 0
DMSO
EZH2i
H
WSU-DLCL2 (EZH2 Y646F)
sgCTRL
sgPCGF5L #2
sgPCGF5 #2
Relative GFP positive cells (%)
DMSO
EZH2i
Days

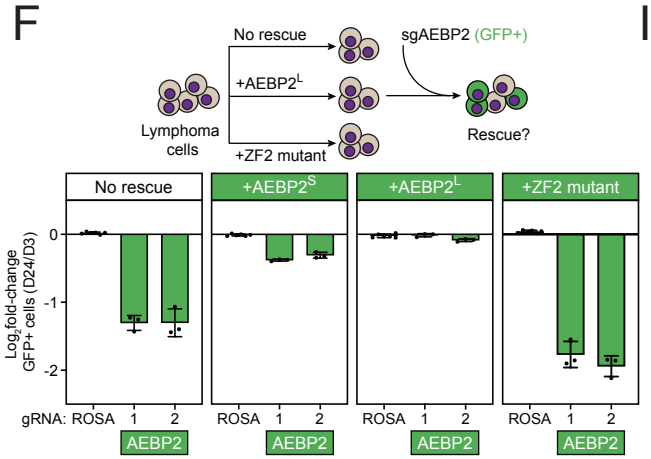
F
No rescue
+AEBP2L
+ZF2 mutant
sgAEBP2 (GFP+)
Lymphoma cells
Rescue?
+AEBP2S
+AEBP2L
+ZF2 mutant
Log2fold-change GFP+ cells (D24/D3)
gRNA: ROSA 1 2
AEBP2

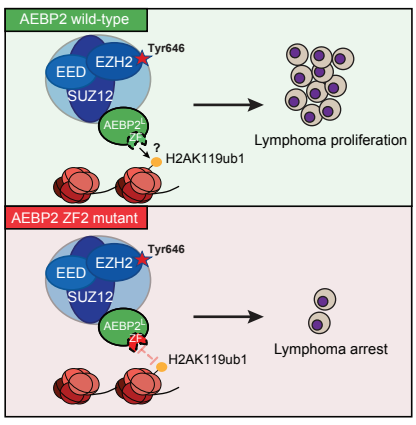
I
AEBP2 wild-type
EED
EZH2
SUZ12
AEBP2L
Tyr646
H2AK119ub1
Lymphoma proliferation
AEBP2 ZF2 mutant
Lymphoma arrest

Figure 5.8: AEBP2 chromatin binding via zinc fingers is critical for its role in lymphoma.

A. Structures of human AEBP2 zinc finger domains, determined by NMR spectroscopy (Sun et al., 2018), with the methionine 319 mutation target indicated.

B. Diagrammatic representation of the HA/FLAG-tagged AEBP2 long, AEBP2 short, and zinc finger 2 (ZF2) mutant constructs expressed in WSU-DLCL2 (EZH2-mutant lymphoma) cells. SBH indicates the SUZ12-binding helix domain.

C. Immunoblots of the indicated proteins from whole cell lysates in WSU-DLCL2 (EZH2-mutant lymphoma) cells expressing the HA/-FLAG-tagged AEBP2 wild-type and mutant constructs.

D. Immunoblots of the indicated proteins in FLAG protein co-immunoprecipitations in WSU-DLCL2 (EZH2-mutant lymphoma) cells expressing the HA/FLAG-tagged AEBP2 wild-type and mutant constructs.

E. Immunoblots showing cellular fractionations in WSU-DLCL2 (EZH2-mutant lymphoma) cells expressing the HA/FLAG-tagged AEBP2 long, AEBP2 short, and zinc finger 2 mutant constructs, using the indicated antibodies. Cells expressing sgROSA (control) or sgAEBP2 are indicated.

F. Schematic representation of AEBP2 rescue experiment (top) and Growth competition assays in WSU-DLCL2 (EZH2-mutant lymphoma) cells expressing sgRNAs targeting endogenous AEBP2 with or without CRISPR-resistant $AEBP2^{L}$, $AEBP2^{S}$ or AEBP2 ZF2 mutant rescue constructs (n=3, data represent mean ± SD).

G. Log2 Fold change of individual sgRNAs relative to D0 from either DMSO-treated or Tazemetostat-treated WSU-DLCL2 cells from the genome-wide CRISPR screen, p value calculated by Mann-Whitney test.

H.Growth competition assays in Cas9-expressing WSU-DLCL2 (EZH2-mutant lymphoma) transduced with sgRNAs targeting the indicated genes followed by treatment with low dose EZH2i (Tazemetostat) (n=3, data represents mean ± SD).

I. Model demonstrating the lymphoma cell phenotype in cells expressing wild-type $AEBP2^{L}$ compared to AEBP2 ZF2 mutant. The recurrent Y646X mutation in EZH2-mutant lymphoma cells is indicated with a red star.

that ZF1-2 of AEBP2 have been shown to interact with H2AK119ub1 (Kasinath et al., 2021), I hypothesised that the Zinc finger domains of AEBP2 play a role in recognising intergenic H2AK119ub1, a modification mediated by PCGF3/PCGF5-containing vPRC1 complexes (Conway et al., 2021; Fursova et al., 2019b). Supporting this hypothesis, I noted that *PCGF5* was one of the most significant sensitiser genes (55/16,808) in the genome-wide CRISPR screen (**Figure 5.8G**). To investigate whether the loss of *PCGF5* synergises with Tazemetostat, I performed CRISPR-Cas9 negative selection assays with and without Tazemetostat treatment (**Figure 5.8H**). Two independent sgRNAs targeting *PCGF5* sensitised lymphoma cells to Tazemetostat, confirming it as a genetic sensitiser similar to *AEBP2*.

Taken together, these results demonstrate that the zinc-finger domains of AEBP2 are essential in EZH2-mutant lymphoma, primarily due to their role in mediating chromatin binding. Furthermore, the findings presented here suggest AEBP2-PRC2 functions downstream of PCGF5-vPRC1 as a reader of intergenic H2AK119ub1 (**Figure 5.8I**).

5.2.9 AEBP2 sustains residual H3K27me2 essential for continued proliferation of EZH2-mutant lymphoma

Next, given that the essential role of AEBP2^{L} in EZH2-mutant lymphoma appears to be independent of its effects on H3K27me3 levels, I hypothesised that its primary function could be to promote PRC2-mediated H3K27me2 deposition at intergenic regions. This idea was supported by prior work from the Bracken Lab showing that both AEBP2 and H3K27me2 increase at intergenic regions upon *JARID2* loss (Healy et al., 2019). Here, in EZH2-mutant B-cell lymphoma cells, which I have shown lack JARID2, AEBP2 appears to be relatively more enriched at intergenic regions than MTF2. Additionally, I've previously established that the ZF domains AEBP2^{L}, responsible for chromatin-binding, are functionally essential (**Figure 5.8**). Since H3K27me3 levels do not correlate with lymphoma proliferation (**Figure 5.4** and **Figure 4.10**), I reasoned that H3K27me2, the other major

PRC2-mediated modification, could be a critical determinant of EZH2 inhibitor sensitivity. Importantly, it has previously been shown that H3K27me2 is already markedly depleted in EZH2-mutant B-cell lymphomas (Beguelin et al., 2013; Romero et al., 2024; Sneeringer et al., 2010).

To test this hypothesis, using CUT&RUN-Rx for H3K27me2, I explored the consequences of CRISPR-mediated loss of *AEBP2* or *MTF2*. This demonstrated that loss of *AEBP2* significantly reduced H3K27me2 at intergenic regions, whereas loss of *MTF2* led to increased H3K27me2 at those same regions (**Figure 5.9A-C**). Thus, the changes in H3K27me2 levels correspond to the opposite sensitivities of AEBP2- versus *MTF2*-depleted cells to EZH2 inhibition (**Figure 5.2**). This led me to speculate that H3K27me2 levels could be central to resistance of cells to EZH2 inhibitors. In another link to Chapter 4 and NSD2-mediated EZH2i resistance, I noted that in **Figure 4.10**, *NSD2* loss resulted in significant gains in H3K27me2 at intergenic and genome-wide regions. Notably, the extent of H3K27me2 gain correlated with the degree of resistance to EZH2 inhibitors: *NSD2* knockout conferred strong resistance, while *MTF2* knockout conferred mild resistance, suggesting a dose-dependent relationship between H3K27me2 levels and EZH2 inhibitor resistance.

Finally, I examined whether restoring AEBP2^{L} could rescue H3K27me2 levels in *AEBP2*-deficient cells (**Figure 5.9D**). Ectopic expression of AEBP2^{L}, but not the chromatin-binding deficient M319D ZF2 mutant, restored H3K27me2 at intergenic regions (**Figure 5.9E-G**). This supports a model in which the ZF domains of AEBP2^{L} are required for PRC2 engagement with chromatin at intergenic regions to maintain H3K27me2. Together, these findings suggest that the characteristically low H3K27me2 levels in EZH2-mutant lymphomas create an Achilles' heel through a specific dependency on AEBP2-PRC2.2 to maintain this essential modification, with H3K27me2 abundance closely correlating with cellular sensitivity or resistance to EZH2 inhibitors.

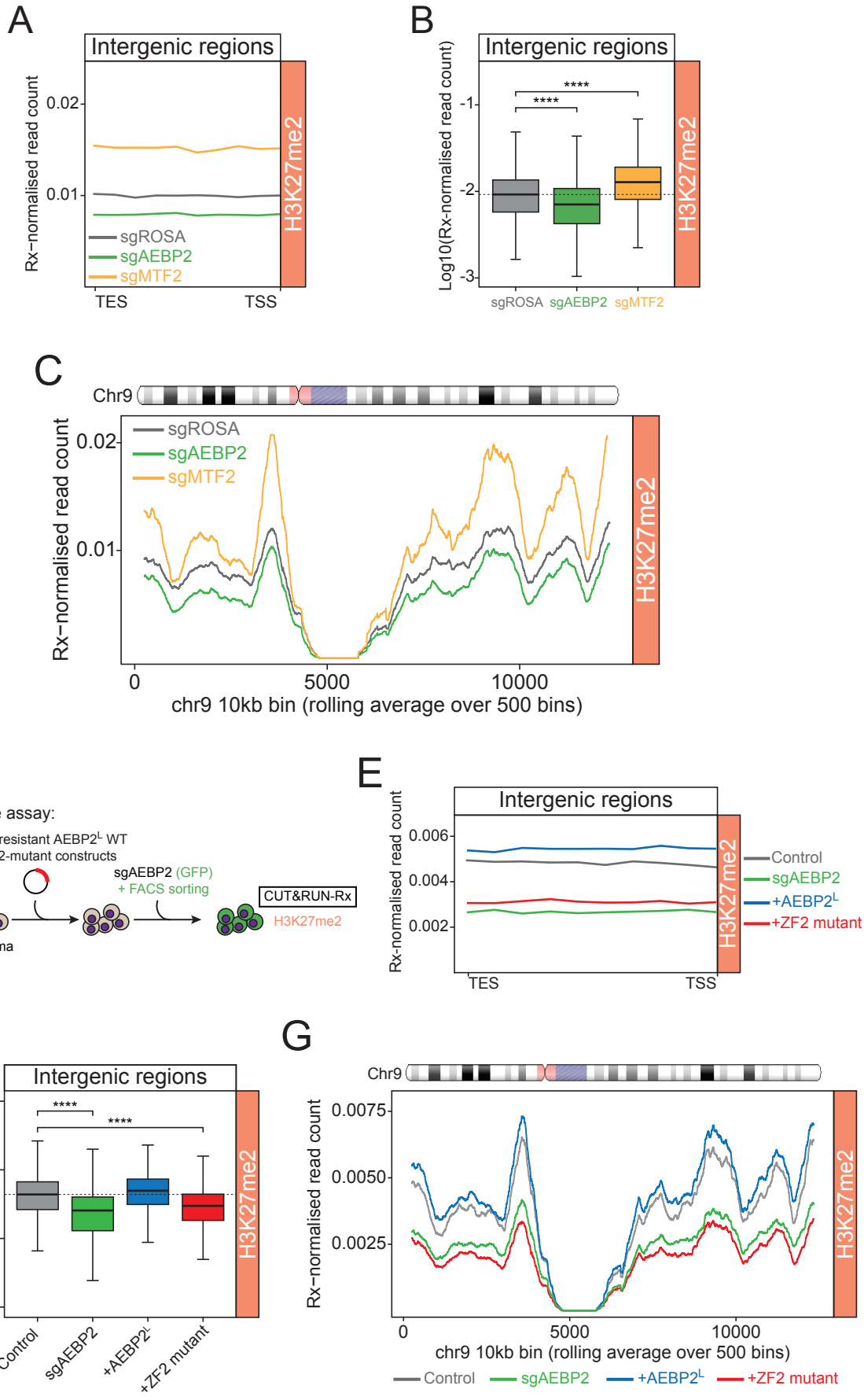
A
Intergenic regions
Rx−normalised read count
0.02
0.01
sgROSA
sgAEBP2
sgMTF2
TES
TSS
H3K27me2
B
Intergenic regions
Log10(Rx-normalised read count)
-1
-2
-3
****
****
sgROSA
sgAEBP2
sgMTF2
H3K27me2
C
Chr9
Rx−normalised read count
0.02
0.01
sgROSA
sgAEBP2
sgMTF2
H3K27me2
0
5000
10000
chr9 10kb bin (rolling average over 500 bins)
D
Rescue assay:
sgRNA-resistant AEBP2L WT
or ZF2-mutant constructs
sgAEBP2 (GFP)
+ FACS sorting
CUT&RUN-Rx
H3K27me2
Lymphoma
cells
E
Intergenic regions
Rx−normalised read count
0.006
0.004
0.002
TES
TSS
H3K27me2
Control
sgAEBP2
+AEBP2L
+ZF2 mutant
F
Intergenic regions
Log10(Rx-normalised read count)
-1
-2
-3
-4
****
****
Control
sgAEBP2
+AEBP2L
+ZF2 mutant
H3K27me2
G
Chr9
Rx−normalised read count
0.0075
0.0050
0.0025
H3K27me2
0
5000
10000
chr9 10kb bin (rolling average over 500 bins)
Control
sgAEBP2
+AEBP2L
+ZF2 mutant

Figure 5.9: AEBP2 sustains residual H3K27me2 essential for continued proliferation of EZH2-mutant lymphoma.
A. Average plots showing H3K27me2 CUT&RUN-Rx enrichment at all intergenic sites in Cas9-expressing WSU-DLCL2 (EZH2-mutant lymphoma) cells transduced with sgRNAs targeting the indicated PRC2 genes.
B. Boxplots of H3K27me2 CUT&RUN-Rx signal at all intergenic regions in Cas9-expressing WSU-DLCL2 (EZH2-mutant lymphoma) cells transduced with sgRNAs targeting the indicated PRC2 genes. Significance determined using pairwise Wilcoxon rank-sum tests, ****p value ≤ 0.0001.
C. Rolling average plots presenting H3K27me2 CUT&RUN-Rx signal across the whole of chromosome 9 in Cas9-expressing WSU-DLCL2 (EZH2-mutant lymphoma) cells transduced with sgRNAs targeting the indicated PRC2 genes. Visualised using 10kb genomic windows.
D. Schematic of CUT&RUN-Rx experiment in WSU-DLCL2 (EZH2-mutant lymphoma) cells expressing AEBP2 wild-type or mutant constructs and using CRISPR to KO endogenous AEBP2.
E. Average plots showing H3K27me2 CUT&RUN-Rx enrichment at all intergenic sites in WSU-DLCL2 (EZH2-mutant lymphoma) cells expressing the indicated AEBP2 constructs.
F. Boxplots of H3K27me2 CUT&RUN-Rx signal at all intergenic regions in in WSU-DLCL2 (EZH2-mutant lymphoma) cells expressing the indicated AEBP2 constructs. Significance determined using pairwise Wilcoxon rank-sum tests, ****p value ≤ 0.0001.
G. Rolling average plots presenting H3K27me2 CUT&RUN-Rx signal across the whole of chromosome 9 in WSU-DLCL2 (EZH2-mutant lymphoma) cells expressing the indicated AEBP2 constructs. Visualised using 10kb genomic windows.

5.2.10 AEBP2 contributes to genome-wide H3K27me2 and loss of AEBP2 leads to increased cPRC1, PRC2.1 and ultimately H3K27me3 at Polycomb target genes in embryonic stem cells

The work in this research project has thus far focused on cancer specific contexts. However, a previous PhD student and now Post-Doc Dr Marlena Mucha had a sister project investigating the functional mechanisms of *Aebp2* in mouse embryonic stem cells (mESCs). Drs Mucha and Glancy (previous Bracken Lab members) created a stable *Aebp2* knockout mESC cell line with which to study the mechanisms of AEBP2 function in this context and showed that the two AEBP2 isoforms, $AEBP2^{S}$ and $AEBP2^{L}$, possess dichotomous roles related to PRC2 regulation (Mucha et al., 2025). The long isoform of AEBP2, which I have shown is by far the predominant isoform in germinal centre lymphoma cells, is a negative regulator of PRC2 function, consistent with the effects of AEBP2 modulation on H3K27me3 levels in lymphoma cells (**Figure 5.4**).

Using spike-in normalised CUT&RUN assays (with human NTERA-2 as exogenous spike-in), I first performed CUT&RUN qPCR for AEBP2, MTF2, H3K27me3, and the cPRC1 member PHC1 in *Aebp2*-KO and control mESCs. As expected, AEBP2 was lost from a strong Polycomb target gene promoter, while MTF2 was increased, in the *Aebp2*-KO cells (**Figure 5.10A-B**). Consistent with published data (Grijzenhout et al., 2016; Mucha et al., 2025) and previous results in the lymphoma context (**Figure 5.5**), I saw an increase in H3K27me3 and, not unexpectedly, a concomitant increase in PHC1 at a Polycomb target gene promoter in *Aebp2*-KO cells (**Figure 5.10C-D**). Interestingly, while H3K27me3 was indeed increased at Polycomb target genes in *Aebp2*-KO cells, it was relatively unchanged throughout the rest of the genome (**Figure 5.10E-G**). Strikingly, H3K27me2 levels were significantly reduced at intergenic, and indeed genome-wide, regions in *Aebp2*-KO mESCs (**Figure 5.10H-J**). Taken together, these results suggest a central role of AEBP2-PRC2 is to promote H3K27me2 deposition, even in non-cancer contexts.

5.2.11 AEBP2 is essential in EZH2 wild-type B-cell lymphoma, with different effects on PRC2 binding compared with EZH2-mutant lymphoma

In Section 5.2.10 I expanded the functional mechanisms of AEBP2 from a EZH2-mutant lymphoma context to a non-cancer model system in embryonic stem cells, and showed that AEBP2-PRC2 functions to deposit intergenic H3K27me2. Next, I wanted to broaden these findings to EZH2 wild-type lymphoma cells to see if the same mechanisms held true. Firstly, I expressed wild-type AEBP2^{L} as well as two ZF mutants of AEBP2 (ZF1 – I282D and ZF3 – Q342K) in the EZH2 wild-type lymphoma cell line HT (**Figure 5.11A**), which I've previously shown is also dependent on AEBP2 (**Figure 5.2**). Then, I performed CRISPR-Cas9 based functional rescue assays and found that neither AEBP2 ZF mutant was able to restore proliferation in *AEBP2* knockout lymphoma cells (**Figure 5.11B**).

While H3K27me3 are not found to be abnormally increased in EZH2 wild-type lymphomas, I questioned whether AEBP2 would still negatively regulate PRC2 in the same way as EZH2-mutant lymphomas. Using a 'bulk' knockout strategy for *AEBP2* in HT cells, I performed CUT&RUN-Rx and observed increased SUZ12 and MTF2 binding at Polycomb target gene promoters, and a concomitant rise in H3K27me3 at these sites (**Figure 5.11C-E**). Then, similarly to the EZH2-mutant context, I examined whether restoring AEBP2^{L} could rescue H3K27me2 levels in *AEBP2*-deficient cells. Ectopic expression of AEBP2^{L}, but not the ZF mutants, restored H3K27me2 genome-wide (**Figure 5.11F**). Furthermore, while ectopic expression of AEBP2^{L} did not rescue H3K27me3 levels in *AEBP2*-KO cells, it did reduce the increased binding of PRC2 in the KO cells, strengthening the evidence for the model in which the ZF domains of AEBP2^{L} are required for PRC2 engagement with chromatin at intergenic regions. Taken together, these findings broaden the previously mentioned Achilles' heel, and suggest that targeting AEBP2 and thus H3K27me2 in germinal centre lymphomas may be a rational mechanism-informed therapy in this context.

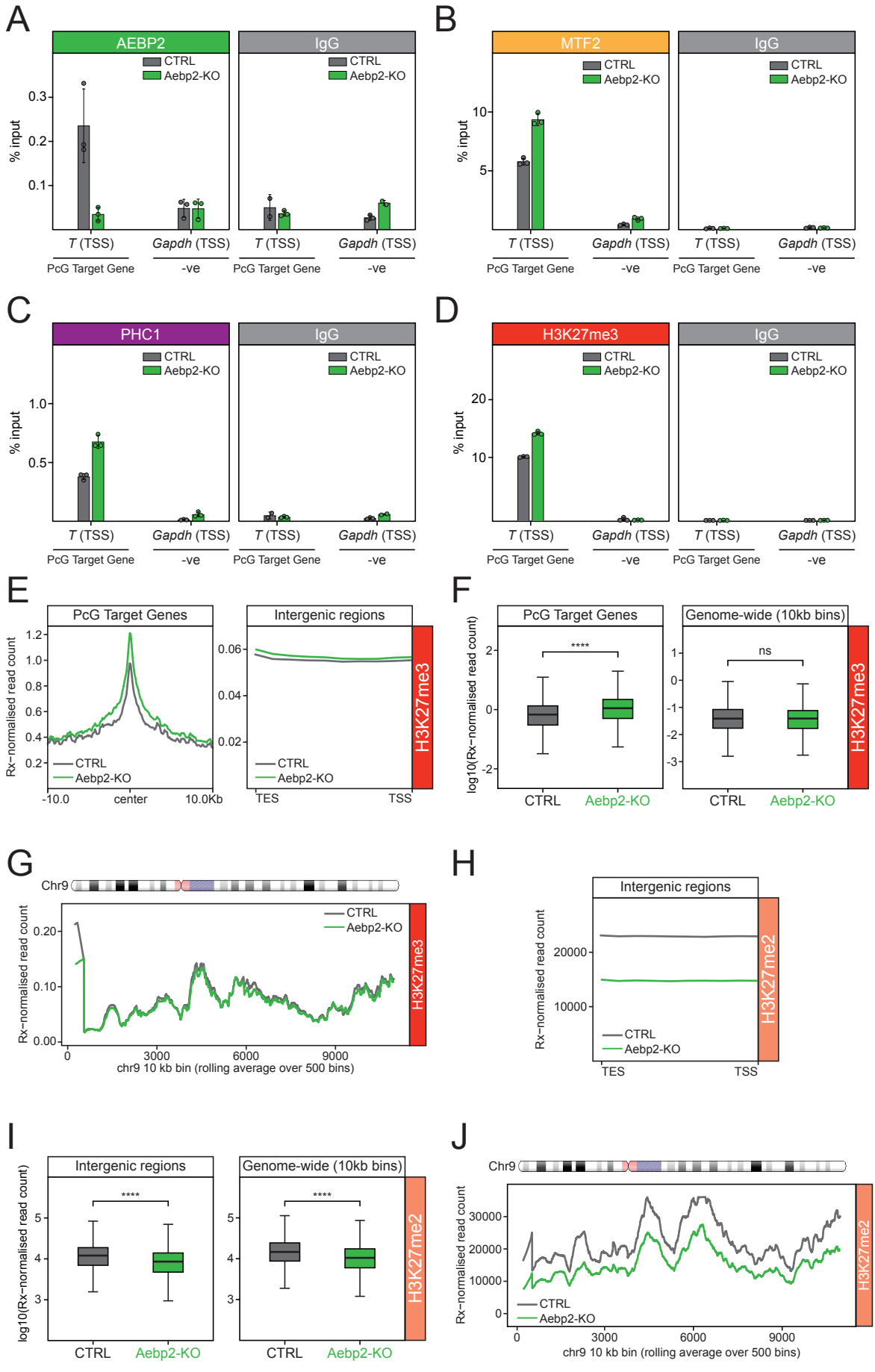
A
AEBP2
IgG
CTRL
Aebp2-KO
% input
T (TSS)
Gapdh (TSS)
PcG Target Gene
-ve
B
MTF2
C
PHC1
D
H3K27me3
E
PcG Target Genes
Intergenic regions
Rx−normalised read count
H3K27me3
-10.0
center
10.0Kb
TES
TSS
F
Genome-wide (10kb bins)
log10(Rx−normalised read count)
****
ns
G
Chr9
chr9 10 kb bin (rolling average over 500 bins)
H
H3K27me2
I
J

Figure 5.10: AEBP2 contributes to genome-wide H3K27me2 and loss of AEBP2 leads to increased cPRC1, PRC2.1 and ultimately H3K27me3 at Polycomb target genes in embryonic stem cells.

A CUT&RUN qPCR analysis of AEBP2 in E14 wild-type and Aebp2-KO mouse embryonic stem cells (mESCs). Data represents mean ± SD of three technical replicates. Each experiment was performed in two biological replicates. A representative experiment is shown.

B CUT&RUN qPCR analysis of MTF2 in E14 wild-type and Aebp2-KO mouse embryonic stem cells (mESCs). Data represents mean ± SD of three technical replicates. Each experiment was performed in two biological replicates. A representative experiment is shown.

C CUT&RUN qPCR analysis of PHC1 in E14 wild-type and Aebp2-KO mouse embryonic stem cells (mESCs). Data represents mean ± SD of three technical replicates. Each experiment was performed in two biological replicates. A representative experiment is shown.

D CUT&RUN qPCR analysis of H3K27me3 in E14 wild-type and Aebp2-KO mouse embryonic stem cells (mESCs). Data represents mean ± SD of three technical replicates. Each experiment was performed in two biological replicates. A representative experiment is shown.

E. Average plots showing H3K27me3 CUT&RUN-Rx enrichment at PRC2 target genes and all intergenic sites in E14 wild-type and Aebp2-KO mouse ESCs. TES and TSS indicate Transcription End Site and Transcription Start Site, respectively.

F. Boxplots of H3K27me3 CUT&RUN-Rx signal at PRC2 target genes and genome-wide 10kb bins in E14 wild-type and Aebp2-KO mouse ESCs. Significance determined using pairwise Wilcoxon rank-sum tests, ****p value ≤ 0.0001.

G. Rolling average plots presenting H3K27me3 CUT&RUN-Rx signal across the whole of chromosome 9 in E14 wild-type and Aebp2-KO mouse ESCs. Visualized using 10kb genomic windows.

H. Average plot showing spike-in normalized H3K27me2 CUT&RUN-Rx enrichment at all intergenic sites in E14 wild-type and Aebp2-KO mouse ESCs. TES and TSS indicate Transcription End Site and Transcription Start Site, respectively.

I. Boxplots of H3K27me2 CUT&RUN-Rx signal at intergenic regions and genome-wide 10kb bins in E14 wild-type and Aebp2-KO mouse ESCs. Significance determined using pairwise Wilcoxon rank-sum tests, ****p value ≤ 0.0001.

J. Rolling average plots presenting H3K27me2 CUT&RUN-Rx signal across the whole of chromosome 9 in E14 wild-type and Aebp2-KO mouse ESCs. Visualized using 10kb genomic windows.

E-J. CUT&RUN-Rx experiments were performed in at least two biological replicates with a representative example shown.

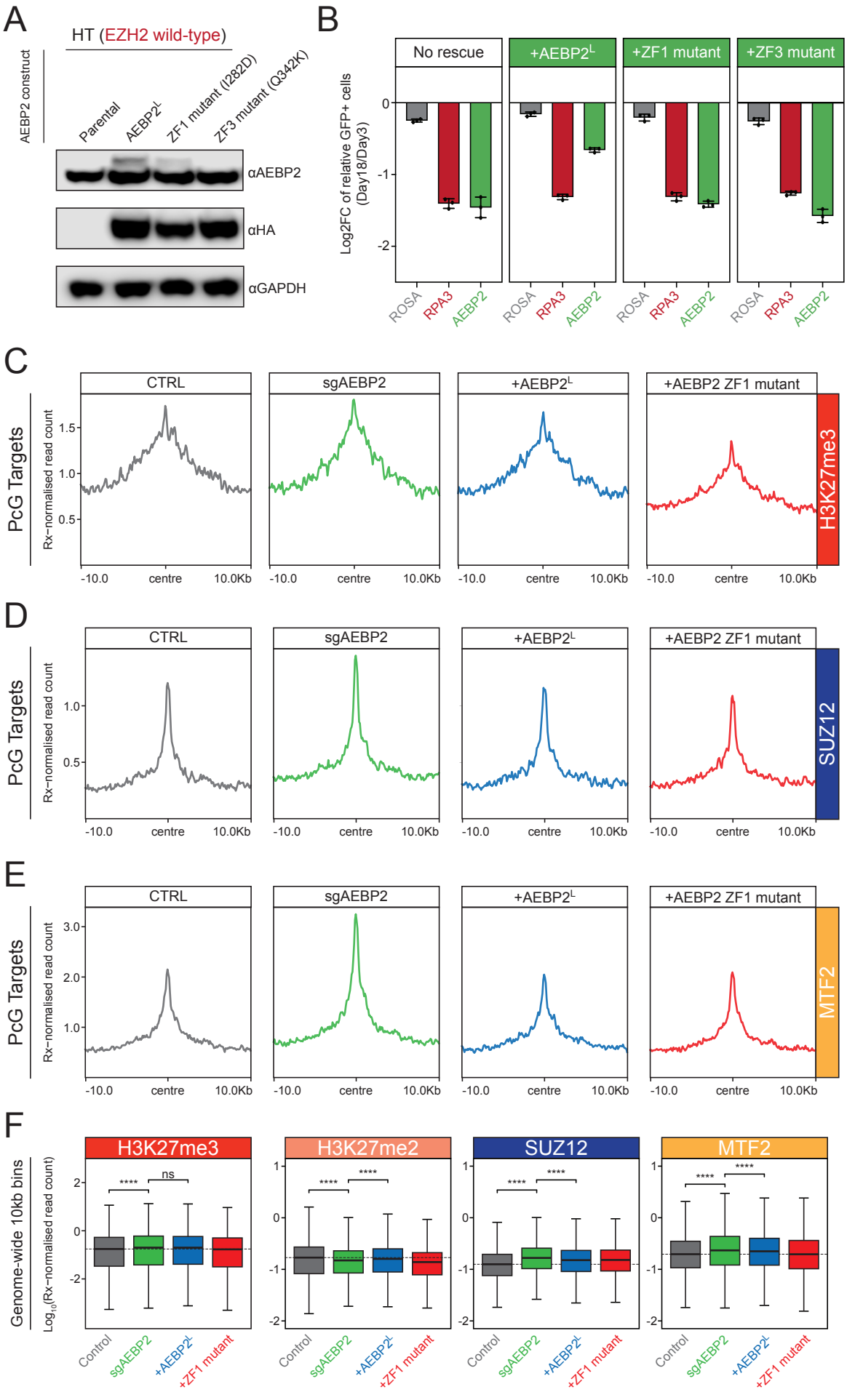
A
HT (EZH2 wild-type)
AEBP2 construct
Parental
AEBP2L
ZF1 mutant (I282D)
ZF3 mutant (Q342K)
αAEBP2
αHA
αGAPDH
B
No rescue
+AEBP2L
+ZF1 mutant
+ZF3 mutant
Log2FC of relative GFP+ cells (Day18/Day3)
ROSA
RPA3
AEBP2
C
PcG Targets
Rx−normalised read count
CTRL
sgAEBP2
+AEBP2L
+AEBP2 ZF1 mutant
H3K27me3
-10.0
centre
10.0Kb
D
SUZ12
E
MTF2
F
Genome-wide 10kb bins
Log10(Rx−normalised read count)
H3K27me3
H3K27me2
SUZ12
MTF2
****
ns
Control
sgAEBP2
+AEBP2L
+ZF1 mutant

Figure 5.11: AEBP2 is essential in EZH2 wild-type B-cell lymphoma, with different effects on PRC2 binding compared with EZH2-mutant lymphoma.

A. Immunoblots from whole cell lysates of the indicated proteins in HT (EZH2 wild-type lymphoma) cells expressing the indicated AEBP2 protein constructs.

B. Growth competition assays in HT (EZH2 wild-type lymphoma) cells expressing sgRNAs targeting ROSA (negative control), RPA3 (positive control) or endogenous AEBP2 with or without CRISPR-resistant AEBP2^{L} or AEBP2 ZF1 or ZF3 mutant rescue constructs (n=3, data represent mean ± SD).

C. Average plots showing H3K27me3 CUT&RUN-Rx enrichment at polycomb target genes in HT (EZH2 wild-type lymphoma) cells expressing the indicated AEBP2 constructs.

D. Average plots showing SUZ12 CUT&RUN-Rx enrichment at polycomb target genes in HT (EZH2 wild-type lymphoma) cells expressing the indicated AEBP2 constructs.

E. Average plots showing MTF2 CUT&RUN-Rx enrichment at polycomb target genes in HT (EZH2 wild-type lymphoma) cells expressing the indicated AEBP2 constructs.

F. Boxplots of H3K27me3, H3K27me2, SUZ12 and MTF2 CUT&RUN-Rx signal at genome-wide 10kb bins in HT (EZH2 wild-type lymphoma) cells expressing the indicated AEBP2 constructs. Significance determined using pairwise Wilcoxon rank-sum tests, ****p value ≤ 0.0001.

5.2.12 In addition to sensitising EZH2-mutant lymphoma cells to EZH2 inhibitors, targeting AEBP2 may overcome acquired EZH2 inhibitor resistance

To conclude the experimental aspects of this PhD research project, I next attempted to link the findings from Chapter 4 relating to *NSD2* loss conferring resistance to EZH2 inhibitors, with the results from Chapter 5 relating to *AEBP2* loss conferring sensitivity to these agents. I've already shown that H3K27me2, and not H3K27me3, appears to be the discriminatory histone post-translational modification relating to sensitivity/resistance to PRC2 inhibitors in germinal centre lymphoma.

I wanted to determine whether the resistance or sensitiser phenotype was stronger in these cells, and from a therapeutic standpoint, could targeting *AEBP2* overcome NSD2-mediated genetic resistance to EZH2 inhibitors, a finding that could have important translational implications. I did this by evaluating *NSD2*-KO lymphoma cells using cell viability assays, analysing populations completely lacking the targeted genes in two EZH2-mutant cell lines (**Figure 5.12A**). As expected, loss of *NSD2* alone conferred resistance to Tazemetostat, whereas AEBP2 loss enhanced sensitivity. Notably, the loss of *AEBP2* in *NSD2*-KO cells could partially overcome Tazemetostat resistance, suggesting that dual targeting of EZH2 and AEBP2 could be an effective strategy to prevent resistance development *in vivo*.

I have summarised the findings of this PhD research project in a set of models set out in **Figure 5.12B-C**. Firstly, PRC2 functions in normal physiology to catalyse all three methylation states on the lysine 27 residue on histone H3 (**Figure 5.12B**), with the complex being more efficient at producing H3K27me1 and H3K27me2 due to a shorter residency time on chromatin required (*top left*). Recurrent SET domain mutations in EZH2 change the substrate preference for the enzyme such that it preferentially tri-methylates H3K27 at the expense of H3K27me2 levels, leading to hyper-repression of gene expression programs required for B-cell maturation (*top right*). EZH2 inhibitors work by inhibiting all methylation

of H3K27, resulting in low levels of H3K27me2 and H3K27me3 and lymphoma cell arrest (*bottom left*). In all these scenarios, NSD1 and NSD2 function to di-methylate H3K36, on the same histone tail, leading to an antagonism on Polycomb function, as previously described (Finogenova et al., 2020). When NSD2 or NSD1 are lost, this Polycomb antagonism is lost, resulting in increased PRC2 activity, with a preference for H3K27me2 over H3K27me3, resulting in enhanced lymphoma cell survival (*bottom right*).

Turning to AEBP2 roles in lymphoma (**Figure 5.12C**), in normal physiology and in the lymphoma context, AEBP2 is bound to SUZ12 and through its ZF domains, it interacts with intergenic chromatin, promoting core PRC2-mediated H3K27me2 deposition (*left*). When AEBP2 is targeted, PRC2 loses its ability to di-methylate H3K27 at intergenic chromatin, leading reductions in this histone post-translational modification, which has negative consequences to lymphoma cell fitness (*right*).

5.3 Discussion

In this Chapter I have identified a previously uncharacterised form of PRC2.2, consisting of the long isoform of AEBP2 (AEBP2^{L}) but lacking JARID2, whose loss represents a specific dependency in EZH2-mutant B-cell lymphoma. I have also shown that AEBP2 is a strong sensitiser to EZH2 inhibition in germinal centre lymphoma. Loss of AEBP2^{L} impairs proliferation in both EZH2-mutant and EZH2 wild-type B-cell lymphomas, but not in other PRC2-dependent cancers such as malignant rhabdoid tumours. While AEBP2^{L} loss causes global increases in H3K27me3, I have demonstrated that the accompanying reduction in H3K27me2, rather than this elevated H3K27me3, drives the proliferation defect.

Interestingly, the lack of gene expression changes in the *NSD2*-KO condition in **Figure 5.3** was notable for how it contrasted with RNA-seq data from Chapter 4. However, in the former experiment cells were harvested 5 days following ‘bulk’ KO of each gene, as a necessity for the difficulties keeping *AEBP2*-KO cells in culture. This contrasts with the Chapter 4 data,

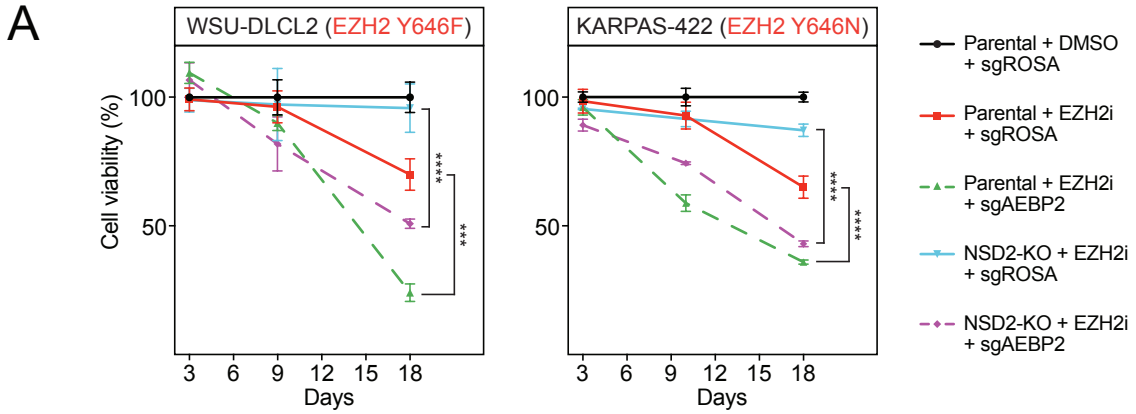
A
WSU-DLCL2 (EZH2 Y646F)
KARPAS-422 (EZH2 Y646N)
Cell viability (%)
100
50
3 6 9 12 15 18
Days
****
***
Parental + DMSO + sgROSA
Parental + EZH2i + sgROSA
Parental + EZH2i + sgAEBP2
NSD2-KO + EZH2i + sgROSA
NSD2-KO + EZH2i + sgAEBP2

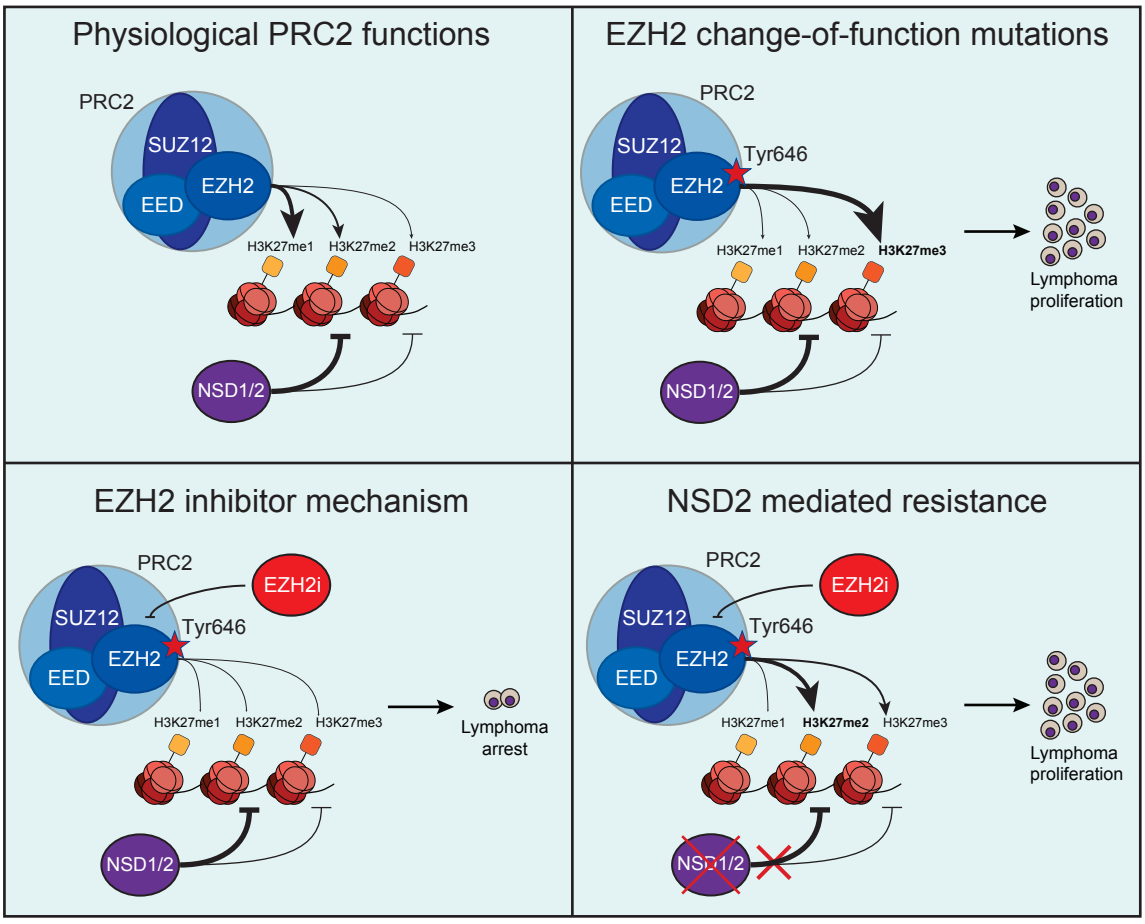
B
Physiological PRC2 functions
EZH2 change-of-function mutations
EZH2 inhibitor mechanism
NSD2 mediated resistance
PRC2
SUZ12
EED
EZH2
Tyr646
EZH2i
H3K27me1
H3K27me2
H3K27me3
NSD1/2
Lymphoma proliferation
Lymphoma arrest

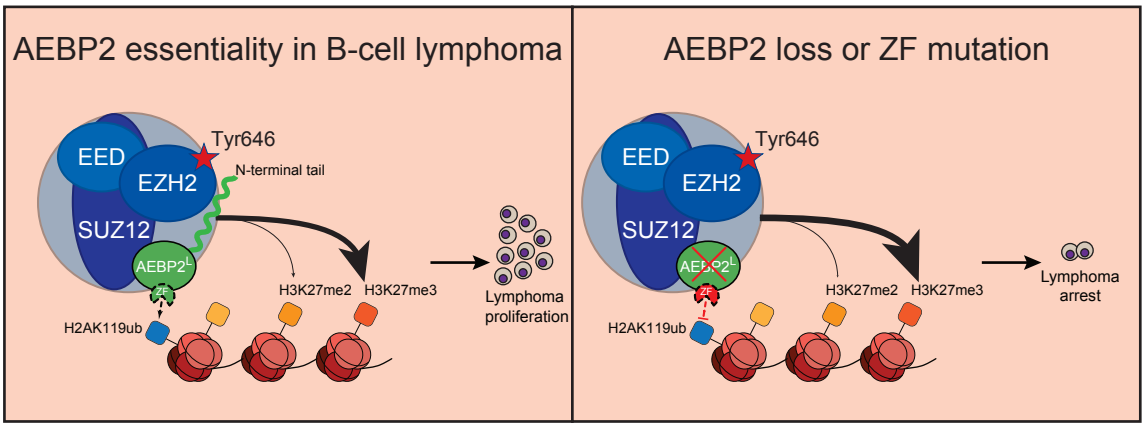
C
AEBP2 essentiality in B-cell lymphoma
AEBP2 loss or ZF mutation
EED
EZH2
SUZ12
Tyr646
N-terminal tail
AEBP2
ZF
H2AK119ub
H3K27me2
H3K27me3
Lymphoma proliferation
Lymphoma arrest

Figure 5.12: In addition to sensitising EZH2-mutant lymphoma cells to EZH2 inhibitors, targeting AEBP2 may overcome acquired EZH2 inhibitor resistance.

A Relative cell viability (normalised to DMSO control) in WSU-DLCL2 and KARPAS-422 (EZH2-mutant lymphoma) cells treated with low dose EZH2 inhibitor (Tazemetostat) and transduced with the indicated sgRNAs over 18 days. Cell viability was measured by CellTiter-Glo. Data are reported as the mean of three biological replicates ± SD. Significance determined using ordinary one-way ANOVA with Tukey's multiple comparisons test, ***p value ≤ 0.001, ****p value ≤ 0.0001.

B Model demonstrating the effects of PRC2 function and dysfunction on histone H3 methylations, and their resulting phenotype in lymphoma cells. Arrow thickness is proportional to the abundance of the specific histone H3 methylation.

C Model demonstrating the effects of PRC2 function and dysfunction on histone H3 methylations, and their resulting phenotype in lymphoma cells. Arrow thickness is proportional to the abundance of the specific histone H3 methylation.

firstly in a different EZH2-mutant cell line (Karpas-422), but also in a clonal and stable *NSD2*-KO model. This suggests that gene expression changes upon *NSD2* loss are likely slow in onset, a hypothesis that could be followed up with RNA-seq over multiple timepoints following *NSD2*-KO.

Furthermore, I have established that the tandem zinc finger domains of AEBP2^{L} are essential for promoting PRC2-mediated H3K27me2 deposition at intergenic regions. Through comparative profiling of cell proliferation rates and H3K27me2 deposition across *MTF2* and *AEBP2* knockout lymphoma lines, and combining with similar data from Chapter 4 on *NSD2* knockout, I have defined a critical threshold of intergenic H3K27me2 required to sustain cell growth and confer resistance to PRC2 inhibitors. Additionally in this chapter, I highlighted that targeting *AEBP2* can overcome EZH2 inhibitor resistance in the previously unreported mechanism of resistance by *NSD2* loss. Collectively, these findings highlight AEBP2^{L}-PRC2.2-dependent maintenance of intergenic H3K27me2 as a new therapeutic vulnerability for these tumours. More broadly, I have established that H2K27me2 functions as a key modulator of sensitivity or resistance to PRC2 inhibitors and that its dysregulation represents a previously underappreciated form of PRC2 dysfunction in cancer. Collectively, these findings highlight AEBP2^{L}-PRC2.2-dependent maintenance of intergenic H3K27me2 as a new therapeutic vulnerability for these tumours.

CHAPTER 6

General Discussion

6.1 General Summary

EZH2-mutant lymphomas are characterised by globally elevated H3K27me3 and reduced H3K27me2 levels, yet the full functional consequences of this altered PRC2 activity remain unclear. This research project identifies a critical requirement for PRC2-mediated intergenic H3K27me2 in sustaining EZH2-mutant lymphoma proliferation and shows that modulation of this mark impacts both sensitivity and resistance to EZH2 inhibitors. In the course of this project I have identified a form of PRC2.2 containing AEBP2L but lacking JARID2 that is required for maintaining H3K27me2 at intergenic regions. These findings uncover a previously unrecognized role for AEBP2-PRC2.2 in mediating H3K27me2 in EZH2-mutant B-cell lymphomas, highlighting it as a potential therapeutic opportunity. More broadly, this project establishes that H3K27me2 functions as a key modulator of sensitivity or resistance to PRC2 inhibitors, revealing its dysregulation as a previously underappreciated form of PRC2 dysfunction in cancer.

6.2 *AEBP2*^{L} joins *MEN1* and *DOT1L* as genes whose loss confer sensitivity to PRC2 inhibitors, albeit via a distinct mechanism

In this project I have identified the long isoform of AEBP2 (AEBP2^{L}) as a novel EZH2 co-dependency in EZH2-mutant lymphoma, expanding on previous studies that uncovered *MEN1* and *DOT1L* as synthetic genetic vulnerabilities, findings that we also observe in this study (Chen et al., 2023; Nguyen et al., 2025; Sparbier et al., 2023). While inhibition of MEN1 and DOT1L synergize with EZH2 inhibition by enhancing de-repression of PRC2-target genes (Göbel et al., 2025; Nguyen et al., 2025; Sparbier et al., 2023), this data suggest that AEBP2 loss functions through a distinct mechanism. Specifically, I showed that AEBP2 loss does not reduce H3K27me3 or induce transcriptional activation of PRC2 target genes. Instead, I have demonstrated that AEBP2^{L} operates within a form of JARID2-free form of PRC2.2 to promote H3K27me2 deposition at intergenic regions - a chromatin

modification that is strikingly diminished in EZH2-mutant B-cell lymphomas (McCabe, Graves, et al., 2012; Romero et al., 2024; Yap et al., 2011).

6.3 AEBP2^{L} is in a JARID2-free form of PRC2.2 that mediates intergenic H3K27me2 deposition

I have identified a distinct form of PRC2.2 in EZH2-mutant B-cell lymphoma that contains the long isoform of AEBP2 (AEBP2^{L}) but lacks JARID2. Most prior studies of PRC2.2 function have been conducted in mouse ESCs, where both AEBP2 and JARID2 proteins are present as sub-stoichiometric components (Glancy et al., 2023; Healy et al., 2019; Højfeldt et al., 2019). However, JARID2 expression is reduced or lost in some non-embryonic tissue types, including lymphomas (Adhikari & Davie, 2018; McCole et al., 2025). The data from this project thus illuminate a JARID2-independent function of AEBP2–PRC2.2 which is both sufficient and capable of targeting PRC2 to intergenic chromatin to mediate H3K27me2 deposition. While JARID2 recruits PRC2.2 to Polycomb target genes in ESCs, at least in part through the recognition of variant PRC1 (vPRC1) mediated H2AK119ub1 (Grijzenhout et al., 2016; Holoch & Margueron, 2017), AEBP2 can also engage this histone mark via its tandem ZF domains, potentially stabilizing PRC2.2 on chromatin (Kalb et al., 2014; Kasinath et al., 2021; Kim et al., 2009). However, unlike *JARID2* loss, which reduces PRC2 occupancy at target genes, AEBP2 loss does not impair PRC2 binding at Polycomb target genes (Grijzenhout et al., 2016; Mucha et al., 2025). Instead, I show here that it leads to reductions in intergenic H3K27me2 deposition. Therefore, I propose that AEBP2^{L}-PRC2.2 sustains H3K27me2 at intergenic regions through recognition of H2AK119ub1 deposited by variant PRC1 complexes containing PCGF3, or PCGF5 (Conway et al., 2021; Kalb et al., 2014). Supporting this, work from the Bracken Lab has demonstrated in ESCs that AEBP2 is relatively more bound at intergenic chromatin compared to MTF2 and JARID2, and that *JARID2* loss results in increased AEBP2-PRC2.2 binding and enhanced H3K27me2 at these regions (Healy et al., 2019).

Furthermore, I propose that AEBP2^{L}-PRC2.2 could act downstream of PCGF5-vPRC1, which functions to mediate intergenic H2AK119ub1 (Conway et al., 2021; Fursova et al., 2019b). Supporting this, I observed *PCGF5* in the top 60 sensitiser genes in the genome-wide CRISPR screen and validated that its loss sensitises lymphoma cells to Tazemetostat treatment. These findings highlight a potential strategy for overcoming resistance to EZH2 inhibitors by disrupting the PCGF5-vPRC1-AEBP2-PRC2.2 axis.

6.4 The potential function of H3K27me2 in B-cell lymphoma

To my knowledge, this is the first study to link a cancer specific genetic vulnerability to aberrantly low H3K27me2 levels and to propose that this may be exploited in cancer therapeutics. I have illustrated that intergenic H3K27me2 is essential in DLBCL, and that reductions below a critical level impair cellular proliferation, despite no detectable changes in gene expression. In non-cancer cells, H3K27me2 is the most abundant PRC2-mediated histone post translational modification and is mostly located at intergenic chromatin, but its function remains unclear (Conway et al., 2015; Ferrari et al., 2014). H3K27me2 deposition has been reported to accumulate during early development and *Jarid2* KO leads to increases in H3K27ac at enhancers, coupled with gene activation (Matsuwaka et al., 2024). However, I did not observe gene activation following the targeted loss of PRC2.2 in EZH2-mutant B-cell lymphoma, via knock-out of AEBP2. Given the lack of gene expression changes in *AEBP2* KO, I speculate that H3K27me2 may alternatively function to maintain 3D chromatin structure, genome stability, or impact DNA replication rate or centromere function. Alternatively, it may facilitate recruitment of other chromatin regulators, such as the EHMT1/EHMT2 complex or the H3K27me2-reader NuRD complex (Hou et al., 2020; Liu et al., 2021; Meng et al., 2020).

To date, the impact of reduced H3K27me2 and its relationship to H3K27me3 has not been examined in EZH2-mutant B-cell lymphomas. While EZH2 inhibitors target both H3K27

methylation states, their putative mechanism of efficacy in B-cell lymphoma is thought to be related to their reduction of H3K27me3 specifically (McCabe, Ott, et al., 2012; Morschhauser et al., 2022). A previously underappreciated aspect of their efficacy may be their further reduction of H3K27me2, which is already diminished due to the *EZH2* mutation (Knutson et al., 2012; McCabe, Ott, et al., 2012). Supporting this, I have shown that *AEBP2* KO synergizes with EZH2 inhibition likely resulting in additional reductions in H3K27me2. Recent work has shown that H3K27me2 and H3K27ac are deposited in a reciprocal fashion, with increasing H3K27ac levels also affecting chromatin compaction (Deevy et al., 2024; Griess et al., 2025). Therefore, it is possible that reductions in H3K27me2, due to *AEBP2* loss, may affect chromatin compaction. Given the known interaction between EZH2 and EHMT2 (Mozzetta et al., 2014; Streubel et al., 2018), and recent work supporting cross talk between H3K9me2 and H3K27me2, rather than H3K27me3 (Griess et al., 2025), the observation that *EHMT2* loss was an EZH2 inhibitor sensitiser in this PhD project warrants further follow up to determine if loci-specific changes in H3K9me2 can point to a mechanism of *AEBP2* dependency .

6.5 Altered H3K27me2 in cancers as an underappreciated modulator of resistance or sensitivity to EZH2 inhibitors

In contrast to *AEBP2*, *MEN1* and *DOT1L*, *NSD1* is a gene whose loss confers resistance to EZH2 inhibitors (Drosos et al., 2022). Here, I have identified *NSD1* and *NSD2* as genes whose loss confer resistance to EZH2 inhibitors in EZH2-mutant B-cell lymphoma, an effect I've established is due to increased intergenic H3K27me2, thus abrogating the efficacy of EZH2 inhibitors. Intriguingly, characterising H3K27me2 levels in SWI/SNF-mutant cancers with and without NSD1 and with and without EZH2 inhibitors could provide a possible mechanistic link between these two divergent cancer types. I demonstrate that AEBP2^{L}-PRC2.2 sustains minimal essential intergenic H3K27me2 in a cancer context where H3K27me2 is markedly scarce, demonstrating also that MTF2-PRC2.1 lacks this function.

Although systematic evaluations of genome-wide H3K27me2 levels in cancers are lacking, other cancers may possess low H3K27me2 and potentially be vulnerable to AEBP2^{L}-PRC2.2 targeting. It is known that the NSD family of enzymes inhibit the deposition of H3K27 methylations by PRC2 (Finogenova et al., 2020; Streubel et al., 2018), and so cancers with NSD1/2/3 gain-of-function would potentially harbour low H3K27me2 levels, and could therefore be sensitive to loss of *AEBP2* (Jaffe et al., 2013; Pierro et al., 2020). In contrast, given the antagonistic role between PRC2 and NSD proteins, cancers with loss-of-function *NSD1/2* mutations or containing the H3K36M oncohistone, would be predicted to have reduced H3K36me2 and consequent elevated H3K27me2 levels, thereby rendering them less sensitive to PRC2 inhibitors (Fang et al., 2016; Farhangdoost et al., 2021; Streubel et al., 2018; Su et al., 2017). Therefore, I suggest assessing H3K27me2 levels across a broader range of cancers to assess its relevance as a predictive marker of vulnerability to AEBP2 loss and EZH2 inhibition. More broadly, I propose grouping cancers by dysregulated histone modification states rather than specific mutations, to expand the therapeutic scope of targeted chromatin-based drugs.

6.6 AEBP2^{L} as a potential therapeutic target

The biology of AEBP2^{L}-PRC2-mediated H3K27me2 offers an interesting potential alternative to targeting the enzymatic activity of EZH2, which faces the challenge of acquired resistance and risks of secondary malignancies (Hsu et al., 2024; Kazansky et al., 2024; Yamagishi et al., 2024). Given that loss-of-function mutations in *AEBP2* are rarely observed in cancers, whereas inactivating mutations/loss of core PRC2 components are well-described (Liu et al., 2017; Neumann et al., 2015; Ntziachristos et al., 2012), targeting the biology of AEBP2^{L} may be an attractive alternative strategy to EZH2 inhibition in EZH2-mutant B-cell lymphoma (Hsu et al., 2024; Huether et al., 2014; Mochizuki-Kashio et al., 2015; Ntziachristos et al., 2012; M. Zhang et al., 2014). Although AEBP2^{L} lacks a tractable enzymatic domain, targeting its ZF domains (Słabicki et al., 2025) or its interaction with SUZ12 may be feasible. Indeed if AEBP2-binding ligands could be developed it may be

targeted using PROTAC-mediated degradation, an emerging therapeutic modality in several cancer types (Bekes et al., 2022; Brien et al., 2018; Robbins et al., 2024). Further work to elucidate the potential upstream function of PCGF3/5-vPRC1-mediated intergenic deposition of H2AK119ub1 could open new avenues for targeting the biology of AEBP2^{L} in lymphoma.

6.7 Conclusions

This PhD research project has provided evidence to support the following conclusions:

1. Genetic sensitisers to EZH2 inhibition in EZH2-mutant lymphoma are enriched for chromatin regulatory genes including *EHMT2*, *BRD9*, *MEN1*, *DOT1L*, *KMT2D*, and *EP300*.
2. *NSD2* loss results in resistance to EZH2 inhibitors in EZH2-mutant lymphoma, due to its effects on H3K36 methylation, H3K27 methylation and H3K27 acetylation at distal regulatory elements.
3. Identification of a previously uncharacterised form of PRC2.2, consisting of the long isoform of AEBP2 (AEBP2^{L}) but lacking JARID2, which represents a specific dependency in EZH2-mutant B-cell lymphoma.
4. Loss of AEBP2^{L} impairs proliferation specifically in EZH2-mutant B-cell lymphomas, but not in other PRC2-dependent cancers such as malignant rhabdoid tumours.
5. Loss of AEBP2^{L} acts synergistically with PRC2 inhibition as a genetic sensitiser in germinal centre B-cell lymphomas.
6. While AEBP2^{L} loss causes global increases in H3K27me3, the accompanying reduction in H3K27me2, rather than this elevated H3K27me3, drives the proliferation defect.
7. The tandem zinc finger domains of AEBP2^{L} are essential for promoting PRC2-mediated H3K27me2 deposition at intergenic regions.
8. Targeting AEBP2 can overcome EZH2 inhibitor resistance driven by the previously unreported mechanism of resistance by NSD2 loss.
9. AEBP2^{L}-PRC2.2-dependent maintenance of intergenic H3K27me2 is a new therapeutic vulnerability for B-cell lymphomas.
10. H2K27me2 functions as a key modulator of sensitivity or resistance to PRC2 inhibitors and that its dysregulation represents a previously underappreciated form of PRC2 dysfunction in cancer.

References

Abu-Farha, M., Lambert, J. P., Al-Madhoun, A. S., Elisma, F., Skerjanc, I. S., & Figeys, D. (2008). The tale of two domains: proteomics and genomics analysis of SMYD2, a new histone methyltransferase. Mol Cell Proteomics, 7(3), 560-572. https://doi.org/10.1074/mcp.M700271-MCP200

Adhikari, A., & Davie, J. (2018). JARID2 and the PRC2 complex regulate skeletal muscle differentiation through regulation of canonical Wnt signaling. Epigenetics Chromatin, 11(1), 46. https://doi.org/10.1186/s13072-018-0217-x

Administration, U. S. F. a. D. (2020). FDA granted accelerated approval to tazemetostat for follicular lymphoma. https://www.fda.gov/drugs/fda-granted-accelerated-approval-tazemetostat-follicular-lymphoma

Agger, K., Cloos, P. A., Christensen, J., Pasini, D., Rose, S., Rappsilber, J., Issaeva, I., Canaani, E., Salcini, A. E., & Helin, K. (2007). UTX and JMJD3 are histone H3K27 demethylases involved in HOX gene regulation and development. Nature, 449(7163), 731-734. https://doi.org/10.1038/nature06145

Aguirre, A. J., Meyers, R. M., Weir, B. A., Vazquez, F., Zhang, C. Z., Ben-David, U., Cook, A., Ha, G., Harrington, W. F., Doshi, M. B., Kost-Alimova, M., Gill, S., Xu, H., Ali, L. D., Jiang, G., Pantel, S., Lee, Y., Goodale, A., Cherniack, A. D., . . . Hahn, W. C. (2016). Genomic Copy Number Dictates a Gene-Independent Cell Response to CRISPR/Cas9 Targeting. Cancer Discov, 6(8), 914-929. https://doi.org/10.1158/2159-8290.CD-16-0154

Alizadeh, A. A., Eisen, M. B., Davis, R. E., Ma, C., Lossos, I. S., Rosenwald, A., Boldrick, J. C., Sabet, H., Tran, T., Yu, X., Powell, J. I., Yang, L., Marti, G. E., Moore, T., Hudson, J., Jr., Lu, L., Lewis, D. B., Tibshirani, R., Sherlock, G., . . . Staudt, L. M. (2000). Distinct types of diffuse large B-cell lymphoma identified by gene expression profiling. Nature, 403(6769), 503-511. https://doi.org/10.1038/35000501

Allfrey, V. G., Faulkner, R., & Mirsky, A. E. (1964). Acetylation and Methylation of Histones and Their Possible Role in the Regulation of Rna Synthesis. Proc Natl Acad Sci U S A, 51(5), 786-794. https://doi.org/10.1073/pnas.51.5.786

Allis, C. D., & Jenuwein, T. (2016). The molecular hallmarks of epigenetic control. Nat Rev Genet, 17(8), 487-500. https://doi.org/10.1038/nrg.2016.59

Alqazzaz, M. A., Luciani, G. M., Vu, V., Machado, R. A. C., Szewczyk, M. M., Adamson, E. C., Cheon, S., Li, F., Arrowsmith, C. H., Minden, M. D., & Barsyte-Lovejoy, D. (2024). Epigenetic vulnerabilities of leukemia harboring inactivating EZH2 mutations. Exp Hematol, 130, 104135. https://doi.org/10.1016/j.exphem.2023.11.009

Amengual, J. E., Johannet, P., Lombardo, M., Zullo, K., Hoehn, D., Bhagat, G., Scotto, L., Jirau-Serrano, X., Radeski, D., Heinen, J., Jiang, H., Cremers, S., Zhang, Y., Jones, S., & O'Connor, O. A. (2015). Dual Targeting of Protein Degradation Pathways with the Selective HDAC6 Inhibitor ACY-1215 and Bortezomib Is Synergistic in Lymphoma. Clin Cancer Res, 21(20), 4663-4675. https://doi.org/10.1158/1078-0432.CCR-14-3068

An, W., Kim, J., & Roeder, R. G. (2004). Ordered cooperative functions of PRMT1, p300, and CARM1 in transcriptional activation by p53. Cell, 117(6), 735-748. https://doi.org/10.1016/j.cell.2004.05.009

Angelov, D., Nolan, J., Holland, G., Nimmo, D., Davies, M., Monger, C., Dillon, E., Mucha, M., Wang, C., Gannon, D., Lagan, E., Malcolm, A., Yang, L., Chen, A., Vandenberghe, E., Flaus, A., Chen, C.-W., Brien, G. L., Conway, E., & Bracken, A. P. (2025). AEBP2-Directed H3K27me2 Defines a Specific Vulnerability in EZH2-mutant Lymphoma. bioRxiv, 2025.2010.2014.682307. https://doi.org/10.1101/2025.10.14.682307

Angrand, P. O., Apiou, F., Stewart, A. F., Dutrillaux, B., Losson, R., & Chambon, P. (2001). NSD3, a new SET domain-containing gene, maps to 8p12 and is amplified in human breast cancer cell lines. Genomics, 74(1), 79-88. https://doi.org/10.1006/geno.2001.6524

Arellano, M. L., Thirman, M. J., DiPersio, J. F., Heiblig, M., Stein, E. M., Schuh, A. C., Zucenka, A., de Botton, S., Grove, C. S., Mannis, G. N., Papayannidis, C., Perl, A. E., Issa, G. C., Aldoss, I., Bajel, A., Dickens, D. S., Kuhn, M. W. M., Mantzaris, I., Raffoux, E., . . . Blachly, J. S. (2025). Menin inhibition with revumenib for NPM1-mutated relapsed or refractory acute myeloid leukemia: the AUGMENT-101 study. Blood, 146(9), 1065-1077. https://doi.org/10.1182/blood.2025028357

Baker, L. A., Allis, C. D., & Wang, G. G. (2008). PHD fingers in human diseases: disorders arising from misinterpreting epigenetic marks. Mutat Res, 647(1-2), 3-12. https://doi.org/10.1016/j.mrfmmm.2008.07.004

Baker, T., Nerle, S., Pritchard, J., Zhao, B., Rivera, V. M., Garner, A., & Gonzalvez, F. (2015). Acquisition of a single EZH2 D1 domain mutation confers acquired resistance to EZH2-targeted inhibitors. Oncotarget, 6(32), 32646-32655. https://doi.org/10.18632/oncotarget.5066

Barisic, D., Chin, C. R., Meydan, C., Teater, M., Tsialta, I., Mlynarczyk, C., Chadburn, A., Wang, X., Sarkozy, M., Xia, M., Carson, S. E., Raggiri, S., Debek, S., Pelzer, B., Durmaz, C., Deng, Q., Lakra, P., Rivas, M., Steidl, C., . . . Melnick, A. (2024). ARID1A orchestrates SWI/SNF-mediated sequential binding of transcription factors with ARID1A loss driving pre-memory B cell fate and lymphomagenesis. Cancer Cell, 42(4), 583-604 e511. https://doi.org/10.1016/j.ccell.2024.02.010

Barrangou, R., Fremaux, C., Deveau, H., Richards, M., Boyaval, P., Moineau, S., Romero, D. A., & Horvath, P. (2007). CRISPR provides acquired resistance against viruses in prokaryotes. Science, 315(5819), 1709-1712. https://doi.org/10.1126/science.1138140

Bartram, C. R., de Klein, A., Hagemeijer, A., van Agthoven, T., Geurts van Kessel, A., Bootsma, D., Grosveld, G., Ferguson-Smith, M. A., Davies, T., Stone, M., & et al. (1983). Translocation of c-ab1 oncogene correlates with the presence of a Philadelphia chromosome in chronic myelocytic leukaemia. Nature, 306(5940), 277-280. https://doi.org/10.1038/306277a0

Basso, K., & Dalla-Favera, R. (2012). Roles of BCL6 in normal and transformed germinal center B cells. Immunol Rev, 247(1), 172-183. https://doi.org/10.1111/j.1600-065X.2012.01112.x

Basso, K., & Dalla-Favera, R. (2015). Germinal centres and B cell lymphomagenesis. Nat Rev Immunol, 15(3), 172-184. https://doi.org/10.1038/nri3814

Bates, S. E. (2020). Epigenetic Therapies for Cancer. N Engl J Med, 383(7), 650-663. https://doi.org/10.1056/NEJMra1805035

Bea, S., Valdes-Mas, R., Navarro, A., Salaverria, I., Martin-Garcia, D., Jares, P., Gine, E., Pinyol, M., Royo, C., Nadeu, F., Conde, L., Juan, M., Clot, G., Vizan, P., Di Croce, L., Puente, D. A., Lopez-Guerra, M., Moros, A., Roue, G., . . . Campo, E. (2013). Landscape of somatic mutations and clonal evolution in mantle cell lymphoma. Proc Natl Acad Sci U S A, 110(45), 18250-18255. https://doi.org/10.1073/pnas.1314608110

Beguelin, W., Popovic, R., Teater, M., Jiang, Y., Bunting, K. L., Rosen, M., Shen, H., Yang, S. N., Wang, L., Ezponda, T., Martinez-Garcia, E., Zhang, H., Zheng, Y., Verma, S. K., McCabe, M. T., Ott, H. M., Van Aller, G. S., Kruger, R. G., Liu, Y., . . . Melnick, A. M. (2013). EZH2 is required for germinal center formation and somatic EZH2 mutations promote lymphoid transformation. Cancer Cell, 23(5), 677-692. https://doi.org/10.1016/j.ccr.2013.04.011

Beguelin, W., Rivas, M. A., Calvo Fernandez, M. T., Teater, M., Purwada, A., Redmond, D., Shen, H., Challman, M. F., Elemento, O., Singh, A., & Melnick, A. M. (2017). EZH2 enables germinal centre formation through epigenetic silencing of CDKN1A and an Rb-E2F1 feedback loop. Nat Commun, 8(1), 877. https://doi.org/10.1038/s41467-017-01029-x

Béguelin, W., Teater, M., Gearhart, M. D., Calvo Fernández, M. T., Goldstein, R. L., Cárdenas, M. G., Hatzi, K., Rosen, M., Shen, H., Corcoran, C. M., Hamline, M. Y., Gascoyne, R. D., Levine, R. L., Abdel-Wahab, O., Licht, J. D., Shaknovich, R., Elemento, O., Bardwell, V. J., & Melnick, A. M. (2016). EZH2 and BCL6 Cooperate to Assemble CBX8-BCOR Complex to Repress Bivalent Promoters, Mediate

Germinal Center Formation and Lymphomagenesis. Cancer Cell, 30(2), 197-213. https://doi.org/10.1016/j.ccell.2016.07.006

Beguelin, W., Teater, M., Meydan, C., Hoehn, K. B., Phillip, J. M., Soshnev, A. A., Venturutti, L., Rivas, M. A., Calvo-Fernandez, M. T., Gutierrez, J., Camarillo, J. M., Takata, K., Tarte, K., Kelleher, N. L., Steidl, C., Mason, C. E., Elemento, O., Allis, C. D., Kleinstein, S. H., & Melnick, A. M. (2020). Mutant EZH2 Induces a Pre-malignant Lymphoma Niche by Reprogramming the Immune Response. Cancer Cell, 37(5), 655-673 e611. https://doi.org/10.1016/j.ccell.2020.04.004

Behjati, S., Tarpey, P. S., Presneau, N., Scheipl, S., Pillay, N., Van Loo, P., Wedge, D. C., Cooke, S. L., Gundem, G., Davies, H., Nik-Zainal, S., Martin, S., McLaren, S., Goodie, V., Robinson, B., Butler, A., Teague, J. W., Halai, D., Khatri, B., . . . Flanagan, A. M. (2013). Distinct H3F3A and H3F3B driver mutations define chondroblastoma and giant cell tumor of bone. Nat Genet, 45(12), 1479-1482. https://doi.org/10.1038/ng.2814

Bekes, M., Langley, D. R., & Crews, C. M. (2022). PROTAC targeted protein degraders: the past is prologue. Nat Rev Drug Discov, 21(3), 181-200. https://doi.org/10.1038/s41573-021-00371-6

Bennett, R. L., Swaroop, A., Troche, C., & Licht, J. D. (2017). The Role of Nuclear Receptor-Binding SET Domain Family Histone Lysine Methyltransferases in Cancer. Cold Spring Harb Perspect Med, 7(6). https://doi.org/10.1101/cshperspect.a026708

Bernstein, B. E., Mikkelsen, T. S., Xie, X., Kamal, M., Huebert, D. J., Cuff, J., Fry, B., Meissner, A., Wernig, M., Plath, K., Jaenisch, R., Wagschal, A., Feil, R., Schreiber, S. L., & Lander, E. S. (2006). A bivalent chromatin structure marks key developmental genes in embryonic stem cells. Cell, 125(2), 315-326. https://doi.org/10.1016/j.cell.2006.02.041

Bernt, K. M., Zhu, N., Sinha, A. U., Vempati, S., Faber, J., Krivtsov, A. V., Feng, Z., Punt, N., Daigle, A., Bullinger, L., Pollock, R. M., Richon, V. M., Kung, A. L., & Armstrong, S. A. (2011). MLL-rearranged leukemia is dependent on aberrant H3K79 methylation by DOT1L. Cancer Cell, 20(1), 66-78. https://doi.org/10.1016/j.ccr.2011.06.010

Bisserier, M., & Wajapeyee, N. (2018). Mechanisms of resistance to EZH2 inhibitors in diffuse large B-cell lymphomas. Blood, 131(19), 2125-2137. https://doi.org/10.1182/blood-2017-08-804344

Blackledge, N. P., Farcas, A. M., Kondo, T., King, H. W., McGouran, J. F., Hanssen, L. L. P., Ito, S., Cooper, S., Kondo, K., Koseki, Y., Ishikura, T., Long, H. K., Sheahan, T. W., Brockdorff, N., Kessler, B. M., Koseki, H., & Klose, R. J. (2014). Variant PRC1 complex-dependent H2A ubiquitylation drives PRC2 recruitment and polycomb

domain formation. Cell, 157(6), 1445-1459. https://doi.org/10.1016/j.cell.2014.05.004

Blackledge, N. P., Fursova, N. A., Kelley, J. R., Huseyin, M. K., Feldmann, A., & Klose, R. J. (2020). PRC1 Catalytic Activity Is Central to Polycomb System Function. Mol Cell, 77(4), 857-874 e859. https://doi.org/10.1016/j.molcel.2019.12.001

Blackledge, N. P., & Klose, R. J. (2021). The molecular principles of gene regulation by Polycomb repressive complexes. Nat Rev Mol Cell Biol, 22(12), 815-833. https://doi.org/10.1038/s41580-021-00398-y

Bock, C., Datlinger, P., Chardon, F., Coelho, M. A., Dong, M. B., Lawson, K. A., Lu, T., Maroc, L., Norman, T. M., Song, B., Stanley, G., Chen, S., Garnett, M., Li, W., Moffat, J., Qi, L. S., Shapiro, R. S., Shendure, J., Weissman, J. S., & Zhuang, X. (2022). High-content CRISPR screening. Nat Rev Methods Primers, 2(1). https://doi.org/10.1038/s43586-022-00098-7

Bodor, C., Grossmann, V., Popov, N., Okosun, J., O'Riain, C., Tan, K., Marzec, J., Araf, S., Wang, J., Lee, A. M., Clear, A., Montoto, S., Matthews, J., Iqbal, S., Rajnai, H., Rosenwald, A., Ott, G., Campo, E., Rimsza, L. M., . . . Fitzgibbon, J. (2013). EZH2 mutations are frequent and represent an early event in follicular lymphoma. Blood, 122(18), 3165-3168. https://doi.org/10.1182/blood-2013-04-496893

Bodor, C., O'Riain, C., Wrench, D., Matthews, J., Iyengar, S., Tayyib, H., Calaminici, M., Clear, A., Iqbal, S., Quentmeier, H., Drexler, H. G., Montoto, S., Lister, A. T., Gribben, J. G., Matolcsy, A., & Fitzgibbon, J. (2011). EZH2 Y641 mutations in follicular lymphoma. Leukemia, 25(4), 726-729. https://doi.org/10.1038/leu.2010.311

Bonnet, J., Boichenko, I., Kalb, R., Le Jeune, M., Maltseva, S., Pieropan, M., Finkl, K., Fierz, B., & Muller, J. (2022). PR-DUB preserves Polycomb repression by preventing excessive accumulation of H2Aub1, an antagonist of chromatin compaction. Genes Dev, 36(19-20), 1046-1061. https://doi.org/10.1101/gad.350014.122

Borkin, D., He, S., Miao, H., Kempinska, K., Pollock, J., Chase, J., Purohit, T., Malik, B., Zhao, T., Wang, J., Wen, B., Zong, H., Jones, M., Danet-Desnoyers, G., Guzman, M. L., Talpaz, M., Bixby, D. L., Sun, D., Hess, J. L., . . . Grembecka, J. (2015). Pharmacologic inhibition of the Menin-MLL interaction blocks progression of MLL leukemia in vivo. Cancer Cell, 27(4), 589-602. https://doi.org/10.1016/j.ccell.2015.02.016

Bottcher, J., Dilworth, D., Reiser, U., Neumuller, R. A., Schleicher, M., Petronczki, M., Zeeb, M., Mischerikow, N., Allali-Hassani, A., Szewczyk, M. M., Li, F., Kennedy, S., Vedadi, M., Barsyte-Lovejoy, D., Brown, P. J., Huber, K. V. M., Rogers, C. M., Wells, C. I., Fedorov, O., . . . McConnell, D. B. (2019). Fragment-based discovery

of a chemical probe for the PWWP1 domain of NSD3. Nat Chem Biol, 15(8), 822-829. https://doi.org/10.1038/s41589-019-0310-x

Bracken, A. P., Brien, G. L., & Verrijzer, C. P. (2019). Dangerous liaisons: interplay between SWI/SNF, NuRD, and Polycomb in chromatin regulation and cancer. Genes Dev, 33(15-16), 936-959. https://doi.org/10.1101/gad.326066.119

Bracken, A. P., Dietrich, N., Pasini, D., Hansen, K. H., & Helin, K. (2006). Genome-wide mapping of Polycomb target genes unravels their roles in cell fate transitions. Genes Dev, 20(9), 1123-1136. https://doi.org/10.1101/gad.381706

Bracken, A. P., Pasini, D., Capra, M., Prosperini, E., Colli, E., & Helin, K. (2003). EZH2 is downstream of the pRB-E2F pathway, essential for proliferation and amplified in cancer. EMBO J, 22(20), 5323-5335. https://doi.org/10.1093/emboj/cdg542

Brien, G. L., Remillard, D., Shi, J., Hemming, M. L., Chabon, J., Wynne, K., Dillon, E. T., Cagney, G., Van Mierlo, G., Baltissen, M. P., Vermeulen, M., Qi, J., Frohling, S., Gray, N. S., Bradner, J. E., Vakoc, C. R., & Armstrong, S. A. (2018). Targeted degradation of BRD9 reverses oncogenic gene expression in synovial sarcoma. Elife, 7. https://doi.org/10.7554/eLife.41305

Bushnell, B. (2014). BBMap: A Fast, Accurate, Splice-Aware Aligner. https://escholarship.org/uc/item/1h3515gn

Caganova, M., Carrisi, C., Varano, G., Mainoldi, F., Zanardi, F., Germain, P. L., George, L., Alberghini, F., Ferrarini, L., Talukder, A. K., Ponzoni, M., Testa, G., Nojima, T., Doglioni, C., Kitamura, D., Toellner, K. M., Su, I. H., & Casola, S. (2013). Germinal center dysregulation by histone methyltransferase EZH2 promotes lymphomagenesis. J Clin Invest, 123(12), 5009-5022. https://doi.org/10.1172/JCI70626

Calado, D. P., Sasaki, Y., Godinho, S. A., Pellerin, A., Kochert, K., Sleckman, B. P., de Alboran, I. M., Janz, M., Rodig, S., & Rajewsky, K. (2012). The cell-cycle regulator c-Myc is essential for the formation and maintenance of germinal centers. Nat Immunol, 13(11), 1092-1100. https://doi.org/10.1038/ni.2418

Cancer Genome Atlas, N. (2015). Comprehensive genomic characterization of head and neck squamous cell carcinomas. Nature, 517(7536), 576-582. https://doi.org/10.1038/nature14129

Cao, R., Wang, L., Wang, H., Xia, L., Erdjument-Bromage, H., Tempst, P., Jones, R. S., & Zhang, Y. (2002). Role of histone H3 lysine 27 methylation in Polycomb-group silencing. Science, 298(5595), 1039-1043. https://doi.org/10.1126/science.1076997

Cao, R., & Zhang, Y. (2004). SUZ12 is required for both the histone methyltransferase activity and the silencing function of the EED-EZH2 complex. Mol Cell, 15(1), 57-67. https://doi.org/10.1016/j.molcel.2004.06.020

Cenik, B. K., & Shilatifard, A. (2021). COMPASS and SWI/SNF complexes in development and disease. Nat Rev Genet, 22(1), 38-58. https://doi.org/10.1038/s41576-020-0278-0

Cerami, E., Gao, J., Dogrusoz, U., Gross, B. E., Sumer, S. O., Aksoy, B. A., Jacobsen, A., Byrne, C. J., Heuer, M. L., Larsson, E., Antipin, Y., Reva, B., Goldberg, A. P., Sander, C., & Schultz, N. (2012). The cBio cancer genomics portal: an open platform for exploring multidimensional cancer genomics data. Cancer Discov, 2(5), 401-404. https://doi.org/10.1158/2159-8290.CD-12-0095

Chang, M. T., Asthana, S., Gao, S. P., Lee, B. H., Chapman, J. S., Kandoth, C., Gao, J., Socci, N. D., Solit, D. B., Olshen, A. B., Schultz, N., & Taylor, B. S. (2016). Identifying recurrent mutations in cancer reveals widespread lineage diversity and mutational specificity. Nat Biotechnol, 34(2), 155-163. https://doi.org/10.1038/nbt.3391

Chapuy, B., Stewart, C., Dunford, A. J., Kim, J., Kamburov, A., Redd, R. A., Lawrence, M. S., Roemer, M. G. M., Li, A. J., Ziepert, M., Staiger, A. M., Wala, J. A., Ducar, M. D., Leshchiner, I., Rheinbay, E., Taylor-Weiner, A., Coughlin, C. A., Hess, J. M., Pedamallu, C. S., . . . Shipp, M. A. (2018). Molecular subtypes of diffuse large B cell lymphoma are associated with distinct pathogenic mechanisms and outcomes. Nat Med, 24(5), 679-690. https://doi.org/10.1038/s41591-018-0016-8

Cheah, C. Y., & Fowler, N. H. (2016). Idelalisib in the management of lymphoma. Blood, 128(3), 331-336. https://doi.org/10.1182/blood-2016-02-702761

Chen, S., Jiao, L., Shubbar, M., Yang, X., & Liu, X. (2018). Unique Structural Platforms of Suz12 Dictate Distinct Classes of PRC2 for Chromatin Binding. Mol Cell, 69(5), 840-852 e845. https://doi.org/10.1016/j.molcel.2018.01.039

Chen, S., Zhou, Y., Chen, Y., & Gu, J. (2018). fastp: an ultra-fast all-in-one FASTQ preprocessor. Bioinformatics, 34(17), i884-i890. https://doi.org/10.1093/bioinformatics/bty560

Chen, X., Li, Y., Zhu, F., Xu, X., Estrella, B., Pazos, M. A., 2nd, McGuire, J. T., Karagiannis, D., Sahu, V., Mustafokulov, M., Scuoppo, C., Sanchez-Rivera, F. J., Soto-Feliciano, Y. M., Pasqualucci, L., Ciccia, A., Amengual, J. E., & Lu, C. (2023). Context-defined cancer co-dependency mapping identifies a functional interplay between PRC2 and MLL-MEN1 complex in lymphoma. Nat Commun, 14(1), 4259. https://doi.org/10.1038/s41467-023-39990-5

Chesi, M., Nardini, E., Lim, R. S., Smith, K. D., Kuehl, W. M., & Bergsagel, P. L. (1998). The t(4;14) translocation in myeloma dysregulates both FGFR3 and a novel gene, MMSET, resulting in IgH/MMSET hybrid transcripts. Blood, 92(9), 3025-3034. https://www.ncbi.nlm.nih.gov/pubmed/9787135

Ciapponi, M., Karlukova, E., Schkolziger, S., Benda, C., & Muller, J. (2024). Structural basis of the histone ubiquitination read-write mechanism of RYBP-PRC1. Nat Struct Mol Biol, 31(7), 1023-1027. https://doi.org/10.1038/s41594-024-01258-x

Ciferri, C., Lander, G. C., Maiolica, A., Herzog, F., Aebersold, R., & Nogales, E. (2012). Molecular architecture of human polycomb repressive complex 2. Elife, 1, e00005. https://doi.org/10.7554/eLife.00005

Clapier, C. R., Iwasa, J., Cairns, B. R., & Peterson, C. L. (2017). Mechanisms of action and regulation of ATP-dependent chromatin-remodelling complexes. Nat Rev Mol Cell Biol, 18(7), 407-422. https://doi.org/10.1038/nrm.2017.26

Clayton, E., Bardi, G., Bell, S. E., Chantry, D., Downes, C. P., Gray, A., Humphries, L. A., Rawlings, D., Reynolds, H., Vigorito, E., & Turner, M. (2002). A crucial role for the p110delta subunit of phosphatidylinositol 3-kinase in B cell development and activation. J Exp Med, 196(6), 753-763. https://doi.org/10.1084/jem.20020805

Comet, I., Riising, E. M., Leblanc, B., & Helin, K. (2016). Maintaining cell identity: PRC2-mediated regulation of transcription and cancer. Nat Rev Cancer, 16(12), 803-810. https://doi.org/10.1038/nrc.2016.83

Cong, L., Ran, F. A., Cox, D., Lin, S., Barretto, R., Habib, N., Hsu, P. D., Wu, X., Jiang, W., Marraffini, L. A., & Zhang, F. (2013). Multiplex genome engineering using CRISPR/Cas systems. Science, 339(6121), 819-823. https://doi.org/10.1126/science.1231143

Conway, E., Healy, E., & Bracken, A. P. (2015). PRC2 mediated H3K27 methylations in cellular identity and cancer. Curr Opin Cell Biol, 37, 42-48. https://doi.org/10.1016/j.ceb.2015.10.003

Conway, E., Jerman, E., Healy, E., Ito, S., Holoch, D., Oliviero, G., Deevy, O., Glancy, E., Fitzpatrick, D. J., Mucha, M., Watson, A., Rice, A. M., Chammas, P., Huang, C., Pratt-Kelly, I., Koseki, Y., Nakayama, M., Ishikura, T., Streubel, G., . . . Bracken, A. P. (2018). A Family of Vertebrate-Specific Polycombs Encoded by the LCOR/LCORL Genes Balance PRC2 Subtype Activities. Mol Cell, 70(3), 408-421 e408. https://doi.org/10.1016/j.molcel.2018.03.005

Conway, E., Rossi, F., Fernandez-Perez, D., Ponzo, E., Ferrari, K. J., Zanotti, M., Manganaro, D., Rodighiero, S., Tamburri, S., & Pasini, D. (2021). BAP1 enhances Polycomb repression by counteracting widespread H2AK119ub1 deposition and chromatin condensation. Mol Cell, 81(17), 3526-3541 e3528. https://doi.org/10.1016/j.molcel.2021.06.020

Cortes, J., Pavlovsky, C., & Saussele, S. (2021). Chronic myeloid leukaemia. Lancet, 398(10314), 1914-1926. https://doi.org/10.1016/S0140-6736(21)01204-6

Cosgrove, M. S., Boeke, J. D., & Wolberger, C. (2004). Regulated nucleosome mobility and the histone code. Nat Struct Mol Biol, 11(11), 1037-1043. https://doi.org/10.1038/nsmb851

Coussens, N. P., Kales, S. C., Henderson, M. J., Lee, O. W., Horiuchi, K. Y., Wang, Y., Chen, Q., Kuznetsova, E., Wu, J., Chakka, S., Cheff, D. M., Cheng, K. C., Shinn, P., Brimacombe, K. R., Shen, M., Simeonov, A., Lal-Nag, M., Ma, H., Jadhav, A., & Hall, M. D. (2018). High-throughput screening with nucleosome substrate identifies small-molecule inhibitors of the human histone lysine methyltransferase NSD2. J Biol Chem, 293(35), 13750-13765. https://doi.org/10.1074/jbc.RA118.004274

Curry, E., Green, I., Chapman-Rothe, N., Shamsaei, E., Kandil, S., Cherblanc, F. L., Payne, L., Bell, E., Ganesh, T., Srimongkolpithak, N., Caron, J., Li, F., Uren, A. G., Snyder, J. P., Vedadi, M., Fuchter, M. J., & Brown, R. (2015). Dual EZH2 and EHMT2 histone methyltransferase inhibition increases biological efficacy in breast cancer cells. Clin Epigenetics, 7(1), 84. https://doi.org/10.1186/s13148-015-0118-9

Czermin, B., Melfi, R., McCabe, D., Seitz, V., Imhof, A., & Pirrotta, V. (2002). Drosophila enhancer of Zeste/ESC complexes have a histone H3 methyltransferase activity that marks chromosomal Polycomb sites. Cell, 111(2), 185-196. https://doi.org/10.1016/s0092-8674(02)00975-3

Daigle, S. R., Olhava, E. J., Therkelsen, C. A., Basavapathruni, A., Jin, L., Boriack-Sjodin, P. A., Allain, C. J., Klaus, C. R., Raimondi, A., Scott, M. P., Waters, N. J., Chesworth, R., Moyer, M. P., Copeland, R. A., Richon, V. M., & Pollock, R. M. (2013). Potent inhibition of DOT1L as treatment of MLL-fusion leukemia. Blood, 122(6), 1017-1025. https://doi.org/10.1182/blood-2013-04-497644

Dawson, M. A., Prinjha, R. K., Dittmann, A., Giotopoulos, G., Bantscheff, M., Chan, W. I., Robson, S. C., Chung, C. W., Hopf, C., Savitski, M. M., Huthmacher, C., Gudgin, E., Lugo, D., Beinke, S., Chapman, T. D., Roberts, E. J., Soden, P. E., Auger, K. R., Mirguet, O., . . . Kouzarides, T. (2011). Inhibition of BET recruitment to chromatin as an effective treatment for MLL-fusion leukaemia. Nature, 478(7370), 529-533. https://doi.org/10.1038/nature10509

de Matos Simoes, R., Shirasaki, R., Downey-Kopyscinski, S. L., Matthews, G. M., Barwick, B. G., Gupta, V. A., Dupere-Richer, D., Yamano, S., Hu, Y., Sheffer, M., Dhimolea, E., Dashevsky, O., Gandolfi, S., Ishiguro, K., Meyers, R. M., Bryan, J. G., Dharia, N. V., Hengeveld, P. J., Bruggenthies, J. B., . . . Mitsiades, C. S. (2023). Genome-scale functional genomics identify genes preferentially essential for multiple myeloma cells compared to other neoplasias. Nat Cancer, 4(5), 754-773. https://doi.org/10.1038/s43018-023-00550-x

De Silva, N. S., & Klein, U. (2015). Dynamics of B cells in germinal centres. Nat Rev Immunol, 15(3), 137-148. https://doi.org/10.1038/nri3804

Deevy, O., & Bracken, A. P. (2019). PRC2 functions in development and congenital disorders. Development, 146(19). https://doi.org/10.1242/dev.181354

Deevy, O., Monger, C., Matrà, F., Tuck, E., Conway, E., Badonyi, M., Nimmo, D., Rodighiero, S., Zhang, Q., Davidovich, C., Marsh, J. A., Pasini, D., & Bracken, A. P. (2024). Dominant negative effects on H3K27 methylation by Weaver syndrome-associated EZH2 variants. bioRxiv, 2023.2006.2001.543208. https://doi.org/10.1101/2023.06.01.543208

Dempster, J. M., Rossen, J., Kazachkova, M., Pan, J., Kugener, G., Root, D.E., Tsherniak, A. (2019). Extracting Biological Insights from the Project Achilles Genome-Scale CRISPR Screens in Cancer Cell Lines. bioRxiv. https://doi.org/10.1101/720243

Deng, Q., Lakra, P., Gou, P., Yang, H., Meydan, C., Teater, M., Chin, C., Zhang, W., Dinh, T., Hussein, U., Li, X., Rojas, E., Liu, W., Reville, P. K., Kizhakeyil, A., Barisic, D., Parsons, S., Wilson, A., Henderson, J., . . . Green, M. R. (2024). SMARCA4 is a haploinsufficient B cell lymphoma tumor suppressor that fine-tunes centrocyte cell fate decisions. Cancer Cell, 42(4), 605-622 e611. https://doi.org/10.1016/j.ccell.2024.02.011

Dhayalan, A., Rajavelu, A., Rathert, P., Tamas, R., Jurkowska, R. Z., Ragozin, S., & Jeltsch, A. (2010). The Dnmt3a PWWP domain reads histone 3 lysine 36 trimethylation and guides DNA methylation. J Biol Chem, 285(34), 26114-26120. https://doi.org/10.1074/jbc.M109.089433

Dilworth, D., Hanley, R. P., Ferreira de Freitas, R., Allali-Hassani, A., Zhou, M., Mehta, N., Marunde, M. R., Ackloo, S., Carvalho Machado, R. A., Khalili Yazdi, A., Owens, D. D. G., Vu, V., Nie, D. Y., Alqazzaz, M., Marcon, E., Li, F., Chau, I., Bolotokova, A., Qin, S., . . . Schapira, M. (2022). A chemical probe targeting the PWWP domain alters NSD2 nucleolar localization. Nat Chem Biol, 18(1), 56-63. https://doi.org/10.1038/s41589-021-00898-0

Ding, L. W., Sun, Q. Y., Tan, K. T., Chien, W., Mayakonda, A., Yeoh, A. E. J., Kawamata, N., Nagata, Y., Xiao, J. F., Loh, X. Y., Lin, D. C., Garg, M., Jiang, Y. Y., Xu, L., Lim, S. L., Liu, L. Z., Madan, V., Sanada, M., Fernandez, L. T., . . . Koeffler, H. P. (2017). Mutational Landscape of Pediatric Acute Lymphoblastic Leukemia. Cancer Res, 77(2), 390-400. https://doi.org/10.1158/0008-5472.CAN-16-1303

Doench, J. G. (2018). Am I ready for CRISPR? A user's guide to genetic screens. Nat Rev Genet, 19(2), 67-80. https://doi.org/10.1038/nrg.2017.97

Doench, J. G., Fusi, N., Sullender, M., Hegde, M., Vaimberg, E. W., Donovan, K. F., Smith, I., Tothova, Z., Wilen, C., Orchard, R., Virgin, H. W., Listgarten, J., & Root, D. E. (2016). Optimized sgRNA design to maximize activity and minimize off-target effects of CRISPR-Cas9. Nat Biotechnol, 34(2), 184-191. https://doi.org/10.1038/nbt.3437

Doench, J. G., Hartenian, E., Graham, D. B., Tothova, Z., Hegde, M., Smith, I., Sullender, M., Ebert, B. L., Xavier, R. J., & Root, D. E. (2014). Rational design of highly active sgRNAs for CRISPR-Cas9-mediated gene inactivation. Nat Biotechnol, 32(12), 1262-1267. https://doi.org/10.1038/nbt.3026

Dominguez-Sola, D., Victora, G. D., Ying, C. Y., Phan, R. T., Saito, M., Nussenzweig, M. C., & Dalla-Favera, R. (2012). The proto-oncogene MYC is required for selection in the germinal center and cyclic reentry. Nat Immunol, 13(11), 1083-1091. https://doi.org/10.1038/ni.2428

Donaldson-Collier, M. C., Sungalee, S., Zufferey, M., Tavernari, D., Katanayeva, N., Battistello, E., Mina, M., Douglass, K. M., Rey, T., Raynaud, F., Manley, S., Ciriello, G., & Oricchio, E. (2019). EZH2 oncogenic mutations drive epigenetic, transcriptional, and structural changes within chromatin domains. Nat Genet, 51(3), 517-528. https://doi.org/10.1038/s41588-018-0338-y

Drake, K. M., Watson, V. G., Kisielewski, A., Glynn, R., & Napper, A. D. (2014). A sensitive luminescent assay for the histone methyltransferase NSD1 and other SAM-dependent enzymes. Assay Drug Dev Technol, 12(5), 258-271. https://doi.org/10.1089/adt.2014.583

Dreyling, M., Ghielmini, M., Rule, S., Salles, G., Ladetto, M., Tonino, S. H., Herfarth, K., Seymour, J. F., Jerkeman, M., & clinicalguidelines@esmo.org, E. G. C. E. a. (2021). Newly diagnosed and relapsed follicular lymphoma: ESMO Clinical Practice Guidelines for diagnosis, treatment and follow-up. Ann Oncol, 32(3), 298-308. https://doi.org/10.1016/j.annonc.2020.11.008

Drosos, Y., Myers, J. A., Xu, B., Mathias, K. M., Beane, E. C., Radko-Juettner, S., Mobley, R. J., Larsen, M. E., Piccioni, F., Ma, X., Low, J., Hansen, B. S., Peters, S. T., Bhanu, N. V., Dhanda, S. K., Chen, T., Upadhyaya, S. A., Pruett-Miller, S. M., Root, D. E., . . . Roberts, C. W. M. (2022). NSD1 mediates antagonism between SWI/SNF and polycomb complexes and is required for transcriptional activation upon EZH2 inhibition. Mol Cell, 82(13), 2472-2489 e2478. https://doi.org/10.1016/j.molcel.2022.04.015

Druker, B. J. (2009). Perspectives on the development of imatinib and the future of cancer research. Nat Med, 15(10), 1149-1152. https://doi.org/10.1038/nm1009-1149

Druker, B. J., O'Brien, S. G., Cortes, J., & Radich, J. (2002). Chronic myelogenous leukemia. Hematology Am Soc Hematol Educ Program, 111-135. https://doi.org/10.1182/asheducation-2002.1.111

Druker, B. J., Tamura, S., Buchdunger, E., Ohno, S., Segal, G. M., Fanning, S., Zimmermann, J., & Lydon, N. B. (1996). Effects of a selective inhibitor of the Abl tyrosine kinase on the growth of Bcr-Abl positive cells. Nat Med, 2(5), 561-566. https://doi.org/10.1038/nm0596-561

Eagen, K. P., Aiden, E. L., & Kornberg, R. D. (2017). Polycomb-mediated chromatin loops revealed by a subkilobase-resolution chromatin interaction map. Proc Natl Acad Sci U S A, 114(33), 8764-8769. https://doi.org/10.1073/pnas.1701291114

Eden, E., Navon, R., Steinfeld, I., Lipson, D., & Yakhini, Z. (2009). GOrilla: a tool for discovery and visualization of enriched GO terms in ranked gene lists. BMC Bioinformatics, 10, 48. https://doi.org/10.1186/1471-2105-10-48

Eisen, M. B., Spellman, P. T., Brown, P. O., & Botstein, D. (1998). Cluster analysis and display of genome-wide expression patterns. Proc Natl Acad Sci U S A, 95(25), 14863-14868. https://doi.org/10.1073/pnas.95.25.14863

El-Khoueiry, A. B., Clarke, J., Neff, T., Crossman, T., Ratia, N., Rathi, C., Noto, P., Tarkar, A., Garrido-Laguna, I., Calvo, E., Rodon, J., Tran, B., O'Dwyer, P. J., Cuker, A., & Abdul Razak, A. R. (2023). Phase 1 study of GSK3368715, a type I PRMT inhibitor, in patients with advanced solid tumors. Br J Cancer, 129(2), 309-317. https://doi.org/10.1038/s41416-023-02276-0

Eom, G. H., Kim, K. B., Kim, J. H., Kim, J. Y., Kim, J. R., Kee, H. J., Kim, D. W., Choe, N., Park, H. J., Son, H. J., Choi, S. Y., Kook, H., & Seo, S. B. (2011). Histone methyltransferase SETD3 regulates muscle differentiation. J Biol Chem, 286(40), 34733-34742. https://doi.org/10.1074/jbc.M110.203307

Ernst, T., Chase, A. J., Score, J., Hidalgo-Curtis, C. E., Bryant, C., Jones, A. V., Waghorn, K., Zoi, K., Ross, F. M., Reiter, A., Hochhaus, A., Drexler, H. G., Duncombe, A., Cervantes, F., Oscier, D., Boultwood, J., Grand, F. H., & Cross, N. C. (2010). Inactivating mutations of the histone methyltransferase gene EZH2 in myeloid disorders. Nat Genet, 42(8), 722-726. https://doi.org/10.1038/ng.621

Eskeland, R., Leeb, M., Grimes, G. R., Kress, C., Boyle, S., Sproul, D., Gilbert, N., Fan, Y., Skoultchi, A. I., Wutz, A., & Bickmore, W. A. (2010). Ring1B compacts chromatin structure and represses gene expression independent of histone ubiquitination. Mol Cell, 38(3), 452-464. https://doi.org/10.1016/j.molcel.2010.02.032

Fabbri, G., Rasi, S., Rossi, D., Trifonov, V., Khiabanian, H., Ma, J., Grunn, A., Fangazio, M., Capello, D., Monti, S., Cresta, S., Gargiulo, E., Forconi, F., Guarini, A., Arcaini, L., Paulli, M., Laurenti, L., Larocca, L. M., Marasca, R., . . . Gaidano, G. (2011). Analysis of the chronic lymphocytic leukemia coding genome: role of NOTCH1 mutational activation. J Exp Med, 208(7), 1389-1401. https://doi.org/10.1084/jem.20110921

Fang, D., Gan, H., Lee, J. H., Han, J., Wang, Z., Riester, S. M., Jin, L., Chen, J., Zhou, H., Wang, J., Zhang, H., Yang, N., Bradley, E. W., Ho, T. H., Rubin, B. P., Bridge, J. A., Thibodeau, S. N., Ordog, T., Chen, Y., . . . Zhang, Z. (2016). The histone

H3.3K36M mutation reprograms the epigenome of chondroblastomas. Science, 352(6291), 1344-1348. https://doi.org/10.1126/science.aae0065

Farhangdoost, N., Horth, C., Hu, B., Bareke, E., Chen, X., Li, Y., Coradin, M., Garcia, B. A., Lu, C., & Majewski, J. (2021). Chromatin dysregulation associated with NSD1 mutation in head and neck squamous cell carcinoma. Cell Rep, 34(8), 108769. https://doi.org/10.1016/j.celrep.2021.108769

Feinberg, A. P., & Tycko, B. (2004). The history of cancer epigenetics. Nat Rev Cancer, 4(2), 143-153. https://doi.org/10.1038/nrc1279

Feng, Q., Wang, H., Ng, H. H., Erdjument-Bromage, H., Tempst, P., Struhl, K., & Zhang, Y. (2002). Methylation of H3-lysine 79 is mediated by a new family of HMTases without a SET domain. Curr Biol, 12(12), 1052-1058. https://doi.org/10.1016/s0960-9822(02)00901-6

Feng, X., Tang, M., Dede, M., Su, D., Pei, G., Jiang, D., Wang, C., Chen, Z., Li, M., Nie, L., Xiong, Y., Li, S., Park, J. M., Zhang, H., Huang, M., Szymonowicz, K., Zhao, Z., Hart, T., & Chen, J. (2022). Genome-wide CRISPR screens using isogenic cells reveal vulnerabilities conferred by loss of tumor suppressors. Sci Adv, 8(19), eabm6638. https://doi.org/10.1126/sciadv.abm6638

Ferrari, K. J., Scelfo, A., Jammula, S., Cuomo, A., Barozzi, I., Stutzer, A., Fischle, W., Bonaldi, T., & Pasini, D. (2014). Polycomb-dependent H3K27me1 and H3K27me2 regulate active transcription and enhancer fidelity. Mol Cell, 53(1), 49-62. https://doi.org/10.1016/j.molcel.2013.10.030

Ferreira de Freitas, R., Liu, Y., Szewczyk, M. M., Mehta, N., Li, F., McLeod, D., Zepeda-Velazquez, C., Dilworth, D., Hanley, R. P., Gibson, E., Brown, P. J., Al-Awar, R., James, L. I., Arrowsmith, C. H., Barsyte-Lovejoy, D., Min, J., Vedadi, M., Schapira, M., & Allali-Hassani, A. (2021). Discovery of Small-Molecule Antagonists of the PWWP Domain of NSD2. J Med Chem, 64(3), 1584-1592. https://doi.org/10.1021/acs.jmedchem.0c01768

Finogenova, K., Bonnet, J., Poepsel, S., Schafer, I. B., Finkl, K., Schmid, K., Litz, C., Strauss, M., Benda, C., & Muller, J. (2020). Structural basis for PRC2 decoding of active histone methylation marks H3K36me2/3. Elife, 9. https://doi.org/10.7554/eLife.61964

Fischle, W., Wang, Y., Jacobs, S. A., Kim, Y., Allis, C. D., & Khorasanizadeh, S. (2003). Molecular basis for the discrimination of repressive methyl-lysine marks in histone H3 by Polycomb and HP1 chromodomains. Genes Dev, 17(15), 1870-1881. https://doi.org/10.1101/gad.1110503

Freeman, C. L., & Sehn, L. H. (2018). A tale of two antibodies: obinutuzumab versus rituximab. Br J Haematol, 182(1), 29-45. https://doi.org/10.1111/bjh.15232

French, C. A., Rahman, S., Walsh, E. M., Kuhnle, S., Grayson, A. R., Lemieux, M. E., Grunfeld, N., Rubin, B. P., Antonescu, C. R., Zhang, S., Venkatramani, R., Dal Cin, P., & Howley, P. M. (2014). NSD3-NUT fusion oncoprotein in NUT midline carcinoma: implications for a novel oncogenic mechanism. Cancer Discov, 4(8), 928-941. https://doi.org/10.1158/2159-8290.CD-14-0014

Frey, F., Sheahan, T., Finkl, K., Stoehr, G., Mann, M., Benda, C., & Muller, J. (2016). Molecular basis of PRC1 targeting to Polycomb response elements by PhoRC. Genes Dev, 30(9), 1116-1127. https://doi.org/10.1101/gad.279141.116

Fu, Y., Foden, J. A., Khayter, C., Maeder, M. L., Reyon, D., Joung, J. K., & Sander, J. D. (2013). High-frequency off-target mutagenesis induced by CRISPR-Cas nucleases in human cells. Nat Biotechnol, 31(9), 822-826. https://doi.org/10.1038/nbt.2623

Fujisawa, T., & Filippakopoulos, P. (2017). Functions of bromodomain-containing proteins and their roles in homeostasis and cancer. Nat Rev Mol Cell Biol, 18(4), 246-262. https://doi.org/10.1038/nrm.2016.143

Fursova, N. A., Blackledge, N. P., Nakayama, M., Ito, S., Koseki, Y., Farcas, A. M., King, H. W., Koseki, H., & Klose, R. J. (2019a). Synergy between Variant PRC1 Complexes Defines Polycomb-Mediated Gene Repression. Mol Cell, 74(5), 1020-1036.e1028. https://doi.org/10.1016/j.molcel.2019.03.024

Fursova, N. A., Blackledge, N. P., Nakayama, M., Ito, S., Koseki, Y., Farcas, A. M., King, H. W., Koseki, H., & Klose, R. J. (2019b). Synergy between Variant PRC1 Complexes Defines Polycomb-Mediated Gene Repression. Mol Cell, 74(5), 1020-1036 e1028. https://doi.org/10.1016/j.molcel.2019.03.024

Gao, J., Aksoy, B. A., Dogrusoz, U., Dresdner, G., Gross, B., Sumer, S. O., Sun, Y., Jacobsen, A., Sinha, R., Larsson, E., Cerami, E., Sander, C., & Schultz, N. (2013). Integrative analysis of complex cancer genomics and clinical profiles using the cBioPortal. Sci Signal, 6(269), pl1. https://doi.org/10.1126/scisignal.2004088

Gao, Z., Zhang, J., Bonasio, R., Strino, F., Sawai, A., Parisi, F., Kluger, Y., & Reinberg, D. (2012). PCGF homologs, CBX proteins, and RYBP define functionally distinct PRC1 family complexes. Mol Cell, 45(3), 344-356. https://doi.org/10.1016/j.molcel.2012.01.002

Garnett, M. J., Edelman, E. J., Heidorn, S. J., Greenman, C. D., Dastur, A., Lau, K. W., Greninger, P., Thompson, I. R., Luo, X., Soares, J., Liu, Q., Iorio, F., Surdez, D., Chen, L., Milano, R. J., Bignell, G. R., Tam, A. T., Davies, H., Stevenson, J. A., . . . Benes, C. H. (2012). Systematic identification of genomic markers of drug sensitivity in cancer cells. Nature, 483(7391), 570-575. https://doi.org/10.1038/nature11005

Gibaja, V., Shen, F., Harari, J., Korn, J., Ruddy, D., Saenz-Vash, V., Zhai, H., Rejtar, T., Paris, C. G., Yu, Z., Lira, M., King, D., Qi, W., Keen, N., Hassan, A. Q., & Chan, H.

M. (2016). Development of secondary mutations in wild-type and mutant EZH2 alleles cooperates to confer resistance to EZH2 inhibitors. Oncogene, 35(5), 558-566. https://doi.org/10.1038/onc.2015.114

Glancy, E., Ciferri, C., & Bracken, A. P. (2021). Structural basis for PRC2 engagement with chromatin. Curr Opin Struct Biol, 67, 135-144. https://doi.org/10.1016/j.sbi.2020.10.017

Glancy, E., Wang, C., Tuck, E., Healy, E., Amato, S., Neikes, H. K., Mariani, A., Mucha, M., Vermeulen, M., Pasini, D., & Bracken, A. P. (2023). PRC2.1- and PRC2.2-specific accessory proteins drive recruitment of different forms of canonical PRC1. Mol Cell, 83(9), 1393-1411 e1397. https://doi.org/10.1016/j.molcel.2023.03.018

Göbel, C., Niccolai, R., de Groot, M. H. P., Jayachandran, J., Traets, J., Kloosterman, D. J., Gregoricchio, S., Morris, B., Kreft, M., Song, J. Y., Azarang, L., Kasa, E., Oskam, N., de Groot, D., Hoekman, L., Bleijerveld, O. B., Kersten, M. J., Aslam, M. A., van Leeuwen, F., & Jacobs, H. (2025). Targeting DOT1L and EZH2 synergizes in breaking the germinal center identity of diffuse large B-cell lymphoma. Blood, 145(16), 1802-1813. https://doi.org/10.1182/blood.2024025500

Gopal, A. K., Kahl, B. S., de Vos, S., Wagner-Johnston, N. D., Schuster, S. J., Jurczak, W. J., Flinn, I. W., Flowers, C. R., Martin, P., Viardot, A., Blum, K. A., Goy, A. H., Davies, A. J., Zinzani, P. L., Dreyling, M., Johnson, D., Miller, L. L., Holes, L., Li, D., . . . Salles, G. A. (2014). PI3Kdelta inhibition by idelalisib in patients with relapsed indolent lymphoma. N Engl J Med, 370(11), 1008-1018. https://doi.org/10.1056/NEJMoa1314583

Gopal, A. K., Kahl, B. S., Flowers, C. R., Martin, P., Ansell, S. M., Abella-Dominicis, E., Koh, B., Ye, W., Barr, P. M., Salles, G. A., & Friedberg, J. W. (2017). Idelalisib is effective in patients with high-risk follicular lymphoma and early relapse after initial chemoimmunotherapy. Blood, 129(22), 3037-3039. https://doi.org/10.1182/blood-2016-12-757740

Grau, D. J., Chapman, B. A., Garlick, J. D., Borowsky, M., Francis, N. J., & Kingston, R. E. (2011). Compaction of chromatin by diverse Polycomb group proteins requires localized regions of high charge. Genes Dev, 25(20), 2210-2221. https://doi.org/10.1101/gad.17288211

Green, M. R., Gentles, A. J., Nair, R. V., Irish, J. M., Kihira, S., Liu, C. L., Kela, I., Hopmans, E. S., Myklebust, J. H., Ji, H., Plevritis, S. K., Levy, R., & Alizadeh, A. A. (2013). Hierarchy in somatic mutations arising during genomic evolution and progression of follicular lymphoma. Blood, 121(9), 1604-1611. https://doi.org/10.1182/blood-2012-09-457283

Green, M. R., Kihira, S., Liu, C. L., Nair, R. V., Salari, R., Gentles, A. J., Irish, J., Stehr, H., Vicente-Duenas, C., Romero-Camarero, I., Sanchez-Garcia, I., Plevritis, S. K.,

Arber, D. A., Batzoglou, S., Levy, R., & Alizadeh, A. A. (2015). Mutations in early follicular lymphoma progenitors are associated with suppressed antigen presentation. Proc Natl Acad Sci U S A, 112(10), E1116-1125. https://doi.org/10.1073/pnas.1501199112

Griess, O., Furth, N., Harpaz, N., Di Bernardo, N., Salame, T. M., Dassa, B., Karagiannidis, I., Isshiki, Y., Gross, M., Melnick, A. M., Beguelin, W., Ron, G., & Shema, E. (2025). Mutant EZH2 alters the epigenetic network and increases epigenetic heterogeneity in B cell lymphoma. PLoS Biol, 23(6), e3003191. https://doi.org/10.1371/journal.pbio.3003191

Grijzenhout, A., Godwin, J., Koseki, H., Gdula, M. R., Szumska, D., McGouran, J. F., Bhattacharya, S., Kessler, B. M., Brockdorff, N., & Cooper, S. (2016). Functional analysis of AEBP2, a PRC2 Polycomb protein, reveals a Trithorax phenotype in embryonic development and in ESCs. Development, 143(15), 2716-2723. https://doi.org/10.1242/dev.123935

Guo, Q., Liao, S., Kwiatkowski, S., Tomaka, W., Yu, H., Wu, G., Tu, X., Min, J., Drozak, J., & Xu, C. (2019). Structural insights into SETD3-mediated histidine methylation on beta-actin. Elife, 8. https://doi.org/10.7554/eLife.43676

Hanley, R. P., Nie, D. Y., Tabor, J. R., Li, F., Sobh, A., Xu, C., Barker, N. K., Dilworth, D., Hajian, T., Gibson, E., Szewczyk, M. M., Brown, P. J., Barsyte-Lovejoy, D., Herring, L. E., Wang, G. G., Licht, J. D., Vedadi, M., Arrowsmith, C. H., & James, L. I. (2023). Discovery of a Potent and Selective Targeted NSD2 Degrader for the Reduction of H3K36me2. J Am Chem Soc, 145(14), 8176-8188. https://doi.org/10.1021/jacs.3c01421

Harb, W., Abramson, J., Lunning, M., Goy, A., Maddocks, K., Lebedinsky, C., Senderowicz, A., Trojer, P., Bradley, W.D., Flinn, I. (2018). A phase 1 study of CPI-1205, a small molecule inhibitor of EZH2, preliminary safety in patients with B-cell lymphomas. Annals of Oncology, 29(III7). https://doi.org/10.1093/annonc/mdy048.001

Hartenian, E., & Doench, J. G. (2015). Genetic screens and functional genomics using CRISPR/Cas9 technology. FEBS J, 282(8), 1383-1393. https://doi.org/10.1111/febs.13248

Hatzi, K., Jiang, Y., Huang, C., Garrett-Bakelman, F., Gearhart, M. D., Giannopoulou, E. G., Zumbo, P., Kirouac, K., Bhaskara, S., Polo, J. M., Kormaksson, M., MacKerell, A. D., Jr., Xue, F., Mason, C. E., Hiebert, S. W., Prive, G. G., Cerchietti, L., Bardwell, V. J., Elemento, O., & Melnick, A. (2013). A hybrid mechanism of action for BCL6 in B cells defined by formation of functionally distinct complexes at enhancers and promoters. Cell Rep, 4(3), 578-588. https://doi.org/10.1016/j.celrep.2013.06.016

Hauri, S., Comoglio, F., Seimiya, M., Gerstung, M., Glatter, T., Hansen, K., Aebersold, R., Paro, R., Gstaiger, M., & Beisel, C. (2016). A High-Density Map for Navigating the Human Polycomb Complexome. Cell Rep, 17(2), 583-595. https://doi.org/10.1016/j.celrep.2016.08.096

He, C., Liu, C., Wang, L., Sun, Y., Jiang, Y., & Hao, Y. (2019). Histone methyltransferase NSD2 regulates apoptosis and chemosensitivity in osteosarcoma. Cell Death Dis, 10(2), 65. https://doi.org/10.1038/s41419-019-1347-1

He, G.P., Kim, S., Ro, H.S. (1999). Cloning and characterization of a novel zinc finger transcriptional repressor. A direct role of the zinc finger motif in repression. J Biol Chem, 274(21), 14678-84. https://doi.org/10.1074/jbc.274.21.14678

He, W., Zhang, L., Villarreal, O. D., Fu, R., Bedford, E., Dou, J., Patel, A. Y., Bedford, M. T., Shi, X., Chen, T., Bartholomew, B., & Xu, H. (2019). De novo identification of essential protein domains from CRISPR-Cas9 tiling-sgRNA knockout screens. Nat Commun, 10(1), 4541. https://doi.org/10.1038/s41467-019-12489-8

He, Y., Selvaraju, S., Curtin, M. L., Jakob, C. G., Zhu, H., Comess, K. M., Shaw, B., The, J., Lima-Fernandes, E., Szewczyk, M. M., Cheng, D., Klinge, K. L., Li, H. Q., Pliushchev, M., Algire, M. A., Maag, D., Guo, J., Dietrich, J., Panchal, S. C., . . . Pappano, W. N. (2017). The EED protein-protein interaction inhibitor A-395 inactivates the PRC2 complex. Nat Chem Biol, 13(4), 389-395. https://doi.org/10.1038/nchembio.2306

Healy, E., Mucha, M., Glancy, E., Fitzpatrick, D. J., Conway, E., Neikes, H. K., Monger, C., Van Mierlo, G., Baltissen, M. P., Koseki, Y., Vermeulen, M., Koseki, H., & Bracken, A. P. (2019). PRC2.1 and PRC2.2 Synergize to Coordinate H3K27 Trimethylation. Mol Cell, 76(3), 437-452 e436. https://doi.org/10.1016/j.molcel.2019.08.012

Hedehus, L., Mas, A. M., Alpsoy, A., Armstrong, R. L., Koche, R., Tatar, T., Wang, H., & Helin, K. (2025). Addressing the specific roles of histone modifications in transcriptional repression. Nat Commun, 16(1), 11326. https://doi.org/10.1038/s41467-025-66426-z

Heikamp, E. B., Henrich, J. A., Perner, F., Wong, E. M., Hatton, C., Wen, Y., Barwe, S. P., Gopalakrishnapillai, A., Xu, H., Uckelmann, H. J., Takao, S., Kazansky, Y., Pikman, Y., McGeehan, G. M., Kolb, E. A., Kentsis, A., & Armstrong, S. A. (2022). The menin-MLL1 interaction is a molecular dependency in NUP98-rearranged AML. Blood, 139(6), 894-906. https://doi.org/10.1182/blood.2021012806

Heinz, S., Benner, C., Spann, N., Bertolino, E., Lin, Y. C., Laslo, P., Cheng, J. X., Murre, C., Singh, H., & Glass, C. K. (2010). Simple combinations of lineage-determining transcription factors prime cis-regulatory elements required for macrophage and B cell identities. Mol Cell, 38(4), 576-589. https://doi.org/10.1016/j.molcel.2010.05.004

Helin, K., & Dhanak, D. (2013). Chromatin proteins and modifications as drug targets. Nature, 502(7472), 480-488. https://doi.org/10.1038/nature12751

Helming, K. C., Wang, X., Wilson, B. G., Vazquez, F., Haswell, J. R., Manchester, H. E., Kim, Y., Kryukov, G. V., Ghandi, M., Aguirre, A. J., Jagani, Z., Wang, Z., Garraway, L. A., Hahn, W. C., & Roberts, C. W. (2014). ARID1B is a specific vulnerability in ARID1A-mutant cancers. Nat Med, 20(3), 251-254. https://doi.org/10.1038/nm.3480

Heward, J., Konali, L., D'Avola, A., Close, K., Yeomans, A., Philpott, M., Dunford, J., Rahim, T., Al Seraihi, A. F., Wang, J., Korfi, K., Araf, S., Iqbal, S., Bewicke-Copley, F., Kumar, E., Barisic, D., Calaminici, M., Clear, A., Gribben, J., . . . Fitzgibbon, J. (2021). KDM5 inhibition offers a novel therapeutic strategy for the treatment of KMT2D mutant lymphomas. Blood, 138(5), 370-381. https://doi.org/10.1182/blood.2020008743

Højfeldt, J. W., Hedehus, L., Laugesen, A., Tatar, T., Wiehle, L., & Helin, K. (2019). Non-core Subunits of the PRC2 Complex Are Collectively Required for Its Target-Site Specificity. Mol Cell, 76(3), 423-436.e423. https://doi.org/10.1016/j.molcel.2019.07.031

Holoch, D., & Margueron, R. (2017). Mechanisms Regulating PRC2 Recruitment and Enzymatic Activity. Trends Biochem Sci, 42(7), 531-542. https://doi.org/10.1016/j.tibs.2017.04.003

Holohan, C., Van Schaeybroeck, S., Longley, D. B., & Johnston, P. G. (2013). Cancer drug resistance: an evolving paradigm. Nat Rev Cancer, 13(10), 714-726. https://doi.org/10.1038/nrc3599

Horsman, D. E., Gascoyne, R. D., Coupland, R. W., Coldman, A. J., & Adomat, S. A. (1995). Comparison of cytogenetic analysis, southern analysis, and polymerase chain reaction for the detection of t(14; 18) in follicular lymphoma. Am J Clin Pathol, 103(4), 472-478. https://doi.org/10.1093/ajcp/103.4.472

Horvath, P., & Barrangou, R. (2010). CRISPR/Cas, the immune system of bacteria and archaea. Science, 327(5962), 167-170. https://doi.org/10.1126/science.1179555

Hou, X., Xu, M., Zhu, C., Gao, J., Li, M., Chen, X., Sun, C., Nashan, B., Zang, J., Zhou, Y., Guang, S., & Feng, X. (2023). Systematic characterization of chromodomain proteins reveals an H3K9me1/2 reader regulating aging in C. elegans. Nat Commun, 14(1), 1254. https://doi.org/10.1038/s41467-023-36898-y

Hou, Y., Liu, W., Yi, X., Yang, Y., Su, D., Huang, W., Yu, H., Teng, X., Yang, Y., Feng, W., Zhang, T., Gao, J., Zhang, K., Qiu, R., & Wang, Y. (2020). PHF20L1 as a H3K27me2 reader coordinates with transcriptional repressors to promote breast tumorigenesis. Sci Adv, 6(16), eaaz0356. https://doi.org/10.1126/sciadv.aaz0356

Hsu, C., Konner, J. A., & Gounder, M. M. (2024). Epigenetic Therapy in a Rare Ovarian Cancer - A Double-Edged Sword. N Engl J Med, 391(8), 770-772. https://doi.org/10.1056/NEJMc2407971

Hsu, J. H., Rasmusson, T., Robinson, J., Pachl, F., Read, J., Kawatkar, S., DH, O. D., Bagal, S., Code, E., Rawlins, P., Argyrou, A., Tomlinson, R., Gao, N., Zhu, X., Chiarparin, E., Jacques, K., Shen, M., Woods, H., Bednarski, E., . . . Bloecher, A. (2020). EED-Targeted PROTACs Degrade EED, EZH2, and SUZ12 in the PRC2 Complex. Cell Chem Biol, 27(1), 41-46 e17. https://doi.org/10.1016/j.chembiol.2019.11.004

Hsu, P. D., Scott, D. A., Weinstein, J. A., Ran, F. A., Konermann, S., Agarwala, V., Li, Y., Fine, E. J., Wu, X., Shalem, O., Cradick, T. J., Marraffini, L. A., Bao, G., & Zhang, F. (2013). DNA targeting specificity of RNA-guided Cas9 nucleases. Nat Biotechnol, 31(9), 827-832. https://doi.org/10.1038/nbt.2647

Huang, N., vom Baur, E., Garnier, J. M., Lerouge, T., Vonesch, J. L., Lutz, Y., Chambon, P., & Losson, R. (1998). Two distinct nuclear receptor interaction domains in NSD1, a novel SET protein that exhibits characteristics of both corepressors and coactivators. EMBO J, 17(12), 3398-3412. https://doi.org/10.1093/emboj/17.12.3398

Huang, X., LeDuc, R. D., Fornelli, L., Schunter, A. J., Bennett, R. L., Kelleher, N. L., & Licht, J. D. (2019). Defining the NSD2 interactome: PARP1 PARylation reduces NSD2 histone methyltransferase activity and impedes chromatin binding. J Biol Chem, 294(33), 12459-12471. https://doi.org/10.1074/jbc.RA118.006159

Hubner, J. M., Muller, T., Papageorgiou, D. N., Mauermann, M., Krijgsveld, J., Russell, R. B., Ellison, D. W., Pfister, S. M., Pajtler, K. W., & Kool, M. (2019). EZHIP/CXorf67 mimics K27M mutated oncohistones and functions as an intrinsic inhibitor of PRC2 function in aggressive posterior fossa ependymoma. Neuro Oncol, 21(7), 878-889. https://doi.org/10.1093/neuonc/noz058

Hudlebusch, H. R., Santoni-Rugiu, E., Simon, R., Ralfkiaer, E., Rossing, H. H., Johansen, J. V., Jorgensen, M., Sauter, G., & Helin, K. (2011). The histone methyltransferase and putative oncoprotein MMSET is overexpressed in a large variety of human tumors. Clin Cancer Res, 17(9), 2919-2933. https://doi.org/10.1158/1078-0432.CCR-10-1302

Huether, R., Dong, L., Chen, X., Wu, G., Parker, M., Wei, L., Ma, J., Edmonson, M. N., Hedlund, E. K., Rusch, M. C., Shurtleff, S. A., Mulder, H. L., Boggs, K., Vadordaria, B., Cheng, J., Yergeau, D., Song, G., Becksfort, J., Lemmon, G., . . . Downing, J. R. (2014). The landscape of somatic mutations in epigenetic regulators across 1,000 paediatric cancer genomes. Nat Commun, 5, 3630. https://doi.org/10.1038/ncomms4630

Husmann, D., & Gozani, O. (2019). Histone lysine methyltransferases in biology and disease. Nat Struct Mol Biol, 26(10), 880-889. https://doi.org/10.1038/s41594-019-0298-7

Iorio, F., Knijnenburg, T. A., Vis, D. J., Bignell, G. R., Menden, M. P., Schubert, M., Aben, N., Goncalves, E., Barthorpe, S., Lightfoot, H., Cokelaer, T., Greninger, P., van Dyk, E., Chang, H., de Silva, H., Heyn, H., Deng, X., Egan, R. K., Liu, Q., . . . Garnett, M. J. (2016). A Landscape of Pharmacogenomic Interactions in Cancer. Cell, 166(3), 740-754. https://doi.org/10.1016/j.cell.2016.06.017

Iqbal, J., Greiner, T. C., Patel, K., Dave, B. J., Smith, L., Ji, J., Wright, G., Sanger, W. G., Pickering, D. L., Jain, S., Horsman, D. E., Shen, Y., Fu, K., Weisenburger, D. D., Hans, C. P., Campo, E., Gascoyne, R. D., Rosenwald, A., Jaffe, E. S., . . . Leukemia/Lymphoma Molecular Profiling, P. (2007). Distinctive patterns of BCL6 molecular alterations and their functional consequences in different subgroups of diffuse large B-cell lymphoma. Leukemia, 21(11), 2332-2343. https://doi.org/10.1038/sj.leu.2404856

Isono, K., Endo, T. A., Ku, M., Yamada, D., Suzuki, R., Sharif, J., Ishikura, T., Toyoda, T., Bernstein, B. E., & Koseki, H. (2013). SAM domain polymerization links subnuclear clustering of PRC1 to gene silencing. Dev Cell, 26(6), 565-577. https://doi.org/10.1016/j.devcel.2013.08.016

Issa, G. C., Aldoss, I., DiPersio, J., Cuglievan, B., Stone, R., Arellano, M., Thirman, M. J., Patel, M. R., Dickens, D. S., Shenoy, S., Shukla, N., Kantarjian, H., Armstrong, S. A., Perner, F., Perry, J. A., Rosen, G., Bagley, R. G., Meyers, M. L., Ordentlich, P., . . . Stein, E. M. (2023). The menin inhibitor revumenib in KMT2A-rearranged or NPM1-mutant leukaemia. Nature, 615(7954), 920-924. https://doi.org/10.1038/s41586-023-05812-3

Issa, G. C., Aldoss, I., Thirman, M. J., DiPersio, J., Arellano, M., Blachly, J. S., Mannis, G. N., Perl, A., Dickens, D. S., McMahon, C. M., Traer, E., Zwaan, C. M., Grove, C. S., Stone, R., Shami, P. J., Mantzaris, I., Greenwood, M., Shukla, N., Cuglievan, B., . . . Stein, E. M. (2025). Menin Inhibition With Revumenib for KMT2A-Rearranged Relapsed or Refractory Acute Leukemia (AUGMENT-101). J Clin Oncol, 43(1), 75-84. https://doi.org/10.1200/JCO.24.00826

Isshiki, Y., Chen, X., Teater, M., Karagiannidis, I., Nam, H., Cai, W., Meydan, C., Xia, M., Shen, H., Gutierrez, J., Easwar Kumar, V., Carrasco, S. E., Ouseph, M. M., Yamshon, S., Martin, P., Griess, O., Shema, E., Porazzi, P., Ruella, M., . . . Beguelin, W. (2025). EZH2 inhibition enhances T cell immunotherapies by inducing lymphoma immunogenicity and improving T cell function. Cancer Cell, 43(1), 49-68 e49. https://doi.org/10.1016/j.ccell.2024.11.006

Italiano, A., Soria, J. C., Toulmonde, M., Michot, J. M., Lucchesi, C., Varga, A., Coindre, J. M., Blakemore, S. J., Clawson, A., Suttle, B., McDonald, A. A., Woodruff, M., Ribich, S., Hedrick, E., Keilhack, H., Thomson, B., Owa, T., Copeland, R. A., Ho, P. T. C., & Ribrag, V. (2018). Tazemetostat, an EZH2 inhibitor, in relapsed or refractory B-cell non-Hodgkin lymphoma and advanced solid tumours: a first-in-human, open-label, phase 1 study. Lancet Oncol, 19(5), 649-659. https://doi.org/10.1016/S1470-2045(18)30145-1

Jaffe, J. D., Wang, Y., Chan, H. M., Zhang, J., Huether, R., Kryukov, G. V., Bhang, H. E., Taylor, J. E., Hu, M., Englund, N. P., Yan, F., Wang, Z., Robert McDonald, E., 3rd, Wei, L., Ma, J., Easton, J., Yu, Z., deBeaumount, R., Gibaja, V., . . . Stegmeier, F. (2013). Global chromatin profiling reveals NSD2 mutations in pediatric acute lymphoblastic leukemia. Nat Genet, 45(11), 1386-1391. https://doi.org/10.1038/ng.2777

Jain, S. U., Rashoff, A. Q., Krabbenhoft, S. D., Hoelper, D., Do, T. J., Gibson, T. J., Lundgren, S. M., Bondra, E. R., Deshmukh, S., Harutyunyan, A. S., Juretic, N., Jabado, N., Harrison, M. M., & Lewis, P. W. (2020). H3 K27M and EZHIP Impede H3K27-Methylation Spreading by Inhibiting Allosterically Stimulated PRC2. Mol Cell, 80(4), 726-735 e727. https://doi.org/10.1016/j.molcel.2020.09.028

Jaju, R. J., Fidler, C., Haas, O. A., Strickson, A. J., Watkins, F., Clark, K., Cross, N. C., Cheng, J. F., Aplan, P. D., Kearney, L., Boultwood, J., & Wainscoat, J. S. (2001). A novel gene, NSD1, is fused to NUP98 in the t(5;11)(q35;p15.5) in de novo childhood acute myeloid leukemia. Blood, 98(4), 1264-1267. https://doi.org/10.1182/blood.v98.4.1264

Jeong, J., Hausmann, S., Dong, H., Szczepski, K., Flores, N. M., Garcia Gonzalez, A., Shi, L., Lu, X., Lempiainen, J., Jakab, M., Zeng, L., Chasan, T., Bareke, E., Dong, R., Carlson, E., Padilla, R., Husmann, D., Thompson, J., Shipman, G. A., . . . Gozani, O. (2026). NSD2 inhibitors rewire chromatin to treat lung and pancreatic cancers. Nature, 649(8095), 205-215. https://doi.org/10.1038/s41586-025-09299-y

Jiang, Y., Ortega-Molina, A., Geng, H., Ying, H. Y., Hatzi, K., Parsa, S., McNally, D., Wang, L., Doane, A. S., Agirre, X., Teater, M., Meydan, C., Li, Z., Poloway, D., Wang, S., Ennishi, D., Scott, D. W., Stengel, K. R., Kranz, J. E., . . . Melnick, A. M. (2017). CREBBP Inactivation Promotes the Development of HDAC3-Dependent Lymphomas. Cancer Discov, 7(1), 38-53. https://doi.org/10.1158/2159-8290.CD-16-0975

Jiao, L., & Liu, X. (2015). Structural basis of histone H3K27 trimethylation by an active polycomb repressive complex 2. Science, 350(6258), aac4383. https://doi.org/10.1126/science.aac4383

Jin, H., Zhang, C., Zwahlen, M., von Feilitzen, K., Karlsson, M., Shi, M., Yuan, M., Song, X., Li, X., Yang, H., Turkez, H., Fagerberg, L., Uhlen, M., & Mardinoglu, A. (2023). Systematic transcriptional analysis of human cell lines for gene expression landscape and tumor representation. Nat Commun, 14(1), 5417. https://doi.org/10.1038/s41467-023-41132-w

Jinek, M., Chylinski, K., Fonfara, I., Hauer, M., Doudna, J. A., & Charpentier, E. (2012). A programmable dual-RNA-guided DNA endonuclease in adaptive bacterial immunity. Science, 337(6096), 816-821. https://doi.org/10.1126/science.1225829

Kadoch, C., & Crabtree, G. R. (2015). Mammalian SWI/SNF chromatin remodeling complexes and cancer: Mechanistic insights gained from human genomics. Sci Adv, 1(5), e1500447. https://doi.org/10.1126/sciadv.1500447

Kalb, R., Latwiel, S., Baymaz, H. I., Jansen, P. W., Muller, C. W., Vermeulen, M., & Muller, J. (2014). Histone H2A monoubiquitination promotes histone H3 methylation in Polycomb repression. Nat Struct Mol Biol, 21(6), 569-571. https://doi.org/10.1038/nsmb.2833

Kaminskas, E., Farrell, A., Abraham, S., Baird, A., Hsieh, L. S., Lee, S. L., Leighton, J. K., Patel, H., Rahman, A., Sridhara, R., Wang, Y. C., Pazdur, R., & Fda. (2005). Approval summary: azacitidine for treatment of myelodysplastic syndrome subtypes. Clin Cancer Res, 11(10), 3604-3608. https://doi.org/10.1158/1078-0432.CCR-04-2135

Kanno, T., Kanno, Y., Siegel, R. M., Jang, M. K., Lenardo, M. J., & Ozato, K. (2004). Selective recognition of acetylated histones by bromodomain proteins visualized in living cells. Mol Cell, 13(1), 33-43. https://doi.org/10.1016/s1097-2765(03)00482-9

Kasinath, V., Beck, C., Sauer, P., Poepsel, S., Kosmatka, J., Faini, M., Toso, D., Aebersold, R., & Nogales, E. (2021). JARID2 and AEBP2 regulate PRC2 in the presence of H2AK119ub1 and other histone modifications. Science, 371(6527). https://doi.org/10.1126/science.abc3393

Kazansky, Y., Cameron, D., Demarest, P., Zaffaroni, N., Arrighetti, N., Zuco, V., Kuwahara, Y., Qu, R., De Stanchina, E., Cruz, F. D., Kung, A., Gounder, M., & Kentsis, A. (2023). Overcoming clinical resistance to EZH2 inhibition using rational epigenetic combination therapy. bioRxiv. https://doi.org/10.1101/2023.02.06.527192

Kazansky, Y., Cameron, D., Mueller, H. S., Demarest, P., Zaffaroni, N., Arrighetti, N., Zuco, V., Kuwahara, Y., Somwar, R., Ladanyi, M., Qu, R., de Stanchina, E., Dela Cruz, F. S., Kung, A. L., Gounder, M. M., & Kentsis, A. (2024). Overcoming Clinical Resistance to EZH2 Inhibition Using Rational Epigenetic Combination Therapy. Cancer Discov, 14(6), 965-981. https://doi.org/10.1158/2159-8290.CD-23-0110

Keats, J. J., Maxwell, C. A., Taylor, B. J., Hendzel, M. J., Chesi, M., Bergsagel, P. L., Larratt, L. M., Mant, M. J., Reiman, T., Belch, A. R., & Pilarski, L. M. (2005).

Overexpression of transcripts originating from the MMSET locus characterizes all t(4;14)(p16;q32)-positive multiple myeloma patients. Blood, 105(10), 4060-4069. https://doi.org/10.1182/blood-2004-09-3704

Keats, J. J., Reiman, T., Belch, A. R., & Pilarski, L. M. (2006). Ten years and counting: so what do we know about t(4;14)(p16;q32) multiple myeloma. Leuk Lymphoma, 47(11), 2289-2300. https://doi.org/10.1080/10428190600822128

Keck, M. K., Zuo, Z., Khattri, A., Stricker, T. P., Brown, C. D., Imanguli, M., Rieke, D., Endhardt, K., Fang, P., Bragelmann, J., DeBoer, R., El-Dinali, M., Aktolga, S., Lei, Z., Tan, P., Rozen, S. G., Salgia, R., Weichselbaum, R. R., Lingen, M. W., . . . Seiwert, T. Y. (2015). Integrative analysis of head and neck cancer identifies two biologically distinct HPV and three non-HPV subtypes. Clin Cancer Res, 21(4), 870-881. https://doi.org/10.1158/1078-0432.CCR-14-2481

Kennison, J. A., & Tamkun, J. W. (1988). Dosage-dependent modifiers of polycomb and antennapedia mutations in Drosophila. Proc Natl Acad Sci U S A, 85(21), 8136-8140. https://doi.org/10.1073/pnas.85.21.8136

Khan, J., Whaley, R., Cheng, L. (2020). Primary Pulmonary NUT Carcinoma with NSD3-NUTM1 Fusion. Am J Clin Pathol, 154, S83-S84. https://doi.org/10.1093/ajcp/aqaa161.183

Kim, E., Dede, M., Lenoir, W. F., Wang, G., Srinivasan, S., Colic, M., & Hart, T. (2019). A network of human functional gene interactions from knockout fitness screens in cancer cells. Life Sci Alliance, 2(2). https://doi.org/10.26508/lsa.201800278

Kim, H., Ekram, M. B., Bakshi, A., & Kim, J. (2015). AEBP2 as a transcriptional activator and its role in cell migration. Genomics, 105(2), 108-115. https://doi.org/10.1016/j.ygeno.2014.11.007

Kim, H., Kang, K., & Kim, J. (2009). AEBP2 as a potential targeting protein for Polycomb Repression Complex PRC2. Nucleic Acids Res, 37(9), 2940-2950. https://doi.org/10.1093/nar/gkp149

Kim, J. J., & Kingston, R. E. (2022). Context-specific Polycomb mechanisms in development. Nat Rev Genet, 23(11), 680-695. https://doi.org/10.1038/s41576-022-00499-0

Kim, K. H., Kim, W., Howard, T. P., Vazquez, F., Tsherniak, A., Wu, J. N., Wang, W., Haswell, J. R., Walensky, L. D., Hahn, W. C., Orkin, S. H., & Roberts, C. W. (2015). SWI/SNF-mutant cancers depend on catalytic and non-catalytic activity of EZH2. Nat Med, 21(12), 1491-1496. https://doi.org/10.1038/nm.3968

Kim, K. H., & Roberts, C. W. (2016). Targeting EZH2 in cancer. Nat Med, 22(2), 128-134. https://doi.org/10.1038/nm.4036

Kirschbaum, M., Frankel, P., Popplewell, L., Zain, J., Delioukina, M., Pullarkat, V., Matsuoka, D., Pulone, B., Rotter, A. J., Espinoza-Delgado, I., Nademanee, A.,

Forman, S. J., Gandara, D., & Newman, E. (2011). Phase II study of vorinostat for treatment of relapsed or refractory indolent non-Hodgkin's lymphoma and mantle cell lymphoma. J Clin Oncol, 29(9), 1198-1203. https://doi.org/10.1200/JCO.2010.32.1398

Kitano, M., Moriyama, S., Ando, Y., Hikida, M., Mori, Y., Kurosaki, T., & Okada, T. (2011). Bcl6 protein expression shapes pre-germinal center B cell dynamics and follicular helper T cell heterogeneity. Immunity, 34(6), 961-972. https://doi.org/10.1016/j.immuni.2011.03.025

Kleer, C. G., Cao, Q., Varambally, S., Shen, R., Ota, I., Tomlins, S. A., Ghosh, D., Sewalt, R. G., Otte, A. P., Hayes, D. F., Sabel, M. S., Livant, D., Weiss, S. J., Rubin, M. A., & Chinnaiyan, A. M. (2003). EZH2 is a marker of aggressive breast cancer and promotes neoplastic transformation of breast epithelial cells. Proc Natl Acad Sci U S A, 100(20), 11606-11611. https://doi.org/10.1073/pnas.1933744100

Klein, U., & Dalla-Favera, R. (2008). Germinal centres: role in B-cell physiology and malignancy. Nat Rev Immunol, 8(1), 22-33. https://doi.org/10.1038/nri2217

Knutson, S. K., Wigle, T. J., Warholic, N. M., Sneeringer, C. J., Allain, C. J., Klaus, C. R., Sacks, J. D., Raimondi, A., Majer, C. R., Song, J., Scott, M. P., Jin, L., Smith, J. J., Olhava, E. J., Chesworth, R., Moyer, M. P., Richon, V. M., Copeland, R. A., Keilhack, H., . . . Kuntz, K. W. (2012). A selective inhibitor of EZH2 blocks H3K27 methylation and kills mutant lymphoma cells. Nat Chem Biol, 8(11), 890-896. https://doi.org/10.1038/nchembio.1084

Kooistra, S. M., & Helin, K. (2012). Molecular mechanisms and potential functions of histone demethylases. Nat Rev Mol Cell Biol, 13(5), 297-311. https://doi.org/10.1038/nrm3327

Kornberg, R. D. (1974). Chromatin structure: a repeating unit of histones and DNA. Science, 184(4139), 868-871. https://doi.org/10.1126/science.184.4139.868

Kornberg, R. D., & Lorch, Y. (1999). Twenty-five years of the nucleosome, fundamental particle of the eukaryote chromosome. Cell, 98(3), 285-294. https://doi.org/10.1016/s0092-8674(00)81958-3

Kornberg, R. D., & Lorch, Y. (2020). Primary Role of the Nucleosome. Mol Cell, 79(3), 371-375. https://doi.org/10.1016/j.molcel.2020.07.020

Krivtsov, A. V., Feng, Z., Lemieux, M. E., Faber, J., Vempati, S., Sinha, A. U., Xia, X., Jesneck, J., Bracken, A. P., Silverman, L. B., Kutok, J. L., Kung, A. L., & Armstrong, S. A. (2008). H3K79 methylation profiles define murine and human MLL-AF4 leukemias. Cancer Cell, 14(5), 355-368. https://doi.org/10.1016/j.ccr.2008.10.001

Kuhn, M. W., Song, E., Feng, Z., Sinha, A., Chen, C. W., Deshpande, A. J., Cusan, M., Farnoud, N., Mupo, A., Grove, C., Koche, R., Bradner, J. E., de Stanchina, E.,

Vassiliou, G. S., Hoshii, T., & Armstrong, S. A. (2016). Targeting Chromatin Regulators Inhibits Leukemogenic Gene Expression in NPM1 Mutant Leukemia. Cancer Discov, 6(10), 1166-1181. https://doi.org/10.1158/2159-8290.CD-16-0237

Kuleshov, M. V., Jones, M. R., Rouillard, A. D., Fernandez, N. F., Duan, Q., Wang, Z., Koplev, S., Jenkins, S. L., Jagodnik, K. M., Lachmann, A., McDermott, M. G., Monteiro, C. D., Gundersen, G. W., & Ma'ayan, A. (2016). Enrichr: a comprehensive gene set enrichment analysis web server 2016 update. Nucleic Acids Res, 44(W1), W90-97. https://doi.org/10.1093/nar/gkw377

Kuo, A. J., Cheung, P., Chen, K., Zee, B. M., Kioi, M., Lauring, J., Xi, Y., Park, B. H., Shi, X., Garcia, B. A., Li, W., & Gozani, O. (2011). NSD2 links dimethylation of histone H3 at lysine 36 to oncogenic programming. Mol Cell, 44(4), 609-620. https://doi.org/10.1016/j.molcel.2011.08.042

Kuppers, R., Klein, U., Hansmann, M. L., & Rajewsky, K. (1999). Cellular origin of human B-cell lymphomas. N Engl J Med, 341(20), 1520-1529. https://doi.org/10.1056/NEJM199911113412007

Kurotaki, N., Harada, N., Yoshiura, K., Sugano, S., Niikawa, N., & Matsumoto, N. (2001). Molecular characterization of NSD1, a human homologue of the mouse Nsd1 gene. Gene, 279(2), 197-204. https://doi.org/10.1016/s0378-1119(01)00750-8

Kuzmichev, A., Nishioka, K., Erdjument-Bromage, H., Tempst, P., & Reinberg, D. (2002). Histone methyltransferase activity associated with a human multiprotein complex containing the Enhancer of Zeste protein. Genes Dev, 16(22), 2893-2905. https://doi.org/10.1101/gad.1035902

Kwok, H. S., Freedy, A. M., Siegenfeld, A. P., Morriss, J. W., Waterbury, A. L., Kissler, S. M., & Liau, B. B. (2023). Drug addiction unveils a repressive methylation ceiling in EZH2-mutant lymphoma. Nat Chem Biol, 19(9), 1105-1115. https://doi.org/10.1038/s41589-023-01299-1

La Starza, R., Gorello, P., Rosati, R., Riezzo, A., Veronese, A., Ferrazzi, E., Martelli, M. F., Negrini, M., & Mecucci, C. (2004). Cryptic insertion producing two NUP98/NSD1 chimeric transcripts in adult refractory anemia with an excess of blasts. Genes Chromosomes Cancer, 41(4), 395-399. https://doi.org/10.1002/gcc.20103

Lagan, E., Gannon, D., Silva, A. J., Bibawi, P., Doherty, A. M., Nimmo, D., McCole, R., Monger, C., Genesi, G. L., Vanderlinden, A., Innes, J. A., Jones, C. L. E., Yang, L., Chen, B., van Mierlo, G., Jansen, P., Pednekar, C., Von Kriegsheim, A., Wynne, K., . . . Brien, G. L. (2025). A specific form of cPRC1 containing CBX4 is co-opted to mediate oncogenic gene repression in diffuse midline glioma. Mol Cell, 85(11), 2110-2127 e2117. https://doi.org/10.1016/j.molcel.2025.04.026

Lan, F., Bayliss, P. E., Rinn, J. L., Whetstine, J. R., Wang, J. K., Chen, S., Iwase, S., Alpatov, R., Issaeva, I., Canaani, E., Roberts, T. M., Chang, H. Y., & Shi, Y. (2007).

A histone H3 lysine 27 demethylase regulates animal posterior development. Nature, 449(7163), 689-694. https://doi.org/10.1038/nature06192

Landau, D. A., Carter, S. L., Stojanov, P., McKenna, A., Stevenson, K., Lawrence, M. S., Sougnez, C., Stewart, C., Sivachenko, A., Wang, L., Wan, Y., Zhang, W., Shukla, S. A., Vartanov, A., Fernandes, S. M., Saksena, G., Cibulskis, K., Tesar, B., Gabriel, S., . . . Wu, C. J. (2013). Evolution and impact of subclonal mutations in chronic lymphocytic leukemia. Cell, 152(4), 714-726. https://doi.org/10.1016/j.cell.2013.01.019

Langmead, B., & Salzberg, S. L. (2012). Fast gapped-read alignment with Bowtie 2. Nat Methods, 9(4), 357-359. https://doi.org/10.1038/nmeth.1923

Launay, E., Pangault, C., Bertrand, P., Jardin, F., Lamy, T., Tilly, H., Tarte, K., Bastard, C., & Fest, T. (2012). High rate of TNFRSF14 gene alterations related to 1p36 region in de novo follicular lymphoma and impact on prognosis. Leukemia, 26(3), 559-562. https://doi.org/10.1038/leu.2011.266

Lee, Y. H., Coonrod, S. A., Kraus, W. L., Jelinek, M. A., & Stallcup, M. R. (2005). Regulation of coactivator complex assembly and function by protein arginine methylation and demethylimination. Proc Natl Acad Sci U S A, 102(10), 3611-3616. https://doi.org/10.1073/pnas.0407159102

Lenz, G., Davis, R. E., Ngo, V. N., Lam, L., George, T. C., Wright, G. W., Dave, S. S., Zhao, H., Xu, W., Rosenwald, A., Ott, G., Muller-Hermelink, H. K., Gascoyne, R. D., Connors, J. M., Rimsza, L. M., Campo, E., Jaffe, E. S., Delabie, J., Smeland, E. B., . . . Staudt, L. M. (2008). Oncogenic CARD11 mutations in human diffuse large B cell lymphoma. Science, 319(5870), 1676-1679. https://doi.org/10.1126/science.1153629

LeRoy, G., Rickards, B., & Flint, S. J. (2008). The double bromodomain proteins Brd2 and Brd3 couple histone acetylation to transcription. Mol Cell, 30(1), 51-60. https://doi.org/10.1016/j.molcel.2008.01.018

Lewis, E. B. (1978). A gene complex controlling segmentation in Drosophila. Nature, 276(5688), 565-570. https://doi.org/10.1038/276565a0

Li, H., Handsaker, B., Wysoker, A., Fennell, T., Ruan, J., Homer, N., Marth, G., Abecasis, G., & Durbin, R. (2009). The Sequence Alignment/Map format and SAMtools. Bioinformatics, 25(16), 2078-2079. https://doi.org/10.1093/bioinformatics/btp352

Li, J. J., Vasciaveo, A., Karagiannis, D., Sun, Z., Gretarsson, K. H., Chen, X., Ouerfelli, O., Socciarelli, F., Frankenstein, Z., Dong, H., Zou, M., Yuan, W., Yang, G., Aizenman, G. M., Pannellini, T., Xu, X., Beltran, H., Chen, Y., Gardner, K., . . . Shen, M. M. (2026). NSD2 targeting reverses plasticity and drug resistance in prostate cancer. Nature, 649(8095), 216-226. https://doi.org/10.1038/s41586-025-09727-z

Li, W., Tian, W., Yuan, G., Deng, P., Sengupta, D., Cheng, Z., Cao, Y., Ren, J., Qin, Y., Zhou, Y., Jia, Y., Gozani, O., Patel, D. J., & Wang, Z. (2021). Molecular basis of nucleosomal H3K36 methylation by NSD methyltransferases. Nature, 590(7846), 498-503. https://doi.org/10.1038/s41586-020-03069-8

Li, W., Xu, H., Xiao, T., Cong, L., Love, M. I., Zhang, F., Irizarry, R. A., Liu, J. S., Brown, M., & Liu, X. S. (2014). MAGeCK enables robust identification of essential genes from genome-scale CRISPR/Cas9 knockout screens. Genome Biol, 15(12), 554. https://doi.org/10.1186/s13059-014-0554-4

Li, Y., Trojer, P., Xu, C. F., Cheung, P., Kuo, A., Drury, W. J., 3rd, Qiao, Q., Neubert, T. A., Xu, R. M., Gozani, O., & Reinberg, D. (2009). The target of the NSD family of histone lysine methyltransferases depends on the nature of the substrate. J Biol Chem, 284(49), 34283-34295. https://doi.org/10.1074/jbc.M109.034462

Li, Z., Wang, B., Gu, S., Jiang, P., Sahu, A., Chen, C. H., Han, T., Shi, S., Wang, X., Traugh, N., Liu, H., Liu, Y., Wu, Q., Brown, M., Xiao, T., Boland, G. M., & Shirley Liu, X. (2020). CRISPR Screens Identify Essential Cell Growth Mediators in BRAF Inhibitor-resistant Melanoma. Genomics Proteomics Bioinformatics, 18(1), 26-40. https://doi.org/10.1016/j.gpb.2020.02.002

Liao, Y., Smyth, G. K., & Shi, W. (2014). featureCounts: an efficient general purpose program for assigning sequence reads to genomic features. Bioinformatics, 30(7), 923-930. https://doi.org/10.1093/bioinformatics/btt656

Liberzon, A., Birger, C., Thorvaldsdottir, H., Ghandi, M., Mesirov, J. P., & Tamayo, P. (2015). The Molecular Signatures Database (MSigDB) hallmark gene set collection. Cell Syst, 1(6), 417-425. https://doi.org/10.1016/j.cels.2015.12.004

Lim, S. H., Beers, S. A., French, R. R., Johnson, P. W., Glennie, M. J., & Cragg, M. S. (2010). Anti-CD20 monoclonal antibodies: historical and future perspectives. Haematologica, 95(1), 135-143. https://doi.org/10.3324/haematol.2008.001628

Lin, P. N., Park, J., Kang, Y. A., & Souroullas, G. P. (2025). ARID1A and ARID1B preserve B cell identity, prevent myeloid transformation and reveal therapeutic vulnerabilities. bioRxiv. https://doi.org/10.1101/2025.09.16.676393

Lindsley, A. W., Saal, H. M., Burrow, T. A., Hopkin, R. J., Shchelochkov, O., Khandelwal, P., Xie, C., Bleesing, J., Filipovich, L., Risma, K., Assa'ad, A. H., Roehrs, P. A., & Bernstein, J. A. (2016). Defects of B-cell terminal differentiation in patients with type-1 Kabuki syndrome. J Allergy Clin Immunol, 137(1), 179-187 e110. https://doi.org/10.1016/j.jaci.2015.06.002

Liu, F., Chen, X., Allali-Hassani, A., Quinn, A. M., Wasney, G. A., Dong, A., Barsyte, D., Kozieradzki, I., Senisterra, G., Chau, I., Siarheyeva, A., Kireev, D. B., Jadhav, A., Herold, J. M., Frye, S. V., Arrowsmith, C. H., Brown, P. J., Simeonov, A., Vedadi, M., & Jin, J. (2009). Discovery of a 2,4-diamino-7-aminoalkoxyquinazoline as a

potent and selective inhibitor of histone lysine methyltransferase G9a. J Med Chem, 52(24), 7950-7953. https://doi.org/10.1021/jm901543m

Liu, Y., Easton, J., Shao, Y., Maciaszek, J., Wang, Z., Wilkinson, M. R., McCastlain, K., Edmonson, M., Pounds, S. B., Shi, L., Zhou, X., Ma, X., Sioson, E., Li, Y., Rusch, M., Gupta, P., Pei, D., Cheng, C., Smith, M. A., . . . Mullighan, C. G. (2017). The genomic landscape of pediatric and young adult T-lineage acute lymphoblastic leukemia. Nat Genet, 49(8), 1211-1218. https://doi.org/10.1038/ng.3909

Liu, Y., Piorczynski, T. B., Estrella, B., Ricker, E. C., Pazos, M., Gonzalez, Y., Tolu, S. S., Ryu Tiger, Y. K., Karan, C., Cremers, S., Nandakumar, R., Honig, B., Hwang, H., Kelleher, N. L., Camarillo, J. M., Abshiru, N. A., & Amengual, J. E. (2025). Targeting Monoallelic CREBBP / EP300 Mutations in Germinal Center-Derived B-Cell Lymphoma with a First-in-Class Histone Acetyltransferase Activator. bioRxiv. https://doi.org/10.1101/2025.03.13.642871

Liu, Y., Yuan, J., Jia, G., Ye, W., Jeffrey Chen, Z., & Song, Q. (2021). Histone H3K27 dimethylation landscapes contribute to genome stability and genetic recombination during wheat polyploidization. Plant J, 105(3), 678-690. https://doi.org/10.1111/tpj.15063

Livingston, J. A., Blay, J. Y., Trent, J., Valverde, C., Agulnik, M., Gounder, M., Le Cesne, A., McKean, M., Wagner, M. J., Stacchiotti, S., Agresta, S., Quintas-Cardama, A., Reilly, S. A., Healy, K., Hickman, D., Zhao, T., Ballesteros-Perez, A., Khalil, A., Collins, M. P., . . . Wagner, A. J. (2025). A Phase I Study of FHD-609, a Heterobifunctional Degrader of Bromodomain-Containing Protein 9, in Patients with Advanced Synovial Sarcoma or SMARCB1-Deficient Tumors. Clin Cancer Res, 31(4), 628-638. https://doi.org/10.1158/1078-0432.CCR-24-2583

Love, M. I., Huber, W., & Anders, S. (2014). Moderated estimation of fold change and dispersion for RNA-seq data with DESeq2. Genome Biol, 15(12), 550. https://doi.org/10.1186/s13059-014-0550-8

Lu, C., Jain, S. U., Hoelper, D., Bechet, D., Molden, R. C., Ran, L., Murphy, D., Venneti, S., Hameed, M., Pawel, B. R., Wunder, J. S., Dickson, B. C., Lundgren, S. M., Jani, K. S., De Jay, N., Papillon-Cavanagh, S., Andrulis, I. L., Sawyer, S. L., Grynspan, D., . . . Lewis, P. W. (2016). Histone H3K36 mutations promote sarcomagenesis through altered histone methylation landscape. Science, 352(6287), 844-849. https://doi.org/10.1126/science.aac7272

Lu, T., Jackson, M. W., Wang, B., Yang, M., Chance, M. R., Miyagi, M., Gudkov, A. V., & Stark, G. R. (2010). Regulation of NF-kappaB by NSD1/FBXL11-dependent reversible lysine methylation of p65. Proc Natl Acad Sci U S A, 107(1), 46-51. https://doi.org/10.1073/pnas.0912493107

Luger, K., Mader, A. W., Richmond, R. K., Sargent, D. F., & Richmond, T. J. (1997). Crystal structure of the nucleosome core particle at 2.8 A resolution. Nature, 389(6648), 251-260. https://doi.org/10.1038/38444

Lunning, M. A., & Green, M. R. (2015). Mutation of chromatin modifiers; an emerging hallmark of germinal center B-cell lymphomas. Blood Cancer J, 5(10), e361. https://doi.org/10.1038/bcj.2015.89

Lydon, N. (2009). Attacking cancer at its foundation. Nat Med, 15(10), 1153-1157. https://doi.org/10.1038/nm1009-1153

Mali, P., Yang, L., Esvelt, K. M., Aach, J., Guell, M., DiCarlo, J. E., Norville, J. E., & Church, G. M. (2013). RNA-guided human genome engineering via Cas9. Science, 339(6121), 823-826. https://doi.org/10.1126/science.1232033

Malone, H. A., & Roberts, C. W. M. (2024). Chromatin remodellers as therapeutic targets. Nat Rev Drug Discov, 23(9), 661-681. https://doi.org/10.1038/s41573-024-00978-5

Manning, B. D., & Toker, A. (2017). AKT/PKB Signaling: Navigating the Network. Cell, 169(3), 381-405. https://doi.org/10.1016/j.cell.2017.04.001

Margueron, R., Li, G., Sarma, K., Blais, A., Zavadil, J., Woodcock, C. L., Dynlacht, B. D., & Reinberg, D. (2008). Ezh1 and Ezh2 maintain repressive chromatin through different mechanisms. Mol Cell, 32(4), 503-518. https://doi.org/10.1016/j.molcel.2008.11.004

Margueron, R., & Reinberg, D. (2011). The Polycomb complex PRC2 and its mark in life. Nature, 469(7330), 343-349. https://doi.org/10.1038/nature09784

Martinez-Garcia, E., Popovic, R., Min, D. J., Sweet, S. M., Thomas, P. M., Zamdborg, L., Heffner, A., Will, C., Lamy, L., Staudt, L. M., Levens, D. L., Kelleher, N. L., & Licht, J. D. (2011). The MMSET histone methyl transferase switches global histone methylation and alters gene expression in t(4;14) multiple myeloma cells. Blood, 117(1), 211-220. https://doi.org/10.1182/blood-2010-07-298349

Matsuwaka, M., Kumon, M., & Inoue, A. (2024). H3K27 dimethylation dynamics reveal stepwise establishment of facultative heterochromatin in early mouse embryos. Nat Cell Biol. https://doi.org/10.1038/s41556-024-01553-1

Mattson, N. M., Chan, A. K. N., Miyashita, K., Mukhaleva, E., Chang, W. H., Yang, L., Ma, N., Wang, Y., Pokharel, S. P., Li, M., Liu, Q., Xu, X., Chen, R., Singh, P., Zhang, L., Elsayed, Z., Chen, B., Keen, D., Pirrotte, P., . . . Chen, C. W. (2024). A novel class of inhibitors that disrupts the stability of integrin heterodimers identified by CRISPR-tiling-instructed genetic screens. Nat Struct Mol Biol, 31(3), 465-475. https://doi.org/10.1038/s41594-024-01211-y

McBride, M. J., Pulice, J. L., Beird, H. C., Ingram, D. R., D'Avino, A. R., Shern, J. F., Charville, G. W., Hornick, J. L., Nakayama, R. T., Garcia-Rivera, E. M., Araujo, D. M., Wang, W. L., Tsai, J. W., Yeagley, M., Wagner, A. J., Futreal, P. A., Khan, J.,

Lazar, A. J., & Kadoch, C. (2018). The SS18-SSX Fusion Oncoprotein Hijacks BAF Complex Targeting and Function to Drive Synovial Sarcoma. Cancer Cell, 33(6), 1128-1141 e1127. https://doi.org/10.1016/j.ccell.2018.05.002

McCabe, M. T., Graves, A. P., Ganji, G., Diaz, E., Halsey, W. S., Jiang, Y., Smitheman, K. N., Ott, H. M., Pappalardi, M. B., Allen, K. E., Chen, S. B., Della Pietra, A., 3rd, Dul, E., Hughes, A. M., Gilbert, S. A., Thrall, S. H., Tummino, P. J., Kruger, R. G., Brandt, M., . . . Creasy, C. L. (2012). Mutation of A677 in histone methyltransferase EZH2 in human B-cell lymphoma promotes hypertrimethylation of histone H3 on lysine 27 (H3K27). Proc Natl Acad Sci U S A, 109(8), 2989-2994. https://doi.org/10.1073/pnas.1116418109

McCabe, M. T., Ott, H. M., Ganji, G., Korenchuk, S., Thompson, C., Van Aller, G. S., Liu, Y., Graves, A. P., Della Pietra, A., 3rd, Diaz, E., LaFrance, L. V., Mellinger, M., Duquenne, C., Tian, X., Kruger, R. G., McHugh, C. F., Brandt, M., Miller, W. H., Dhanak, D., . . . Creasy, C. L. (2012). EZH2 inhibition as a therapeutic strategy for lymphoma with EZH2-activating mutations. Nature, 492(7427), 108-112. https://doi.org/10.1038/nature11606

McCole, R., Nolan, J., Reck, D. M., Monger, C., Rustichelli, S., Conway, E., Brien, G. L., Wang, C., Deevy, O., Neikes, H. K., Bashore, F. M., Mooney, A., Flavin, R., Vandenberghe, E., Flanigan, S. F., Pasini, D., Davidovich, C., Vermeulen, M., James, L. I., . . . Bracken, A. P. (2025). A conserved switch to less catalytically active Polycomb repressive complexes in non-dividing cells. Cell Rep, 44(1), 115192. https://doi.org/10.1016/j.celrep.2024.115192

McFarland, J. M., Ho, Z. V., Kugener, G., Dempster, J. M., Montgomery, P. G., Bryan, J. G., Krill-Burger, J. M., Green, T. M., Vazquez, F., Boehm, J. S., Golub, T. R., Hahn, W. C., Root, D. E., & Tsherniak, A. (2018). Improved estimation of cancer dependencies from large-scale RNAi screens using model-based normalization and data integration. Nat Commun, 9(1), 4610. https://doi.org/10.1038/s41467-018-06916-5

McNamara, C., Montoto, S., Eyre, T. A., Ardeshna, K., Burton, C., Illidge, T., Linton, K., Rule, S., Townsend, W., Wong, W. L., & McKay, P. (2020). The investigation and management of follicular lymphoma. Br J Haematol, 191(3), 363-381. https://doi.org/10.1111/bjh.16872

Meng, T. G., Zhou, Q., Ma, X. S., Liu, X. Y., Meng, Q. R., Huang, X. J., Liu, H. L., Lei, W. L., Zhao, Z. H., Ouyang, Y. C., Hou, Y., Schatten, H., Ou, X. H., Wang, Z. B., Gao, S. R., & Sun, Q. Y. (2020). PRC2 and EHMT1 regulate H3K27me2 and H3K27me3 establishment across the zygote genome. Nat Commun, 11(1), 6354. https://doi.org/10.1038/s41467-020-20242-9

Mertz, J. A., Conery, A. R., Bryant, B. M., Sandy, P., Balasubramanian, S., Mele, D. A., Bergeron, L., & Sims, R. J., 3rd. (2011). Targeting MYC dependence in cancer by inhibiting BET bromodomains. Proc Natl Acad Sci U S A, 108(40), 16669-16674. https://doi.org/10.1073/pnas.1108190108

Mesin, L., Ersching, J., & Victora, G. D. (2016). Germinal Center B Cell Dynamics. Immunity, 45(3), 471-482. https://doi.org/10.1016/j.immuni.2016.09.001

Meyer, S. N., Scuoppo, C., Vlasevska, S., Bal, E., Holmes, A. B., Holloman, M., Garcia-Ibanez, L., Nataraj, S., Duval, R., Vantrimpont, T., Basso, K., Brooks, N., Dalla-Favera, R., & Pasqualucci, L. (2019). Unique and Shared Epigenetic Programs of the CREBBP and EP300 Acetyltransferases in Germinal Center B Cells Reveal Targetable Dependencies in Lymphoma. Immunity, 51(3), 535-547 e539. https://doi.org/10.1016/j.immuni.2019.08.006

Millan-Zambrano, G., Burton, A., Bannister, A. J., & Schneider, R. (2022). Histone post-translational modifications - cause and consequence of genome function. Nat Rev Genet, 23(9), 563-580. https://doi.org/10.1038/s41576-022-00468-7

Milojkovic, D., & Apperley, J. (2009). Mechanisms of Resistance to Imatinib and Second-Generation Tyrosine Inhibitors in Chronic Myeloid Leukemia. Clin Cancer Res, 15(24), 7519-7527. https://doi.org/10.1158/1078-0432.CCR-09-1068

Min, J., Zhang, Y., & Xu, R. M. (2003). Structural basis for specific binding of Polycomb chromodomain to histone H3 methylated at Lys 27. Genes Dev, 17(15), 1823-1828. https://doi.org/10.1101/gad.269603

Mishima, Y., Wang, C., Miyagi, S., Saraya, A., Hosokawa, H., Mochizuki-Kashio, M., Nakajima-Takagi, Y., Koide, S., Negishi, M., Sashida, G., Naito, T., Ishikura, T., Onodera, A., Nakayama, T., Tenen, D. G., Yamaguchi, N., Koseki, H., Taniuchi, I., & Iwama, A. (2014). Histone acetylation mediated by Brd1 is crucial for Cd8 gene activation during early thymocyte development. Nat Commun, 5, 5872. https://doi.org/10.1038/ncomms6872

Mittal, P., & Roberts, C. W. M. (2020). The SWI/SNF complex in cancer - biology, biomarkers and therapy. Nat Rev Clin Oncol, 17(7), 435-448. https://doi.org/10.1038/s41571-020-0357-3

Mlynarczyk, C., Fontan, L., & Melnick, A. (2019). Germinal center-derived lymphomas: The darkest side of humoral immunity. Immunol Rev, 288(1), 214-239. https://doi.org/10.1111/imr.12755

Mochizuki-Kashio, M., Aoyama, K., Sashida, G., Oshima, M., Tomioka, T., Muto, T., Wang, C., & Iwama, A. (2015). Ezh2 loss in hematopoietic stem cells predisposes mice to develop heterogeneous malignancies in an Ezh1-dependent manner. Blood, 126(10), 1172-1183. https://doi.org/10.1182/blood-2015-03-634428

Moreau, P., Facon, T., Leleu, X., Morineau, N., Huyghe, P., Harousseau, J. L., Bataille, R., Avet-Loiseau, H., & Intergroupe Francophone du, M. (2002). Recurrent 14q32 translocations determine the prognosis of multiple myeloma, especially in patients receiving intensive chemotherapy. Blood, 100(5), 1579-1583. https://doi.org/10.1182/blood-2002-03-0749

Moreau, P., Richardson, P. G., Cavo, M., Orlowski, R. Z., San Miguel, J. F., Palumbo, A., & Harousseau, J. L. (2012). Proteasome inhibitors in multiple myeloma: 10 years later. Blood, 120(5), 947-959. https://doi.org/10.1182/blood-2012-04-403733

Moreno, V., Vieito, M., Sepulveda, J. M., Galvao, V., Hernandez-Guerrero, T., Doger, B., Saavedra, O., Carlo-Stella, C., Michot, J. M., Italiano, A., Magagnoli, M., Carpio, C., Pinto, A., Sarmiento, R., Amoroso, B., Aronchik, I., Filvaroff, E., Hanna, B., Wei, X., . . . Brana, I. (2023). BET inhibitor trotabresib in heavily pretreated patients with solid tumors and diffuse large B-cell lymphomas. Nat Commun, 14(1), 1359. https://doi.org/10.1038/s41467-023-36976-1

Morin, R. D., Johnson, N. A., Severson, T. M., Mungall, A. J., An, J., Goya, R., Paul, J. E., Boyle, M., Woolcock, B. W., Kuchenbauer, F., Yap, D., Humphries, R. K., Griffith, O. L., Shah, S., Zhu, H., Kimbara, M., Shashkin, P., Charlot, J. F., Tcherpakov, M., . . . Marra, M. A. (2010). Somatic mutations altering EZH2 (Tyr641) in follicular and diffuse large B-cell lymphomas of germinal-center origin. Nat Genet, 42(2), 181-185. https://doi.org/10.1038/ng.518

Morin, R. D., Mendez-Lago, M., Mungall, A. J., Goya, R., Mungall, K. L., Corbett, R. D., Johnson, N. A., Severson, T. M., Chiu, R., Field, M., Jackman, S., Krzywinski, M., Scott, D. W., Trinh, D. L., Tamura-Wells, J., Li, S., Firme, M. R., Rogic, S., Griffith, M., . . . Marra, M. A. (2011). Frequent mutation of histone-modifying genes in non-Hodgkin lymphoma. Nature, 476(7360), 298-303. https://doi.org/10.1038/nature10351

Morrison, M. J., Boriack-Sjodin, P. A., Swinger, K. K., Wigle, T. J., Sadalge, D., Kuntz, K. W., Scott, M. P., Janzen, W. P., Chesworth, R., Duncan, K. W., Harvey, D. M., Lampe, J. W., Mitchell, L. H., & Copeland, R. A. (2018). Identification of a peptide inhibitor for the histone methyltransferase WHSC1. PLoS One, 13(5), e0197082. https://doi.org/10.1371/journal.pone.0197082

Morschhauser, F., Salles, G., Batlevi, C. L., Tilly, H., Chaidos, A., Phillips, T., Burke, J., & Melnick, A. (2022). Taking the EZ way: Targeting enhancer of zeste homolog 2 in B-cell lymphomas. Blood Rev, 56, 100988. https://doi.org/10.1016/j.blre.2022.100988

Morschhauser, F., Tilly, H., Chaidos, A., McKay, P., Phillips, T., Assouline, S., Batlevi, C. L., Campbell, P., Ribrag, V., Damaj, G. L., Dickinson, M., Jurczak, W., Kazmierczak, M., Opat, S., Radford, J., Schmitt, A., Yang, J., Whalen, J., Agarwal, S., . . . Salles,

G. (2020). Tazemetostat for patients with relapsed or refractory follicular lymphoma: an open-label, single-arm, multicentre, phase 2 trial. Lancet Oncol, 21(11), 1433-1442. https://doi.org/10.1016/S1470-2045(20)30441-1

Mozzetta, C., Pontis, J., Fritsch, L., Robin, P., Portoso, M., Proux, C., Margueron, R., & Ait-Si-Ali, S. (2014). The histone H3 lysine 9 methyltransferases G9a and GLP regulate polycomb repressive complex 2-mediated gene silencing. Mol Cell, 53(2), 277-289. https://doi.org/10.1016/j.molcel.2013.12.005

Mucha, M., Lai, Z., McKenzie, N. J., Matra, F., Boudes, M., Flanigan, S. F., Alejo-Vinogradova, M. T., Monger, C., Zhang, Q., Nimmo, D., Healy, E., Silva, A. J., Angelov, D., Reck, D. M., Holland, G., Atmaca, Z. E., King, H. E., Hamilton, M., Glancy, E., . . . Bracken, A. P. (2025). Auto-inhibition of PRC2 by the broadly expressed long isoform of AEBP2. EMBO J, 44(23), 6979-7020. https://doi.org/10.1038/s44318-025-00616-9

Muller, J., Hart, C. M., Francis, N. J., Vargas, M. L., Sengupta, A., Wild, B., Miller, E. L., O'Connor, M. B., Kingston, R. E., & Simon, J. A. (2002). Histone methyltransferase activity of a Drosophila Polycomb group repressor complex. Cell, 111(2), 197-208. https://doi.org/10.1016/s0092-8674(02)00976-5

Nakayama, K., Szewczyk, M. M., Dela Sena, C., Wu, H., Dong, A., Zeng, H., Li, F., de Freitas, R. F., Eram, M. S., Schapira, M., Baba, Y., Kunitomo, M., Cary, D. R., Tawada, M., Ohashi, A., Imaeda, Y., Saikatendu, K. S., Grimshaw, C. E., Vedadi, M., . . . Brown, P. J. (2018). TP-064, a potent and selective small molecule inhibitor of PRMT4 for multiple myeloma. Oncotarget, 9(26), 18480-18493. https://doi.org/10.18632/oncotarget.24883

NCRI. (2021). *National Cancer Registry Ireland (2021) Cancer in Ireland 1994-2019: Annual report of the National Cancery Registry.* www.ncri.ie

Neff, T., & Armstrong, S. A. (2013). Recent progress toward epigenetic therapies: the example of mixed lineage leukemia. Blood, 121(24), 4847-4853. https://doi.org/10.1182/blood-2013-02-474833

Neumann, M., Vosberg, S., Schlee, C., Heesch, S., Schwartz, S., Gökbuget, N., Hoelzer, D., Graf, A., Krebs, S., Bartram, I., Blum, H., Brüggemann, M., Hecht, J., Bohlander, S. K., Greif, P. A., & Baldus, C. D. (2015). Mutational spectrum of adult T-ALL. Oncotarget, 6(5), 2754-2766. https://doi.org/10.18632/oncotarget.2218

Ng, H. H., Feng, Q., Wang, H., Erdjument-Bromage, H., Tempst, P., Zhang, Y., & Struhl, K. (2002). Lysine methylation within the globular domain of histone H3 by Dot1 is important for telomeric silencing and Sir protein association. Genes Dev, 16(12), 1518-1527. https://doi.org/10.1101/gad.1001502

Ng, S. B., Bigham, A. W., Buckingham, K. J., Hannibal, M. C., McMillin, M. J., Gildersleeve, H. I., Beck, A. E., Tabor, H. K., Cooper, G. M., Mefford, H. C., Lee,

C., Turner, E. H., Smith, J. D., Rieder, M. J., Yoshiura, K., Matsumoto, N., Ohta, T., Niikawa, N., Nickerson, D. A., . . . Shendure, J. (2010). Exome sequencing identifies MLL2 mutations as a cause of Kabuki syndrome. Nat Genet, 42(9), 790-793. https://doi.org/10.1038/ng.646

Ngo, V. N., Young, R. M., Schmitz, R., Jhavar, S., Xiao, W., Lim, K. H., Kohlhammer, H., Xu, W., Yang, Y., Zhao, H., Shaffer, A. L., Romesser, P., Wright, G., Powell, J., Rosenwald, A., Muller-Hermelink, H. K., Ott, G., Gascoyne, R. D., Connors, J. M., . . . Staudt, L. M. (2011). Oncogenically active MYD88 mutations in human lymphoma. Nature, 470(7332), 115-119. https://doi.org/10.1038/nature09671

Nguyen, V. T. M., Namba, H., Porter, H., Shlyueva, D., Lopez, E., Melcher, A., Béguelin, W., Melnick, A. M., & Helin, K. (2025). Synergistic antitumor effect of combined EZH2 and DOT1L inhibition in B-cell lymphoma. Blood, 145(24), 2873-2886. https://doi.org/10.1182/blood.2024026534

Nicosia, L., Boffo, F. L., Ceccacci, E., Conforti, F., Pallavicini, I., Bedin, F., Ravasio, R., Massignani, E., Somervaille, T. C. P., Minucci, S., & Bonaldi, T. (2022). Pharmacological inhibition of LSD1 triggers myeloid differentiation by targeting GSE1 oncogenic functions in AML. Oncogene, 41(6), 878-894. https://doi.org/10.1038/s41388-021-02123-7

Nimura, K., Ura, K., Shiratori, H., Ikawa, M., Okabe, M., Schwartz, R. J., & Kaneda, Y. (2009). A histone H3 lysine 36 trimethyltransferase links Nkx2-5 to Wolf-Hirschhorn syndrome. Nature, 460(7252), 287-291. https://doi.org/10.1038/nature08086

Ntziachristos, P., Tsirigos, A., Van Vlierberghe, P., Nedjic, J., Trimarchi, T., Flaherty, M. S., Ferres-Marco, D., da Ros, V., Tang, Z., Siegle, J., Asp, P., Hadler, M., Rigo, I., De Keersmaecker, K., Patel, J., Huynh, T., Utro, F., Poglio, S., Samon, J. B., . . . Aifantis, I. (2012). Genetic inactivation of the polycomb repressive complex 2 in T cell acute lymphoblastic leukemia. Nat Med, 18(2), 298-301. https://doi.org/10.1038/nm.2651

Nurk, S., Koren, S., Rhie, A., Rautiainen, M., Bzikadze, A. V., Mikheenko, A., Vollger, M. R., Altemose, N., Uralsky, L., Gershman, A., Aganezov, S., Hoyt, S. J., Diekhans, M., Logsdon, G. A., Alonge, M., Antonarakis, S. E., Borchers, M., Bouffard, G. G., Brooks, S. Y., . . . Phillippy, A. M. (2022). The complete sequence of a human genome. Science, 376(6588), 44-53. https://doi.org/10.1126/science.abj6987

Ogawa, H., Ishiguro, K., Gaubatz, S., Livingston, D. M., & Nakatani, Y. (2002). A complex with chromatin modifiers that occupies E2F- and Myc-responsive genes in G0 cells. Science, 296(5570), 1132-1136. https://doi.org/10.1126/science.1069861

Ogiyama, Y., Schuettengruber, B., Papadopoulos, G. L., Chang, J. M., & Cavalli, G. (2018). Polycomb-Dependent Chromatin Looping Contributes to Gene Silencing

during Drosophila Development. Mol Cell, 71(1), 73-88 e75. https://doi.org/10.1016/j.molcel.2018.05.032

Ogura, M., Ando, K., Suzuki, T., Ishizawa, K., Oh, S. Y., Itoh, K., Yamamoto, K., Au, W. Y., Tien, H. F., Matsuno, Y., Terauchi, T., Yamamoto, K., Mori, M., Tanaka, Y., Shimamoto, T., Tobinai, K., & Kim, W. S. (2014). A multicentre phase II study of vorinostat in patients with relapsed or refractory indolent B-cell non-Hodgkin lymphoma and mantle cell lymphoma. Br J Haematol, 165(6), 768-776. https://doi.org/10.1111/bjh.12819

Okada, Y., Feng, Q., Lin, Y., Jiang, Q., Li, Y., Coffield, V. M., Su, L., Xu, G., & Zhang, Y. (2005). hDOT1L links histone methylation to leukemogenesis. Cell, 121(2), 167-178. https://doi.org/10.1016/j.cell.2005.02.020

Okkenhaug, K., Bilancio, A., Farjot, G., Priddle, H., Sancho, S., Peskett, E., Pearce, W., Meek, S. E., Salpekar, A., Waterfield, M. D., Smith, A. J., & Vanhaesebroeck, B. (2002). Impaired B and T cell antigen receptor signaling in p110delta PI 3-kinase mutant mice. Science, 297(5583), 1031-1034. https://doi.org/10.1126/science.1073560

Okosun, J., Bodor, C., Wang, J., Araf, S., Yang, C. Y., Pan, C., Boller, S., Cittaro, D., Bozek, M., Iqbal, S., Matthews, J., Wrench, D., Marzec, J., Tawana, K., Popov, N., O'Riain, C., O'Shea, D., Carlotti, E., Davies, A., . . . Fitzgibbon, J. (2014). Integrated genomic analysis identifies recurrent mutations and evolution patterns driving the initiation and progression of follicular lymphoma. Nat Genet, 46(2), 176-181. https://doi.org/10.1038/ng.2856

Ortega-Molina, A., Boss, I. W., Canela, A., Pan, H., Jiang, Y., Zhao, C., Jiang, M., Hu, D., Agirre, X., Niesvizky, I., Lee, J. E., Chen, H. T., Ennishi, D., Scott, D. W., Mottok, A., Hother, C., Liu, S., Cao, X. J., Tam, W., . . . Wendel, H. G. (2015). The histone lysine methyltransferase KMT2D sustains a gene expression program that represses B cell lymphoma development. Nat Med, 21(10), 1199-1208. https://doi.org/10.1038/nm.3943

Oyer, J. A., Huang, X., Zheng, Y., Shim, J., Ezponda, T., Carpenter, Z., Allegretta, M., Okot-Kotber, C. I., Patel, J. P., Melnick, A., Levine, R. L., Ferrando, A., Mackerell, A. D., Jr., Kelleher, N. L., Licht, J. D., & Popovic, R. (2014). Point mutation E1099K in MMSET/NSD2 enhances its methyltranferase activity and leads to altered global chromatin methylation in lymphoid malignancies. Leukemia, 28(1), 198-201. https://doi.org/10.1038/leu.2013.204

Parolia, A., Eyunni, S., Verma, B. K., Young, E., Liu, Y., Liu, L., George, J., Aras, S., Das, C. K., Mannan, R., Ur Rasool, R., Mitchell-Velasquez, E., Mahapatra, S., Luo, J., Carson, S. E., Xiao, L., Gajjala, P. R., Venkatesh, S., Jaber, M., . . . Asangani, I. A. (2024). NSD2 is a requisite subunit of the AR/FOXA1 neo-enhanceosome in

promoting prostate tumorigenesis. Nat Genet, 56(10), 2132-2143. https://doi.org/10.1038/s41588-024-01893-6

Pasini, D., Bracken, A. P., Jensen, M. R., Lazzerini Denchi, E., & Helin, K. (2004). Suz12 is essential for mouse development and for EZH2 histone methyltransferase activity. EMBO J, 23(20), 4061-4071. https://doi.org/10.1038/sj.emboj.7600402

Pasqualucci, L., Dominguez-Sola, D., Chiarenza, A., Fabbri, G., Grunn, A., Trifonov, V., Kasper, L. H., Lerach, S., Tang, H., Ma, J., Rossi, D., Chadburn, A., Murty, V. V., Mullighan, C. G., Gaidano, G., Rabadan, R., Brindle, P. K., & Dalla-Favera, R. (2011). Inactivating mutations of acetyltransferase genes in B-cell lymphoma. Nature, 471(7337), 189-195. https://doi.org/10.1038/nature09730

Patil, A., Manzano, M., & Gottwein, E. (2019). Genome-wide CRISPR screens reveal genetic mediators of cereblon modulator toxicity in primary effusion lymphoma. Blood Adv, 3(14), 2105-2117. https://doi.org/10.1182/bloodadvances.2019031732

Perner, F., Stein, E. M., Wenge, D. V., Singh, S., Kim, J., Apazidis, A., Rahnamoun, H., Anand, D., Marinaccio, C., Hatton, C., Wen, Y., Stone, R. M., Schaller, D., Mowla, S., Xiao, W., Gamlen, H. A., Stonestrom, A. J., Persaud, S., Ener, E., . . . Cai, S. F. (2023). MEN1 mutations mediate clinical resistance to menin inhibition. Nature, 615(7954), 913-919. https://doi.org/10.1038/s41586-023-05755-9

Pertea, M., Kim, D., Pertea, G. M., Leek, J. T., & Salzberg, S. L. (2016). Transcript-level expression analysis of RNA-seq experiments with HISAT, StringTie and Ballgown. Nat Protoc, 11(9), 1650-1667. https://doi.org/10.1038/nprot.2016.095

Pierro, J., Saliba, J., Narang, S., Sethia, G., Saint Fleur-Lominy, S., Chowdhury, A., Qualls, A., Fay, H., Kilberg, H. L., Moriyama, T., Fuller, T. J., Teachey, D. T., Schmiegelow, K., Yang, J. J., Loh, M. L., Brown, P. A., Zhang, J., Ma, X., Tsirigos, A., . . . Carroll, W. L. (2020). The NSD2 p.E1099K Mutation Is Enriched at Relapse and Confers Drug Resistance in a Cell Context-Dependent Manner in Pediatric Acute Lymphoblastic Leukemia. Mol Cancer Res, 18(8), 1153-1165. https://doi.org/10.1158/1541-7786.MCR-20-0092

Piovesan, A., Pelleri, M. C., Antonaros, F., Strippoli, P., Caracausi, M., & Vitale, L. (2019). On the length, weight and GC content of the human genome. BMC Res Notes, 12(1), 106. https://doi.org/10.1186/s13104-019-4137-z

Piunti, A., Smith, E. R., Morgan, M. A. J., Ugarenko, M., Khaltyan, N., Helmin, K. A., Ryan, C. A., Murray, D. C., Rickels, R. A., Yilmaz, B. D., Rendleman, E. J., Savas, J. N., Singer, B. D., Bulun, S. E., & Shilatifard, A. (2019). CATACOMB: An endogenous inducible gene that antagonizes H3K27 methylation activity of Polycomb repressive complex 2 via an H3K27M-like mechanism. Sci Adv, 5(7), eaax2887. https://doi.org/10.1126/sciadv.aax2887

Plass, C., Pfister, S. M., Lindroth, A. M., Bogatyrova, O., Claus, R., & Lichter, P. (2013). Mutations in regulators of the epigenome and their connections to global chromatin patterns in cancer. Nat Rev Genet, 14(11), 765-780. https://doi.org/10.1038/nrg3554

Popovic, R., Martinez-Garcia, E., Giannopoulou, E. G., Zhang, Q., Zhang, Q., Ezponda, T., Shah, M. Y., Zheng, Y., Will, C. M., Small, E. C., Hua, Y., Bulic, M., Jiang, Y., Carrara, M., Calogero, R. A., Kath, W. L., Kelleher, N. L., Wang, J. P., Elemento, O., & Licht, J. D. (2014). Histone methyltransferase MMSET/NSD2 alters EZH2 binding and reprograms the myeloma epigenome through global and focal changes in H3K36 and H3K27 methylation. PLoS Genet, 10(9), e1004566. https://doi.org/10.1371/journal.pgen.1004566

Porazzi, P., Nason, S., Yang, Z., Carturan, A., Ghilardi, G., Guruprasad, P., Patel, R. P., Tan, M., Padmanabhan, A. A., Lemoine, J., Fardella, E., Zhang, Y., Pajarillo, R., Chen, L., Ugwuanyi, O., Markowitz, K., Delman, D., Angelos, M. G., Shestova, O., . . . Ruella, M. (2025). EZH1/EZH2 inhibition enhances adoptive T cell immunotherapy against multiple cancer models. Cancer Cell, 43(3), 537-551 e537. https://doi.org/10.1016/j.ccell.2025.01.013

Potjewyd, F., Turner, A. W., Beri, J., Rectenwald, J. M., Norris-Drouin, J. L., Cholensky, S. H., Margolis, D. M., Pearce, K. H., Herring, L. E., & James, L. I. (2020). Degradation of Polycomb Repressive Complex 2 with an EED-Targeted Bivalent Chemical Degrader. Cell Chem Biol, 27(1), 47-56 e15. https://doi.org/10.1016/j.chembiol.2019.11.006

Puvvada, S. D., Li, H., Rimsza, L. M., Bernstein, S. H., Fisher, R. I., LeBlanc, M., Schmelz, M., Glinsmann-Gibson, B., Miller, T. P., Maddox, A. M., Friedberg, J. W., Smith, S. M., & Persky, D. O. (2016). A phase II study of belinostat (PXD101) in relapsed and refractory aggressive B-cell lymphomas: SWOG S0520. Leuk Lymphoma, 57(10), 2359-2369. https://doi.org/10.3109/10428194.2015.1135431

Qi, W., Chan, H., Teng, L., Li, L., Chuai, S., Zhang, R., Zeng, J., Li, M., Fan, H., Lin, Y., Gu, J., Ardayfio, O., Zhang, J. H., Yan, X., Fang, J., Mi, Y., Zhang, M., Zhou, T., Feng, G., . . . Li, E. (2012). Selective inhibition of Ezh2 by a small molecule inhibitor blocks tumor cells proliferation. Proc Natl Acad Sci U S A, 109(52), 21360-21365. https://doi.org/10.1073/pnas.1210371110

Qi, W., Zhao, K., Gu, J., Huang, Y., Wang, Y., Zhang, H., Zhang, M., Zhang, J., Yu, Z., Li, L., Teng, L., Chuai, S., Zhang, C., Zhao, M., Chan, H., Chen, Z., Fang, D., Fei, Q., Feng, L., . . . Li, E. (2017). An allosteric PRC2 inhibitor targeting the H3K27me3 binding pocket of EED. Nat Chem Biol, 13(4), 381-388. https://doi.org/10.1038/nchembio.2304

Qiao, Q., Li, Y., Chen, Z., Wang, M., Reinberg, D., & Xu, R. M. (2011). The structure of NSD1 reveals an autoregulatory mechanism underlying histone H3K36 methylation. J Biol Chem, 286(10), 8361-8368. https://doi.org/10.1074/jbc.M110.204115

Raaphorst, F. M., van Kemenade, F. J., Fieret, E., Hamer, K. M., Satijn, D. P., Otte, A. P., & Meijer, C. J. (2000). Cutting edge: polycomb gene expression patterns reflect distinct B cell differentiation stages in human germinal centers. J Immunol, 164(1), 1-4. https://doi.org/10.4049/jimmunol.164.1.1

Radko-Juettner, S., Yue, H., Myers, J. A., Carter, R. D., Robertson, A. N., Mittal, P., Zhu, Z., Hansen, B. S., Donovan, K. A., Hunkeler, M., Rosikiewicz, W., Wu, Z., McReynolds, M. G., Roy Burman, S. S., Schmoker, A. M., Mageed, N., Brown, S. A., Mobley, R. J., Partridge, J. F., . . . Roberts, C. W. M. (2024). Targeting DCAF5 suppresses SMARCB1-mutant cancer by stabilizing SWI/SNF. Nature, 628(8007), 442-449. https://doi.org/10.1038/s41586-024-07250-1

Rajagopalan, K. N., Chen, X., Weinberg, D. N., Chen, H., Majewski, J., Allis, C. D., & Lu, C. (2021). Depletion of H3K36me2 recapitulates epigenomic and phenotypic changes induced by the H3.3K36M oncohistone mutation. Proc Natl Acad Sci U S A, 118(9). https://doi.org/10.1073/pnas.2021795118

Ramirez, F., Ryan, D. P., Gruning, B., Bhardwaj, V., Kilpert, F., Richter, A. S., Heyne, S., Dundar, F., & Manke, T. (2016). deepTools2: a next generation web server for deep-sequencing data analysis. Nucleic Acids Res, 44(W1), W160-165. https://doi.org/10.1093/nar/gkw257

Rathert, P. (2021). Structure, Activity and Function of the NSD3 Protein Lysine Methyltransferase. Life (Basel), 11(8). https://doi.org/10.3390/life11080726

Rayasam, G. V., Wendling, O., Angrand, P. O., Mark, M., Niederreither, K., Song, L., Lerouge, T., Hager, G. L., Chambon, P., & Losson, R. (2003). NSD1 is essential for early post-implantation development and has a catalytically active SET domain. EMBO J, 22(12), 3153-3163. https://doi.org/10.1093/emboj/cdg288

Reddy, A., Zhang, J., Davis, N. S., Moffitt, A. B., Love, C. L., Waldrop, A., Leppa, S., Pasanen, A., Meriranta, L., Karjalainen-Lindsberg, M. L., Norgaard, P., Pedersen, M., Gang, A. O., Hogdall, E., Heavican, T. B., Lone, W., Iqbal, J., Qin, Q., Li, G., . . . Dave, S. S. (2017). Genetic and Functional Drivers of Diffuse Large B Cell Lymphoma. Cell, 171(2), 481-494 e415. https://doi.org/10.1016/j.cell.2017.09.027

Robbins, D. W., Noviski, M. A., Tan, Y. S., Konst, Z. A., Kelly, A., Auger, P., Brathaban, N., Cass, R., Chan, M. L., Cherala, G., Clifton, M. C., Gajewski, S., Ingallinera, T. G., Karr, D., Kato, D., Ma, J., McKinnell, J., McIntosh, J., Mihalic, J., . . . Cohen, F. (2024). Discovery and Preclinical Pharmacology of NX-2127, an Orally Bioavailable Degrader of Bruton's Tyrosine Kinase with Immunomodulatory Activity

for the Treatment of Patients with B Cell Malignancies. J Med Chem, 67(4), 2321-2336. https://doi.org/10.1021/acs.jmedchem.3c01007

Roberts, C. W., & Orkin, S. H. (2004). The SWI/SNF complex--chromatin and cancer. Nat Rev Cancer, 4(2), 133-142. https://doi.org/10.1038/nrc1273

Romero, P., Richart, L., Aflaki, S., Petitalot, A., Burton, M., Michaud, A., Masliah-Planchon, J., Kuhnowski, F., Le Cam, S., Baliñas-Gavira, C., Méaudre, C., Luscan, A., Hamza, A., Legoix, P., Vincent-Salomon, A., Wassef, M., Holoch, D., & Margueron, R. (2024). EZH2 mutations in follicular lymphoma distort H3K27me3 profiles and alter transcriptional responses to PRC2 inhibition. Nat Commun, 15(1), 3452. https://doi.org/10.1038/s41467-024-47701-x

Rosati, R., La Starza, R., Veronese, A., Aventin, A., Schwienbacher, C., Vallespi, T., Negrini, M., Martelli, M. F., & Mecucci, C. (2002). NUP98 is fused to the NSD3 gene in acute myeloid leukemia associated with t(8;11)(p11.2;p15). Blood, 99(10), 3857-3860. https://doi.org/10.1182/blood.v99.10.3857

Rose, N. R., King, H. W., Blackledge, N. P., Fursova, N. A., Ember, K. J., Fischer, R., Kessler, B. M., & Klose, R. J. (2016). RYBP stimulates PRC1 to shape chromatin-based communication between Polycomb repressive complexes. Elife, 5. https://doi.org/10.7554/eLife.18591

Rosenthal, A. C., Munoz, J. L., & Villasboas, J. C. (2023). Clinical advances in epigenetic therapies for lymphoma. Clin Epigenetics, 15(1), 39. https://doi.org/10.1186/s13148-023-01452-6

Roulland, S., Kelly, R. S., Morgado, E., Sungalee, S., Solal-Celigny, P., Colombat, P., Jouve, N., Palli, D., Pala, V., Tumino, R., Panico, S., Sacerdote, C., Quiros, J. R., Gonzales, C. A., Sanchez, M. J., Dorronsoro, M., Navarro, C., Barricarte, A., Tjonneland, A., . . . Nadel, B. (2014). t(14;18) Translocation: A predictive blood biomarker for follicular lymphoma. J Clin Oncol, 32(13), 1347-1355. https://doi.org/10.1200/JCO.2013.52.8190

Roulland, S., Navarro, J. M., Grenot, P., Milili, M., Agopian, J., Montpellier, B., Gauduchon, P., Lebailly, P., Schiff, C., & Nadel, B. (2006). Follicular lymphoma-like B cells in healthy individuals: a novel intermediate step in early lymphomagenesis. J Exp Med, 203(11), 2425-2431. https://doi.org/10.1084/jem.20061292

Rowley, J. D. (1973). Letter: A new consistent chromosomal abnormality in chronic myelogenous leukaemia identified by quinacrine fluorescence and Giemsa staining. Nature, 243(5405), 290-293. https://doi.org/10.1038/243290a0

Rowley, J. D. (1988). Chromosome studies in the non-Hodgkin's lymphomas: the role of the 14;18 translocation. J Clin Oncol, 6(5), 919-925. https://doi.org/10.1200/JCO.1988.6.5.919

Ryan, R. J., Nitta, M., Borger, D., Zukerberg, L. R., Ferry, J. A., Harris, N. L., Iafrate, A. J., Bernstein, B. E., Sohani, A. R., & Le, L. P. (2011). EZH2 codon 641 mutations are common in BCL2-rearranged germinal center B cell lymphomas. PLoS One, 6(12), e28585. https://doi.org/10.1371/journal.pone.0028585

Saloura, V., Vougiouklakis, T., Zewde, M., Deng, X., Kiyotani, K., Park, J. H., Matsuo, Y., Lingen, M., Suzuki, T., Dohmae, N., Hamamoto, R., & Nakamura, Y. (2017). WHSC1L1-mediated EGFR mono-methylation enhances the cytoplasmic and nuclear oncogenic activity of EGFR in head and neck cancer. Sci Rep, 7, 40664. https://doi.org/10.1038/srep40664

Sanjana, N. E., Shalem, O., & Zhang, F. (2014). Improved vectors and genome-wide libraries for CRISPR screening. Nat Methods, 11(8), 783-784. https://doi.org/10.1038/nmeth.3047

Sankaran, S. M., Wilkinson, A. W., Elias, J. E., & Gozani, O. (2016). A PWWP Domain of Histone-Lysine N-Methyltransferase NSD2 Binds to Dimethylated Lys-36 of Histone H3 and Regulates NSD2 Function at Chromatin. J Biol Chem, 291(16), 8465-8474. https://doi.org/10.1074/jbc.M116.720748

Sato, K., Kumar, A., Hamada, K., Okada, C., Oguni, A., Machiyama, A., Sakuraba, S., Nishizawa, T., Nureki, O., Kono, H., Ogata, K., & Sengoku, T. (2021). Structural basis of the regulation of the normal and oncogenic methylation of nucleosomal histone H3 Lys36 by NSD2. Nat Commun, 12(1), 6605. https://doi.org/10.1038/s41467-021-26913-5

Schenk, T., Chen, W. C., Gollner, S., Howell, L., Jin, L., Hebestreit, K., Klein, H. U., Popescu, A. C., Burnett, A., Mills, K., Casero, R. A., Jr., Marton, L., Woster, P., Minden, M. D., Dugas, M., Wang, J. C., Dick, J. E., Muller-Tidow, C., Petrie, K., & Zelent, A. (2012). Inhibition of the LSD1 (KDM1A) demethylase reactivates the all-trans-retinoic acid differentiation pathway in acute myeloid leukemia. Nat Med, 18(4), 605-611. https://doi.org/10.1038/nm.2661

Scheuermann, J. C., de Ayala Alonso, A. G., Oktaba, K., Ly-Hartig, N., McGinty, R. K., Fraterman, S., Wilm, M., Muir, T. W., & Muller, J. (2010). Histone H2A deubiquitinase activity of the Polycomb repressive complex PR-DUB. Nature, 465(7295), 243-247. https://doi.org/10.1038/nature08966

Schmitges, F. W., Prusty, A. B., Faty, M., Stutzer, A., Lingaraju, G. M., Aiwazian, J., Sack, R., Hess, D., Li, L., Zhou, S., Bunker, R. D., Wirth, U., Bouwmeester, T., Bauer, A., Ly-Hartig, N., Zhao, K., Chan, H., Gu, J., Gut, H., . . . Thoma, N. H. (2011). Histone methylation by PRC2 is inhibited by active chromatin marks. Mol Cell, 42(3), 330-341. https://doi.org/10.1016/j.molcel.2011.03.025

Schmitz, R., Wright, G. W., Huang, D. W., Johnson, C. A., Phelan, J. D., Wang, J. Q., Roulland, S., Kasbekar, M., Young, R. M., Shaffer, A. L., Hodson, D. J., Xiao, W.,

Yu, X., Yang, Y., Zhao, H., Xu, W., Liu, X., Zhou, B., Du, W., . . . Staudt, L. M. (2018). Genetics and Pathogenesis of Diffuse Large B-Cell Lymphoma. N Engl J Med, 378(15), 1396-1407. https://doi.org/10.1056/NEJMoa1801445

Scholze, H., Stephenson, R. E., Reynolds, R., Shah, S., Puri, R., Butler, S. D., Trujillo-Alonso, V., Teater, M. R., van Besien, H., Gibbs-Curtis, D., Ueno, H., Parvin, S., Letai, A., Mathew, S., Singh, A., Cesarman, E., Melnick, A., & Giulino-Roth, L. (2020). Combined EZH2 and Bcl-2 inhibitors as precision therapy for genetically defined DLBCL subtypes. Blood Adv, 4(20), 5226-5231. https://doi.org/10.1182/bloodadvances.2020002580

Schuettengruber, B., Bourbon, H. M., Di Croce, L., & Cavalli, G. (2017). Genome Regulation by Polycomb and Trithorax: 70 Years and Counting. Cell, 171(1), 34-57. https://doi.org/10.1016/j.cell.2017.08.002

Schwartzentruber, J., Korshunov, A., Liu, X. Y., Jones, D. T., Pfaff, E., Jacob, K., Sturm, D., Fontebasso, A. M., Quang, D. A., Tonjes, M., Hovestadt, V., Albrecht, S., Kool, M., Nantel, A., Konermann, C., Lindroth, A., Jager, N., Rausch, T., Ryzhova, M., . . . Jabado, N. (2012). Driver mutations in histone H3.3 and chromatin remodelling genes in paediatric glioblastoma. Nature, 482(7384), 226-231. https://doi.org/10.1038/nature10833

Schweizer, M., Penkov., K.D., Tolcher, A.W., Choudhury, A.D., Doronin, V., Aljumaily, R., Calvo, E., Frank, R.C., Hamm, J.T., Moreno Garcia, V., Vorobyev V., Billotte, S., Bowler, T., Chen, J., Lin, T., Liu, L., Maity, A., Sharma, S., Johnson, M.L. (2022). 488P Phase I trial of PF-06821497, a potent and selective inhibitor of enhancer of zeste homolog 2 (EZH2), in follicular lymphoma (FL), small cell lung cancer (SCLC) and castration-resistant prostate cancer (CRPC). Ann Oncol, 33, S763-S764. https://doi.org/10.1016/j.annonc.2022.07.616

Scott, D. W., Mottok, A., Ennishi, D., Wright, G. W., Farinha, P., Ben-Neriah, S., Kridel, R., Barry, G. S., Hother, C., Abrisqueta, P., Boyle, M., Meissner, B., Telenius, A., Savage, K. J., Sehn, L. H., Slack, G. W., Steidl, C., Staudt, L. M., Connors, J. M., . . . Gascoyne, R. D. (2015). Prognostic Significance of Diffuse Large B-Cell Lymphoma Cell of Origin Determined by Digital Gene Expression in Formalin-Fixed Paraffin-Embedded Tissue Biopsies. J Clin Oncol, 33(26), 2848-2856. https://doi.org/10.1200/JCO.2014.60.2383

Sehn, L. H., & Salles, G. (2021). Diffuse Large B-Cell Lymphoma. N Engl J Med, 384(9), 842-858. https://doi.org/10.1056/NEJMra2027612

Sengupta, D., Zeng, L., Li, Y., Hausmann, S., Ghosh, D., Yuan, G., Nguyen, T. N., Lyu, R., Caporicci, M., Morales Benitez, A., Coles, G. L., Kharchenko, V., Czaban, I., Azhibek, D., Fischle, W., Jaremko, M., Wistuba, II, Sage, J., Jaremko, L., . . . Gozani, O. (2021). NSD2 dimethylation at H3K36 promotes lung adenocarcinoma

pathogenesis. Mol Cell, 81(21), 4481-4492 e4489. https://doi.org/10.1016/j.molcel.2021.08.034

Sermer, D., Pasqualucci, L., Wendel, H. G., Melnick, A., & Younes, A. (2019). Emerging epigenetic-modulating therapies in lymphoma. Nat Rev Clin Oncol, 16(8), 494-507. https://doi.org/10.1038/s41571-019-0190-8

Shen, Y., Morishita, M., Lee, D., Kim, S., Lee, T., Mevius, D., Roh, Y., & di Luccio, E. (2019). Identification of LEM-14 inhibitor of the oncoprotein NSD2. Biochem Biophys Res Commun, 508(1), 102-108. https://doi.org/10.1016/j.bbrc.2018.11.037

Shipman, G. A., Padilla, R., Horth, C., Hu, B., Bareke, E., Vitorino, F. N., Gongora, J. M., Garcia, B. A., Lu, C., & Majewski, J. (2024). Systematic perturbations of SETD2, NSD1, NSD2, NSD3, and ASH1L reveal their distinct contributions to H3K36 methylation. Genome Biol, 25(1), 263. https://doi.org/10.1186/s13059-024-03415-3

Shogren-Knaak, M., Ishii, H., Sun, J. M., Pazin, M. J., Davie, J. R., & Peterson, C. L. (2006). Histone H4-K16 acetylation controls chromatin structure and protein interactions. Science, 311(5762), 844-847. https://doi.org/10.1126/science.1124000

Słabicki, M., Park, J., Nowak, R. P., Roy Burman, S. S., Pellman, J., Zou, C., Razumkov, H., Carreiro, J., Rastogi, S., Goldstein, A., Nagiec, M. M., Donovan, K. A., Che, J., Hunkeler, M., Geng, Q., Hsu, C. L., Lakshminarayan, M., Shu, C., Zon, R. L., . . . Ebert, B. L. (2025). Expanding the druggable zinc-finger proteome defines properties of drug-induced degradation. Mol Cell, 85(16), 3184-3201.e3114. https://doi.org/10.1016/j.molcel.2025.07.019

Smits, A. H., Jansen, P. W., Poser, I., Hyman, A. A., & Vermeulen, M. (2013). Stoichiometry of chromatin-associated protein complexes revealed by label-free quantitative mass spectrometry-based proteomics. Nucleic Acids Res, 41(1), e28. https://doi.org/10.1093/nar/gks941

Sneeringer, C. J., Scott, M. P., Kuntz, K. W., Knutson, S. K., Pollock, R. M., Richon, V. M., & Copeland, R. A. (2010). Coordinated activities of wild-type plus mutant EZH2 drive tumor-associated hypertrimethylation of lysine 27 on histone H3 (H3K27) in human B-cell lymphomas. Proc Natl Acad Sci U S A, 107(49), 20980-20985. https://doi.org/10.1073/pnas.1012525107

Song, D., Lan, J., Chen, Y., Liu, A., Wu, Q., Zhao, C., Feng, Y., Wang, J., Luo, X., Cao, Z., Cao, X., Hu, J., & Wang, G. (2021). NSD2 promotes tumor angiogenesis through methylating and activating STAT3 protein. Oncogene, 40(16), 2952-2967. https://doi.org/10.1038/s41388-021-01747-z

Soto-Feliciano, Y. M., Sanchez-Rivera, F. J., Perner, F., Barrows, D. W., Kastenhuber, E. R., Ho, Y. J., Carroll, T., Xiong, Y., Anand, D., Soshnev, A. A., Gates, L., Beytagh, M. C., Cheon, D., Gu, S., Liu, X. S., Krivtsov, A. V., Meneses, M., de Stanchina, E.,

Stone, R. M., . . . Allis, C. D. (2023). A Molecular Switch between Mammalian MLL Complexes Dictates Response to Menin-MLL Inhibition. Cancer Discov, 13(1), 146-169. https://doi.org/10.1158/2159-8290.CD-22-0416

Spahn, P. N., Bath, T., Weiss, R. J., Kim, J., Esko, J. D., Lewis, N. E., & Harismendy, O. (2017). PinAPL-Py: A comprehensive web-application for the analysis of CRISPR/Cas9 screens. Sci Rep, 7(1), 15854. https://doi.org/10.1038/s41598-017-16193-9

Sparbier, C. E., Gillespie, A., Gomez, J., Kumari, N., Motazedian, A., Chan, K. L., Bell, C. C., Gilan, O., Chan, Y. C., Popp, S., Gough, D. J., Eckersley-Maslin, M. A., Dawson, S. J., Lehner, P. J., Sutherland, K. D., Ernst, P., McGeehan, G. M., Lam, E. Y. N., Burr, M. L., & Dawson, M. A. (2023). Targeting Menin disrupts the KMT2A/B and polycomb balance to paradoxically activate bivalent genes. Nat Cell Biol, 25(2), 258-272. https://doi.org/10.1038/s41556-022-01056-x

Srinivasan, L., Sasaki, Y., Calado, D. P., Zhang, B., Paik, J. H., DePinho, R. A., Kutok, J. L., Kearney, J. F., Otipoby, K. L., & Rajewsky, K. (2009). PI3 kinase signals BCR-dependent mature B cell survival. Cell, 139(3), 573-586. https://doi.org/10.1016/j.cell.2009.08.041

Stec, I., van Ommen, G. J., & den Dunnen, J. T. (2001). WHSC1L1, on human chromosome 8p11.2, closely resembles WHSC1 and maps to a duplicated region shared with 4p16.3. Genomics, 76(1-3), 5-8. https://doi.org/10.1006/geno.2001.6581

Stec, I., Wright, T. J., van Ommen, G. J., de Boer, P. A., van Haeringen, A., Moorman, A. F., Altherr, M. R., & den Dunnen, J. T. (1998). WHSC1, a 90 kb SET domain-containing gene, expressed in early development and homologous to a Drosophila dysmorphy gene maps in the Wolf-Hirschhorn syndrome critical region and is fused to IgH in t(4;14) multiple myeloma. Hum Mol Genet, 7(7), 1071-1082. https://doi.org/10.1093/hmg/7.7.1071

Stein, E. M., Garcia-Manero, G., Rizzieri, D. A., Tibes, R., Berdeja, J. G., Savona, M. R., Jongen-Lavrenic, M., Altman, J. K., Thomson, B., Blakemore, S. J., Daigle, S. R., Waters, N. J., Suttle, A. B., Clawson, A., Pollock, R., Krivtsov, A., Armstrong, S. A., DiMartino, J., Hedrick, E., . . . Tallman, M. S. (2018). The DOT1L inhibitor pinometostat reduces H3K79 methylation and has modest clinical activity in adult acute leukemia. Blood, 131(24), 2661-2669. https://doi.org/10.1182/blood-2017-12-818948

Stewart, A. K., Bergsagel, P. L., Greipp, P. R., Dispenzieri, A., Gertz, M. A., Hayman, S. R., Kumar, S., Lacy, M. Q., Lust, J. A., Russell, S. J., Witzig, T. E., Zeldenrust, S. R., Dingli, D., Reeder, C. B., Roy, V., Kyle, R. A., Rajkumar, S. V., & Fonseca, R. (2007). A practical guide to defining high-risk myeloma for clinical trials, patient

counseling and choice of therapy. Leukemia, 21(3), 529-534. https://doi.org/10.1038/sj.leu.2404516

Stewart, A. K., Chang, H., Trudel, S., Anderson, K. C., Richardson, P., Alsina, M., Reece, D., Young, S., Sable-Hunt, A., Li, Z., Keats, J., Van Wier, S., Ahmann, G., Price-Troska, T., Giusti, K., Bergsagel, P. L., Chesi, M., & Fonseca, R. (2007). Diagnostic evaluation of t(4;14) in multiple myeloma and evidence for clonal evolution. Leukemia, 21(11), 2358-2359. https://doi.org/10.1038/sj.leu.2404800

Strahl, B. D., & Allis, C. D. (2000). The language of covalent histone modifications. Nature, 403(6765), 41-45. https://doi.org/10.1038/47412

Streubel, G., Watson, A., Jammula, S. G., Scelfo, A., Fitzpatrick, D. J., Oliviero, G., McCole, R., Conway, E., Glancy, E., Negri, G. L., Dillon, E., Wynne, K., Pasini, D., Krogan, N. J., Bracken, A. P., & Cagney, G. (2018). The H3K36me2 Methyltransferase Nsd1 Demarcates PRC2-Mediated H3K27me2 and H3K27me3 Domains in Embryonic Stem Cells. Mol Cell, 70(2), 371-379 e375. https://doi.org/10.1016/j.molcel.2018.02.027

Su, X., Zhang, J., Mouawad, R., Compérat, E., Rouprêt, M., Allanic, F., Parra, J., Bitker, M. O., Thompson, E. J., Gowrishankar, B., Houldsworth, J., Weinstein, J. N., Tost, J., Broom, B. M., Khayat, D., Spano, J. P., Tannir, N. M., & Malouf, G. G. (2017). NSD1 Inactivation and SETD2 Mutation Drive a Convergence toward Loss of Function of H3K36 Writers in Clear Cell Renal Cell Carcinomas. Cancer Res, 77(18), 4835-4845. https://doi.org/10.1158/0008-5472.Can-17-0143

Sun, A., Li, F., Liu, Z., Jiang, Y., Zhang, J., Wu, J., & Shi, Y. (2018). Structural and biochemical insights into human zinc finger protein AEBP2 reveals interactions with RBBP4. Protein Cell, 9(8), 738-742. https://doi.org/10.1007/s13238-017-0483-6

Sun, K. Y., Bai, X., Chen, S., Bao, S., Zhang, C., Kapoor, M., Backman, J., Joseph, T., Maxwell, E., Mitra, G., Gorovits, A., Mansfield, A., Boutkov, B., Gokhale, S., Habegger, L., Marcketta, A., Locke, A. E., Ganel, L., Hawes, A., . . . Balasubramanian, S. (2024). A deep catalogue of protein-coding variation in 983,578 individuals. Nature, 631(8021), 583-592. https://doi.org/10.1038/s41586-024-07556-0

Sun, X. J., Wei, J., Wu, X. Y., Hu, M., Wang, L., Wang, H. H., Zhang, Q. H., Chen, S. J., Huang, Q. H., & Chen, Z. (2005). Identification and characterization of a novel human histone H3 lysine 36-specific methyltransferase. J Biol Chem, 280(42), 35261-35271. https://doi.org/10.1074/jbc.M504012200

Sun, Z., Lin, Y., Islam, M. T., Koche, R., Hedehus, L., Liu, D., Huang, C., Vierbuchen, T., Sawyers, C. L., & Helin, K. (2023). Chromatin regulation of transcriptional

enhancers and cell fate by the Sotos syndrome gene NSD1. Mol Cell, 83(14), 2398-2416 e2312. https://doi.org/10.1016/j.molcel.2023.06.007

Swaroop, A., Oyer, J. A., Will, C. M., Huang, X., Yu, W., Troche, C., Bulic, M., Durham, B. H., Wen, Q. J., Crispino, J. D., MacKerell, A. D., Jr., Bennett, R. L., Kelleher, N. L., & Licht, J. D. (2019). An activating mutation of the NSD2 histone methyltransferase drives oncogenic reprogramming in acute lymphocytic leukemia. Oncogene, 38(5), 671-686. https://doi.org/10.1038/s41388-018-0474-y

Swerdlow, S., Campo, E., Harris, N., Jaffe, E., Pileri, S., Stein, H., & Thiele, J. E. (2017). WHO Classification of Tumours of Haematopoietic and Lymphoid Tissues (Revised 4th edition). International Agency for Research on Cancer.

Swigut, T., & Wysocka, J. (2007). H3K27 demethylases, at long last. Cell, 131(1), 29-32. https://doi.org/10.1016/j.cell.2007.09.026

Tamburri, S., Lavarone, E., Fernandez-Perez, D., Conway, E., Zanotti, M., Manganaro, D., & Pasini, D. (2020). Histone H2AK119 Mono-Ubiquitination Is Essential for Polycomb-Mediated Transcriptional Repression. Mol Cell, 77(4), 840-856 e845. https://doi.org/10.1016/j.molcel.2019.11.021

Tarumoto, Y., Lu, B., Somerville, T. D. D., Huang, Y. H., Milazzo, J. P., Wu, X. S., Klingbeil, O., El Demerdash, O., Shi, J., & Vakoc, C. R. (2018). LKB1, Salt-Inducible Kinases, and MEF2C Are Linked Dependencies in Acute Myeloid Leukemia. Mol Cell, 69(6), 1017-1027.e1016. https://doi.org/10.1016/j.molcel.2018.02.011

Tisi, D., Chiarparin, E., Tamanini, E., Pathuri, P., Coyle, J. E., Hold, A., Holding, F. P., Amin, N., Martin, A. C., Rich, S. J., Berdini, V., Yon, J., Acklam, P., Burke, R., Drouin, L., Harmer, J. E., Jeganathan, F., van Montfort, R. L., Newbatt, Y., . . . Heightman, T. D. (2016). Structure of the Epigenetic Oncogene MMSET and Inhibition by N-Alkyl Sinefungin Derivatives. ACS Chem Biol, 11(11), 3093-3105. https://doi.org/10.1021/acschembio.6b00308

Tomassi, S., Romanelli, A., Zwergel, C., Valente, S., & Mai, A. (2021). Polycomb Repressive Complex 2 Modulation through the Development of EZH2-EED Interaction Inhibitors and EED Binders. J Med Chem, 64(16), 11774-11797. https://doi.org/10.1021/acs.jmedchem.1c00226

Topchu, I., Pangeni, R. P., Bychkov, I., Miller, S. A., Izumchenko, E., Yu, J., Golemis, E., Karanicolas, J., & Boumber, Y. (2022). The role of NSD1, NSD2, and NSD3 histone methyltransferases in solid tumors. Cell Mol Life Sci, 79(6), 285. https://doi.org/10.1007/s00018-022-04321-2

Trojer, P., & Reinberg, D. (2007). Facultative heterochromatin: is there a distinctive molecular signature? Mol Cell, 28(1), 1-13. https://doi.org/10.1016/j.molcel.2007.09.011

Tsherniak, A., Vazquez, F., Montgomery, P. G., Weir, B. A., Kryukov, G., Cowley, G. S., Gill, S., Harrington, W. F., Pantel, S., Krill-Burger, J. M., Meyers, R. M., Ali, L., Goodale, A., Lee, Y., Jiang, G., Hsiao, J., Gerath, W. F. J., Howell, S., Merkel, E., . . . Hahn, W. C. (2017). Defining a Cancer Dependency Map. Cell, 170(3), 564-576 e516. https://doi.org/10.1016/j.cell.2017.06.010

Turner, B. M. (1993). Decoding the nucleosome. Cell, 75(1), 5-8. https://www.ncbi.nlm.nih.gov/pubmed/8402900

Tzelepis, K., Koike-Yusa, H., De Braekeleer, E., Li, Y., Metzakopian, E., Dovey, O. M., Mupo, A., Grinkevich, V., Li, M., Mazan, M., Gozdecka, M., Ohnishi, S., Cooper, J., Patel, M., McKerrell, T., Chen, B., Domingues, A. F., Gallipoli, P., Teichmann, S., . . . Yusa, K. (2016). A CRISPR Dropout Screen Identifies Genetic Vulnerabilities and Therapeutic Targets in Acute Myeloid Leukemia. Cell Rep, 17(4), 1193-1205. https://doi.org/10.1016/j.celrep.2016.09.079

Varambally, S., Dhanasekaran, S. M., Zhou, M., Barrette, T. R., Kumar-Sinha, C., Sanda, M. G., Ghosh, D., Pienta, K. J., Sewalt, R. G., Otte, A. P., Rubin, M. A., & Chinnaiyan, A. M. (2002). The polycomb group protein EZH2 is involved in progression of prostate cancer. Nature, 419(6907), 624-629. https://doi.org/10.1038/nature01075

Veazey K.J., Cheng D., Lin K., Villarreal O.D., Gao G., Perez-Oquendo M., Van H.T., Stratton S.A., Green M., Xu H., Lu Y., Bedford M.T., Almeida Santos M. (2020). CARM1 inhibition reduces histone acetyltransferase activity causing synthetic lethality in CREBBP/EP300-mutated lymphomas. Leukemia, 34(12), 3269-3285. https://doi.org/10.1038/s41375-020-0908-8

Vedadi, M., Barsyte-Lovejoy, D., Liu, F., Rival-Gervier, S., Allali-Hassani, A., Labrie, V., Wigle, T. J., Dimaggio, P. A., Wasney, G. A., Siarheyeva, A., Dong, A., Tempel, W., Wang, S. C., Chen, X., Chau, I., Mangano, T. J., Huang, X. P., Simpson, C. D., Pattenden, S. G., . . . Jin, J. (2011). A chemical probe selectively inhibits G9a and GLP methyltransferase activity in cells. Nat Chem Biol, 7(8), 566-574. https://doi.org/10.1038/nchembio.599

Velichutina, I., Shaknovich, R., Geng, H., Johnson, N. A., Gascoyne, R. D., Melnick, A. M., & Elemento, O. (2010). EZH2-mediated epigenetic silencing in germinal center B cells contributes to proliferation and lymphomagenesis. Blood, 116(24), 5247-5255. https://doi.org/10.1182/blood-2010-04-280149

Vogelstein, B., Papadopoulos, N., Velculescu, V. E., Zhou, S., Diaz, L. A., Jr., & Kinzler, K. W. (2013). Cancer genome landscapes. Science, 339(6127), 1546-1558. https://doi.org/10.1126/science.1235122

Vogl, D. T., Raje, N., Jagannath, S., Richardson, P., Hari, P., Orlowski, R., Supko, J. G., Tamang, D., Yang, M., Jones, S. S., Wheeler, C., Markelewicz, R. J., & Lonial, S.

(2017). Ricolinostat, the First Selective Histone Deacetylase 6 Inhibitor, in Combination with Bortezomib and Dexamethasone for Relapsed or Refractory Multiple Myeloma. Clin Cancer Res, 23(13), 3307-3315. https://doi.org/10.1158/1078-0432.CCR-16-2526

Voigt, P., LeRoy, G., Drury, W. J., 3rd, Zee, B. M., Son, J., Beck, D. B., Young, N. L., Garcia, B. A., & Reinberg, D. (2012). Asymmetrically modified nucleosomes. Cell, 151(1), 181-193. https://doi.org/10.1016/j.cell.2012.09.002

Vougiouklakis, T., Hamamoto, R., Nakamura, Y., & Saloura, V. (2015). The NSD family of protein methyltransferases in human cancer. Epigenomics, 7(5), 863-874. https://doi.org/10.2217/epi.15.32

Waddington, C. H. (1942a). Canalization of development and the inheritance of acquired characters. Nature, 150(3811), 563-565.

Waddington, C. H. (1942b). The epigenotype. Endeavour, 1, 18-20.

Wagner, A., Regev, A., & Yosef, N. (2016). Revealing the vectors of cellular identity with single-cell genomics. Nat Biotechnol, 34(11), 1145-1160. https://doi.org/10.1038/nbt.3711

Wagner, E. J., & Carpenter, P. B. (2012). Understanding the language of Lys36 methylation at histone H3. Nat Rev Mol Cell Biol, 13(2), 115-126. https://doi.org/10.1038/nrm3274

Wainberg, M., Kamber, R. A., Balsubramani, A., Meyers, R. M., Sinnott-Armstrong, N., Hornburg, D., Jiang, L., Chan, J., Jian, R., Gu, M., Shcherbina, A., Dubreuil, M. M., Spees, K., Meuleman, W., Snyder, M. P., Bassik, M. C., & Kundaje, A. (2021). A genome-wide atlas of co-essential modules assigns function to uncharacterized genes. Nat Genet, 53(5), 638-649. https://doi.org/10.1038/s41588-021-00840-z

Walport, L. J., Hopkinson, R. J., Vollmar, M., Madden, S. K., Gileadi, C., Oppermann, U., Schofield, C. J., & Johansson, C. (2014). Human UTY(KDM6C) is a male-specific Nε-methyl lysyl demethylase. J Biol Chem, 289(26), 18302-18313. https://doi.org/10.1074/jbc.M114.555052

Wang, E. S., Issa, G. C., Erba, H. P., Altman, J. K., Montesinos, P., DeBotton, S., Walter, R. B., Pettit, K., Savona, M. R., Shah, M. V., Kremyanskaya, M., Baer, M. R., Foran, J. M., Schiller, G., Ades, L., Heiblig, M., Berthon, C., Peterlin, P., Rodriguez-Arboli, E., . . . Fathi, A. T. (2024). Ziftomenib in relapsed or refractory acute myeloid leukaemia (KOMET-001): a multicentre, open-label, multi-cohort, phase 1 trial. Lancet Oncol, 25(10), 1310-1324. https://doi.org/10.1016/S1470-2045(24)00386-3

Wang, G. G., Cai, L., Pasillas, M. P., & Kamps, M. P. (2007). NUP98-NSD1 links H3K36 methylation to Hox-A gene activation and leukaemogenesis. Nat Cell Biol, 9(7), 804-812. https://doi.org/10.1038/ncb1608

Wang, H., Wang, L., Erdjument-Bromage, H., Vidal, M., Tempst, P., Jones, R. S., & Zhang, Y. (2004). Role of histone H2A ubiquitination in Polycomb silencing. Nature, 431(7010), 873-878. https://doi.org/10.1038/nature02985

Wang, H., Yang, H., Shivalila, C. S., Dawlaty, M. M., Cheng, A. W., Zhang, F., & Jaenisch, R. (2013). One-step generation of mice carrying mutations in multiple genes by CRISPR/Cas-mediated genome engineering. Cell, 153(4), 910-918. https://doi.org/10.1016/j.cell.2013.04.025

Wang, L., Zhao, Z., Meyer, M. B., Saha, S., Yu, M., Guo, A., Wisinski, K. B., Huang, W., Cai, W., Pike, J. W., Yuan, M., Ahlquist, P., & Xu, W. (2014). CARM1 methylates chromatin remodeling factor BAF155 to enhance tumor progression and metastasis. Cancer Cell, 25(1), 21-36. https://doi.org/10.1016/j.ccr.2013.12.007

Wang, T., Wei, J. J., Sabatini, D. M., & Lander, E. S. (2014). Genetic screens in human cells using the CRISPR-Cas9 system. Science, 343(6166), 80-84. https://doi.org/10.1126/science.1246981

Wang, W., Chen, Y., Zhao, J., Chen, L., Song, W., Li, L., & Lin, G. N. (2021). Alternatively Splicing Interactomes Identify Novel Isoform-Specific Partners for NSD2. Front Cell Dev Biol, 9, 612019. https://doi.org/10.3389/fcell.2021.612019

Wang, X., & Roberts, C. W. (2014). CARMA: CARM1 methylation of SWI/SNF in breast cancer. Cancer Cell, 25(1), 3-4. https://doi.org/10.1016/j.ccr.2013.12.017

Wang, X., Wang, S., Troisi, E. C., Howard, T. P., Haswell, J. R., Wolf, B. K., Hawk, W. H., Ramos, P., Oberlick, E. M., Tzvetkov, E. P., Ross, A., Vazquez, F., Hahn, W. C., Park, P. J., & Roberts, C. W. M. (2019). BRD9 defines a SWI/SNF sub-complex and constitutes a specific vulnerability in malignant rhabdoid tumors. Nat Commun, 10(1), 1881. https://doi.org/10.1038/s41467-019-09891-7

Wang, Y., Zhao, J., Wang, Y., Chen, G., Zhao, S., Xu, J., Yin, C., Xu, Y., Kang, Y., Dong, Y., & Chen, X. (2025). G9a-mediated H3K9 di-methylation protects centromere integrity and chromosome stability. Sci Bull (Beijing), 70(21), 3489-3493. https://doi.org/10.1016/j.scib.2025.08.023

Weinberg, D. N., Papillon-Cavanagh, S., Chen, H., Yue, Y., Chen, X., Rajagopalan, K. N., Horth, C., McGuire, J. T., Xu, X., Nikbakht, H., Lemiesz, A. E., Marchione, D. M., Marunde, M. R., Meiners, M. J., Cheek, M. A., Keogh, M. C., Bareke, E., Djedid, A., Harutyunyan, A. S., . . . Lu, C. (2019). The histone mark H3K36me2 recruits DNMT3A and shapes the intergenic DNA methylation landscape. Nature, 573(7773), 281-286. https://doi.org/10.1038/s41586-019-1534-3

Weinert, B. T., Narita, T., Satpathy, S., Srinivasan, B., Hansen, B. K., Scholz, C., Hamilton, W. B., Zucconi, B. E., Wang, W. W., Liu, W. R., Brickman, J. M., Kesicki, E. A., Lai, A., Bromberg, K. D., Cole, P. A., & Choudhary, C. (2018). Time-Resolved Analysis

Reveals Rapid Dynamics and Broad Scope of the CBP/p300 Acetylome. Cell, 174(1), 231-244 e212. https://doi.org/10.1016/j.cell.2018.04.033

Wickham, H. (2016). ggplot2: Elegant Graphics for Data Analysis. Springer-Verlag. https://ggplot2.tidyverse.org

Wiedenheft, B., Sternberg, S. H., & Doudna, J. A. (2012). RNA-guided genetic silencing systems in bacteria and archaea. Nature, 482(7385), 331-338. https://doi.org/10.1038/nature10886

Wilson, B. G., & Roberts, C. W. (2011). SWI/SNF nucleosome remodellers and cancer. Nat Rev Cancer, 11(7), 481-492. https://doi.org/10.1038/nrc3068

Xu C., Schaffer L., Head S.R., Feeney A.J. (2008). Reciprocal patterns of methylation of H3K36 and H3K27 on proximal vs. distal IgVH genes are modulated by IL-7 and Pax5. Proc Natl Acad Sci U S A, 105(25), 8685-90. https://doi.org/10.1073/pnas.0711758105

Xu, W., Chen, H., Du, K., Asahara, H., Tini, M., Emerson, B. M., Montminy, M., & Evans, R. M. (2001). A transcriptional switch mediated by cofactor methylation. Science, 294(5551), 2507-2511. https://doi.org/10.1126/science.1065961

Yamagishi, M., Kuze, Y., Kobayashi, S., Nakashima, M., Morishima, S., Kawamata, T., Makiyama, J., Suzuki, K., Seki, M., Abe, K., Imamura, K., Watanabe, E., Tsuchiya, K., Yasumatsu, I., Takayama, G., Hizukuri, Y., Ito, K., Taira, Y., Nannya, Y., . . . Uchimaru, K. (2024). Mechanisms of action and resistance in histone methylation-targeted therapy. Nature, 627(8002), 221-228. https://doi.org/10.1038/s41586-024-07103-x

Yang, H., Wang, H., Shivalila, C. S., Cheng, A. W., Shi, L., & Jaenisch, R. (2013). One-step generation of mice carrying reporter and conditional alleles by CRISPR/Cas-mediated genome engineering. Cell, 154(6), 1370-1379. https://doi.org/10.1016/j.cell.2013.08.022

Yang, L., Chan, A. K. N., Miyashita, K., Delaney, C. D., Wang, X., Li, H., Pokharel, S. P., Li, S., Li, M., Xu, X., Lu, W., Liu, Q., Mattson, N., Chen, K. Y., Wang, J., Yuan, Y. C., Horne, D., Rosen, S. T., Soto-Feliciano, Y., . . . Chen, C. W. (2021). High-resolution characterization of gene function using single-cell CRISPR tiling screen. Nat Commun, 12(1), 4063. https://doi.org/10.1038/s41467-021-24324-0

Yap, D. B., Chu, J., Berg, T., Schapira, M., Cheng, S. W., Moradian, A., Morin, R. D., Mungall, A. J., Meissner, B., Boyle, M., Marquez, V. E., Marra, M. A., Gascoyne, R. D., Humphries, R. K., Arrowsmith, C. H., Morin, G. B., & Aparicio, S. A. (2011). Somatic mutations at EZH2 Y641 act dominantly through a mechanism of selectively altered PRC2 catalytic activity, to increase H3K27 trimethylation. Blood, 117(8), 2451-2459. https://doi.org/10.1182/blood-2010-11-321208

Yokoyama, A., Somervaille, T. C., Smith, K. S., Rozenblatt-Rosen, O., Meyerson, M., & Cleary, M. L. (2005). The menin tumor suppressor protein is an essential oncogenic cofactor for MLL-associated leukemogenesis. Cell, 123(2), 207-218. https://doi.org/10.1016/j.cell.2005.09.025

Younes, A., Berdeja, J. G., Patel, M. R., Flinn, I., Gerecitano, J. F., Neelapu, S. S., Kelly, K. R., Copeland, A. R., Akins, A., Clancy, M. S., Gong, L., Wang, J., Ma, A., Viner, J. L., & Oki, Y. (2016). Safety, tolerability, and preliminary activity of CUDC-907, a first-in-class, oral, dual inhibitor of HDAC and PI3K, in patients with relapsed or refractory lymphoma or multiple myeloma: an open-label, dose-escalation, phase 1 trial. Lancet Oncol, 17(5), 622-631. https://doi.org/10.1016/S1470-2045(15)00584-7

Young, C., & Brink, R. (2021). The unique biology of germinal center B cells. Immunity, 54(8), 1652-1664. https://doi.org/10.1016/j.immuni.2021.07.015

Young, N. L., DiMaggio, P. A., Plazas-Mayorca, M. D., Baliban, R. C., Floudas, C. A., & Garcia, B. A. (2009). High throughput characterization of combinatorial histone codes. Mol Cell Proteomics, 8(10), 2266-2284. https://doi.org/10.1074/mcp.M900238-MCP200

Yuan, G., Ma, B., Yuan, W., Zhang, Z., Chen, P., Ding, X., Feng, L., Shen, X., Chen, S., Li, G., & Zhu, B. (2013). Histone H2A ubiquitination inhibits the enzymatic activity of H3 lysine 36 methyltransferases. J Biol Chem, 288(43), 30832-30842. https://doi.org/10.1074/jbc.M113.475996

Yuan, W., Xie, J., Long, C., Erdjument-Bromage, H., Ding, X., Zheng, Y., Tempst, P., Chen, S., Zhu, B., & Reinberg, D. (2009). Heterogeneous nuclear ribonucleoprotein L Is a subunit of human KMT3a/Set2 complex required for H3 Lys-36 trimethylation activity in vivo. J Biol Chem, 284(23), 15701-15707. https://doi.org/10.1074/jbc.M808431200

Yuan, W., Xu, M., Huang, C., Liu, N., Chen, S., & Zhu, B. (2011). H3K36 methylation antagonizes PRC2-mediated H3K27 methylation. J Biol Chem, 286(10), 7983-7989. https://doi.org/10.1074/jbc.M110.194027

Zentner, G. E., & Henikoff, S. (2013). Regulation of nucleosome dynamics by histone modifications. Nat Struct Mol Biol, 20(3), 259-266. https://doi.org/10.1038/nsmb.2470

Zhang, J., Ding, L., Holmfeldt, L., Wu, G., Heatley, S. L., Payne-Turner, D., Easton, J., Chen, X., Wang, J., Rusch, M., Lu, C., Chen, S. C., Wei, L., Collins-Underwood, J. R., Ma, J., Roberts, K. G., Pounds, S. B., Ulyanov, A., Becksfort, J., . . . Mullighan, C. G. (2012). The genetic basis of early T-cell precursor acute lymphoblastic leukaemia. Nature, 481(7380), 157-163. https://doi.org/10.1038/nature10725

Zhang, J., Dominguez-Sola, D., Hussein, S., Lee, J. E., Holmes, A. B., Bansal, M., Vlasevska, S., Mo, T., Tang, H., Basso, K., Ge, K., Dalla-Favera, R., & Pasqualucci, L. (2015). Disruption of KMT2D perturbs germinal center B cell development and promotes lymphomagenesis. Nat Med, 21(10), 1190-1198. https://doi.org/10.1038/nm.3940

Zhang, J., Grubor, V., Love, C. L., Banerjee, A., Richards, K. L., Mieczkowski, P. A., Dunphy, C., Choi, W., Au, W. Y., Srivastava, G., Lugar, P. L., Rizzieri, D. A., Lagoo, A. S., Bernal-Mizrachi, L., Mann, K. P., Flowers, C., Naresh, K., Evens, A., Gordon, L. I., . . . Dave, S. S. (2013). Genetic heterogeneity of diffuse large B-cell lymphoma. Proc Natl Acad Sci U S A, 110(4), 1398-1403. https://doi.org/10.1073/pnas.1205299110

Zhang, J., Jima, D., Moffitt, A. B., Liu, Q., Czader, M., Hsi, E. D., Fedoriw, Y., Dunphy, C. H., Richards, K. L., Gill, J. I., Sun, Z., Love, C., Scotland, P., Lock, E., Levy, S., Hsu, D. S., Dunson, D., & Dave, S. S. (2014). The genomic landscape of mantle cell lymphoma is related to the epigenetically determined chromatin state of normal B cells. Blood, 123(19), 2988-2996. https://doi.org/10.1182/blood-2013-07-517177

Zhang, M., Wang, Y., Jones, S., Sausen, M., McMahon, K., Sharma, R., Wang, Q., Belzberg, A. J., Chaichana, K., Gallia, G. L., Gokaslan, Z. L., Riggins, G. J., Wolinksy, J. P., Wood, L. D., Montgomery, E. A., Hruban, R. H., Kinzler, K. W., Papadopoulos, N., Vogelstein, B., & Bettegowda, C. (2014). Somatic mutations of SUZ12 in malignant peripheral nerve sheath tumors. Nat Genet, 46(11), 1170-1172. https://doi.org/10.1038/ng.3116

Zhang, Y., Liu, T., Meyer, C. A., Eeckhoute, J., Johnson, D. S., Bernstein, B. E., Nusbaum, C., Myers, R. M., Brown, M., Li, W., & Liu, X. S. (2008). Model-based analysis of ChIP-Seq (MACS). Genome Biol, 9(9), R137. https://doi.org/10.1186/gb-2008-9-9-r137

Zhao, J., Wang, M., Chang, L., Yu, J., Song, A., Liu, C., Huang, W., Zhang, T., Wu, X., Shen, X., Zhu, B., & Li, G. (2020). RYBP/YAF2-PRC1 complexes and histone H1-dependent chromatin compaction mediate propagation of H2AK119ub1 during cell division. Nat Cell Biol, 22(4), 439-452. https://doi.org/10.1038/s41556-020-0484-1

Zhao, L. H., Li, Q., Huang, Z. J., Sun, M. X., Lu, J. J., Zhang, X. H., Li, G., & Wu, F. (2021). Identification of histone methyltransferase NSD2 as an important oncogenic gene in colorectal cancer. Cell Death Dis, 12(11), 974. https://doi.org/10.1038/s41419-021-04267-6

APPENDICES

Appendix I

Antibodies used in this study.

REAGENT or RESOURCE	SOURCE	IDENTIFIER
Normal Rabbit IgG (CUT&RUN)	Cell Signaling	Cat#2729
Normal Rabbit IgG (IP)	Millipore	Cat#12-370
Rabbit anti-EZH2 (WB)	Cell Signaling	Cat#3147
Rabbit anti-SUZ12 (WB, IP, CUT&RUN)	Cell Signaling	Cat#3737
Rabbit anti-EED (WB, IP)	Cell Signaling	Cat#85322
Rabbit anti-JARID2 (WB)	Cell Signaling	Cat#13594
Rabbit anti-MTF2 (WB, CUT&RUN)	Proteintech	Cat#16208-1-AP
Rabbit anti-AEBP2 (WB, IP, CUT&RUN)	Cell Signaling	Cat#14129
Rabbit anti-H3K27me2 (WB, CUT&RUN)	Cell Signaling	Cat#9728
Rabbit anti-H3K27me3 (WB, CUT&RUN)	Cell Signaling	Cat#9733
Rabbit anti-H3K27ac (WB, CUT&RUN)	Abcam	Cat#4729
Rabbit anti-H3K4me3 (WB)	Abcam	Cat#8580
Rabbit anti-H3K36me2 (WB, CUT&RUN)	Abcam	Cat#9049
Rabbit anti-H3K36me3 (WB)	Abcam	Cat#9050
Rabbit anti-H2AK119ub1 (WB)	Cell Signaling	Cat#8240
Mouse anti-Histone H3 (WB)	Active Motif	Cat#39763
Rabbit anti-NSD1 (WB)	Abbexa	Cat#135901
Mouse anti-NSD2 (WB, IP, CUT&RUN)	Abcam	Cat#75359
Mouse anti-NSD3 (WB)	Santa Cruz	Cat#sc-130009
Rabbit anti-Menin (WB, IP)	Bethyl	Cat#A300-105A
Rabbit anti-MLL1 (WB, IP)	Bethyl	Cat#A300-086A
Mouse anti-CCNA2 (WB)	Cell Signaling	Cat#4656
Rabbit anti-BRD9 (WB)	Abcam	Cat#259839
Rabbit anti-HA (WB)	Cell Signaling	Cat#3724
Mouse anti-FLAG (WB, IP)	Sigma-Aldrich	Cat#F1804
Mouse anti-Beta-Actin (WB)	Proteintech	Cat#60008-1-Ig
Mouse anti-GAPDH (WB)	Proteintech	Cat#60004-1-Ig
Rabbit anti-Vinculin (WB)	Cell Signaling	Cat#4650
Goat anti-mouse (red) IRDye 680LT (WB)	LI-COR	Cat#926-68020
Goat anti-rabbit (green) IRDye 800CW (WB)	LI-COR	Cat#926-32211
Goat anti-mouse IgG (chemiluminescent)	Sigma-Aldrich	Cat#401253
Goat anti-rabbit IgG (chemiluminescent)	Sigma-Aldrich	Cat#A0545

Appendix II

sgRNA sequences used in this study.

sgRNA	Target Sequence
ROSA26	GAAGATGGGCGGGAGTCTTC
Luciferase	GATTCTAAAACGGATTACCA
RPA3	GATGAATTGAGCTAGCATGC
MEN1 sg1	AGGATAGAGGGACAGGTCGA
MEN1 sg2	GAACGTTGGTAGGGATGACG
DOT1L sg1	GCAGCAGGTCTACAACCACT
DOT1L sg2	TCAGACCGTGTCTCAGACGG
EHMT2 sg1	CGGACAGGTACAACTGCCGA
EHMT2 sg2	CTCCAGGTGGTTGTTCACCA
PIK3CD sg1	CAGCGGCTGCCGGAACACTG
PIK3CD sg2	TGATGGCGAAGGAGCCTACG
EP300 sg1	ATGGTGAACCATAAGGATTG
EP300 sg2	GTGGCACGAAGATATTACTC
BRD9 sg1	AGAGAGGGAGCACTGTGACA
BRD9 sg2	AGATACCGTGTACTACAAGT
NSD1 sg1	AAGCACATAAAGATGAACGG
NSD1 sg2	TATGCATGATAGTAAGACGA
NSD2 sg1	ACAACGTTGGTGATTTGGTG
NSD2 sg2	GGGTTCTCCATTAAACACCC
EED sg1	AAGAGAATGATCCATACCAC
EED sg2	ACAAACACGCCAAATGCACC
EED sg3	ATTACAGCCAGTGTGACATT
SUZ12 sg1	GAGACTCTCTGAATTTCTAG
SUZ12 sg2	GGAGACTATTCTTGATGGGA
MTF2 sg1	ATGGTTATATGTGACAAGTG
MTF2 sg2	GCAGACATTACCCTATAGTG
JARID2 sg1 (UIM)	ACCACCCGTTCTTCTGACCA
JARID2 sg2 (UIM)	GGATTCCGTGGTCAGAAGAA
CBX4 sg1	CCTTGCAAGATATAACACGT
CBX4 sg2	CGGTCAGGACATTGGAACGA
CBX8 sg1	CTCTATGGCCCCAAAAAGCG
sgRNA	**Target Sequence**
CBX8 sg2	GGGACAAACCCATGTTTCGA
AEBP2 sg1 (ZF1_1)	AGTTGAAGCAAGCCTGGCAC
AEBP2 sg2 (ZF1_2)	GGCTAGAGTTGAAGCAAGCC
AEBP2 sg3 (ZF2_1)	AACCAACTTTGACTGGTAGA

AEBP2 sg4 (ZF2_2)	CCTTTGTAACCAACTTTGAC
AEBP2 sg5 (ZF3_1)	CAGTGGAGACAAACCTTTCA
AEBP2 sg6 (ZF3_2)	ACATGCATCCTTACCTTGAA
AEBP2 sg7 (SBH_1)	CTTTCATTCACCCACACATC
AEBP2 sg8 (SBH_2)	TTCATAGTCTGCCTGATGTG

Appendix III

CUT&RUN qPCR primers for TSS of the following mouse genes used in this study.

Target	**Forward Primer Sequence (5'-3')**	**Reverse Primer Sequence (5'-3')**
T	TCCGCAGAGTGACCCTTTTTC	TACCCAACAGCCACCTTCACTTC
Gapdh	GTGTGCACCAAGGACATCCAG	CCCATTTTACTCGGGAAGCAG

Appendix IV

Compounds used in this study.

Name	**Target**	**Compound Type**	**Source**
Tazemetostat	EZH2	Methyltransferase inhibitor	Stratech
SNDX-5613	Menin	Protein-protein interaction inhibitor	MedChemExpress
dBRD9	BRD9	PROTAC degrader	Dr. Gerry Brien (Gift)
UNC8153	NSD2	PROTAC degrader	Dr. Lindsey James (Gift)
Idelalisib	PI3K	Kinase inhibitor	MedChemExpress
UNC0642	EHMT2	Methyltransferase inhibitor	MedChemExpress
TP-064	CARM1	Methyltransferase inhibitor	MedChemExpress

Appendix V

Primers for amplifying Brunello library from gDNA.

P5 primer	**Sequence (5'-3')**
Brunello_P5_0nt _stagger	AATGATACGGCGACCACCGAGATCTACACTCTTTCCCTACACGAC GCTCTTCCGATCTTTGTGGAAAGGACGAAACACCG
Brunello_P5_1nt _stagger	AATGATACGGCGACCACCGAGATCTACACTCTTTCCCTACACGAC GCTCTTCCGATCTCTTGTGGAAAGGACGAAACACCG
Brunello_P5_2nt _stagger	AATGATACGGCGACCACCGAGATCTACACTCTTTCCCTACACGAC GCTCTTCCGATCTGCTTGTGGAAAGGACGAAACACCG

Brunello_P5_3nt_stagger	AATGATACGGCGACCACCGAGATCTACACTCTTTCCCTACACGACGCTCTTCCGATCTAGCTTGTGGAAAGGACGAAACACCG
Brunello_P5_4nt_stagger	AATGATACGGCGACCACCGAGATCTACACTCTTTCCCTACACGACGCTCTTCCGATCTCAACTTGTGGAAAGGACGAAACACCG
Brunello_P5_6nt_stagger	AATGATACGGCGACCACCGAGATCTACACTCTTTCCCTACACGACGCTCTTCCGATCTTGCACCTTGTGGAAAGGACGAAACACCG
Brunello_P5_7nt_stagger	AATGATACGGCGACCACCGAGATCTACACTCTTTCCCTACACGACGCTCTTCCGATCTACGCAACTTGTGGAAAGGACGAAACACCG
Brunello_P5_8nt_stagger	AATGATACGGCGACCACCGAGATCTACACTCTTTCCCTACACGACGCTCTTCCGATCTGAAGACCCTTGTGGAAAGGACGAAACACCG
P7 primer	**Sequence (5'-3')**
Brunello_P7_NEB_Index30 (e.g.)	CAAGCAGAAGACGGCATACGAGATCCGGTGGTGACTGGAGTTCAGACGTGTGCTCTTCCGATCTTCTACTATTCTTTCCCCTGCACTGT